Author:
Alsadder, Lujain R Z

Title:
Characterisation of post ischaemic cardiac remodelling in rodent and porcine models of cardiac injury

CHARACTERISATION OF POST ISCHAEMIC CARDIAC REMODELLING IN RODENT AND PORCINE MODELS OF CARDIAC INJURY

By: Lujain Alsadder, *BSc, MD*

Supervisors

Prof. Saadeh Suleiman

Prof. Raimondo Ascione

Dr. Tom Johnson

A Dissertation Submitted to the University of Bristol in accordance with the requirements for award of the degree of Doctor of Philosophy in The Faculty of Health Sciences
The Bristol Medical School (THS)
June 2021

Word count: 55998

Abstract

Introduction: Cardiovascular diseases remain a major cause of morbidity and mortality worldwide. There is a large number of patients who suffer from myocardial infarction (MI). However, the a hearts of majority of patients who survive an MI will undergo substantial changes that will lead to heart failure (HF). The aim of this work is to characterise post ischaemic cardiac remodelling in two different experimental models using rats and pigs. A clinical study was also planned to identify acute changes in the blood metabolome of patients undergoing primary percutaneous coronary intervention (PPCI) following ST elevation myocardial infarction (STEMI) and correlate with long term recovery. The obtained information will help in identifying targets for therapeutic interventions, which can reduce the likelihood of adverse cardiac remodelling, and therefore heart failure.

Methods: Adult rats undergoing left anterior descending (LAD) coronary artery ligation and pigs with LAD coronary artery balloon occlusion were used in this work. SHAM operated rats and healthy pigs were used as control. After initiation of cardiac injury, the animals were monitored for 4 weeks before termination. Cardiac injury and function 4 weeks after interventions were assessed using echocardiography and cardiac proteins release in pigs. Hearts and blood samples were extracted and collected. Nuclear magnetic resonance spectroscopy was used to assess metabolic profile of blood and cardiac tissues. Cardiac energy metabolites were measured using high performance liquid chromatography. Cardiac protein and phospho-protein quantification were carried out using liquid chromatography tandem mass spectrometry. Histological analyses of infarcted and control hearts were conducted using light and electron microscopies to detect ultrastructural differences. Ethical application and protocol for the clinical study were granted.

Results: Post ischaemic cardiac remodelling in rodent and porcine hearts was associated with increased cardiac fibrosis and wall thickening of small to medium size arterioles. Ultrastructural analysis showed characteristics of ongoing structural remodelling in the extracellular matrix and the presence of fibroblasts and telocytes. There was disruption to mitochondrial cristae density and distribution. No significant changes were detected in cardiac energetics in infarcted and control tissues of rats and pigs. Proteomics and phosphoproteomics analyses revealed evidence of sustained oxidative stress and inflammation, in addition decrease of mitochondrial respiration and metabolism proteins, modification to calcium cycling, z disc and selected extracellular matrix proteins and collagen subtypes. There was increase in certain metabolites with post ischaemic remodelling, mainly ketone bodies in rodents and porcine blood, and taurine in porcine cardiac tissues. The clinical study was suspended due to Covid-19 pandemic.

Conclusion: Post ischaemic cardiac remodelling is associated with substantial cellular, molecular and metabolic changes in rodent and porcine models of cardiac injury. Importantly, the increase in blood ketone bodies in both models, in addition to decreased porcine blood taurine level could potentially be investigated furthermore in patients to target adverse cardiac remodelling and design therapeutic intervention for heart failure.

Dedication

I would like to dedicate this work to my Mum Lubna and my Dad Reda, the most amazing, beautiful, and genuine persons in my whole life, for their enormous and endless love and continuous support and care throughout my life. No words are good enough to express my great love and gratitude for you!

To my wonderful and brilliant siblings: Razan, Zuhier, Aya, Zubieda and Siham; as well as my sweet grandma and my adorable nephews (Ghassan and Omar), and to all of my family and friends back home and everywhere.

Thank you all for always being there for me, love you most ardently!

Acknowledgement

I am eternally grateful Prof. Tom Sperlinger, the lead for HESPAL scheme at University of Bristol, and HESPAL team in Palestine. This scheme made dream come true for many Palestinian scholars, including myself, to pursue higher education in UK. I am lucky enough to receive such a generous support throughout these years. I am also grateful to staff at An-Najah National University for their encouragement and motivation to pursue PhD, specially Dr. Abdulsalam Khayyat.

I am absolutely grateful to my supervisor, Prof. Saadeh Suleiman for his great support, patience, and wisdom he offered to me ever since I started my PhD, and for everything he has done to refine my research skills and connect me with other researchers and attend meeting and training opportunities. He has been, and always will be, a great role model to me. I would like also to express gratitude to my co-supervisors Prof. Raimondo Ascione and Dr. Tom Johnson for their valuable contribution and feedback to the project.

My great thanks to everyone who helped me throughout this wonderful journey, particularly Mrs. Hua Lin for teaching me several lab techniques and skills. I am greatly thankful to TBRC team, especially Mr. Daniel Baz Lopez, Dr. Eva Sammut and Dr. Domenico Bruno for their amazing help in porcine model. My sincere gratitude to the following amazing University of Bristol staff for their help and technical support: Dr. Simon Bryant, Dr. Erin O'Callghan and Dr. Andy James (rodent model), Dr. Katie Skeffington (HPLC and IPA), Dr. Matt Goodwin (NMR), Dr. Kate Heesom (LC-MS/MS), Hanna and Debbie Martin (histology) and staff at Wolfson Bioimaging facility, University of Bristol (Gini Tilly, Dr. Chris Neal, Dr. Judith Mantell and Sally Hobson) and Dr. Georgia May Connolly at Bristol Heart Institute (clinical study) and staff at Research Floor Level 7.

Finally, I would like to acknowledge and appreciate the amazing moral support and love I received from my amazing parents, siblings, family, and friends everywhere throughout these years, thanks a lot for always believing in me! I also have been very blessed to meet and make many beautiful friends here in UK, who became my second and extended family, namely Haneen, Tasneem, Froso, Faegheh, Sahirah, Suner and Silvia, Shazia and her family, Aunt Khairyia and her family amongst many other great friends. Thank you all for the amazing times we had together, definitely it would not be the same without you!

Author's Declaration

I declare that the work in this dissertation was carried out in accordance with the requirements of the University's Regulations and Code of Practice for Research Degree Programmes and that it has not been submitted for any other academic award. Except where indicated by specific reference in the text, the work is the candidate's own work. Work done in collaboration with, or with the assistance of, others, is indicated as such. Any views expressed in the dissertation are those of the author.

SIGNED: ..... DATE:.....

List of presentations and publication

Published abstracts:

Proteomic And Phosphoproteomic Analyses Of Porcine Post-ischaemic Hearts Reveal Marked Alterations In Z-disc Proteins L Alsadder, K Heesom, DB Lopez, VD Bruno, E Sammut, T Johnson, CARDIOVASCULAR DRUGS AND THERAPY 34 (2), 283-283

Changes in Cardiac Inflammatory Signalling Pathways After Myocardial Infarction L Alsadder, R Ascione, T Johnson, K Heesom, S Bryant, A James, CARDIOVASCULAR DRUGS AND THERAPY 33 (2), 264-264

Remodelling After Myocardial Infarction Involves Changes in Inflammatory Signalling Pathways L Alsadder, R Ascione, T Johnson, K Heesom, S Bryant, A James, CARDIOVASCULAR DRUGS AND THERAPY 33 (2), 271-271

Oral presentation:

University of Bristol Postgraduate Research Day, September 2019

Poster presentation:

British Society of Cardiovascular Research (BSCR) Autumn Meeting 2019 - Heart Failure, New Therapies and strategies, University of Cambridge, September 2019

University of Bristol Postgraduate Research Day, September 2019

Physiological Society Life Sciences 2019- Posttranslational Modification and Cell Signalling Nottingham, March 2019

British Society of Cardiovascular Research (BSCR) Autumn Meeting 2018 - Inflammation and Repair, University of Sheffield, September 2018

Table of Content

List of tables

List of figures

Abbreviations and notes

ANT, Adenine nucleotide translocator
CABG, Coronary Artery Bypass Graft
CICR, Calcium-induced calcium release
CK, Creatine Kinase
DAMP, Danger-associated molecular pattern
ECM, Extracellular matrix
ETC, Electron Transport Chain
EVG, Elastic- Verhoeff's Van Gieson
FA, Fatty acid
FC, Fold Change
GLUT, glucose transporter
GSH, glutathione
GSSG, glutathione disulfide
HPLC, High Pressure Liquid chromatography
IL, Interleukin
IMM, inner mitochondrial membrane
IRI, Ischaemia Reperfusion Injury
KH buffer, Krebs-Henseleit buffer
LAD, Left Anterior Descending
LC-MS, Liquid chromatography–mass spectrometry
LDH, Lactate dehydrogenase
MMP, Matrix metallopeptidase
NCX, Sodium-Calcium exchanger
NMR, Nuclear Magnetic Resonance
OCT, Optimal cutting temperature
OMM, Outer mitochondrial membrane
PBS, Phosphate Buffer Saline
PCI, Percutaneous Coronary Intervention
PFA, Paraformaldehyde
PKA, Protein Kinase A
PKC, Protein Kinase C
PLC, Phospholipase C
ROS, Reactive oxygen species
SEM, Standard error of mean
SMC, Smooth muscle cell
SOD, Superoxide dismutase
SR, Sarcoplasmic reticulum
TCA, Tricarboxylic acid cycle
TLR, Toll-like receptor
TMT, Tandem Mass Tags
Tp, Telopde
TSP, Trimethylsilylpropanoic acid

Note: Unless stated elsewhere, all the work in this thesis was carried out by the student herself, including samples preparation and data analysis. Experimental work on animal models and running samples through NMR, HPLC and LC-MS/MS and samples processing for EM was done by staff from University of Bristol and acknowledged in the methods chapter.

Chapter 1

General Introduction

1.1 Overall impact of cardiovascular diseases

Cardiovascular diseases (CVDs) are a leading cause of death globally, with an estimate of 17.9 million lives lost each year due to CVDs (World Health Organizition WHO). Ischaemic heart disease (IHD) and other diseases like stroke account for most of CVD deaths. In the United Kingdom, it has been estimated that 27% of deaths each year (nearly 160,000 deaths) is caused by or related to cardiovascular diseases (British Heart Foundation). Patients who survive previous heart attack will most likely suffer from deleterious sequela, i.e., Heart Failure, which will dramatically affect quality of life and increase risk of sudden cardiac death. As for 2019, there were around 900,000 patients who survived an episode of myocardial infarction and are living with heart failure (British Heart Foundation). Whereas several heterogenous aetiologies are attributed to heart failure, ischaemic heart disease, however, remains the most common cause (Vedin, Lam et al. 2017). Unfortunately, despite the recent advancements in reperfusion strategies such as percutaneous coronary intervention (PCI) and coronary artery bypass grafting (CABG) surgery, reperfusion substantially exacerbates the initial ischaemic injury, which manifests in decreased cardiac function and expansion of the infarct size in patients with coronary artery disease (CAD). Therefore, expansion of the current knowledge involving the pathophysiological changes contributing toward development of heart failure will assist in identifying new targets, designing new therapeutic interventions and modulating disease progression.

This introduction will review basic knowledge and advances in our understanding of myocardial structure and metabolism in health and during ischaemia reperfusion injury (IRI). Additionally, this introduction will address key concepts related to cardiac remodelling following acute myocardial infarction (MI) and the use of experimental animal models.

1.2 Myocardial structure and metabolism

1.2.1 Structure

Mammalian cardiovascular system consists of heart which continuously pumps blood into pulmonary and systemic circulation through blood vessels. The heart itself consists of two atria and two ventricles, separated by muscular septum and valves as illustrated in figure 1.1. All the heart chambers contract and relax in a well-coordinated manner to facilitate blood pumping into lungs or other organs. Right atrium receives deoxygenated blood from superior and inferior vena cavae, whereas oxygenated blood is carried through pulmonary veins into left atrium. During cardiac diastole, passive filling of blood into right and left ventricles from right and left atria occurs through tricuspid and mitral valves, respectively. Atria contract simultaneously to eject blood into right and left ventricles at the end of diastole, which takes around two thirds of the cardiac cycle. During systole, however, right ventricle ejects deoxygenated blood through pulmonary valve to pulmonary artery. Concurrently, left ventricle contracts against aortic valve, ejecting blood into the systemic circulation through via the aorta. Moreover, the heart function is tightly regulated through central neurological and endocrine mechanisms as well as regional autoregulatory responses to achieve homeostasis (Dampney 2016).

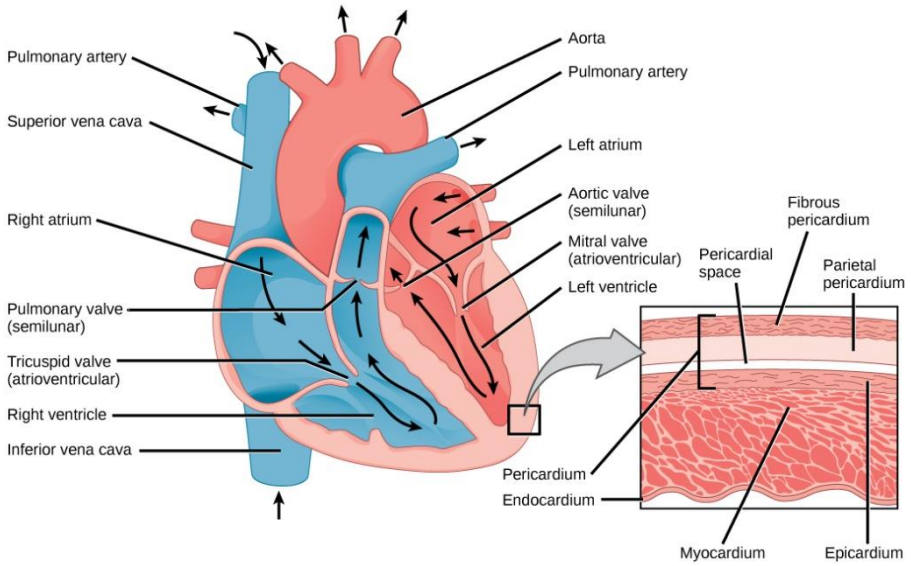

Figure 1.1 The heart and its champers, and the side box showing different layers of cardiac wall. Adapted from Lumenlearning courses website.

The heart wall is made of three distinct layers: innermost endothelial layer, i.e., endocardium, intermediate muscular layer of myocardium and an outermost layer called epicardium. The pericardium consists of serous and fibrous layers, which surrounds the heart for protection and lubrication from pericardial fluid in the pericardial cavity. Myocardium constitutes the bulk of heart wall and contains cardiomyocytes, in which their structural arrangement is inseparable from their main contractile function. Cardiomyocytes occupy majority of cardiac volume (70–85%) and are arranged in in criss-crossing fashion, therefore reducing the longitudinal axis of the chamber to generate the maximum force to pump the blood out (Zhou and Pu 2016). As seen in figure

1.2, the cardiac tissue include a variety of non-cardiomyocytes cells in addition to cardiomyocytes including smooth muscle cells (SMC), endothelial cells, fibroblasts, pericytes, and immune cells, e.g. macrophages, mast and T cells, and cardiac progenitor cells (Takeda and Manabe 2011). Spindle-shaped fibroblasts mediate fibrotic response and produce interstitial collagen, proteoglycans, and proteases. Endothelial cells play central role in release of growth factors and active substances modulating vascular tone, coagulation and inflammatory responses (Esper, Nordaby et al. 2006). Noncardiomyocytes normally resides in the heart stroma, however, massive infiltration of immune cells and fibroblasts occurs following cardiomyocytes death to mediate repair (Hinglais, Heudes et al. 1994). Electron micrographs of these different types of cells with their characteristic morphology are listed in table 1.1. Nonetheless, since adult cardiomyocytes are terminally differentiated, they lack the ability to regenerate after ischaemic injury.

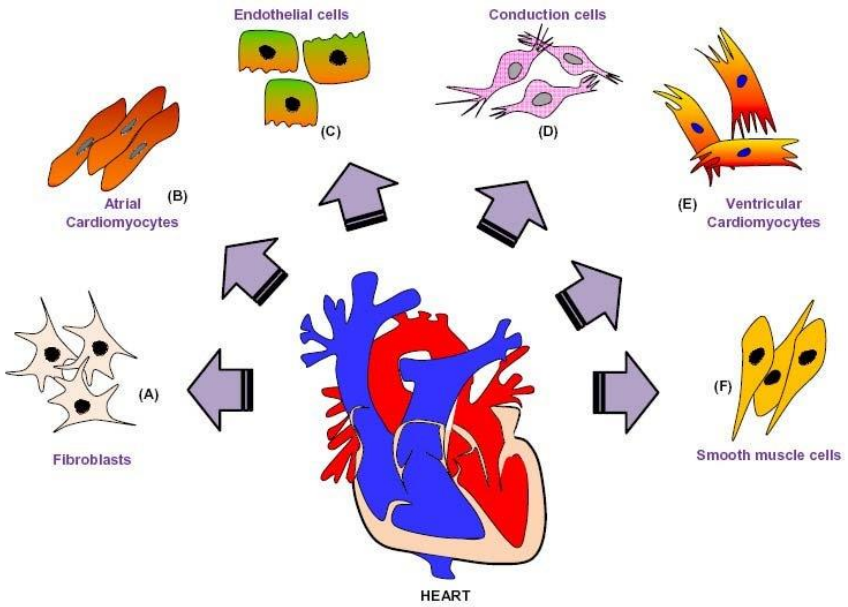

Figure 1.2 Schematic of selected key cardiac cell types, from (Nandi and Mishra 2015).

Table 1.1 Characteristics, function, and electron micrographs of selected cardiac connective tissue cells.

Cell	Characteristics and function	Electron micrograph	Image Source
Fibroblast	Elongated cells of branched cytoplasm, elliptical nucleus with abundant rough endoplasmic reticulum, Mediates production of ECM proteins.	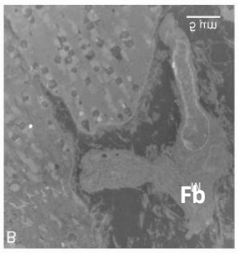 Fb, fibroblast	(Baum and Duffy 2011)
Smooth muscle cell	Elongated spindle shape cells, involved in vascular remodelling and control lumen diameter of blood vessels.	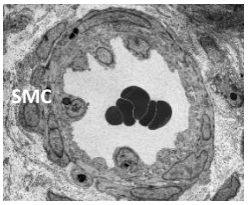 SMC, smooth muscle cell	(Sciencephoto)
Telocyte	Stromal cells with dichotomous pattern of elongated extensions called telopdes, up to hundreds of microns in length. Involved in intercellular signalling and regeneration.	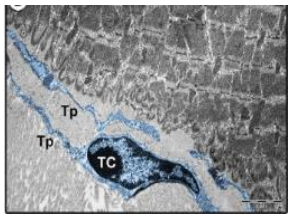 TC, telocyte; Tp, telopodes	(Rosa, Taverna et al. 2019)
Endothelial cell	Cells lining blood vessels, and endocardium and mediates various biological responses related to homeostasis and tissue repair.	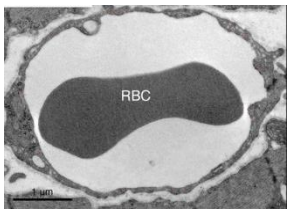	(Cheng, Mendoza-Topaz et al. 2015)
Pericyte	Their cellular extensions wrap around endothelial cells to control capillary blood flow.	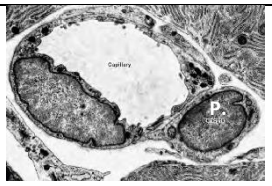 P., pericyte	(Slideshare)
Macrophage	Antigen presentation, phagocytosis and inflammation, regulation of angiogenesis.	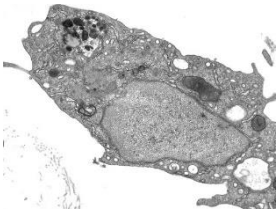	(University of Yale medical lab)

Cardiomyocytes

Cardiac myocyte is striated, branched, multi- nucleated cell where the nuclei are centrally located, however, like other striated skeletal muscle, each cell is composed of many fibres called myofibrils which contain functional units for contraction, the sarcomeres. Figure 1.3 shows the distinctive banding appearance of the striated myocytes.

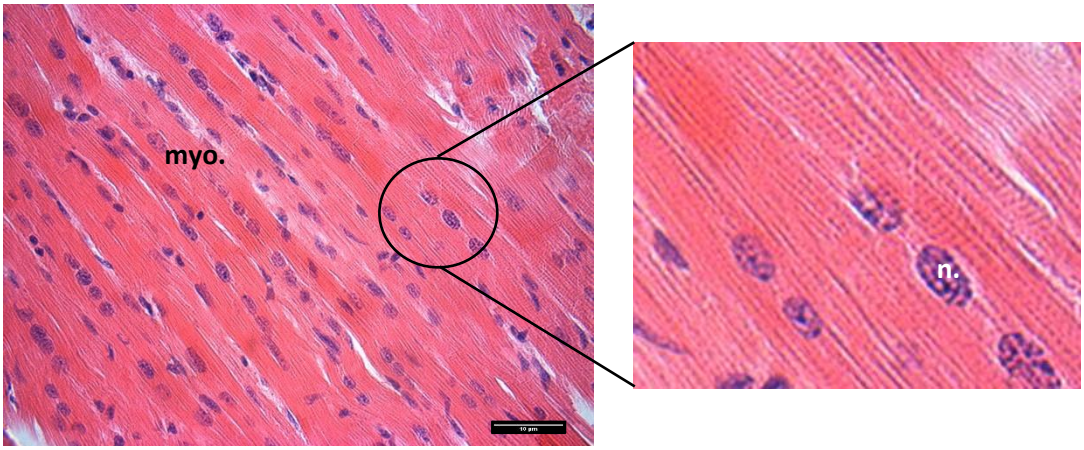

Figure 1.3 Longitudinal section of porcine myocardium stained with eosin and haematoxylin (H&E) stain, showing the distinctive banding appreance. Scale bar set to 10 micron. n. nucleus; myo, cardiomyocyte. (own work)

Sarcomere, the fundamental contractile unit of the myocyte, is primarily made up of parallel overlapping arrangement of thick filaments, myosin, and thin actin filaments, as well as other structural protein elements (Farah and Reinach 1995). Figure 1.4 illustrates the areas and lines recognised within a sarcomere. A band (anisotropic) spans the length of the whole thick filaments. I band (isotropic) is the section which contains only thin filaments that are bound to z discs at the end of each sarcomere. An individual sarcomere, therefore, spans distance between two consecutive z discs, it varies in length depending on state of relaxion and contraction.

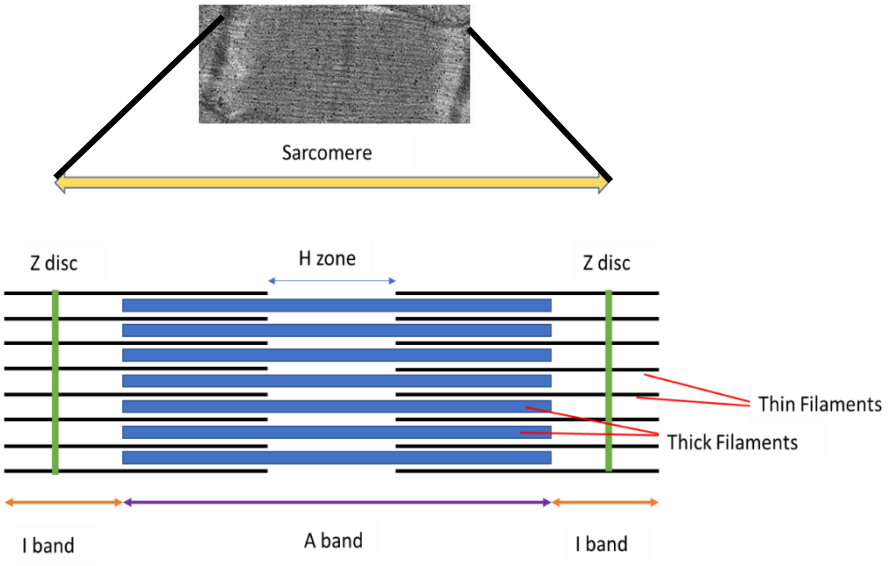

Figure 1.4 Schematic illustration and electron micrograph of sarcomere structure in cardiomyocyte. (own work)

Cardiomyocytes must contract simultaneously for effective pumping, and this requirement is mediated through intercalated discs, which are located at the end of cardiomyocytes. These highly organized structures play an important role in intercellular signalling and simultaneous electrical coupling and contraction. As a result, cardiac myocytes work together as a single functional unit, or syncytium (Manring, Dorn et al. 2018).

Intercalated discs, as illustrated in figure 1.5, are made of three components: gap junctions, desmosomes as well as adherens junctions. Adherens junction directly link the contractile proteins in one cardiomyocyte to the neighbouring cells, thus transmitting the contractile force from cardiomyocyte to the other (Tepass, Truong et al. 2000). Intermediate filaments in each myocyte are connected through desmosomes to filaments in other cells. As a result, desmosomes provide an essential robust structure to allow cardiomyocytes to withstand the force generated during cardiac cycle (Delmar 2004). The gap junctions, consisting of connexin proteins, act like tunnels allowing ions influx to be transmitted from one cardiomyocyte to another rapidly, therefore allowing simultaneous propagation of electrical stimuli to trigger cardiac contraction (Rohr 2004).

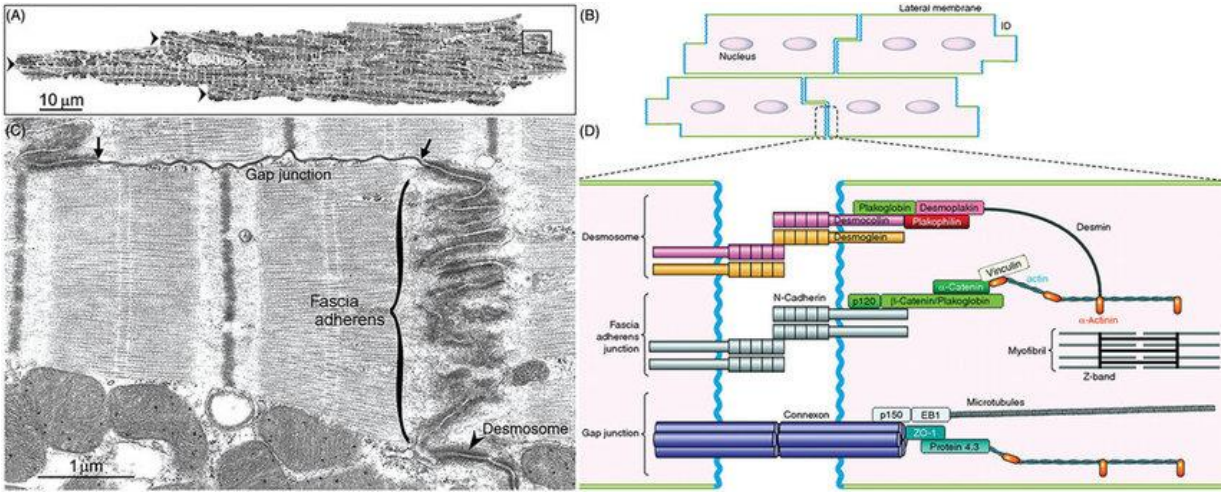

Figure 1.5 Schematic and electron micrograph of intercalated disc structure in cardiomyocyte. Gap junction consists of connexin proteins, fascia adherens junctions in cardiomyocytes are made of N-cadherin, and desmosomes of desmoglein and desmocolin. From (Henderson, Gomez et al. 2017).

1.2.2 Excitation-Contraction coupling

Excitation- Contraction (E-C) coupling is an energy dependant process linking electrical signal that results in action potential to myocyte contraction. Contractile apparatus consumes more than two thirds of hydrolysed myocardial ATP, while the remaining is used to keep ion balance, namely by sarcoplasmic reticulum Ca^{2+}-ATPase and the sarcolemmal Na^{+}/K^{+}-ATPase, in addition to various enzymatic activities (Solaini and Harris 2005, Maack and O'Rourke 2007). Calcium cycling is central in mediating the coupling between excitation and contraction.

In the mammalian hearts, E-C coupling is a calcium dependant process. Calcium influx triggers further release of SR calcium, and together result in transient rise of calcium which a central role in mediating interaction between actin and myosin necessary for contraction. Therefore, calcium transient must be tightly controlled through its release and recycling back to sarcoplasmic reticulum (Bers 2002).

Excitation

Excitation occurs by autonomous generation of action potential in specialized cells in the sinoatrial (SA) node, acting as pacemaker of the heart, which is transmitted throughout the atria until it reaches the atrioventricular (AV) node. Action potential is then transmitted through conduction system by bundle of His, then through the widely distributed Purkinji fibres to the ventricles traveling down to t-tubule to reach cardiomyocytes. Because of gap junctions, membrane depolarisation diffuses rapidly and simultaneously to all neighbouring cells. Action potential changes in different parts of the heart as seen in figure 1.6.

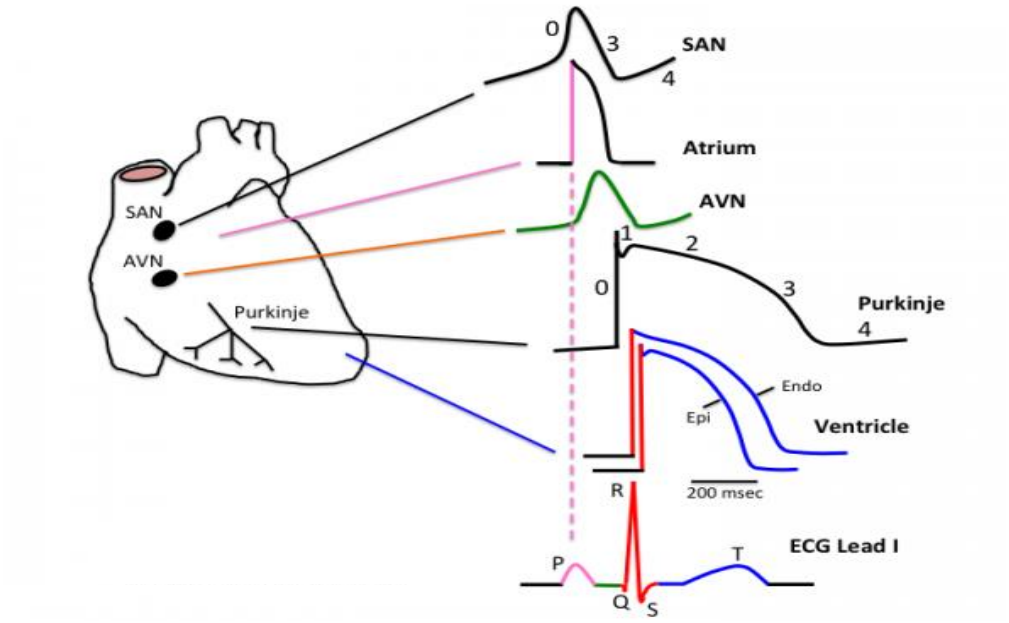

Figure 1.6 Changes in action potential (phases are indicated by numbers (0 - 4) among different areas of the heart with the corresponding ECG signal in lead I. SAN, sinoatrial node; AVN, atrioventricular node. From (Katzung and Trevor 2015)

Ventricular cardiomyocyte has a resting membrane potential nearly of -90 mV (Wright 2004), this is due to selective membrane permeability to potassium ions via inward rectifying potassium channels. At this stage, membrane potential is at phase 4.

As rapid depolarisation occurs as a result of voltage gated Na^+ channels opening, the membrane potential increases leading to an upstroke in membrane potential (phase 0) from rapid influx of sodium into cells with its electrochemical gradient (Reuter and Beeler 1969). Early repolarisation (phase 1) is mediated by inactivation of voltage gated Na^+ channels when the membrane potential reaches positive value, in addition to an outward current of K^+ and Cl^- (Luo and Rudy 1994). However, in phase 2 there is a plateau in membrane potential due to a balance between influx of calcium, through L-type Ca^{2+} channels which open when the potential is higher than -40 mV, and the slow efflux of potassium via delayed rectifier K^+ channels (Orkand and Niedergerke 1964). However, when membrane potential becomes below -40 mV, marking phase 3, delayed rectifier potassium channels remain open, driving repolarisation and a drop in membrane potential toward its resting value (-90

mV). These channels close when the resting membrane potential is achieved at phase 4, when only inward rectifier K^+ channels continue to maintain resting potential as illustrated in figure 1.7.

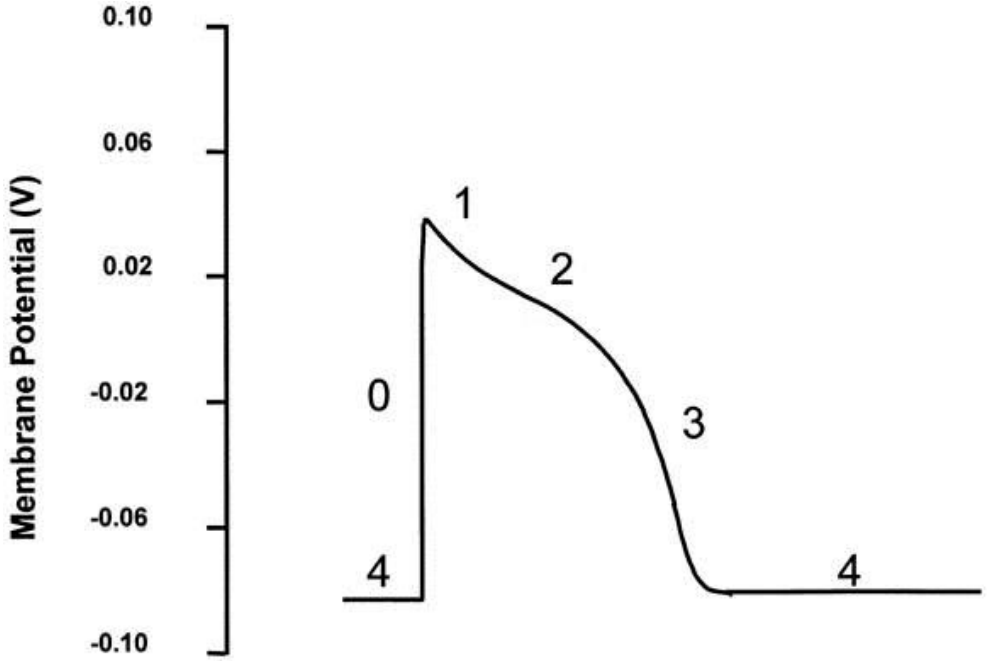

Figure 1.7 Ventricular membrane potential (in voltage). Numbers from 0 to 4 denote phases of action potential production. From (Walker and Spinale 1999)

Contraction

Depolarization-activated opening of calcium channels results in calcium influx as illustrated in figure 1.8. This slight increase in intracellular calcium ions triggers ryanodine receptors (RyR) on sarcoplasmic reticulum (SR) to release even further stored calcium (Bers, Lederer et al. 1990, Lee and Michalak 2010), the net result is a greater increase in cytosolic Ca^{2+} transient, from 0.1 µM to 1 µM (Bers 2002). This effect is known as calcium induced calcium release (CICR) which is the driving signal for cardiomyocyte contraction (Fabiato and Fabiato 1975). Calcium exerts its action through its binding to troponin C, to activate a conformation changes in troponin T and I proteins to displace tropomyosin protein from actin, facilitating myosin-actin binding (Bing, Fraser et al. 1997).

Calcium release and uptake is a highly controlled process. There are several mechanisms to regulate intracellular calcium concentration, including phosphorylation as well as inactivation of ryanodine receptors opening by calsequestrins. These proteins are detached from ryanodine receptors in a relaxed state, i.e. when intraluminal calcium concentration is high (Stevens, Terentyev et al. 2009). However, once ryanodine receptors are triggered by the influx of calcium through L-type Ca^{2+} channels, they release stored calcium. When intraluminal calcium levels are decreased, calsequestrin interacts with ryanodine receptors to block their opening, and subsequently halting release of calcium (Xu, Mann et al. 1996).

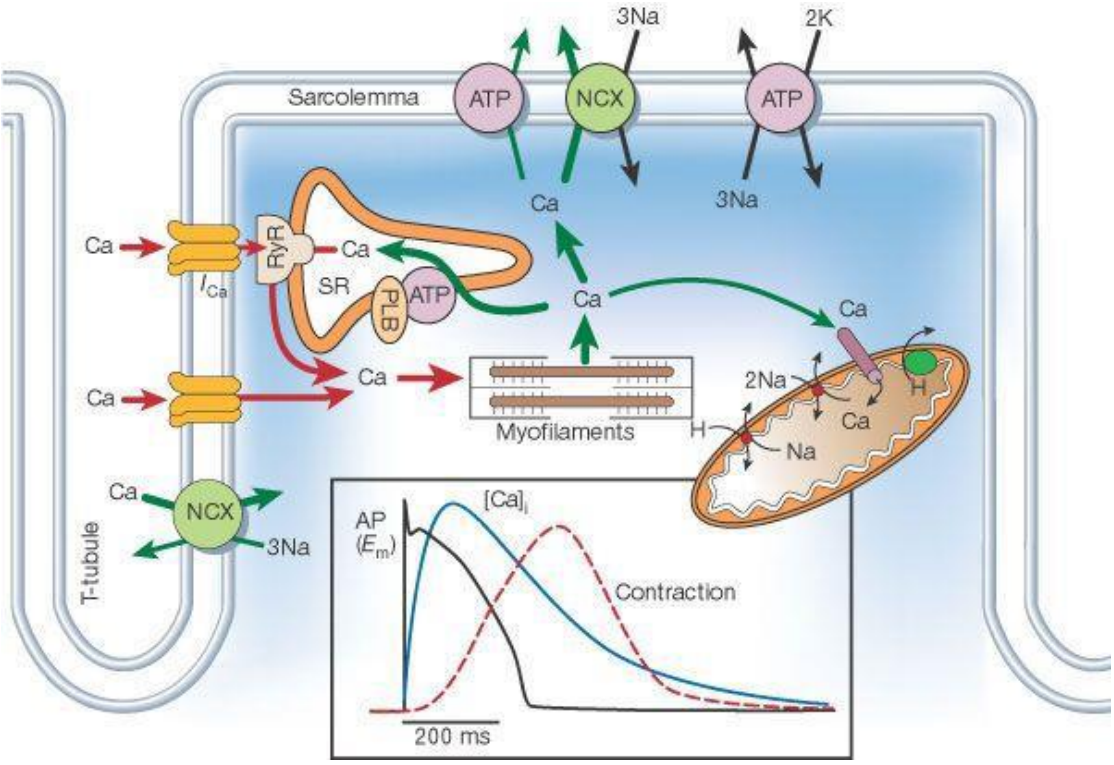

Figure 1.8 Excitation contraction coupling and CICR from sarcoplasmic reticulum (SR). AP action potential, NCX (Na^+ /Ca^{2+} exchanger), RyR (ryanodine receptors). From (Bers 2002)

Relaxation and cross bridge cycle

Myosin has 3 main parts: head to which actin binds, in addition to neck and tail, whereas actin filaments are helical structures of two interwoven globular actin subunits. In a relaxed state, myosin heads are bound to ATP and myosin binding sites on actin are covered by tropomyosin, hindering the myosin-actin interaction. Tropomyosin interacts with Troponin complex by troponin T, which binds to troponin I and C proteins (Yasui, Fuchs et al. 1968). When intracellular Ca^{2+} level increases, calcium binds to troponin C leading to conformational changes which force tropomyosin displacement by troponin I and T (Dong, Jayasundar et al. 2007). This leaves myosin heads vacant to bind with actin. ATP hydrolysis to ADP and Pi occurs on myosin head where conversion of chemical to mechanical energy occurs. When phosphate group is released from myosin head, this results in a power stroke to allow myosin to slide over actin filament, forming a cross-bridge interaction between the two

filaments (Huxley and Hanson 1954). Hydrolysis of ATP molecules therefore leads to shortening of I bands, as z discs come closer, to facilitate cardiomyocytes contraction as demonstrated in figure 1.9.

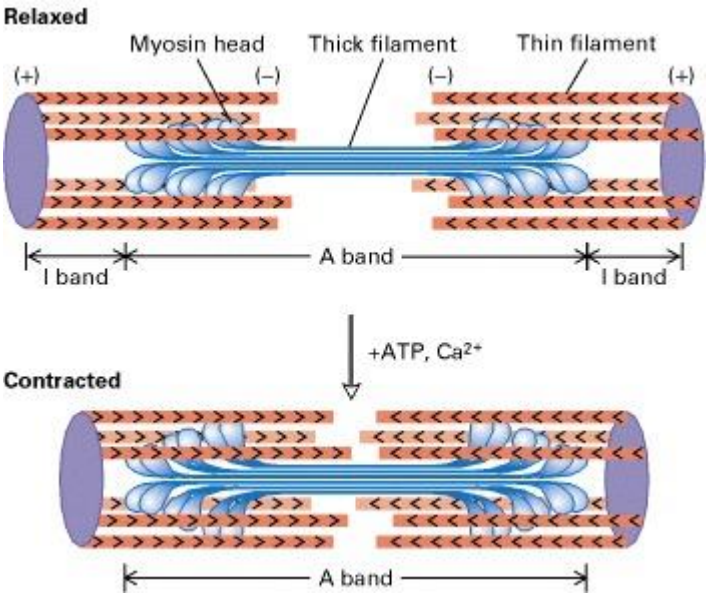

Figure 1.9 Actin and myosin filaments during cardiomyocyte contraction and relaxation. From (Lodish H 2000)

ADP is released from myosin head which, in turn, is released from actin. ATP binds to myosin head to undergo hydrolysis for the next cycle. Calcium is pumped back to SR through sarcoplasmic reticulum Ca^{2+} ATPase (SERCA), sarcolemmal Na^{+}/Ca^{2+} exchanger as well as plasmalemmal Ca^{2+}-ATPase (PMCA)(Bers, Lederer et al. 1990, Maack and O'Rourke 2007). When intracellular calcium level falls, it dissociates from troponin C, allowing tropomyosin to block actin-myosin binding sites.

1.2.3 Cardiac metabolism

1.2.3.1 Energy production

ATP, a molecule with high energy phosphate bonds is constantly demanded as a prerequisite to maintain cardiac contraction and cellular integrity. Cardiac energy pool constitutes of ATP (~ 5 µmol/g wet wt) in addition to phosphocreatine (~ 8 µmol/g wet wt) serving as a buffer system for ATP transport(Beer, Seyfarth et al. 2002). Oxidative phosphorylation produces 90% of cardiomyocytes ATP pool (Mootha, Arai et al. 1997). Other sources being GTP formation from Krebs cycle and ATP production from glycolysis. Figure 1.10 is an overview of metabolic pathways to utilise main substrates in cardiomyocytes.

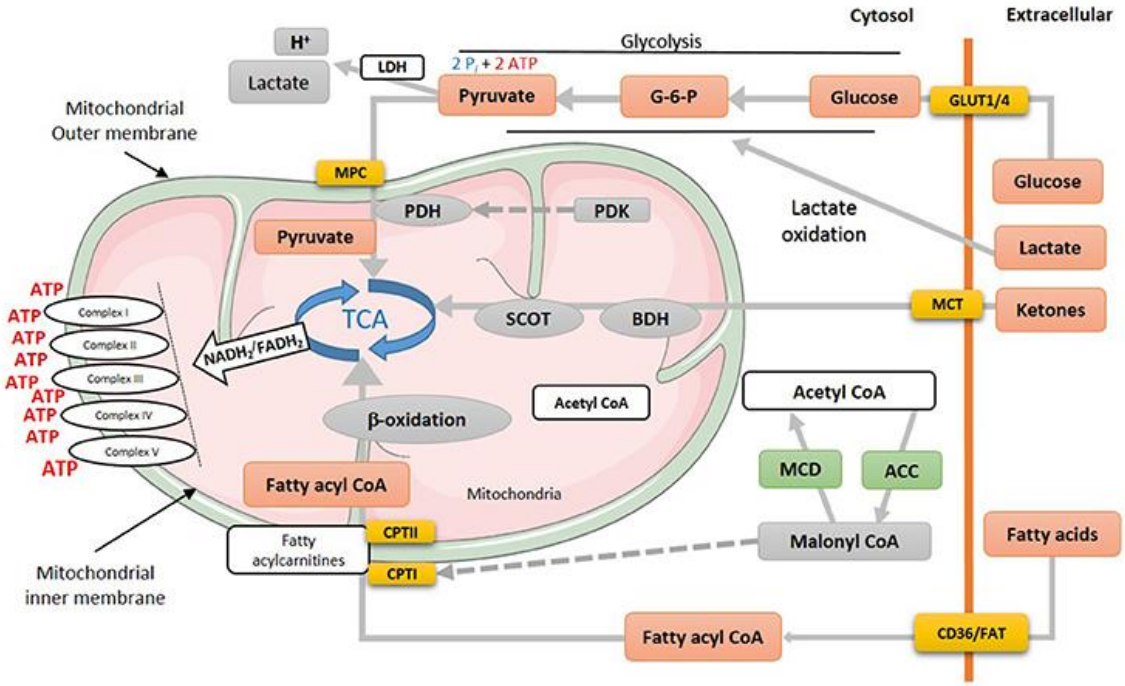

Figure 1.10 Summary of metabolic pathways to utilise various substrates in the cardiomyocyte. CPT I and II; carnitine palmitoyltransferases I and II, FAT/CD 36; fatty acid translocase Cluster of Differentiation CD 36, PDH; pyruvate dehydrogenase, PDK; pyruvate dehydrogenase kinase, GLUT; 1/4 glucose transporter type 1/4, ACC; acetyl CoA carboxylase, MCD; malonyl CoA decarboxylase, SCOT; succinyl-CoA:3-oxoacid-CoA-transferase, βOHB; β-hydroxybutyrate, BDH, βOHB dehydrogenase; MPC; (mitochondrial pyruvate carrier), MCT; monocarboxylate transporters, LDH; Lactate dehydrogenase From (Karwi, Uddin et al. 2018).

Under normoxic conditions, heart utilises fatty acids (FA) through β-oxidation as the primary source of energy, as nearly 60% of ATP production comes from FA oxidation (Doenst, Nguyen et al. 2013). Other substrates include glucose (which contributes to 30% of ATP production), amino acids (10%) and occasionally lactate and ketone bodies (Schutz 1995). Therefore, the heart can upregulate and use several pathways to meet its high energy demands in different physiological conditions, establishing a versatile cardiac metabolism or what is known as metabolic flexibility. Fatty acids, which could be found as free fatty acids that are circulating in blood or released from lipoprotein containing triglycerides, are converted by β-oxidation in the mitochondria into acetyl-CoA to enter Krebs (or TCA/Citric acid) cycle (Lopaschuk, Ussher et al. 2010), while glucose could undergo into the

anaerobic glycolysis in the cytosol, producing 2 pyruvate molecules and 2 ATP molecules. Then pyruvate enters Krebs cycle, and electron transport chain (ETC) in the mitochondria, where oxygen is used as electron acceptor and the resulting proton current is used to synthesise ATP by F0/F1 ATP synthase (Lopaschuk, Ussher et al. 2010).

1.2.3.2 Substrates used by cardiomyocytes for energy production

Glucose

Glucose availability depends on either transportation of exogenous glucose into cardiomyocytes mainly via insulin dependent glucose transporter type 4 (GLUT 4) and type 1 (GLUT 1) or through breakdown of stored cardiac glycogen (Fischer, Thomas et al. 1997, Abel 2004). Once in the cytosol, glucose is phosphorylated to by hexokinase to glucose-6-phosphate (G-6-P). Phosphorylated glucose can be used in glycogen synthesis or enter several metabolic pathways including glycolysis, and Pentose Phosphate Pathway (PPP), for pyrimidine and purine synthesis, as well as Hexosamine Biosynthetic Pathway (HBP) for synthesis of proteoglycans and other glycation end products (Tran and Wang 2019). Initial utilisation of one molecule of glucose by a series of enzymes through glycolytic pathway generates 2 pyruvate molecules, 2 Nicotinamide Adenine Dinucleotide Hydrogen NADH and 2 ATP as illustrated in figure 1.11.

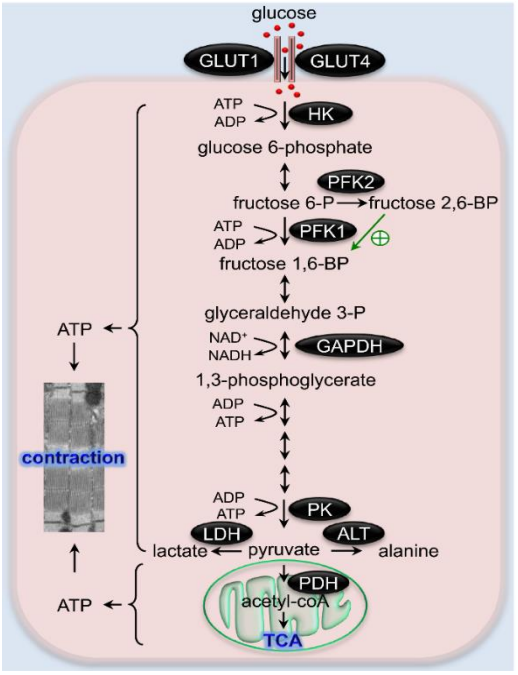

Figure 1.11 Glycolytic pathway for glucose metabolism. PDH; pyruvate dehydrogenase, GLUT 1/4; glucose transporter type 1/4, PK; pyruvate Kinase, HK; Hexokinase, GAPDH; glyceraldehyde-3- phosphate dehydrogenase; PFK 1 and 2; ATP-dependent phosphofructokinase 1 and 2, PK; pyruvate kinase, LDH; lactate dehydrogenase, ALT; alanine aminotransferase. From (Tran and Wang 2019)

This process occurs regardless of oxygen availability in the cytosol (anaerobic glycolysis); however, its ATP yield is not sufficient to maintain the contractile machinery. Therefore, pyruvate can be further utilised by aerobic respiration once it has been transported into mitochondrial matrix, where it is converted by pyruvate

dehydrogenase into acetyl-CoA to feed Krebs cycle (Patel and Korotchkina 2006). Regulation of PDH activity depends on availability of acetyl-CoA and NADH as they exert product inhibition effect. In addition, pyruvate dehydrogenase is regulated by PDH kinase (inhibits PDH through phosphorylation) and PDH phosphatase (activation through dephosphorylation)(Holness and Sugden 2003). Glucose has phosphate to oxygen (P/O) ratio of 2.58, which makes it the most energy efficient substrate; as 6 oxygen molecules are needed to oxidise one molecule of glucose, producing in total 31 ATP (Karwi, Uddin et al. 2018).

Fatty acids

Heart utilises free fatty acids (FFA) that are bound to albumin or released from triglycerides (TAG), which are found in chylomicron or Very Low Density Lipoproteins (VLDL) (Hauton, Bennett et al. 2001). Fatty acids could be either diffused into the cytosol or transported by fatty acid translocase (Cluster of Differentiation CD 36)(van der Vusse, van Bilsen et al. 2000). Esterification of fatty acid to long chain fatty acyl Coenzyme A by fatty acyl CoA synthase takes place in cytosol. This step is necessary to facilitate triglyceride synthesis (cardiac TAG reserve) or, alternatively, direct shuttle of the vast majority of fatty acyl CoA into mitochondria. The later occurs through carnitine shuttle system by carnitine palmitoyltransferases (CPT I and II). CPT I enzyme converts long chain fatty acyl CoA into long chain acylcarnitine to be transported through outer mitochondrial membrane (OMM). Carnitine acylcarnitine translocase on the inner mitochondrial membrane (IMM) transfers acylcarnitine into mitochondrial matrix, where CPT II converts them back into long chain fatty acyl CoA to be utilised via β-oxidation pathway (Murthy and Pande 1984). Figure 1.12 summarises carnitine shuttle system.

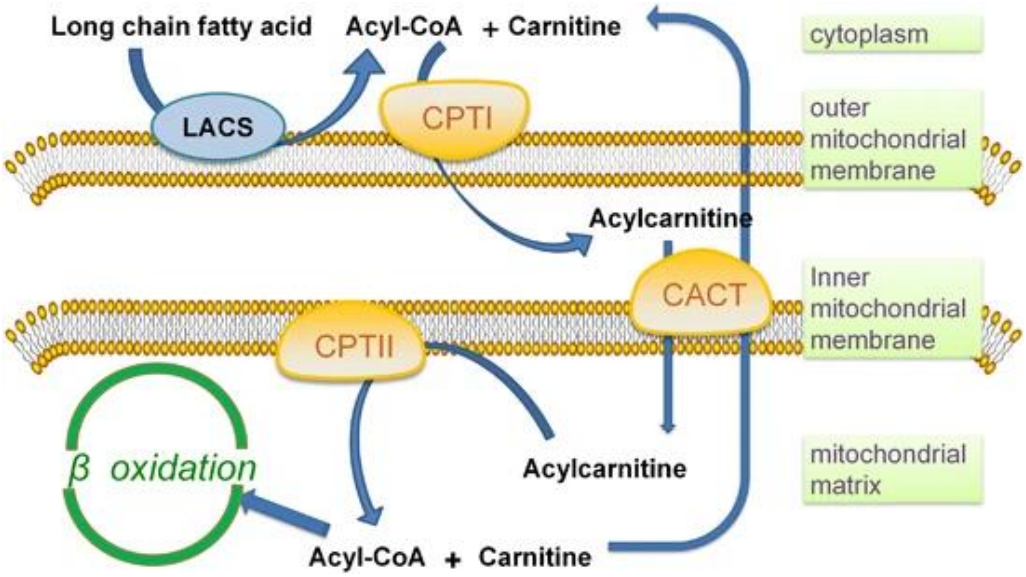

Figure 1.12 Carnitine shuttle pathway. CPT I and II; carnitine palmitoyltransferases I and II, LACS; Long fatty acyl CoA synthase. From (Qu, Zeng et al. 2016)

Regulation of this shuttle system, and β-oxidation, depends on malonyl CoA, made from acetyl-CoA carboxylation by acetyl-CoA carboxylase. Whenever there is excess acetyl-CoA, it is converted into malonyl CoA (which indicates an increased rate of β-oxidation). Malonyl CoA consequently inhibits CPT I, decreasing long chain fatty acyl CoA transport across mitochondrial membranes (McGarry, Mannaerts et al. 1977).

β-oxidation is the sequential derivation of acetyl-CoA (two carbon units) from fatty acyl CoA. Acetyl-CoA then enters TCA cycle, which yields NADH, reduced flavin adenine dinucleotide ($FADH_2$), which are used to generate ATP during mitochondrial oxidative phosphorylation (Cotter, Schugar et al. 2013). In terms of energy efficiency, β-oxidation of a typical FA molecule such as palmitate produces 105 ATPs per 23 oxygen molecules, with P/O ratio of 2.33, making it less energy efficient that glucose. Nonetheless, in terms of the theoretical amount of ATP molecules produced by two carbons unit utilisation, fatty acids supersede any other myocardial substrates (Karwi, Uddin et al. 2018).

Ketone bodies

Ketone bodies are synthesised by liver during prolonged fasting or starvation, and can be oxidised to enter TCA cycle. Acetoacetate, β-hydroxybutyrate (βOHB) are predominant the ketone bodies circulating in blood, while acetone which is easily eliminated by breath(Cotter, Schugar et al. 2013). Cardiomyocytes utilise only ketone bodies in a proportional manner to their delivery since heart lacks the ability to produce ketones, however, it is considered the highest ketones consumer per unit of mass (Young, McNulty et al. 2002). Oxidation of βOHB takes place in the mitochondria by phosphatidylcholine-dependent βOHB dehydrogenase into acetoacetate, thensuccinyl-CoA:3-oxoacid-CoA-transferase (SCOT) converts acetoacetate into acetoacetyl-CoA. Finally, acetoacetyl-CoA is converted by acetyl-CoA acetyltransferase into acetyl-CoA, as shown in figure 1.13, which can subsequently enter TCA cycle and electron transport chain for ATP production (Puchalska and Crawford 2017).

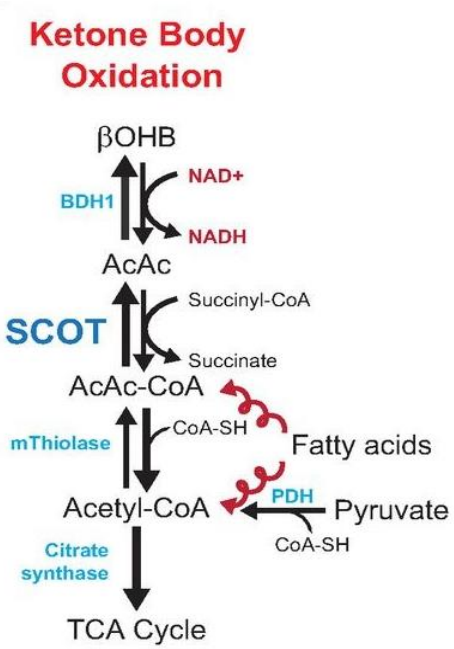

Figure 1.13 Ketone Body oxidation pathway. SCOT; succinyl-CoA:3-oxoacid-CoA-transferase, βOHB; β-hydroxybutyrate, BDH1; βOHB dehydrogenase, AcAc,; Acetoacetate, AcAc-CoA; Acetoacetate-CoA, PDH; Pyruvate dehydrogenase. From (Cotter, Schugar et al. 2013)

Lactate and amino acids

Amino acids have minor contribution to ATP production under normal condition, but this could be greatly challenged during cardiac ischaemia. Unlike lactate, amino acids can be involved in energy production under hypoxic or anoxic conditions, without vastly decreasing cellular pH levels, through conversion into TCA intermediates and participation in substrate-level phosphorylation. Aspartate, asparagine, and the branched chain amino acids (BCAAs) in addition to glutamate and glutamine can be all converted TCA cycle intermediates. As shown in figure 1.14, glutamate (from glutamine conversion) can be transaminated into α-ketoglutarate, a Krebs cycle intermediate, by glutamate-dehydrogenase, leading to production of a single molecule of GTP and one NADH, through conversion of α-ketoglutarate to succinate (Mudge, Mills et al. 1976). Asparagine and aspartate can be converted to oxaloacetate, wheras alanine, on the other hand, is interconvertible with pyruvate (Drake, Sidorov et al. 2012). Pyruvate oxidation results in three NADH and one GTP.

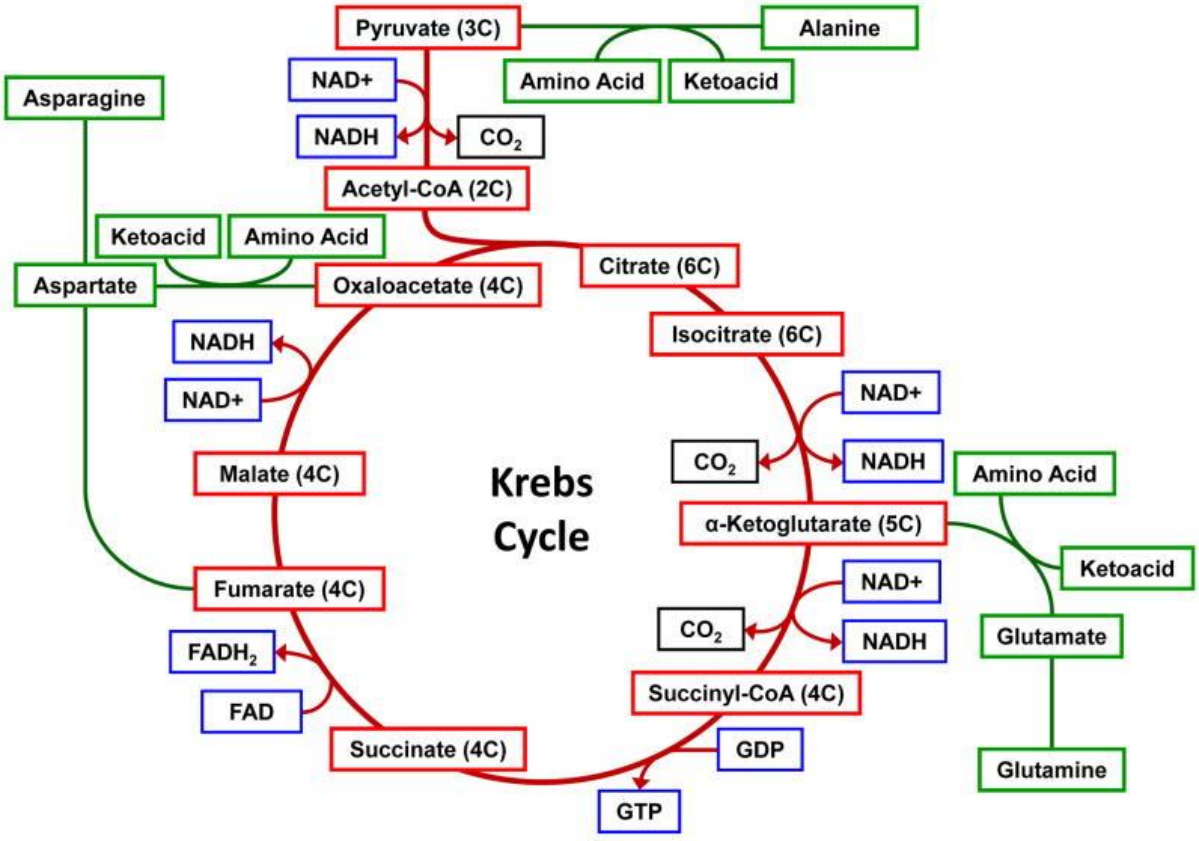

Figure 1.14 Metabolic pathways to replenish cardiac TCA cycle intermediates from amino acids. From (Drake, Sidorov et al. 2012)

Lactate, a by-product of glucose metabolism, is produced in the heart when it is lacking adequate oxygenation to carry on aerobic glycolysis. Lactate dehydrogenase converts pyruvate to lactate, oxidising NADH to NAD+, which will be recycled in anaerobic glycolysis reaction to produce 2 ATP molecules(Berg, Tymoczko et al. 2010).

$$\text{Pyruvate} + \text{NADH} + H^+ \rightarrow \text{lactate} + NAD^+$$

1.2.3.3 TCA cycle and oxidative phosphorylation

As illustrated previously in figure 1.14, acetyl-CoA is combined with oxaloacetate, forming citrate by citrate synthase. Citrate undergoes several consecutive reactions that end up in oxaloacetate formation, to start another cycle. Therefore, one TCA cycle decarboxylates acetyl-CoA into CO_2 and results in 3 NADH, 1 $FADH_2$ and 1 ATP molecule. Since this cycle is fundamental in energy production, its pool of intermediates can be replenished from other metabolites through different collateral metabolic pathways, what is known as anaplerosis (Des Rosiers, Labarthe et al. 2011). An example of anapleric reaction is the conversion of glutamate to α-ketoglutarate as described earlier in the previous section. Electron donors NADH and $FADH_2$ subsequently undergo oxidative phosphorylation in the electron transport chain to contribute for ATP production through ATP synthase.

There are four complexes in the Electron Transport Chain (ETC) located on the inner mitochondrial membrane as seen in figure 1.15, which work together to shuffle electrons from one to another, facilitating coupling of energy to create a proton gradient. Complex I (NADH-quinone oxidoreductase), which accepts NADH as electron donor, pumps protons from the matrix into inter membrane space to initiate proton gradient. However, complex II (succinate dehydrogenase) only accepts electron from $FADH_2$. Both complex I and II transfer their electrons to Coenzyme Q (CoQ), which moves electrons to complex III (ubiquinol-cytochrome c oxidoreductase) to pump further protons. Complex III then passes its electrons to Cytochrome C, which mediates electrons transfer to complex IV (cytochrome c oxidase). In addition to pumping protons, the later uses oxygen as final electron acceptor. The proton gradient created throughout the chain is used by F0/F1 ATP synthase to phosphorylate ADP to ATP (chemiosmosis) as protons flow back to the matrix. In general, four protons are required to produce a single ATP molecule (Saraste 1999). The ATP produced is then exported from mitochondria in exchange for ADP by adenine nucleotide translocase (ANT) found in the mitochondrial inner membrane (Wheaton and Chandel 2011).

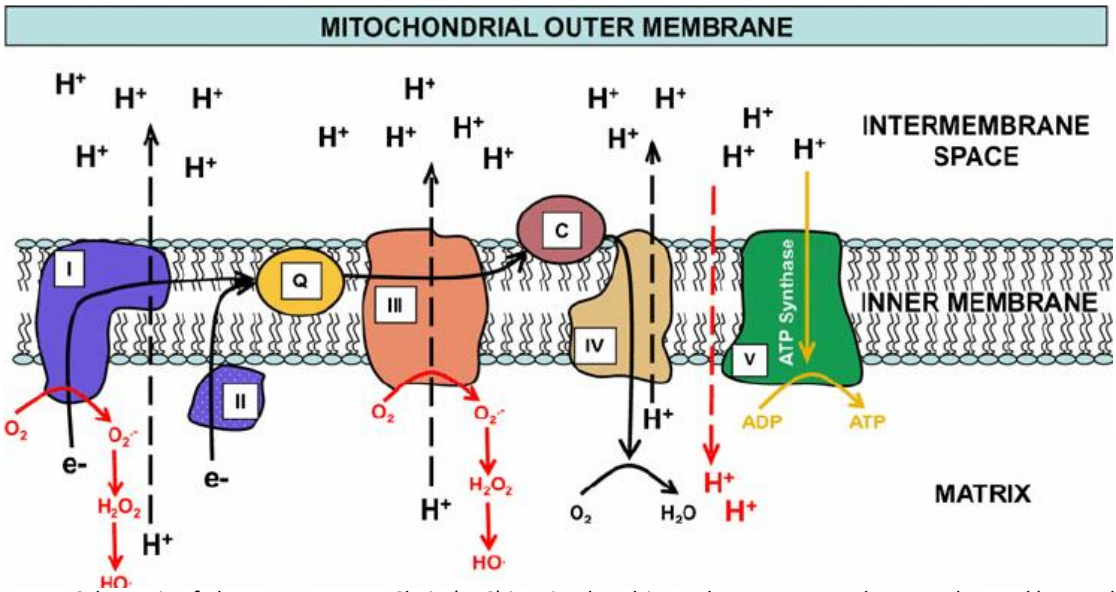

Figure 1.15 Schematic of Electron Transport Chain (ETC) in mitochondria. Redox centres numbers are denoted by numbers I to VI. ATP synthase is essential for ATP synthesis, also known as complex V, although it is not part of ETC. Q, Coenzyme Q (CoQ), C Cytochrome C. From (McEwen, Sullivan et al. 2011)

1.3 Cardiac ischaemia reperfusion injury (IRI)

1.3.1 Overview

Both sustained ischaemia and ischaemia followed by reperfusion trigger series of cellular changes including Ca^{2+} loading and oxidative stress, which lead to mitochondrial permeability transition pore (mPTP) opening and death by necrosis or/and apoptosis (Hausenloy and Yellon 2013). Figure 1.16 is a summary of key changes associated with IRI. Ischaeamia reperfusion injury not only results in infarct size expansion, but also cardiac arrhythmia, myocardial stunning (post ischaemic contractile dysfunction), microvascular obstruction or lethal injury (Krug, De Rochemont et al. 1966, Hearse and Tosaki 1987, Kloner, Bolli et al. 1998).

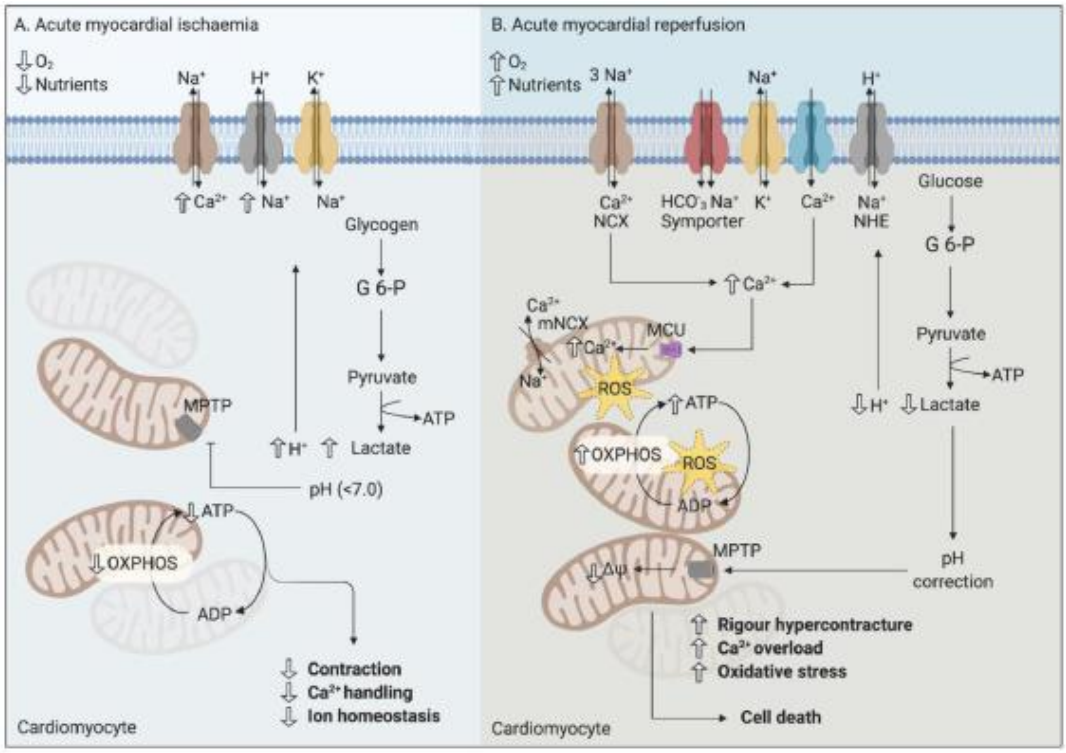

Figure 1.16 Illustration of molecular and metabolic changes following acute myocardial ischaemia (A) and reperfusion (B) injury. G 6-P; Glucose 6-phosphate, OXPHOS; oxidative phosphorylation, NCX; the sodium-calcium exchanger, mNCX; mitochondrial sodium-calcium exchanger, NHE; Na^+/H^+ exchanger, MPTP; mitochondrial permeability transition pore, ROS; reactive oxygen species. From (Ramachandra, Hernandez-Resendiz et al. 2020).

1.3.2 Ischaemia

Cessation or reduction of blood flow in a coronary artery by a thrombus or embolus will deprive cardiomyocytes from blood oxygen and nutrients, i.e., ischaemia. However, in most clinical settings, attempts to restore blood flow and achieve tissue reperfusion with coronary catheterisation, for example, will eventually exacerbate the ischaemic injury. During ischaemia, the oxygen-deprived myocytes switch from oxidative phosphorylation, the primary source to generate ATP for contraction, to anaerobic glycolysis due to decreased ETC complexes and

ATP synthase activity (Rouslin 1983). In these circumstances, cardiomyocytes will rely heavily on glucose to produce energy. However, NAD^+ must be abundant to keep anaerobic glycolysis going. Consequently, pyruvate is converted to either alanine or, most likely, lactate by lactate dehydrogenase (Taegtmeyer 1994).

1.3.2.1 Metabolic and ionic disturbances

Since anaerobic glycolysis is extremely inefficient to provide adequate levels of ATP (2 ATP molecules per one glucose, versus 31 in aerobic respiration), it results in dysfunctional ATP-dependant ion transporters activity and consequently intracellular electrolytes imbalance, which halts myocytes contractility and cellular integrity. Lactic acid concentration increases hence, accumulation of protons in the cytoplasm, i.e. decrease in intracellular pH. The increase in intracellular H^+ will lead to Na^+ accumulation by the action of sarcolemmal Na^+/H^+ exchanger, which is activated to eliminate the excess protons in the cytoplasm. This step, however, leads to Ca^{2+} accumulation by the activated Na^+/Ca^{2+} exchanger (NCX), as the excess sodium cannot be removed by ATP-dependant Na^+/K^+ ATPase (due to ATP deprivation) (Avkiran and Marber 2002). Eventually, elevated intracellular Ca^{2+}, along with ATP depletion causes impaired cardiac contractility (rigor hypercontacture), alterations in membrane potentials, all of which are implicated in cardiomyocytes death.

1.3.2.2 Cardiomyocytes and Mitochondrial swelling

With prolonged ischaemia and ATP depletion, there is a disruption in ion balance, as the increase in intracellular sodium results in osmotic discrepancies in cardiomyocytes, leading to cellular swelling and reduced contractile responsiveness, and no reflow phenomenon if reperfusion occurs (Garcia-Dorado, Andres-Villarreal et al. 2012). Although acidic environment maintains mPTP stability initially, with extended duration of ischaemia the influx of calcium through calcium uniporters into mitochondria triggers mPTP to open, and this provokes mitochondrial swelling, releasing pro-apoptotic enzymes to drive cardiomyocytes to apoptosis (Parlakpınar, Örüm et al. 2013).

1.3.3 Reperfusion

Although it is an apparent necessity needed to limit further injury, blood flow restoration after prolonged ischaemia can lead to precipitation of initial damage caused by ischaemia itself. Reperfusion reintroduces oxygen to the ischaemic tissues, however, this paradoxically provokes excessive reactive oxygen species (ROS) formation by the defective ETC complexes (complex I and complex III), also known as 'Oxygen Paradox'. ROS results in disruption of sarcolemma, lipid peroxidation, proteins, and nucleic acids damage. Calcium ions accumulate due to NCX activity, low activity of Ca^{2+}-ATPases (SERCA & sarcolemma), disruption in plasma membranes, sarcoplasmic reticulum and mitochondria pores from oxidative stress (Hausenloy and Yellon 2013).

1.3.3.1 Ca^{2+} loading

Another element involved in reperfusion injury is the rapid washout of protons via Na^+/H^+ exchanger to restore pH values. Sarcolemmal Na^+/H^+ exchanger retains its activity contributing to increased Na^+ levels, which consequently stimulates an increase in calcium influx through NCX. The inhibitory effect of cellular acidity on mPTP is reduced, which potentiates their susceptibility for opening as they become more permeable to ROS with increased calcium loading (Thind, Agrawal et al. 2015).

1.3.3.2 Reactive Oxygen Species (ROS)

Reactive oxygen species are chemicals derived from oxygen molecules (Taverne, Bogers et al. 2013) that are synthesised naturally as by-products during oxidative phosphorylation, or through enzymatic reactions carried out by certain enzymes such as xanthine oxidase (endothelial cells) and NAD(P)H oxidase (neutrophils)(Droge 2002). ROS include free radicals, e.g., superoxide ($O_2^{\bullet-}$), and hydroxyl radicals ($OH^{\bullet}$), which are characterised by their unpaired free electrons, that is responsible for high chemical reactivity. In addition, there are hydrogen peroxide (H_2O_2)and peroxynitrite ($ONOO^-$), however these chemicals lack the unpaired electron, consequently they only exert oxidising effects (Droge 2002). Imbalance between ROS synthesis and removal creates a state of oxidative stress (Dhalla, Temsah et al. 2000), which leads deleterious effects on cellular membrane through lipids peroxidation, in addition to proteins oxidation and DNA damage (Moris, Spartalis et al. 2017).

The main source of $O_2^{\bullet-}$ in most tissues is derived nonenzymatically from mitochondrial ETC. It is estimated that 1-2% of electrons could be leaked to oxygen during electron shuffle from redox centres(Turrens 2003). Enzymatic ROS production comes from NAD(P)H oxidases in macrophages and neutrophils (to aid in phagocytic activities), xanthine oxidases, and endothelial nitric oxide synthase (eNOS).

Superoxide can undergo several reactions resulting in H_2O_2, $OH^{\bullet}$ and peroxynitrite production. Superoxide Dismutase converts superoxide to hydrogen peroxide, which also could be produced from several oxidases. Although H_2O_2 is not a radical, it has high reactivity as it is a precursor for hypochlorous acid ($HOCl^-$), as well as hydroxyl radical. When H_2O_2 interacts with reduced metal ion, it decomposes leading to OH^- formation through Fenton reaction. Alternatively, H_2O_2 interaction with $O_2^{\bullet-}$ through Harbar-Weiss reaction also produces hydroxyl radial (Koppenol 2001). Figure 1.17 illustrates reactions of ROS production and removal.

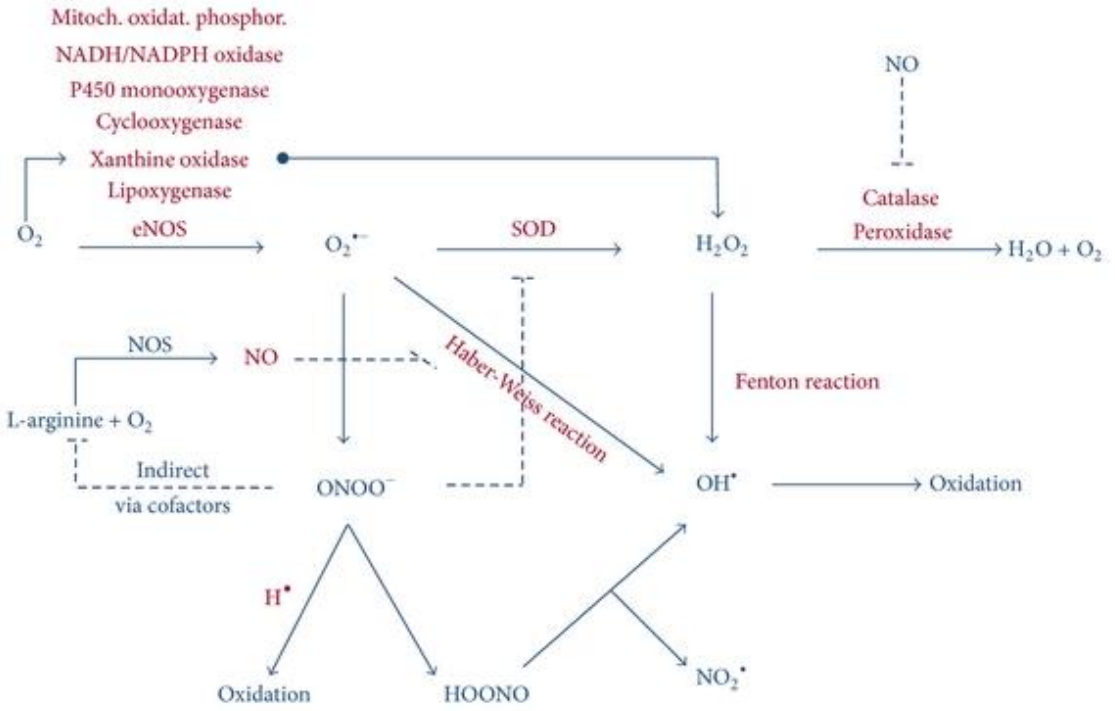

Figure 1.17 Reactions of reactive oxygen species production and removal. NO, nitric oxide, NOS, NO synthase, SOD, superoxide dismutase. From (Taverne, Bogers et al. 2013)

Hydroxyl radical along with peroxynitrite, which is formed from superoxide reaction with nitric oxide, are considered the most reactive species. They induce cellular damage through free chain radial protein oxidation and lipid peroxidation, which consequently alters membrane permeability and stability through disruption of phospholipid bilayer integrity (Turrens 2003) as demonstrated in figure 1.18.

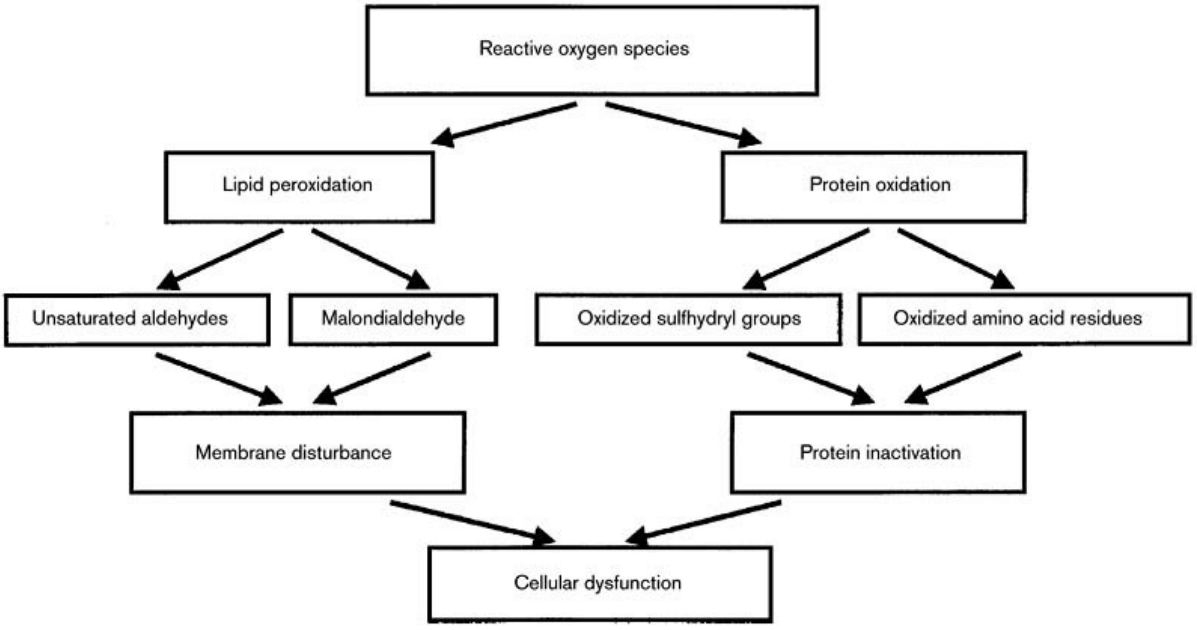

Figure 1.18 Deleterious effect of reactive oxygen species on various cellular targets.From (Dhalla, Temsah et al. 2000)

1.3.3.3 Antioxidant defence mechanisms

Both enzymatic and nonenzymatic defence mechanisms exist intra- and extracellularly to neutralise ROS immediately. Superoxide is converted into H_2O_2 and $O_2^{\bullet-}$ by SOD, which is found in the heart in two isofroms, mitochondrial Mn-SOD and cytoplasmic Cu/Zn- SOD (Freeman and Crapo 1982). Catalase (in peroxisomes) and glutathione peroxidase hydrolyse H_2O_2 into water and oxygen. Glutathione peroxidase (GPx) is particularly important in the heart as it uses abundantly available reduced glutathione (2GSH) in the cytoplasm as a redox buffer to catalyse the reaction:

$$H_2O_2 + 2\ GSH \rightarrow 2\ H_2O + GSSG$$

Reduced glutathione provides protons to cell membrane lipids to maintain them reduced, which helps in cardiac protection specifically during IRI(Curello, Ceconi et al. 1985, Cheung, Wang et al. 2000). Glutathione reductase uses NADPH to covert GSSG to 2GSH, which maintains antioxidant activity of GPx. Therefore, an imbalance between the oxidised and reduced glutathione (GSH : GSSG ratio) is considered as indicator of the oxidative state in the cells(Curello, Ceconi et al. 1987). Other antioxidant proteins include thioredoxin, peroxiredoxin and glutaredoxins. They function as electron donors and maintain redox state through H_2O_2 mediated signal transduction (Hanschmann, Godoy et al. 2013, Netto and Antunes 2016)

Nonenzymatic scavenging mechanisms also exist to reduce the effect of ROS and limit lipid peroxidation, these are present intracellularly such as ubiquinone (Coenzyme Q) and vitamin E (α-tocopherol), and extracellularly such as vitamin C (Dhalla, Temsah et al. 2000).

1.3.3.4 Mitochondria permeability transition pores (mPTP)

Ions and solutes movements across mitochondria, the cellular powerhouses, must be tightly regulated. Outer mitochondria membrane is permeable to solutes up to 5kDa, whereas inner mitochondrial membrane has relative impermeability under normal physiological conditions. Although the exact molecular nature is not fully elaborated, the mitochondrial permeability transition pores are to thought be complex proteinaceous entities consisting of the voltage dependent anion channel (VDAC), adenine nucleotide translocase (ANT), phosphate carrier (PiC), spastic paraplegia 7 (SPG7), and components of the ATP, i.e. synthase oligomycin sensitivity conferring protein (OSCP) (Briston, Roberts et al. 2017). Cyclophilin D (Cyp-D), matrix protein that meditates increased pores sensitivity to Ca^{2+} through binding with PiC and ANT, triggering pores formation (Halestrap 2009).

Dysregulation of cytoplasmic Ca^{2+} levels, and mitochondrial calcium overload in addition to oxidative stress during IRI induce pores opening (Haworth and Hunter 1979), which occurs more prominently during early minutes of reperfusion (Griffiths and Halestrap 1995). Pores formation and opening results in osmotic-induced mitochondrial swelling, oxidative phosphorylation uncoupling, rupture and eventually release of apoptotic enzymes (Crompton 1999). The cardioprotective effects of mPTP inhibition by cyclosporin A, which inhibits CyP-D binding to PiC and ANT complex, were shown to decrease pores sensitivity to increased Ca, and consequently

lead to reduction in infarct size after IRI (Hausenloy, Duchen et al. 2003). Figure 1.19 is an illustration of proposed pores formation during ischaemia reperfusion injury.

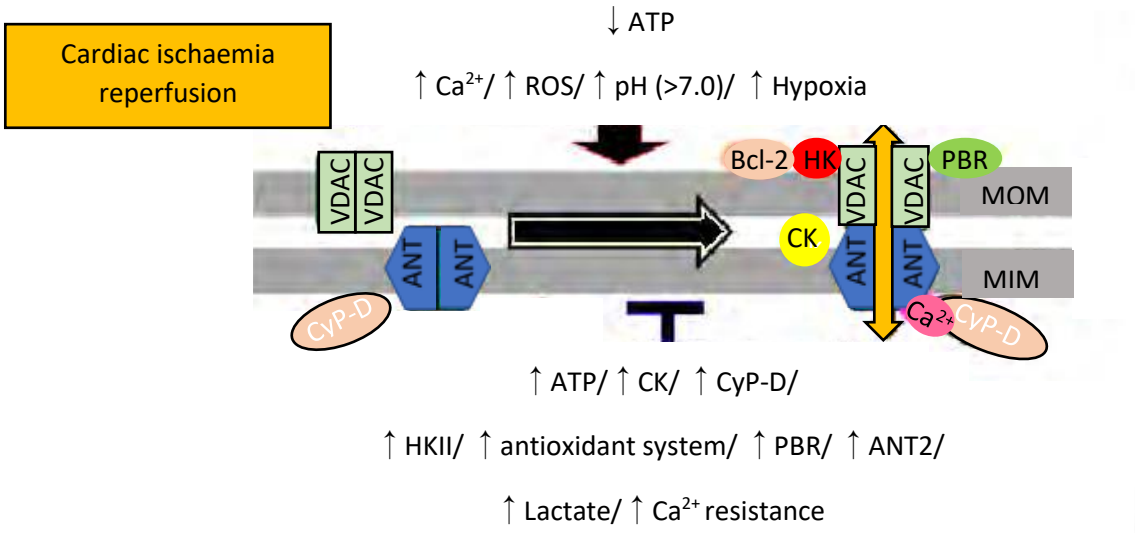

Figure 1.19 Schematic of mPTP opening during ischaemia reperfusion injury. ANT, adenine nucleotide translocase; HK, hexokinase; CK, creatine kinase; MIM, mitochondrial inner membrane; CyP-D, cyclophilin D; MOM, mitochondrial outer membrane; Pi, inorganic phosphate; PBR, peripheral benzodiazepine receptor; SOD, superoxide dismutase; VDAC, voltage-dependent anion channel. Adapted from (Hernandez-Resendiz, Buelna et al. 2012)

1.3.3.5 mPTP as a target for protection against IRI

Since there are several key players involved in mediating ischaemia reperfusion injury to the heart, there were also different approaches to protect the heart, especially during cardiac surgeries when aortic cross clamping and declamping are needed, which result in global cardiac ischaemia reperfusion injury (Beyersdorf 2009), or in the events of myocardial infarction, in which minimising damage that occurs during reperfusion remains the top priority. Cardioprotective interventions and drugs work on specific cellular and molecular targets. Cyclosporin A (as discussed earlier in section 1.3.3.4) and Sanglifehrin A inhibit CyP- D peptidyl-prolyl cis-trans isomerase (PPIase) activity, which is shown to decrease cardiac injury through a decrease in mPTP opening, particularly during early reperfusion (up to 15 min after ischaemia)(Hausenloy, Duchen et al. 2003), as used in reperfused isolated rat heart after induced ischaemia (Clarke, McStay et al. 2002, Xie and Yu 2007). While other drugs such as propofol, $GABA_A$ agonist and a scavenger of free radicals, have shown cardioprotective effects when infused with cardioplegic solution in in porcine model undergoing cardiopulmonary bypass (CPB)(Lim, Halestrap et al. 2005), and decreased calcium-induced mPTP opening in isolated Langendorff perfused rat hearts during reperfusion (Javadov, Lim et al. 2000).

Additionally, there are interventions aiming to decrease impact of ischaemic insult while conferring a varying degree of cardioprotection. Ischaemic preconditioning (IPC), which involves consecutive cycles of ischaemia

prior an extended ischaemic period, halts mPTP opening through decreasing oxidative stress or Ca^{2+} overload, or both, in different experimental models (Murry, Jennings et al. 1986, Javadov, Clarke et al. 2003). Observed changes in signalling pathways, as a result of ischaemic preconditioning, involved pro-survival kinases activation, such as PKB (Akt), ERK1/2) and PKC through phosphorylation (Armstrong, Downey et al. 1994, Hausenloy, Tsang et al. 2005). Similarly, these cycles of brief ischaemic periods could be applied in a remote region away from the heart, for example a peripheral limb, prior to a prolonged cardiac ischaemic insult, as these cycles would still trigger cardioprotective effects. This is known as Remote ischaemic preconditioning (RIPC) and it possibly involves a systemic interplay of neural and humoral mediators that convey stress signals to the myocardium during ischaemic periods (Gho, Schoemaker et al. 1996). Other modalities include ischaemic postconditioning, in which cycles of ischaemia are introduced after a major ischaemic insult, such as myocardial infarction, which result in decrease in infarct size and preservation of endothelial function in a dog model (Zhao, Corvera et al. 2003). Finally, there is temperature preconditioning, in which cycles of hypothermia (optimally at 26 °C) are induced, instead of brief ischaemia, before a lethal ischaemic insult. Effects of temperature preconditioning are linked to reduction in oxidative stress and mPTP inhibition (Khaliulin, Clarke et al. 2007, Khaliulin, Halestrap et al. 2011).

1.4 Cardiac remodelling following acute myocardial infarction

The concept of post infarction ventricular remodelling was first emphasised in 1985 by Pfeffer et. al who examined the causes of left ventricular dilation, and disrupted myocardial function following coronary artery ligation in rodent models (Pfeffer, Pfeffer et al. 1985). Consequently, remodelling was described as a complex alteration in the topography and architecture occurring acutely or chronically and involves infracted and non-infarcted zones of the ventricle (Pfeffer and Braunwald 1990). However, the established evidence a decade later demonstrated that remodelling is not only confined to the structural aspects, but the term also expands to include the molecular, cellular and extracellular alterations, that will clinically manifest as changes in size, shape and function of the heart (Cohn, Ferrari et al. 2000). Indeed, it is a culmination of physical configuration that is driven by a combination of myocytes apoptosis, hypertrophy, fibrosis and myofibroblasts proliferation (Konstam, Kramer et al. 2011). That is why the current emphasis on the inseparable bio-mechanical nature of cardiac remodelling remains the guide to comprehend and address this intricate and ongoing process. Patients suffering from acute myocardial infarction undergo percutaneous coronary intervention (PCI) or coronary artery bypass graft (CABG) surgery to restore coronary flow, however, that will inevitably subject them to ischaemia reperfusion injury, which deleteriously increase the infarct size, and potentially worsen, remodelling. In conclusive prospect, cardiac remodelling could be thought as defined as the molecular, cellular and extracellular alterations that manifests clinically as changes in cardiac shape, size, and function a result of certain pathological or physiological condition(s) (Cohn, Ferrari et al. 2000). Figure 1.20 is a summary of main phases of post ischaemic remodelling.

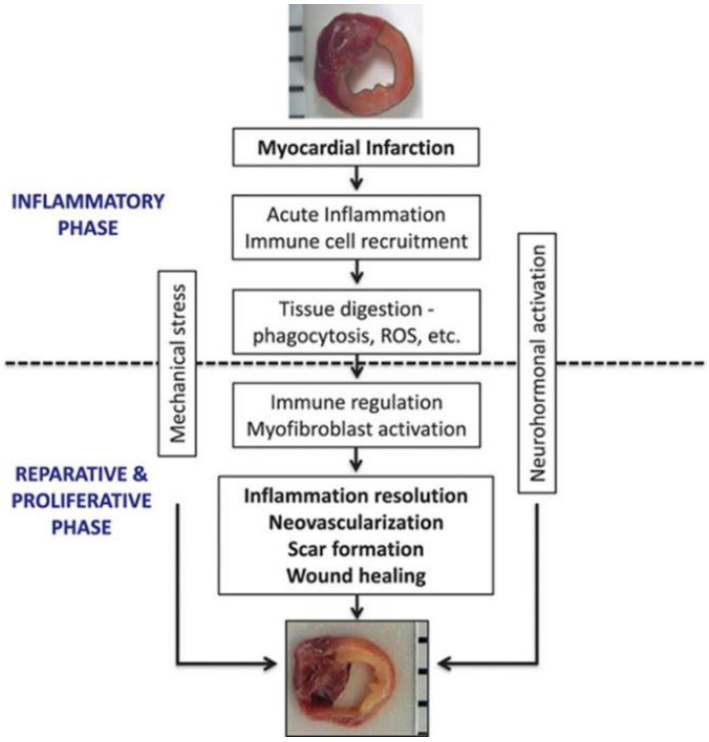

Figure 1.20 Phases of post ischaemic remodelling. From (Prabhu and Frangogiannis 2016)

1.4.1 The role of inflammation in post infarct remodelling

The necrotic myocytes during ischaemia and reperfusion release damage-associated molecular patterns (DAMP) such as ATP, mitochondria DNA (mtDNA) (Birdsall, Green et al. 1997). DAMPs bind to pattern recognition receptor, e.g. Toll-like receptor (TLR), located on the innate immune cells in the parenchyma, as well as the infiltrating white blood cells, to initiate a group of inflammatory mediators (such as cell adhesion molecules, pro inflammatory cytokines and chemokines) (Prabhu and Frangogiannis 2016). Pro-inflammatory cytokines (IL-1, IL-6, TNF-α) and chemokines (monocyte chemoattractant protein-1 MCP, chemokine ligand 5 CCL5) upregulate endothelial cell adhesion molecule synthesis (Kumar, Ballantyne et al. 1997, Frangogiannis 2007), and at the same time, induce leukocyte integrins expression. This interaction between endothelial and leukocytes adhesions molecule results in leukocyte rolling, strong adhesion and extravasation of neutrophils into the infarcted area (Frangogiannis 2008). Neutrophils are initially recruited to clear dead myocytes and cellular debris at the site of infarct, marking the beginning of acute inflammation. Neutrophils degrade and resolve the extracellular matrix (ECM) through secretion of proteases, neutrophil NAPPH oxidase induced ROS release. Monocytes are later recruited by chemokines from neutrophils, and are sequentially activated into M1 proinflammatory type macrophages, which are characterized by their function to phagocytose cellular debris.

Once matrix fragments and cellular debris clearance is completed, the inflammatory response is inhibited, and the previously activated neutrophils undergo apoptosis and clearance by macrophages (Chen and Frangogiannis 2013). Additionally, macrophages and lymphocytes release inhibitory mediators to supress pro-inflammatory

signals, e.g. and transforming growth factor-β (TGF-β(and interleukin (IL)-10 (Nahrendorf, Swirski et al. 2007). Proliferative phase is stimulated by a molecular switch to type M2 macrophages that promote fibroblasts and endothelial infiltration, collagen deposition by fibroblast, myofibroblasts proliferation and matrix reorganisation, all of which are prominent characteristics of the proliferative phase (Willems, Havenith et al. 1994, Troidl, Möllmann et al. 2009). During this phase, extracellular matrix network is dynamically modulated, and directly orchestrates the cellular function and phenotype. Phagocytosis of cellular fragments found in the infarcted area initiates a provisional matrix formation, which is made up mainly by fibrin and fibronectin. The crucial role of fibroblast during the inflammatory phase of cardiac repair is illustrated in figure 1.21.

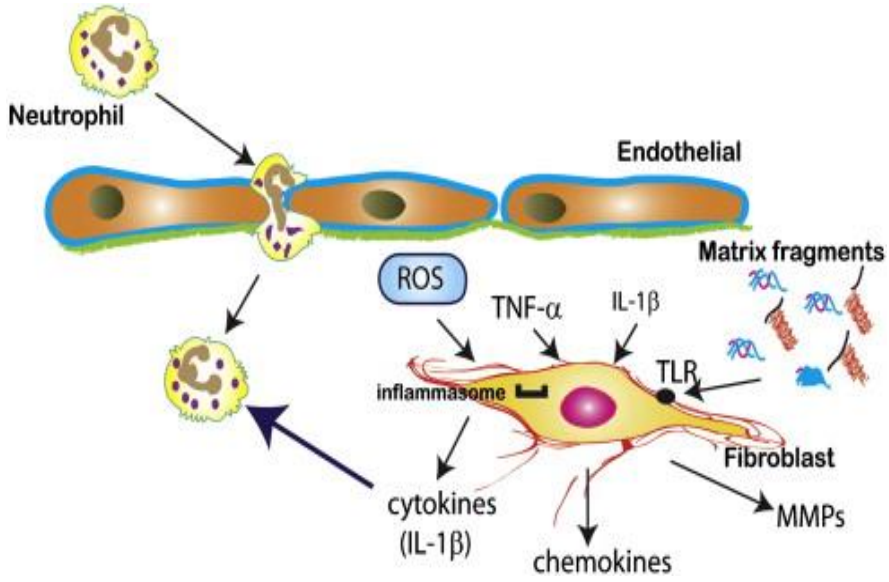

Figure 1.21 The role of fibroblast in mediating inflammatory response. IL-1, interleukin 1, TLR, Toll-Like Receptor, TNF-α, Tumor Necrosis Factor α, MMPs, Matrix Metalloproteases. From (Chen and Frangogiannis 2013).

Endothelial cells proliferation and adherence, labelled by $\alpha_v\beta_3$integrins form new microvessels (angiogenesis) as shown in the Figure 1.22, occur during this phase. Finally, scar condensation and maturation continue while the fibroblasts undergo apoptosis and neovessels regress. The triggers driving reparative cells apoptosis are not yet fully understood, however, removal of fibrogenic growth factors, initiating inhibitory signals which hinders TGF-β and angiotensin II signalling, in addition to elimination of proteins in the matrix, could altogether lead to suppression of proliferation and a reduction of synthetic function of the fibroblasts in the extracellular matrix (Prabhu and Frangogiannis 2016). The resulting outcome is a highly crossed linked scar that replaces the dead myocytes and is progressively modulated as a result of increased wall stress (Willems, Havenith et al. 1994, Troidl, Möllmann et al. 2009).

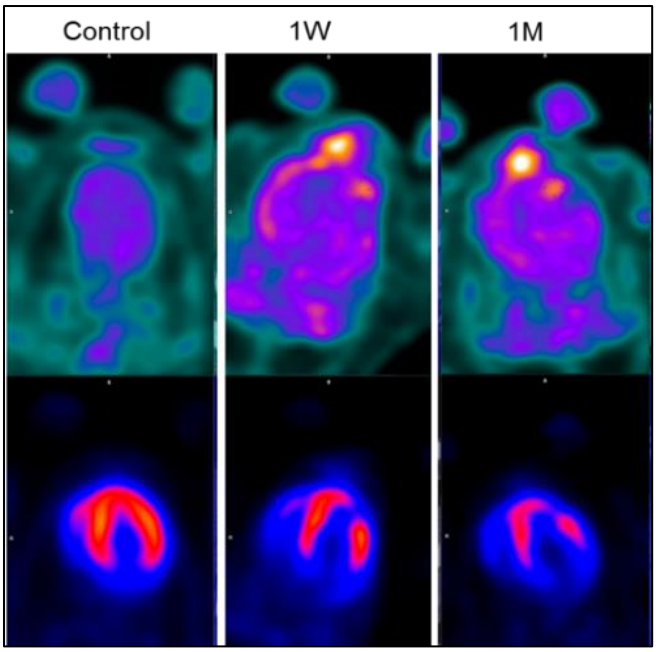

Figure 1.22 Angiogenesis PET. 68Ga-NODAGA-E[c(RGDyK)]2 (RGD) positron emission topography PET (top row, bright colour) and stress PET (bottom row, showing the occlusion) before and after one week (1W) and one month (1M) of induced myocardial infarction (LAD coronary artery occlusion in minipigs). Labelling using αvβ3integrins. From (Rasmussen, Follin et al. 2016)

Recent evidence demonstrated that post myocardial infarction inflammation could potentiate the ischaemic myocardial injury via inflammatory derived cell death or programmed necrosis (necroptosis) mediated by pro-inflammatory cytokines for example IL-1α, IL-6, TNFα (Gao, Liu et al. 2011, Seropian, Toldo et al. 2014), however, the detrimental roles of inflammation and oxidative stress must be thoroughly addressed in animal models and patients suffering from chronic ischaemia and/or ischaemia reperfusion injury, since a comprehensive understanding of roles of the inflammation and oxidative stress in adverse post-infarction LV remodelling are yet to be fully understood.

1.4.2 Manifestations of post ischaemic cardiac remodelling

The major features of cardiac remodelling following acute myocardial infarction are infarct expansion, extension of the infarct to the neighbouring non-ischaemic region as well as the compensated hypertrophy and dilatation of remote myocardium (Cheng, Nguyen et al. 2006). Once the cardiomyocytes are dead due to an ischaemic injury, a subsequent impairment of the contractile force of the diseased heart creates an increased level of strain on the infarct during the ongoing repair process, leading to elongation and thinning of ventricular wall (Opie, Commerford et al. 2006). Moreover, cardiomyocytes contraction in the border zone will be ultimately diminished by the abnormal workload and the increased end diastolic pressure, consequently, these hostile conditions drive an apoptotic cell death response in that area (Narula, Dawson et al. 2000), whereas the remote myocardium displays an adaptive eccentric hypertrophy (Konstam, Kramer et al. 2011). Not only heart

configuration is distorted, but these changes will often precipitate the initial myocardial injury, leading to a progressive deterioration in the left ventricular performance, and indefinitely, heart failure.

1.4.3 Molecular and metabolic aspects of post ischaemic cardiac remodelling

Better understanding of the key changes that draw a link between the initial ischaemic insult and end stage heart failure necessitates a comprehensive study of cardiac remodelling following acute and chronic ischaemia at different, yet highly integrated, perspectives. For this reason, combining and interpreting several different -omics platforms such as genomics, proteomics and metabolomics is invaluable approach to comprehend an inclusive network of the several pathways involved in disease progression and development at several time points. For instance, a porcine model of ischaemia/reperfusion injury was used by Binek et. al to follow the differential cardiac protein expression from early reperfusion (120 minutes) up to 7 days and reported an increase expression of proteins involved in ribosomes, vesicle-mediated protein transport, in addition to collagen and ECM proteins in the ischaemic area. In contrast to mitochondrial and metabolism proteins which were significantly diminished (Binek, Fernández-Jiménez et al. 2017). In this regard, many studies have examined the different metabolic profiles in various cardiovascular diseases, including heart failure of different aetiologies. It has been shown that the failing heart displays an impairment of fatty acid oxidation (Lai, Leone et al. 2014), as well as lactate and ketone body accumulation (Stanley, Recchia et al. 2005), suggesting a disruption to mitochondrial function, in addition to a decrease in essential and nonessential amino acid metabolism (Ussher, Elmariah et al. 2016). Many of the metabolomic studies were notably carried out on patients who often suffer from other co-morbidities or metabolic diseases, reflecting a possible source of heterogeneity, which makes interpretation of metabolomics results quite challenging.

1.5 Experimental models of myocardial infarction

Although there is extensive research investing post MI remodelling in patients, these studies have several limitations which include inability to control disease progression, and unavailability of tissue samples at suitable time points. Therefore, it is critical to use animal models to understand the progression of disease and identify targets for therapeutic interventions. Experimental animal models used to study acute sustained ischaemia or acute ischaemia and reperfusion are quite varied ranging from small rodents to dogs and pigs (Camacho, Fan et al. 2016). Preclinical models (*ex-vivo*, *in-vivo* and *in-vitro*) used to study myocardial infarction in rodents and mice, which include whole animal, isolated perfused heart, and isolated cardiomyocytes (figure 1.23).

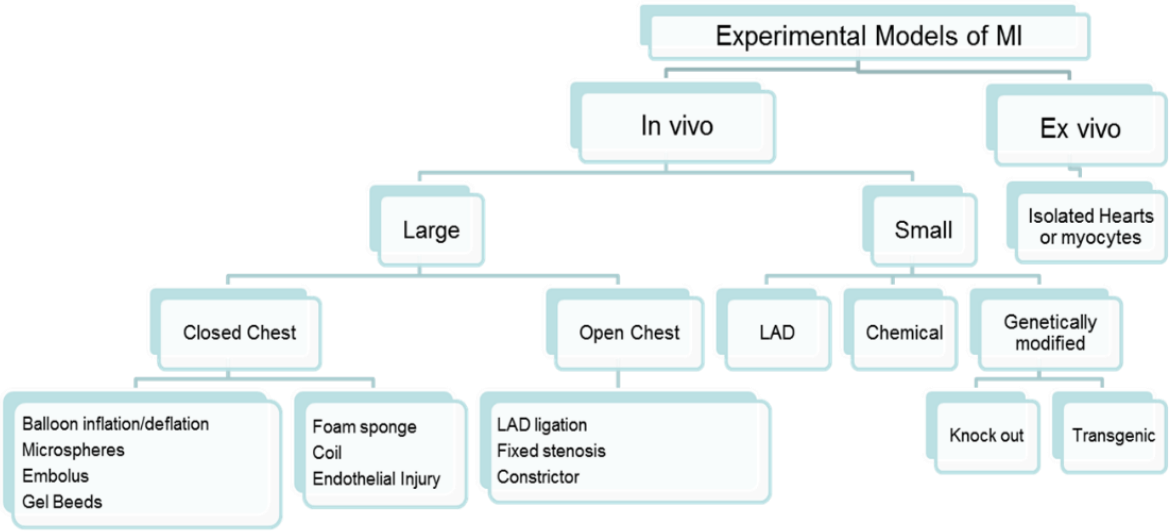

Figure 1.23 Schematic representation of experimental models of MI. Reproduced from (Kumar, Kasala et al. 2016).

In-vivo large animal models are divided into open chest or closed chest models(Kumar, Kasala et al. 2016). Rat hearts with surgically induced MI and heart failure have been extensively used including in our lab (Khaliulin, Halestrap et al. 2014). Percutaneous left anterior descending artery balloon occlusion in pigs is also a popular model for studying heart failure after acute MI and is used largely for investigating therapeutic interventions (Laguens, Cabeza Meckert et al. 2002, Champagne, Su et al. 2003, Jansen of Lorkeers, Gho et al. 2015, Malka, Meerkin et al. 2015, Collantes, Pelacho et al. 2017). Unlike the rodent heart, hearts of pigs, sheep and dogs are very similar to human hearts. Therefore, their use to study interventions prior to clinical trials is very important. Unfortunately, large animals used to study MI tend to be normal animals unlike mice which can be diseased (chemically induced or genetically modified). Moreover, both mice and humans have a completed proteome database available whilst this is not yet applicable for large animals. One important difference between rodents and large animals is the shape, extension, and location of the infarction (figure 1.24).

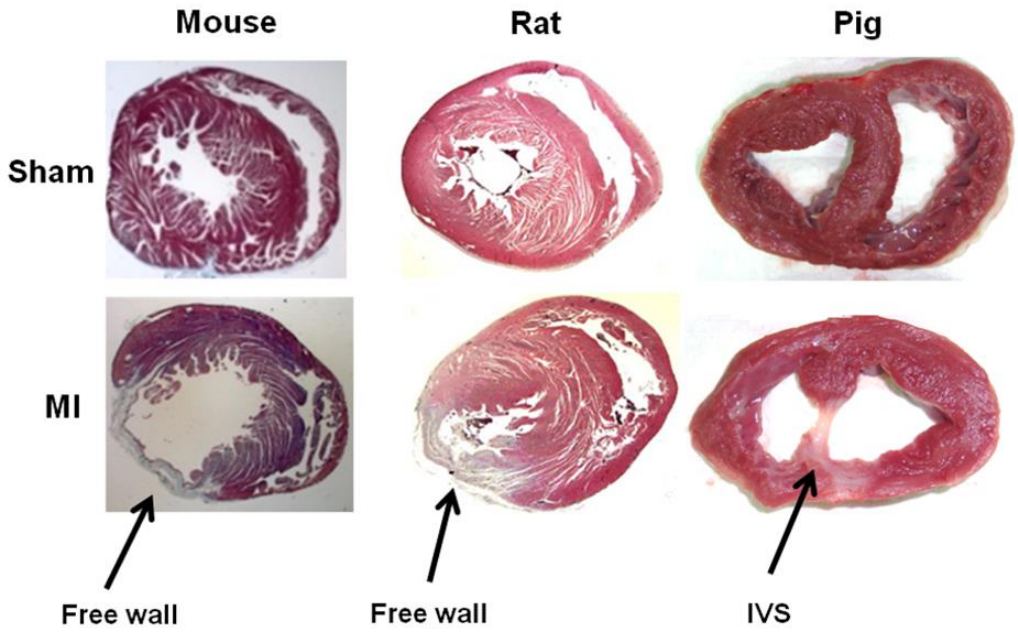

Figure 1.24 Shape and size of infarcts following LAD ligation in mouse, rat and pig heart. IVS, interventricular septum. Image from (Yen and Hsieh).

1.5.1 Relevance of animal models to human cardiovascular disease

Extrapolation of results obtained from animal models of ischaemic heart disease requires careful assessment of advantages and drawbacks of each model. Small animals like mice, and to a lesser degree rat, provide transgenic disease models that could assist in monitoring changes of the diseased heart over their relatively short life span. Nevertheless, key physiological differences in heart rate, being faster in small mammals (e.g. rat resting heart rate ranging from 330 to 480 beats per min) as well as basal metabolic rate should be always considered during interpretation and translation of the obtained data into clinically relevant study designs (Milani-Nejad and Janssen 2014). In this regard, despite being labour intensive and costly, large animal models are, however, of great value to studies investigating cardiac remodelling at the structural and functional levels and in clinically relevant settings.

1.5.2 Rodent model of post ischaemic cardiac remodelling following acute sustained ischaemia

In early 1980s, experimental work on rodents was performed to create MI model via coronary artery ligation (Goldman and Raya 1995). Rat model of MI is considered comparable to human with CAD disease, specifically in terms of pathophysiology and progression toward heart failure following reperfusion (Wayman, McDonald et al. 2003). Due to their availability, lower husbandry costs compared to large animal models, in addition to shorter life span, rats provide an excellent model to study the myocardial changes following myocardial infarction.

1.5.3 Porcine model of post ischaemic cardiac remodelling following ischaemia reperfusion injury

The use of porcine model in cardiovascular research has gained wide acclaim recently due to the anatomical and physiological similarities between human and pig hearts (Spannbauer, Traxler et al. 2019), including energy consumption, left ventricular wall tension and presence of right-dominant coronary vasculature (Kumar, Kasala et al. 2016, Silva and Emter 2020). This great advantage facilitated the translation of numerous therapeutic interventions and devices from small animal models to patients. However, the lack of developed collateral coronary circulation in pigs remains one of the major limitations that challenge the use of this model as a substitute to human heart to study ischaemic heart diseases (Seiler, Stoller et al. 2013). A porcine heart can be always seen as "young heart" for this reason. Nevertheless, the high rate of mortality due to fatal arrhythmias in pigs during surgical induction of ischaemia and/or reperfusion remains an issue for many research centres (Spannbauer, Traxler et al. 2019). In general, the ongoing use of porcine model in cardiovascular diseases facilitated the enhancement of surgical techniques and animal care, all of which aim to advance implementation of this model to test several preclinical therapeutic interventions.

1.6 Clinical studies and cardiac remodelling post MI

Ischaemic heart disease (IHD) is the most common cause of heart attack. However, not all patients die after a heart attack, as it is estimated that 1.4 million people living in the UK who have survived an event of myocardial infarction and a significant number of these patients (estimated at 900,000 people) end up with heart failure (British Heart Foundation annual report 2019). Heart attacks are a consequence of atherosclerosis of the coronary arteries which renders areas of the myocardium ischaemic. Sustained deprivation of cardiomyocytes of oxygen and metabolites results in disruption to intracellular metabolic and ionic homeostasis, Ca^{2+} loading and cardiomyocyte death. However, timely reperfusion of the ischaemic zone (PPCI), can salvage some of the myocardium but can also cause reperfusion injury. Cardiomyocytes are terminally differentiated and therefore are unable to replace the dead ones. Subsequently, the damaged myocardium undergoes a state of cleaning and repair helped by apoptosis and the migration of inflammatory cells to the infarcted area (Zimmer, Bagchi et al. 2019)). In addition to structural changes, cardiac remodelling also includes metabolic, molecular and cellular alterations (Pfeffer and Braunwald 1990, Cohn, Ferrari et al. 2000). Given the intensive functional demands of the myocardium and the associated gradual inflammatory response, apoptosis, hypertrophy, myofibroblasts proliferation and fibrosis, theses will ultimately lead to heart failure (Konstam, Kramer et al. 2011). Heart failure will dramatically affect quality of life and increase risk of sudden cardiac death.

Although there is good understanding of the pathophysiological mechanisms behind ischaemia and reperfusion injury (acute response), little is known about the processes leading to subsequent heart failure (chronic response). More importantly, the link between acute injury and characteristics of heart failure (e.g., onset and intensity) is not yet fully explained. Understanding and identifying the underlying triggers of heart failure early after an ischaemic injury and recognition of early disease signs will help in the design of targeted therapeutic

interventions. Since both acute injury and subsequent chronic remodelling involve metabolic alterations, metabolites are exceedingly being targeted to assess the progression of heart failure to help in prevention, diagnosis, and therapy(Barba, Andres et al. 2019, Cresci, Pereira et al. 2019). This approach in particular is more likely to improve the prediction of heart failure thus adding key clues that could be considered in addition to other established risk factors (e.g., age, sex, low-density and high-density lipoprotein cholesterol, triglycerides, diabetes, body mass index, blood pressure, kidney function, smoking, and MI prior to or during follow-up)(Stenemo, Ganna et al. 2019).

A limited number of clinical studies have attempted in recent years to investigate the changes in blood metabolome in several heart diseases such as hypertrophy, coronary artery disease, diabetic cardiomyopathy, heart failure, atrial fibrillation and resynchronization therapy (McKirnan, Ichikawa et al. 2019, Muller, Heckmann et al. 2019, Pouralijan Amiri, Khoshkam et al. 2019, Sowton, Griffin et al. 2019, Stenemo, Ganna et al. 2019, Zhong, Liu et al. 2019, Zhou, Sun et al. 2019, Zhu, Fulati et al. 2019). There are also recent studies that have reported changes in the metabolome in ST-segment elevation myocardial infarction STEMI patients(Kohlhauer, Dawkins et al. 2018, Goulart, Santos et al. 2019). However, work looking at changes in metabolome throughout early stages of infarction and during chronic remodelling to heart failure is very limited (Chen, Song et al. 2019). Studies of this kind tend to focus on either acute or chronic phases using heterogenous population of patients (sex, age, etc.) who have other diseases with metabolic impact (e.g., diabetes and kidney disease). More importantly, such studies should take in consideration the role of early changes in biomarkers and their ability to predict long term remodelling and outcome.

1.7 Hypothesis

Post ischaemic cardiac remodelling following acute sustained ischaemia or ischaemia reperfusion injury in adult heart occurs at the functional, structural, molecular, and metabolic levels and that investigating these changes will help in identifying pathways and biomarkers that can be targeted to mitigate the deleterious effects of remodelling.

1.8 Aims and objectives

1- Investigate and characterise post ischaemic cardiac proteomic, metabolic, and structural (alterations that occur using the following experimental models:

a. Rodent model of ischaemia-induced infarction by LAD coronary artery ligation.

b. Porcine model of ischaemia reperfusion injury.

2- Identify chronic changes in blood constituents that occur following infarction in both models.

3- Monitor alterations in cardiac function, blood metabolites and markers of cardiac injury in a selected group of STEMI patients both acutely post MI and post ischaemic cardiac remodelling leading to heart failure.

Chapter 2

Materials and Methods

2.1 Materials

2.1.1 Chemicals and reagents

Agar Scientific (Essex, UK)

Glutaraldehyde solution (25 %)

Bio-Rad (Hertfordshire, UK)

Precision Plus Protein™ All Blue Standards

Quick Start™ Bradford 1 x Dye Reagent

BOC Healthcare (Surrey, UK)

95 % oxygen/5 % carbon dioxide medical gas mixture

BOC Industrial Gases (Surrey, UK)

Liquid nitrogen

Fisher Scientific UK Ltd (Leicestershire, UK)

D-glucose anhydrous

Magnesium sulphate ($MgSO_4 \cdot 7H_2O$)

Sodium chloride (NaCl) 68

Sodium dodecyl sulphate (SDS)

Merck (New Jersey, USA)

Magnesium chloride ($MgCl_2$)

Roche (Sussex, UK)

cOmplete, EDTA-free protease inhibitor cocktail tablets

PhosSTOP phosphatase inhibitor cocktail tablets

Sigma-Aldrich™ (Dorset, UK)

Albumin from bovine serum (BSA)

Calcium chloride solution (1 M) ($CaCl_2$)

Chelerythrine Chloride

Ethylene glycol-bis(2-aminoethylether)-N,N,N',N'-tetraacetic acid (EGTA)

Folin and Ciocalteu's phenol reagent

Formaldehyde solution (36.5-38 %)

Glycine

Methanol

Lowry reagent

Nonidet™ P 40 substitute solution

Phosphate buffered saline (PBS) tablets

Sodium deoxycholate

Sodium hydroxide (NaOH)

VWR International Ltd (Leicestershire, UK)

4-(2-Hydroxyethyl) piperazin-1-ylethanesulphonic acid (HEPES)

Di-sodium hydrogen phosphate (Na_2HPO_4)

Hydrochloric acid fuming (37 %) (HCl)

Potassium chloride (KCl)

Potassium dihydrogen phosphate (KH_2PO_4)

Sodium hydrogen carbonate ($NaHCO_3$)

2.1.2 Solutions

Hrebs-Henseleit (KH) buffer

The chemicals used to prepare KH buffer are listed in table 2.1.

Table 2.1 Concentration of chemicals in KH buffer. pH =7.4, solution was equilibrated with 95% O_2-5% CO_2.

Chemical	Concentration (mM)
NaCl	118
$NaHCO_3$	25
KCl	4.8
KH_2PO_4	1.2
$MgSO_4$	1.2
Glucose	11
$CaCl_2$	1.2

Cardioplegia

The chemicals used to make cardioplegia solution are listed in table 2.2.

Table 2.2 Concentration of chemicals in cardioplegia solution. Same pH as above.

Chemical	Concentration (mM)
NaCl	118
$NaHCO_3$	25
KCl	20
KH_2PO_4	1.2
$MgSO_4$	1.2
Glucose	11
$CaCl_2$	1.2
$MgCl_2$	15

2.2 Animals breeding, handling, care & ethics

2.2.1 Rats

Wistar Han male rats, weighing from 220 to 240 g, were provided and delivered by Charles River (Margate, UK). Upon arrival, the animals were placed at University of Bristol animal unit. Animals care and handling were in accordance with Home office guidance (Scientific Procedures) Act of 1986 and the 3R rules (Refinement, Reduction and Replacement). Rats were given *ad libitum* access to food and water.

2.2.2 Pigs

Four months old female Yorkshire (large white) pigs, weighing 58-64 kg, were kept at the Translational Biomedical Research Centre (TBRC), University of Bristol in accordance with the United Kingdom Animal (Scientific Procedures) Act, 1986 and the reduction component of the 3Rs (Refinement, Reduction and Replacement). Diet and nutrition were provided by TBRC team throughout the duration of experiment. A week before the procedure, pigs were given daily a single dose of Aspirin (75 mg), and the night prior to surgical procedure, pigs were starved for 8 hours but allowed a continuous access of water.

2.3 Experimental procedures

2.3.1 *In-vivo* Left Anterior Descending (LAD) artery ligation in rodents

All procedures conform to the Directive 2010/63/EU of the European Parliament and the Guide for the Care and Use of Laboratory Animals published by the US National Institutes of Health (National Research Council Committee for the Update of the Guide for the and Use of Laboratory 2011). Ethical approval was obtained from University of Bristol, and project licence was granted from Home Office under project licence PPL 30/3448, held by Dr. Andrew James.

Adult Wistar male rats were allocated into either SHAM (n = 5) or LAD ligation group (n = 5). Surgical procedures were performed by Dr. Simon Bryant in animal care unit, University of Bristol and I observed the surgery.

2.3.1.1 Anaesthetic drugs

Table 2.3 includes a list of anaesthetic drugs and their dosage, function and route of administration in LAD coronary artery ligation procedure for rodents. Induction of anaesthesia was achieved by injecting medetomidine HCl and ketamine HCl mixture into intraperitoneal space. Followed by Buprenorphine HCl subcutaneous injection to start analgesia and surgery. Finally, Atipamezole was used as a reverse agent to Medetomidine allowing rats to reach recovery after the end of procedure.

Table 2.3 List of anaesthetic drugs used in LAD coronary artery ligation procedure in rats.

Drug	Dose per 100 g (of rat body weight)	Function	Route
Medetomidine HCl (1 mg/ml) and Ketamine HCl (100mg/ml)	125 µl of medetomidine:ketamine 2:3 ratio.	Induction	Intraperitoneal
Buprenorphine HCl (0.3 mg/ml)	17 µl	Analgesia	Subcutaneous
Atipamezole (5 mg/ml)	50 µl	Recovery, reversal of Medetomidine effects	Intraperitoneal

2.3.1.2 Surgical procedure

After ensuring adequate anaesthesia, level of responsiveness was assessed by rear foot reflexes. The rats were intubated via endotracheal tube and ventilated with small animals respirator (Harvard Apparatus) at 250 ± 10 ml flow volume/min. Heat mat was placed under each rat to maintain the body temperature at 37°C throughout the sugery and recovery. A 3 cm longitudinal left parasternal thoracotomy incision was created from 3rd intercostal space. In LAD group, a coated braided polyester round needle 6-0 was used to occlude and tie LAD coronary artery. In SHAM operated rats, no LAD artery occlusion occurred. The surgical incision was closed using 4-0 Vicryl on a cutting needle.

2.3.1.3 Recovery and monitoring

Rats received recovery inside a recovery chamber (Vet Tech Solutions Ltd) where they were ventilated with room air, given glucose saline and followed closely up to 2 hours. All the operated animals survived after the surgery and kept under daily close monitoring and observation at Animal Services Unit, University of Bristol for four weeks after the day of surgery. At the end of the experiment, the rats were culled according to Schedule 1 killing method by stunning and cervical dislocation.

2.3.2 Percutaneous Balloon occlusion of proximal left anterior descending (LAD) artery in pigs

Animal procedures were undertaken at the University of Bristol Translational Biomedical Research Centre (TBRC) in accordance with the United Kingdom Animal (Scientific Procedures) Act, 1986, under project licence PPL 7008975, held by Prof. Raimondo Ascione. TBRC team carried out the intervention, led by Dr. Tom Johnson and

Dr. Domenico Bruno. Four months old female Yorkshire (n=4, weights 62.3 kg ± 5.55 kg) underwent 60-minute closed-chest balloon catheter inflation to occlude the proximal left anterior descending (LAD) coronary artery.

2.3.2.1 Anaesthetic drugs

Table 2.4 includes a list of anaesthetic drugs and their dosage, function and route of administration in LAD coronary artery occlusion procedure for pigs.

Table 2.4 Dose and route of administration of anaesthetic drugs used in LAD coronary artery occlusion procedure in pigs.

Drug	Dose	Function	Route
Dexmedetomine	15 mcg/kg	Sedation	Intramuscular
Ketamine	10 mg/kg	Induction	Intramuscular
Propofol	1 mg/kg	Induction	Intravascular
Isoflorane	(2%)	Maintenance	Inhalation

Anaesthesia was delivered and maintained by veterinary anaesthetists and TBRC team in Langford campus, University of Bristol.

2.3.2.2 Surgical procedure

The pigs underwent closed chest percutaneous balloon occlusion of proximal LAD coronary artery for 60 minutes to induce MI. The mean pressure of occlusion inside the artery was 10.6 atmospheric pressure (atm). Deflation of balloon to achieve reperfusion and animal recovery followed. Amiodarone (300mg) and magnesium (8 mg) were administered through a central line at the time of MI induction and over 4 hours as a measure to decrease the possibility of fatal ventricular arrhythmia. Cardiopulmonary resuscitation (CPR) was performed in case of lethal arrhythmia. CMR and cTnI measurement methods were used to assess cardiac injury after four weeks, and are described fully in appendix.

2.3.2.3 Recovery and monitoring

All the operated animals were kept under daily intensive monitoring and observation at TBRC, University of Bristol for four weeks from the day of intervention before termination.

2.3.2.4 Control Group

Control group was chosen from healthy four months old pigs were (n=4) from abattoir, Langford Campus for veterinary sciences, University of Bristol

2.3.3 Tissue collection, preparation, and storage

2.3.3.1 Rats

Animals were culled according to Schedule 1 killing methods by stunning and cervical dislocation. Hearts were extracted and rapidly transferred into ice-cold KH buffer. Each heart was cannulated into Langendorff system through the aorta and perfused at speed of 10 ml/min for 5 minutes with KH solution then switched to cardioplegia solution by syringe pump.

Tissues from apex, right and left atrium were collected, transferred to cryotubes (Thermo Fisher Scientific, UK) and immediately snap frozen in liquid nitrogen and stored at - 80 °C. Perfusion then switched to electron microscopy fixative before cutting and processing (further explained in section 2.4.4.1.1) as seen in figure 2.1.

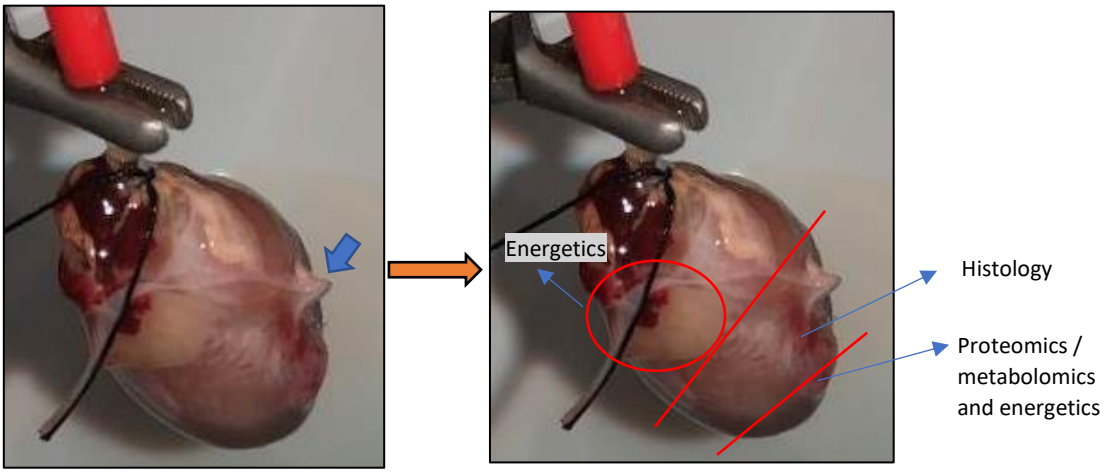

Figure 2.1 Isolated Langendorff perfused rat heart extracted after 4 weeks after LAD coronary artery ligation. Surgical knot outlined in blue arrow. The right panel shows how selected parts of the heart that were collected for different purposes. Following perfusion with cardioplegia, left and right atria and the apex were collected for molecular studies. Sections for histology were taken after perfusion with fixative.

2.3.3.2 Pigs

Cardiac tissues collected from infarcted region from left ventricle from LAD group (four weeks after surgical procedure) and left ventricle from control were transferred immediately into cryotubes, snap frozen in liquid nitrogen and stored at -80°C freezers.

Additionally, tissues from left ventricle of control as well as infracted area of left ventricle in LAD group were placed in 4% paraformaldehyde solution, kept at 4°C for 24 hours and sent for tissue processing and embedding the following day.

2.4 Methods

2.4.1 Proteomics and phosphoproteomics

2.4.1.1 Protein extraction

Tissues from pigs or rats were defrosted but kept on ice and weighed for wet weight. This was followed by the addition of 10 µl RIPA buffer cocktail per 1 mg of tissue wet weight. RIPA buffer cocktail was prepared in 200ml 1X PBS. The following were added to the PBS: 1% (v/v) Nonidet P-40 detergent, 0.5% (w/v) Sodium deoxycholate and 0.1% (w/v) Sodium dodecylsulphate. On the day of the experiment, protease and phosphatase inhibitors were added, these were mini, EDTA-free protease inhibitor cocktail tablets and phosphatase inhibitor cocktail tablets PhosSTOP (Roche, UK).

Up to 20 Zirconium oxide beads (1.4mm) were added as appropriate to the tissues immersed in RIPA buffer cocktail in 0.5 ml soft tissue homogenizing CK 14 tubes (Precellys 24), then each tube was placed in the tissue homogenizer (Bertin technologies, France) at 4°C for 10 seconds, repeated twice at the maximum speed with 5 second break. Tubes containing the homogenised tissues were left in icebox on the shaker for 30 minutes, before centrifugation at 10,000 x g for 10 minutes at 4°C. The supernatant was pipetted and kept in Eppendorf tubes at -80°C for further quantification using Bradford assay. The pallet contained cellular debris and, therefore, was discarded.

2.4.1.2 Protein estimation using Bradford assay

Bradford assay was used to quantify proteins content in the samples prepared in the previous section. First, the samples were diluted three times with distilled water (5 µl sample to 10µl of distilled water) to fit in standard curve range. 5 µl of the diluted samples were then pipetted into LP4 tubes in duplicates and 5 µl of RIPA buffer as a blank. Bovine Serum Albumin (BSA) stock solution 5 mg/ml was used to prepare protein standard curve by pipetting a duplicate of 1, 2, 3, 4 and 5µl into LP4 tubes. Followed by addition of 3ml of Bradford reagent to every single tube plus an empty one serving as standard blank. All the tubes were vortexed and incubated for 15 minutes at room temperature. The light absorbance was measured at 595nm using spectrophotometer. Average absorbance of each BSA concentration was calculated and used to plot the standard curve. The curve line was applied to calculate the samples protein concentration after adjustment to the dilution factor (figure 2.2).

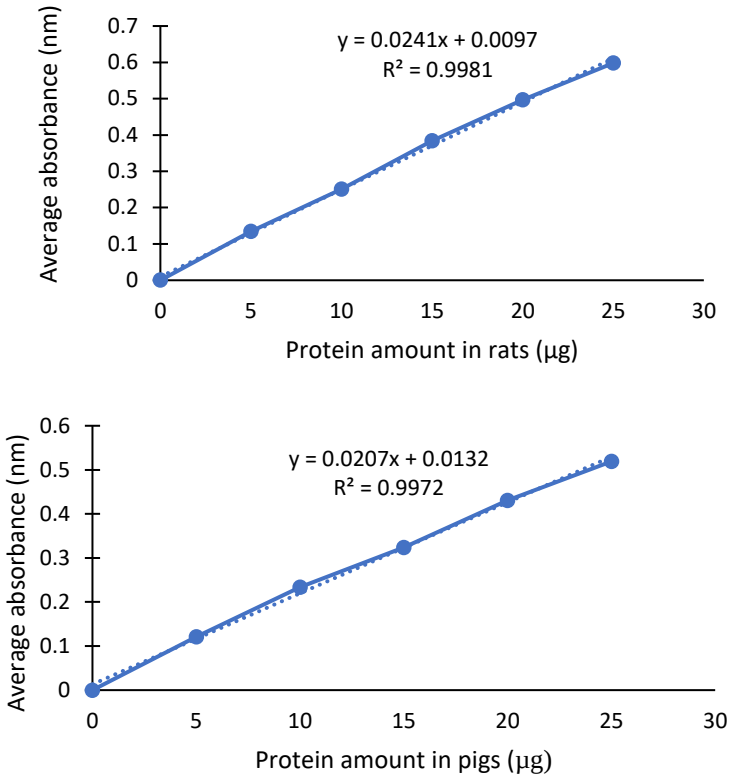

Figure 2.2 Standard curve calculated using the Bradford assay in rats (above) and pigs (below). Absorbance was measured at 595 nm.

Protein concentration of 2mg/ml was prepared by diluting the protein extract with double distilled water, based on Bradford protein quantification method. Protein identification was performed using Tandem Mass Tagging (TMT) (ThermoFisher Scientific, UK) and reverse phase nano-liquid chromatography (RP nano-LC MS/MS) using a LTQ-Orbitrap Velos mass spectrometer at the University of Bristol Proteomics Facility (ThermoFisher Scientific, UK), run by Dr. Kate Heesom.

2.4.1.3 Liquid Chromatography Tandem Mass Spectrometry (LC-MS/MS) setup

Proteins of each sample were digested and processed into amino acids, which were labelled using TMT. Each TMT label consists of a cleavable linker region, and NH2 Reactive group, which allows efficient amine-specific binding to peptides, a Mass Normaliser, which is used to ensure the overall mass of each tag is constant despite the differing reporter groups, in addition to a Mass Reporter group (R), that specifically binds to each sample in a single run (labelled as 126, 127, 128, 129, 130 and 131) (Abdul-Ghani, Heesom et al. 2014). The linker region is cleaved during LC-MS/Ms followed by fragmentation using Collision Induced Dissociation (CID), which releases the Mass Reporter group. This allows the detection of different reporter ions ranging 126-131 Da as they cluster at the low mass end of each LC-MS/MS spectra to indicate the relative abundance of each peptide by sample, as illustrated in figure 2.3.

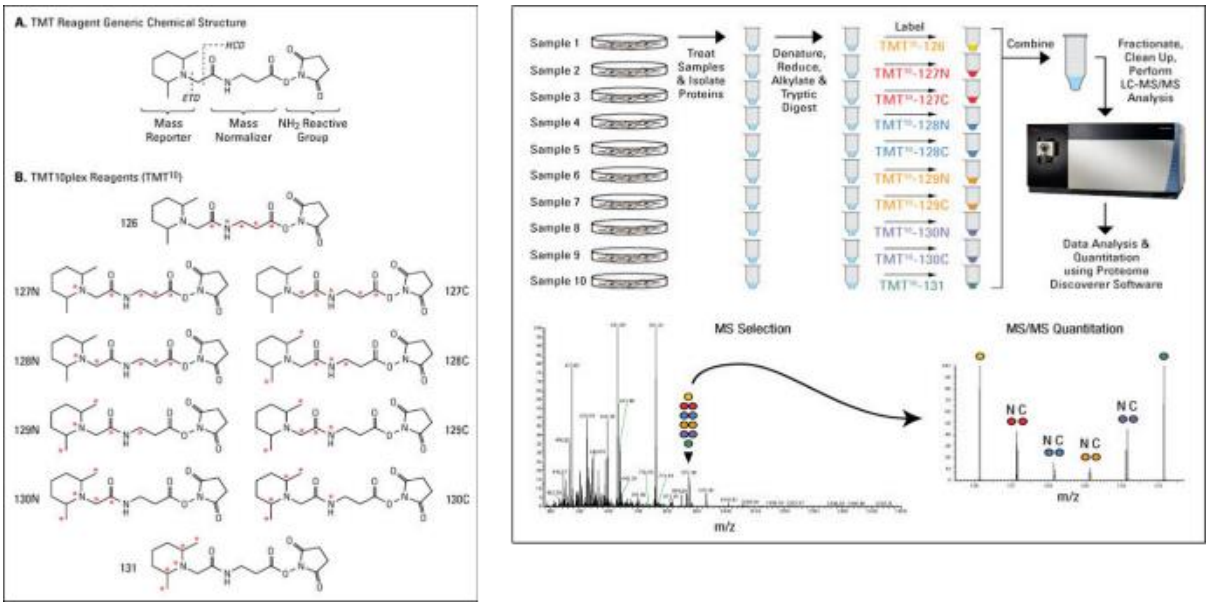

Figure 2.3 (Right and Left): The tandem mass tag reagents. Right**:** Structure of the amine-reactive TMT Reagents. A) Functional regions of the reagent structure. B) Structures ofTMT10plex reagent with 13C and 15N heavy isotope positions (red asterisks) Left: Scheme for MS experiments using TMT Isobaric Mass Tagging Reagents. In this experiment, protein extracts are reduced, alkylated and digested overnight. Samples are labelled with the TMT Reagents and then mixed before sample fractionation. Labelled samples are analysed by high resolution Orbitrap LC-MS/MS right before data analysis to identify peptides and quantify reporter ion relative abundance. From ThermoScientific website

2.4.1.4 Phosphoproteins identification

Phosphopeptide enrichment technique to quantify and determine phosphopetides in the samples was performed through running the tagged samples through a titanium dioxide (TiO_2) column. Unlike the non-phosphorylated peptides, the phosphopeptides in these samples bind to the column, this step was followed by elution and analysis in LC-MS/MS (Abdul-Ghani, Heesom et al. 2014).

2.4.1.5 Proteomics and phosphoproteomics data analysis

Proteins levels were processed using Proteome discoverer software 2.1 (ThermoFisher Scientific, UK) as the sample normalized abundance values by setting the Normalization Mode parameter of the "Peptide and Protein Quantifier" node in Proteome discoverer to either Total Peptide or Specific Protein Amount. Proteins and phosphosites of low confidence rate were excluded from analysis.

Proteomics data were transferred from Proteome discover to be analysed using Microsoft Excel 2016. After correction of each individual sample to the pooled sample, abundance of proteins in each group was displayed as mean and standard error of the mean (SEM). F-test for variance followed by Unpaired student's t-test were used to determine statistical significance ($p < 0.05$) between 2 groups. Data were illustrated as Fold Change (mean LAD abundance/ mean SHAM or Control abundance). Panther GO database was used to classify molecular function of proteins. Pathway analysis was completed using Ingenuity Pathway analysis (IPA) software (QIAGEN, USA) against rodent and human databases for porcine data (using Uniport ID system).

Phosphosites analysis followed same pattern as proteome data, in addition to Proteome Discoverer program to identify the exact phosphorylation site(s) of each phosphoprotein.

2.4.2 High Performance Liquid Chromatography (HPLC)

2.4.2.1 Samples preparation

Frozen tissues, as described in (section 2.3.3), were crushed using a pestle and mortar in liquid nitrogen. The resulting tissue powder was immediately moved into perchloric acid (PCA) containing LP3 tube (4.8% perchloric acid (PCA) made by addition of 8 ml of 60% PCA to 100ml distilled water and cooled to 4°C. The tubes were weighed before and after addition of the tissue powder to obtain wet tissue weight. The mixture was vortexed (Rotamixer 7871, Hook & Tucker Instruments) and centrifuged at 4°C, 4000 g for 10 minutes using Allegra 21R centrifuge (Beckman Coulter, UK). The supernatant was neutralised by mixing with equal volume of 0.44 M K_2CO_3 (400 µl). The mixture was then centrifuged again at 4°C, 4000 g for 10 minutes. The supernatant was collected, aliquoted and stored at -20 °C freezer for HPLC analysis while the pellet, potassium perchlorate and debris, was discarded.

2.4.2.2 HPLC apparatus

The high-performance liquid chromatography (HPLC) instrumentation consists of a solvent module pump (Beckman System Gold 125), an autosampler (Beckman System Gold 507e, Beckman Coulter Ltd, UK), a separation column, and a detector (Beckman System Gold 166, Beckman Coulter Ltd, UK). All the samples were run by Hua Lin. The machine operates through two phases, stationary and mobile phase. Standards or samples were first injected by autosampler to the separation column, which is termed stationary phase, then a high-pressure pump forces the eluent solution through the column, i.e., mobile phase. A chromatographic material is used for compounds separation, in which the absorbance was recorded by a detector that is wired to computer as seen in figure 2.5.

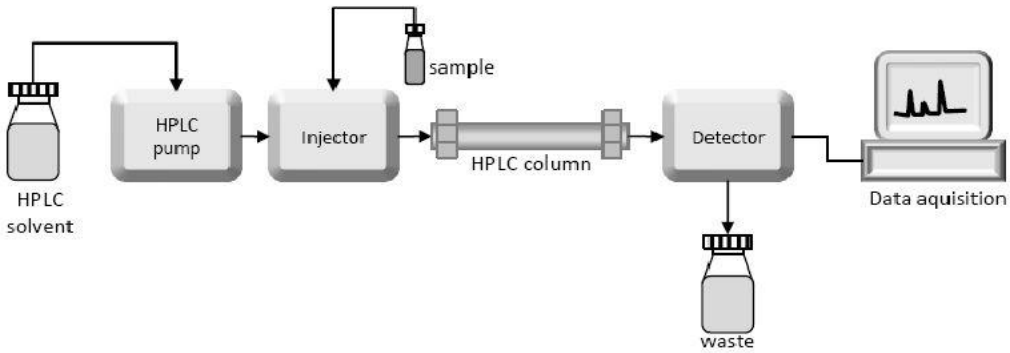

Figure 2.4 A schematic diagram of the high-performance liquid chromatography component. From (French and Kramer 2007)

2.4.2.3 Metabolites Analysis

A 3 µm octadecyl silane Hypersil column (150 mm x 4.6 mm) was used as the separation column (Thermo Scientific, UK). The elution of metabolites is dependent on the composition of the mobile phase, which contained two eluents. Eluent A (150 mM KH_2PO_4 and 150 mM KCl, set at pH 6.0 with KOH) and eluent B (eluent A with 15 % (v/v) HPLC grade acetonitrile added) and a low-pressure gradient mixing device was used to ensure a well-controlled composition of the mobile phase.

At different time points, the amount of eluent B changed linearly as seen in table 2.5. The column temperature was maintained at 17-19 °C and the absorption was measured at 254 nm.

Table 2.5 Mobile phase composition at selected time points.

Time (min)	Flow speed (mL · min-1)	Eluent A (%)	Eluent B (%)
0	0.9	100	0
0.1	0.9	97	3
3.0	0.9	91	9
7.0	0.9	0	100
8.5	0.9	100	0

10 µL of standard samples or 20 µL of tissue extract were injected into HPLC system and bound to the column. ATP, ADP, AMP, GTP, GDP, GMP, IMP, xanthine, hypoxanthine, β-NAD, inosine and adenosine were measured. According to the mobile phase composition, each of these metabolites were eluted at different time points.

2.4.2.4 HPLC Data analysis

The signals generated from HPLC were displayed as chromatograms using OpenLab Software (Aligent, USA). The samples chromatograms were compared to the standards to identify peaks of each metabolite (Figure 2.5). Data analysis was completed by measuring area under curve and adjusting the values to samples recorded weights. Concentration of metabolites is derived from the corrected values, and statistical analysis is done by comparing means of the two groups using unpaired student's t-test.

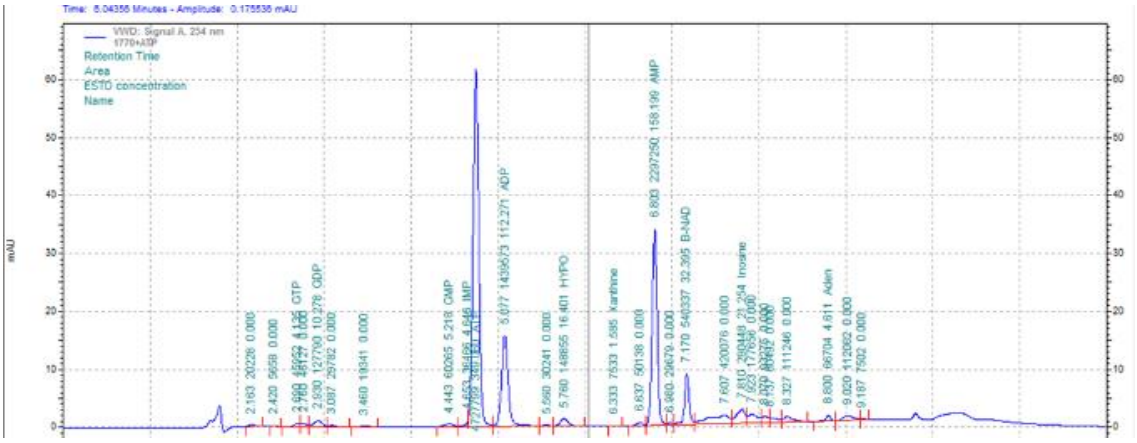

Figure 2.5 Chromatographs for cardiac energetics from one of the samples, measured using high-performance liquid chromatography. Made with Aligent software. (own work)

2.4.3 Nuclear Magnetic Resonance (NMR)

2.4.3.1 NMR apparatus

NMR spectroscope (700 MHz Bruker AVANCE HD, Bruker BioSpin GmbH, Germany) in School of Chemistry at University of Bristol, consists mainly of liquid handling robots, sample holder placed within a magnet (14 Tesla) that is wired with radiofrequency (RF) pulse transmitter and receiver. Once the signal is obtained and detected from RF receiver, it is amplified and strengthened by a recorder that transforms the spectrum for analysis. Figure 2.6 shows a schematic diagram of 1H-NMR experiment workflow.

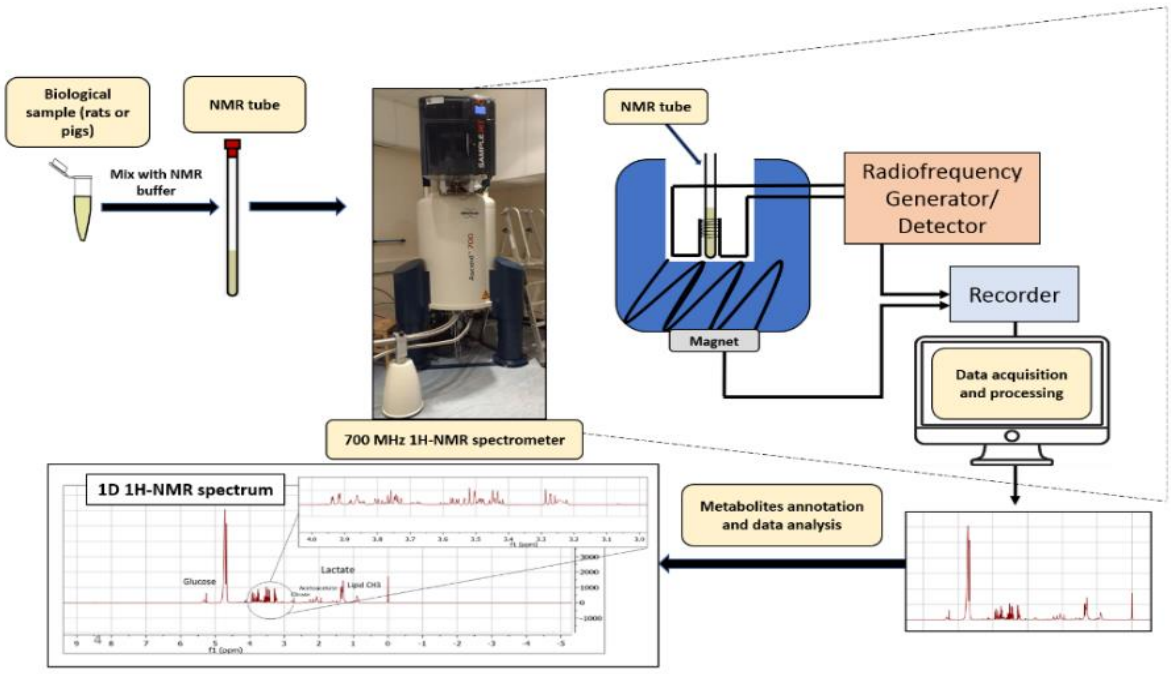

Figure 2.6 NMR experiment workflow. A schematic diagram of Nuclear Magnetic Spectroscopy. Plasma is mixed with NMR buffer, transferred into cryoprobe (tubes) and placed inside NMR magnet. A radiofrequency generator detects the radiofrequency signals of each sample, which are recorded, transformed and processed into NMR spectrum. (own work)

2.4.3.2 Samples preparation for NMR

2.4.3.2.1 Blood

Blood samples taken from rats (baseline and 4 weeks after LAD ligation) or pigs (4 weeks after LAD occlusion and control) were collected into EDTA tubes, centrifuged at 2000 g for rats samples (1000 g for pigs) for 10 minutes, and the resultant plasma was placed into Eppendorf tubes and stored in -80°C freezer until the day of the experiment. Samples (~0.5ml each) were then transferred to School of Chemistry-University of Bristol on dry ice for metabolites analysis using Nuclear Magnetic Resonance spectroscopy (NMR), run by Dr. Matt Goodwin. Once defrosted, plasma is transferred into 1.7 mm CryoProbe and dissolved with NMR buffer (1 PBS tablet, 0.16 g Trimethylsilylpropanoic acid (TSP), 0.2 g sodium azide NaN_3 in 170 ml type I water and 20 ml deuterium oxide (D_2O), adjusted to pH 7.4) and kept at 4°C during running.

2.4.3.2.2 Myocardial tissue extract

Same extraction method, that was used in section (2.4.2.1) using PCA extraction, was also used in NMR study to detect cardiac tissue metabolites from both rodent and porcine models.

2.4.3.3 Running samples in NMR spectroscope

NMR depends on the quantum mechanical properties of the nucleus of the atom, specifically spinning and electrical charge. 1H-NMR uses external magnetic field that is exposed toward hydrogen nuclei of biomolecules, therefore the energy is transferred to a higher level and vice versa, when magnetic field is removed. The energy transfer occurs at a wavelength that is recorded and interpreted based on the known properties of each molecules, since the intra-molecular magnetic field is specific depending on the type, number of hydrogen nuclei and their interactions within one single molecule (Watkins, Jenkins et al. 2017). Figure 2.7 shows a representation of 1H-NMR spectrum.

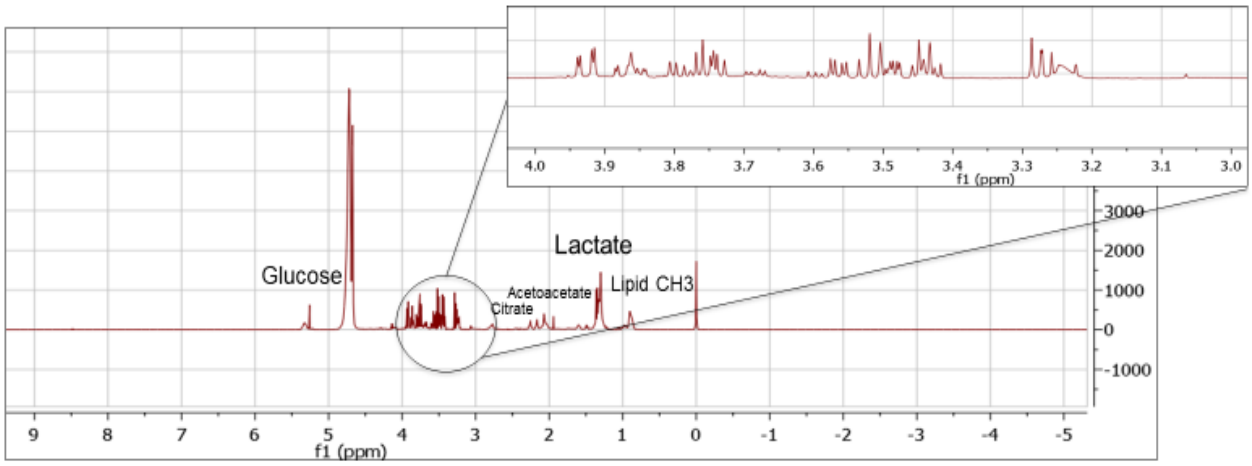

Figure 2.7 1-Dimension (1D) 1H-NMR spectrum generated by 700 MHz spectrometer**.** Some metabolites were annotated based on their chemical shifts (ppm). (own work)

2.4.3.4 NMR Data analysis

1H-NMR spectra were Fourier-transformed using Bruker TopSpin software (Bruker, Germany), 1D-1H Carr–Purcell–Meiboom–Gill (CPMG) pulse sequence was used for data analysis using MestReNova software (Mnova, MestReNova Research SL, Spain) .

Samples were referenced against Trimethylsilylpropanoic acid (TSP) at concentration of 4.6 mM, which had a chemical shift value of 0. Chemical shifts reference for selected metabolites were obtained using Human Metabolome Database (HMDB) and Chenomix metabolites library (Chenomix Inc., Alberta, Canada) and through searching the available literature (Soininen, Kangas et al. 2009) as seen in figure 2.8. Targeted metabolomics was used to determine differences between groups. Peaks areas generated from Mnova files were annotated to their corresponding metabolites, and the average of each metabolite was compared between the two groups (LAD vs. SHAM or control) using unpaired student's t-test for pigs (and paired student's t-test for rat samples).

Statistically significant p value is set to < 0.05. Fold change is calculated by dividing mean metabolites values in intervention group (LAD) by the corresponding ones at the baseline or control.

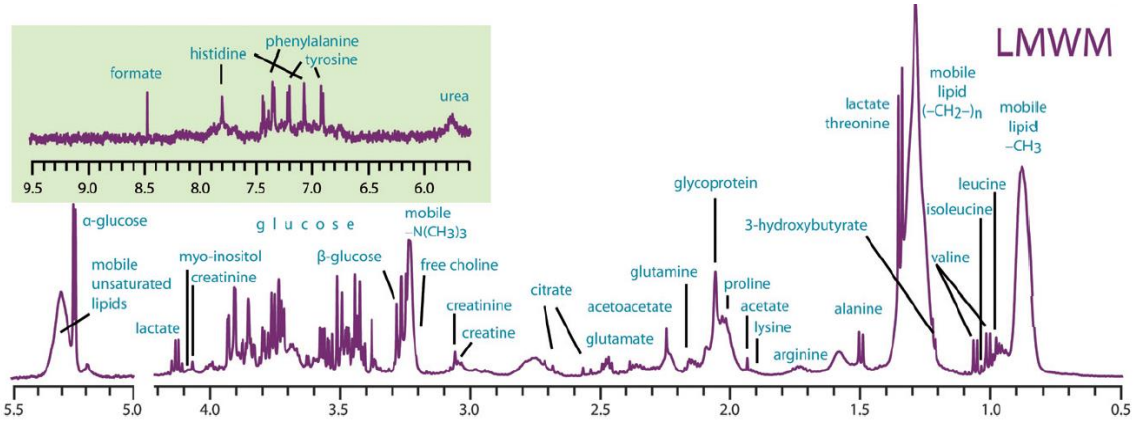

Figure 2.8 1D 1H-NMR spectrum of human plasma. From (Soininen, Kangas et al. 2009)

2.4.4 Light Microscopy

2.4.4.1 Tissue processing and embedding

2.4.4.1.1 rats

Fixed tissues from rat hearts were prepared by Dr Erin O'Callaghan. Mid sections of rat hearts were submerged in 50 mM PBS/EDTA for 5 minutes then switched to 10% formaldehyde solution for 2 minutes, and left in 4% formaldehyde solution at room temperature overnight. Tissues were transversely sliced and washed with PBS buffer twice and kept at 4˚C for one day. Slices were later transferred to 30% sucrose in PBS. At this stage, the samples are floating on the surface, once they sink, indicating that sucrose had fully penetrated the tissues, they were oriented and embedded in OCT (Optimal Cutting Temperature) compound media using a piece of wood placed on dry ice before suspending tissues on the surface of Liquid Nitrogen until frozen. The samples were stored in -80˚C freezer for cryosectioning.

Cryosectioning

Fixed tissues were collected and proceed for sectioning. Scientific Cryostar NX50 Cryostat machine (Thermofisher Scientific, UK) was used to cut the OCT embedded tissue. First, the machine was cooled to -20 ˚C. The samples were transferred from - 80°C freezer on dry ice and left in the cryochamber to equilibrate with chamber temperature. Second, OCT freezing compound was added to specimen chunk to stick the sample on it, and when the chunk is placed on cryobar, the compound became frozen. The slices were cut at thickness of 8 microns, anti-roll glass was used to prevent rolling of slices during cutting (Figure 2.9). Polysaline slides

(Thermofisher Scientific, UK) were used to adhere to the slices briefly after sectioning. Each glass slide was placed to air dry for 5 minutes before bringing it back to cutting chamber. Slides were either placed in acetone for 5 min at -20 ˚C just before staining procedure or directly stored at -80˚C for future staining.

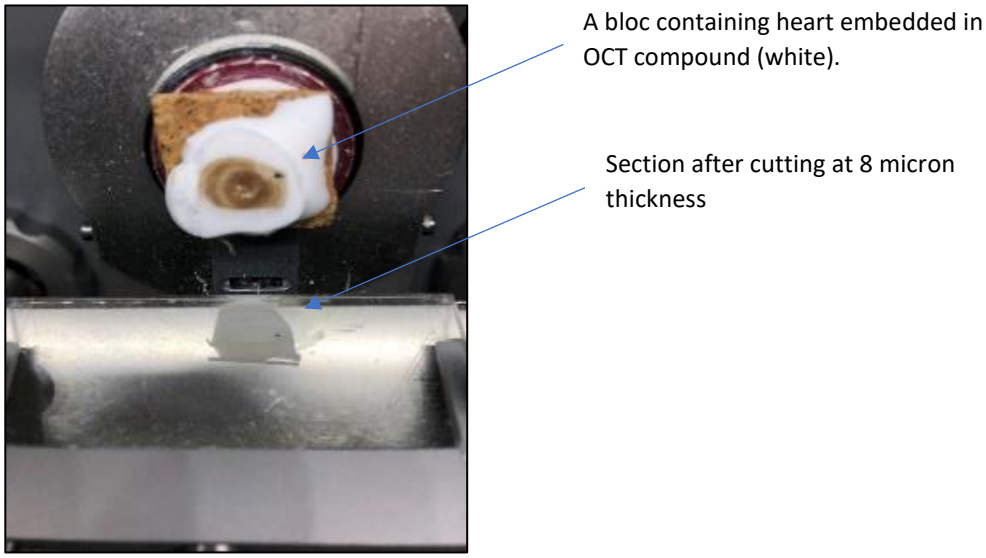

Figure 2.9 Cryosectioning of a rat heart in OCT compound. (own work)

2.4.4.1.2 pigs

Ventricular tissues were taken from left ventricle from both control and LAD groups. Samples were preserved in 4% paraformaldehyde solution at 4°C, for 24 hours and then transferred to PBS buffer to be washed and preserved until processing in tissue processor (ThermoFisher Scientific ExcelsiorTM AS Tissue Processor). Each sample was cut to appropriate size of cassette and placed in tissue processer for gradual dehydration using ethanol, substituting water content in tissues, to allow for paraffin infiltration. Samples were embedded in paraffin blocks using Thermo Scientific™ HistoStar™ Embedding Workstation. Metal moulds were used in embedding by adding a layer of paraffin wax, followed by placing the sample in the desired orientation for cutting, topped with another layer of paraffin and then the plastic cassette. The moulds were cooled before removing the solidified paraffin block.

Sectioning

Paraffin blocks were cooled on ice block, cardiac tissues were cut at 3-micron thickness using Thermo Scientific™ Shandon™ Finesse™ 325 Manual Microtome. Each section was placed in water path before it is placed into microscope slides (Superfrost, Thermo-scientific, UK) and left to dry in an oven at 37°C overnight.

Tissue preparation before staining

Rat slides prepared from cryosectioning were transferred on dry ice and placed in coplin jar and submerged with acetone solution for 5 minutes at -20 °C for further fixation. Then slides were transferred to PBS solution. At this stage, tissues are rehydrated and ready to start staining protocol.

Paraffin-embedded slides prepared from porcine hearts were rinsed with histoclear solutions before staining to dissolve wax and rehydrate tissues as listed in table 2.6.

Table 2.6 List of histoclear solutions and duration in preparation for staining.

Solution	Duration
Clearene 1	5 minutes
Clearene 2	5 minutes
Clearene 3	5 minutes
100 % industrial methylated spirits (IMS)	3 minutes
95 % IMS	3 minutes
70 % IMS	10 minutes
Distilled water	Until staining

Finally, once slides are in distilled water, they are ready for the staining protocol.

2.4.4.2 H&E Staining

Haemtoxylin is a basic dye used to stain acidic structures in the cells (e.g. DNA, RNA) in blue to purple colour, whereas its counterstain, eosin, stains basic acidophilic elements of the cells such as cytoplasm and proteins with pink (Titford 2005). H&E staining is especially helpful when studying architecture and organisation of cells within tissues. Figure 2.10 is a representative image of H&E stain of heart tissue.

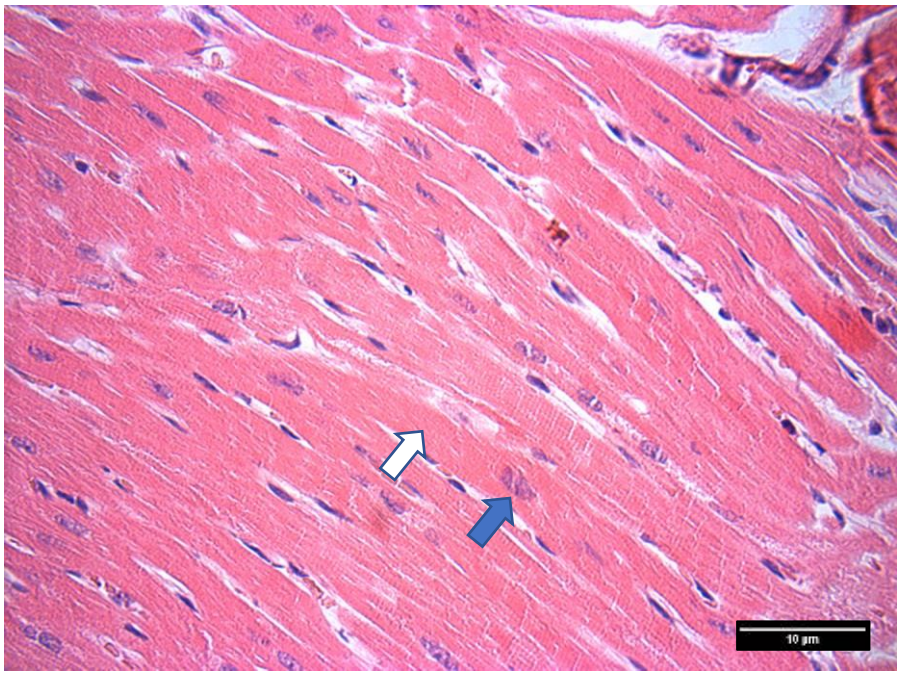

Figure 2.10 Representative mage of H&E stain from porcine heart. Scale bar set to 10 micron. Blue arrow (nucleus) and white arrow (cytoplasm). (own work)

Rehydrated slides (in water or PBS) are first stained with haematoxylin dye to stain nuclei in reddish-purple colour, which is enhanced by addition of weak alkaline. Then, eosin is added to stain different cellular components in pink. Porcine tissues were rinsed, dehydrated with alcohol and finally placed in clearene and mounted with Thermo Scientific™ DPX Mounting Media. A cover slip was placed to cover the specimen, and slides were dried in fume hood overnight.Rat tissues were airdried at the end of staining and then transferred into clearene and mounted in the same manner as porcine samples.

2.4.4.3 EVG Staining

EVG stain uses iron-haematoxylin compound to stain elastin, which is found in elastic fibres in dark purple. Van Gieson's stain, a counterstain, is used as contrast. The result of this stain is appearance of elastic fibres and nuclei with dark purple colour, collagen in red and other components in yellow or orange. EVG stain is used to study blood vessels since they are rich in elastic fibres. Figure 2.11 is a representative image of EVG stain from porcine heart.

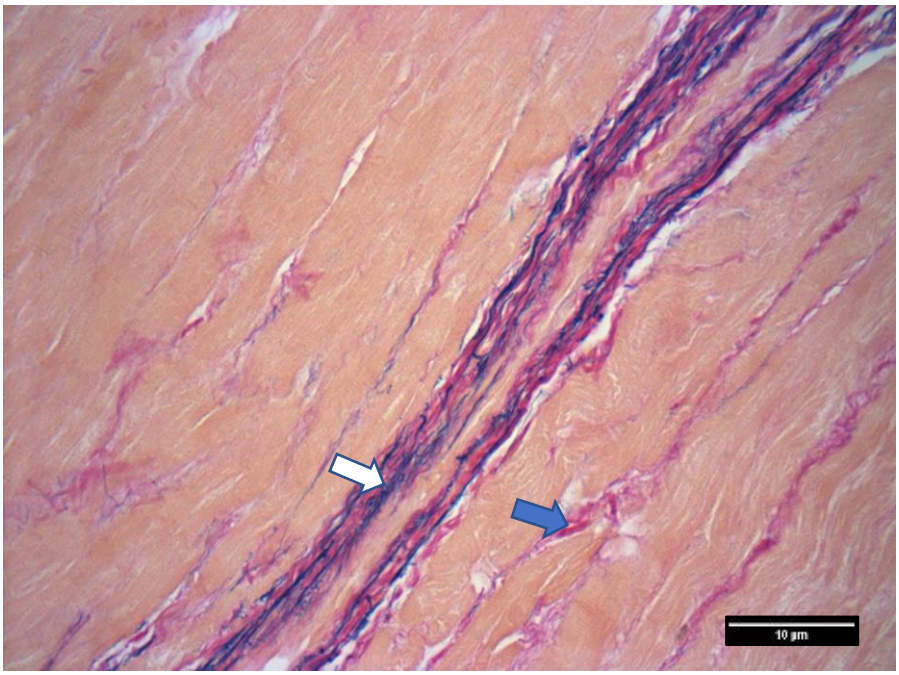

Figure 2.11 Representative image of EVG stain from porcine heart. Scale bar set to 10 micron. Blue arrow (collagen in pink) and white arrow (elastin in purple). (own work)

Rehydrated slides were transferred into 1% oxalic acid, rinsed in water. Slides were rinsed in 70% IMS and stained in Miller's stain for 1 hour. This was followed by another rinse in 70% IMS and water. Then they were stained with the counterstain, Van Gieson's stain, before rinsing and dehydration in alcohol (for porcine samples) and cleared in clearene and mounted with mounting media. Similarly, rodent samples were airdried and placed straight into clearene solution and mounted with Thermo Scientific™ DPX Mounting Media.

Auto staining

H&E and EVG staining were done using the auto-stainer (Thermo Scientific™ Varistain™ 24-4 Automatic Slide Stainer) which contains 24 compartments, 14 of which are used in the H&E staining, whereas 18 are used in the EVG staining. Running time for H&E and EVG staining were 51 min and 2 hours, respectively.

Rat samples were treated similar to porcine samples, with exception of acetone fixation before placing slides into machine, and no gradual hydration and dehydration steps occurred. After staining, slides were mounted with Thermo Scientific™ DPX Mounting Media and left to air-dry in hood.

2.4.4.4 Masson's Trichrome

This stain involves three colours to differentiate three components: Collagen in blue, nuclei in black and cytoplasm and muscle fibres in red. Massan's Trichrome is therefore used to study collagen fibres in skin and muscles, as seen in figure 2.12.

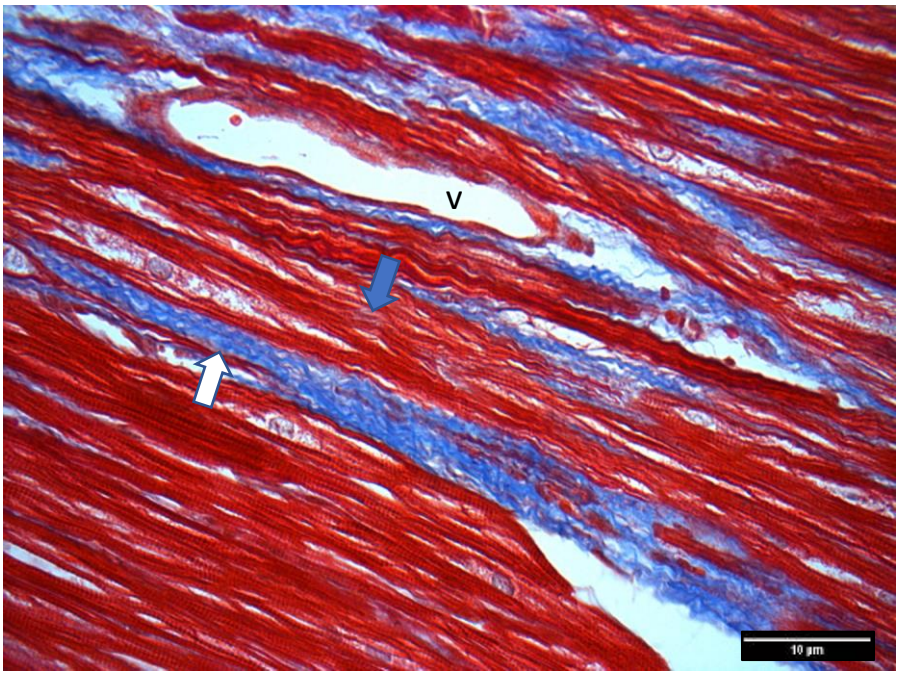

Figure 2.12 Representative image of Masson's trichrome stain from porcine heart. Scale bar set to 10 micron. Blue arrow (cytoplasm in red) and white arrow (collagen in blue), v; blood vessel. (own work)

For porcine samples, nuclei were first stained with Mayor's Haematoxylin for one minute, washed with running tap water for 10 minutes and rinsed in distilled water. Cardiomyocytes were stained with Biebrich scarlet acid fushsin solution (3 ml glacial acetic acid, 2.4 gm of Biebrish scarlet, 0.3 gm of acid fuchsin, and 300 ml distilled water) for 15 minutes, rinsed in distilled water followed by the differentiation step in phosphomolybdic-phosphotungstic acid solution (25 gm of 5% phosphomolybdic acid, 25 gm of 5% phosphotungstic acid, and 1000 ml distilled water) for another 15 minutes until the collagen appears colourless. Slides were placed in aniline blue solution (2.5 gm aniline blue, 1 ml glacial acetic acid, and 100 ml distilled water) for two minutes and in 1% acetic acid for 5 minutes. Finally, slides were dehydrated with 95% ethyl alcohol, and 100% ethyl alcohol, cleared quickly in xylene and mounted resinous medium.

Rat samples, however, had a different staining protocol. Masson's Trichrome stain was prepared by placing acetone-fixed slides in tap water first, then left in Wiegert's Iron haematoxylin (made up of equal volumes of Wiegert's A +B solutions) for 8 minutes. The slides were moved to tap water for blueing, and then, differentiation in 1% acid alcohol, followed by blueing in Scott's water and quick rinse in distilled water. The slides were stained in Masson's red solution for 30 seconds and rinsed in distilled water. They were treated in 1% phosphomolybdic acid for 2 minutes and rinsed again in distilled water. Colour intensity of the red stain was checked at this stage to confirm adequate staining of myocytes. Slides were placed quickly (less than 2 seconds) in 25% Masson's blue solution and rinsed immediately in distilled water, and finally 1% acetic acid for 1 minute. Slides were to air dry, then dehydrated and cleared in histoclear solutions before mounting with mounting medium.

2.4.4.5 Image acquisition and analysis

Image Procapture software 2.1 was used to acquire images for different sections of H&E, EVG and Masson's Trichrome stain under light microscope (Olympus BX40 Microscope and QImaging QICAM Fast 1394 digital camera).

Different magnification at 1.25, 4, 10, 20 and 100X were obtained using different microscopic lenses. Images were coded before analysis, and ImageJ software (Fiji) was used to adjust scale and colour threshold to quantify fibrosis and arteriolar wall thickness.

2.4.5 Electron Microscopy

2.4.5.1 Samples processing, embedding and sectioning

Left ventricular tissues from comparative groups (intervention and control or SHAM) in rodent and porcine hearts were sent to EM to study cellular ultrastructure and changes in mitochondrial morphometry in different subpopulations (subsarcolemmal, interfibrillar and perinuclear).

After perfusion with cardioplegia as described in section (2.3.3.1), tissues from rat were perfused with EM fixative solution (0.1 M phosphate buffer + 1% glutaraldehyde + 1% paraformaldehyde + 0.5 mM $CaCl_2$ and 1.7 mM D-glucose anhydrous) for 2-3 min at rate of 1ml/min. Then tissues were cut and placed in phosphate buffer (76.76 mM $HNa2O_4P$, 22.5 mM $NaH2PO_4.2H_2O$, and 100 ml distilled water; pH = 7.4) for an hour, then samples were washed and preserved in PBS buffer at 4°C, cut into small cubes before processing. Porcine tissues, however, were only preserved in 4% paraformaldehyde solution at 4°C, for 24 hours and then transferred into PBS buffer and cut into small cubes before EM processing. This fixation process is not normally used for EM, however, it was adopted to overcome technical issues with EM perfusion in porcine hearts.

2.4.5.2 Tissue processing

Porcine and rodent fixed heart samples were sent for processing at Wolfson Bioimaging facility, University of Bristol by Gini Tilly. Hearts were placed in 1 % (w/v) OsO_4 in phosphate buffer for 90 min for post-fixation. This was followed by a wash in phosphate buffer (3 times, 10 minutes each) and distilled water. Samples were stained in 3 % (w/v) uranyl acetate in distilled water for 30 min in dark room, followed by rinse in distilled water for 10 minutes. Samples were dehydrated in 70%, 80% and 90% ethanol for 10 minutes in each solution, then rinsed in propylene oxide (3 times, 10 minutes each) before storage in sealed container overnight. Tissues were preserved in EPON epoxy resin for 24 hours, followed by embedding in EPON epoxy resin and polymerise at 60 °C for 48-72 hours. Finally, tissues were cut into different blocks and stained finally with uranyl acetate and lead citrate (94 mM lead nitrate, 140 mM sodium citrate and 0.19 mM NaOH).

2.4.5.3 Image acquisition

The EM sections were examined and captured with a Tecnai 12 bioTWIN transmission electron microscope (EI, Netherlands) using Eagle 4K x 4K CCD camera as seen in figure 2.13.

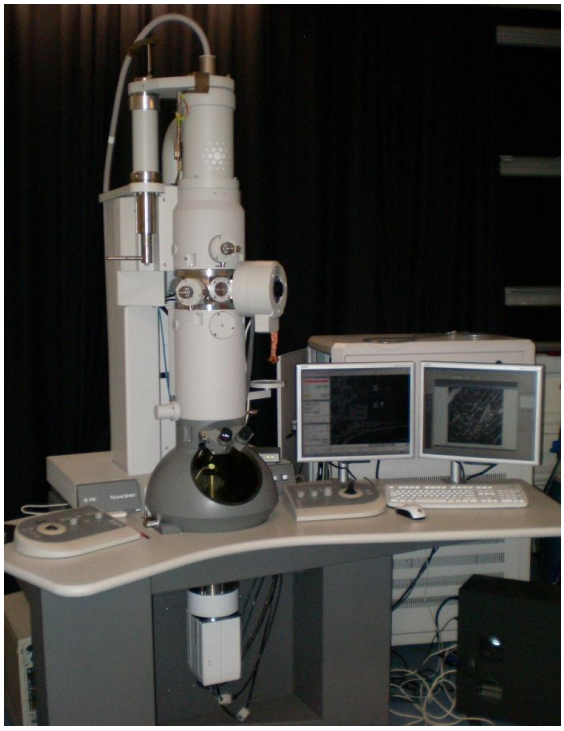

Figure 2.13 An image of T12 electron microscope. CCD = charge-coupled device. From(Littlejohns, University of et al. 2013)

2.4.5.4 Data Analysis

The obtained images were used to measure sarcomere length (micron), mitochondrial morphometry (length, width, perimeter), area and circularity, and aspect ratio (length: width) using ImageJ software.

IBM SPSS software was used to analyse different measurements using student's t-test and compare between the control (or SHAM) and LAD group. One-way anova was used to compare between different mitochondrial subtypes within one group. Level of significance was set to $p < 0.05$.

2.6 Patients protocol and requirements for metabolomics study

As explained in chapter 1, metabolomics is a relatively new omic application with great potential of identifying biomarkers of disease. Progression from acute cardiac injury following interventions (e.g., PPCI) to heart failure involves gradual remodelling (e.g., metabolic, molecular and structural) in infarcted and non-infarcted areas of the heart with inflammatory response (adaptive and innate) playing a central role in remodelling. These changes are likely to be reflected in changes in blood metabolites of patients which will reflect different steps of remodelling from acute (ischaemia/reperfusion) to chronic stage (heart failure). However, despite intense recent work involving measuring the metabolome, this has produced very little to identify early biomarker associated with progression to heart failure. Heterogeneity of patients including those with co-morbidities that a metabolic impact (diabetes, kidney disease, etc.) is likely to be responsible.

The proposed pilot study aims to monitor alterations in the blood metabolome of STEMI patients (n=30) with no major associated disease that would impact upon the metabolome (e.g., diabetes, disease of the kidney, liver and peripheral vasculature). This will ensure the blood metabolome (acutely and chronically) will largely reflect the changes associated with cardiac remodelling. This project intends to assess changes and variations of left ventricular function and cardiac remodelling among STEMI patients using echocardiography soon after in-hospital treatment with Primary Percutaneous Coronary Intervention (PPCI) and 4-6 weeks later. Blood metabolome will be measured and detected with NMR and High-Performance Liquid Chromatography, which are available at the University of Bristol.

This preliminary study will identify metabolite(s) that correlate/predict the inflammatory response and progression to heart failure. The biomarker(s) are likely to be linked mostly to cardiac changes. The next step will expand on this by monitoring the identified metabolites in different populations of patients with different co-morbidities and characteristics. The trial will include more collection of samples, MRI will be deployed to monitor cardiac function to identify relationships between biomarkers and disease progression in patients with different co-morbidities.

Study design

The proposed pilot study will measure the blood metabolome in patients undergoing emergency PCI for STEMI at the time of presentation, 48 hours as part of routine standard clinical treatment, and 4-6 weeks later to assess remodelling and functional parameters. Additionally, cardiac function will be assessed at these intervals using echocardiography. Apart from blood collection during the chronic stage, all steps are part of current standard clinical care treatment in cardiac coronary care. The data will be collected over a 12months duration. In order to obtain a normal metabolome for reference, blood will be collected from age matched normal subject.

Study Population

This pilot study will include adult patients undergoing emergency PCI for STEMI resulting from left main coronary artery. Patients having any of the following will be excluded: diabetes mellitus; chronic kidney disease; lung

disease; previous MI; previous PCI; previous CABG; hypertension; peripheral vascular disease; cerebrovascular disease; valvular heart disease; heart failure.

The obtained data will be analysed to look for any correlation between certain metabolomic profiles and degree of left ventricular dysfunction. If any biomarkers are identified this could be used to help risk stratify patients at risk of adverse remodelling and heart failure with reduced ejection fraction. Information gained will be used to design interventions to prevent adverse remodelling and cardiac fibrosis which is associated with high rates of morbidity and mortality. Copy of full protocol, including eligibility criteria and requirement, and ethics application is included in the appendix, submitted by Dr. Georgia May Connolly and study team.

Chapter 3

Post ischaemic cardiac remodelling in rat model of LAD coronary artery ligation

3.1 Introduction

3.1.1 Overview

The use of rodents as preclinical model to study ischaemic heart diseases has been established for a long time using a variety of surgical and non-surgical methods. Bagdon et al first developed a non-surgical chemical intervention to induce MI in rat heart through sequential subcutaneous administration of isoproterenol, a non-selective β adrenoreceptor agonist (Zbinden and Bagdon 1963). Others have used cauterisation applied to apical epicardium create focal lesions of necrosis (Adler, Camin et al. 1976), however, the most common and widely accepted technique is coronary artery ligation, to induce regional myocardial necrosis in a rat heart, which was first introduced by Pfeffer et al in 1979.

Pfeffer group used left anterior descending coronary artery ligation procedure to investigate the relationship between infarct size and ventricular performance, and the role of captopril, an angiotensin-converting enzyme inhibitor, in modulating the course of LV remodelling in hearts with medium to large infarcts (Pfeffer, Pfeffer et al. 1979). This work established a foundation for several modified versions of the technique (for example, no heart exteriorisation, temporary instead of permanent coronary artery ligation) that are still used today as a classical model of MI in rodents. This procedure can be coupled with electrocardiography (ECG) and echocardiography, as a validation of the cardiac injury instantly, and to assess LV functional parameters and remodelling. It important to take in consideration that all these mentioned models involve normal hearts. Alternatively, other studies have used transgenic mice, particularly those fed high-fat diet, as they showed evidence of atherosclerosis and myocardial infarction (Chase 2007). However, these mice also have limitations, including uncertainty regarding onset of infarction. Although these techniques are extensively employed to evaluate and determine effectiveness of various cardioprotective therapeutic interventions, it must be noted that each has its own drawbacks and limitations, all of which must be considered carefully as attempts to mimic and study cardiovascular diseases (Patten and Hall-Porter 2009).

3.1.2 Integrated studies in small animal models of myocardial infarction

Ischaemic heart disease has complex and inherent nature that involves crosstalk of multiple underlying mechanisms. Therefore, employment of system biology studies (including -omics studies) to trace imminent or consequent changes in the hearts during ischaemia and/or ischaemia reperfusion injury, both in clinical and animal models, provides wider and more inclusive prospects. The data obtained systemically using -omics technologies from several molecular levels at different time points could be collectively integrated to establish the major cellular pathways that result in substantial alterations in cardiac function and structure after acute myocardial injury.

Whilst some studies focused on specific pathophysiological aspects involved in myocardial damage such as inflammation and fibrosis (Frantz, Bauersachs et al. 2009, Prabhu and Frangogiannis 2016, Talman and Ruskoaho

2016), oxidative stress (Byrne, Grieve et al. 2003, Grieve and Shah 2003) and microvascular obstruction (Hamirani, Wong et al. 2014, Yu, Kalogeris et al. 2019) as disease modifying targets, others have used proteomic-metabolomic studies to identify possible mechanisms implicated in acute MI (White, Cordwell et al. 2005, Kim, Lee et al. 2006, Basak, Varshney et al. 2015). For example, Bai et al found significant perturbation in certain myocardial metabolic pathways such as lipid and amino acid metabolism, as well as proteins involved in vascular smooth muscle contraction and gap junction signalling, as measured from rat hearts 24 hours after LAD coronary artery ligation procedure (Bai, Sun et al. 2020). White et al reported marked upregulation in many functional protein groups, notably stress response proteins (Heat Shock Protein 27 kDa, Alpha B-Crystallin) and redox regulatory proteins (e.g. NADH Ubiquinone Oxidoreductase proteins) using isolated and perfused rabbit heart model of ischaemia reperfusion injury (White, Cordwell et al. 2005). Others have conducted metabolomics study in mice 8 weeks after MI, and demonstrated a decrease in metabolites related to lipid and energy metabolism, and an increase in indices of oxidative stress, such as oxidised glutathione (Sansbury, DeMartino et al. 2014). Nonetheless, a comprehensive approach that involves integration of -omics technologies with the observed alterations at the cellular and subcellular levels, such as mitochondria, to investigate and characterise the ongoing post ischaemic cardiac remodelling weeks after MI is highly needed.

Therefore, chapter 3 aims to characterise modifications resulted from chronic MI-induced cardiac remodelling in rat model following LAD coronary artery ligation in the myocardium and blood. Molecular changes manifested as altered expression in cardiac proteomics and phosphoproteomis, integrated with cardiac and systemic metabolomics, in addition to assessment of cardiac cellular and subcellular components, were all presented to provide novel mechanistic aspects that could be translated as potential therapeutic targets to prevent adverse cardiac remodelling in clinically relevant settings.

3.2 Methods

The techniques and methods used in this chapter are fully described in materials and methods chapter (chapter 2). In summary, 10 Wistar male rats (Charles River), weighing from 220 to 240 g, were used in this study. The animals were divided into SHAM or LAD group (n=5 per group). Additionally, a separate group of Wistar Rats (n=4) had also LAD coronary artery ligation surgery and were only used for collecting blood and histology samples. These were carried out by Dr. Erin Callaghan (Bristol Medical School).

3.2.1 Experimental procedure

Details of surgery and anaesthesia are mentioned in detail in section (2.3.1). Briefly, after adjusting the dose to rat total body wight, induction of anaesthetise was achieved with intraperotineal injection of medetomidine and ketamine, while buprenorphine was used to maintain analgesia throughout the procedure. After intubation and ventilation with a respirator, rats body temperature was kept at 37 °C throughout the surgery and during recovery. Left longitudinal parasternal thoracotomy incision was made, and for LAD group, a suture was used to occlude LAD coronary artery. Whereas in SHAM operated rats, no LAD coronary artery occlusion occurred. The surgical wound was closed, and the rats were injected with atipamezole, placed in a chamber for recovery afterward and monitored closely for 2 hours. All operated animals survived after the surgery and kept under daily close monitoring and observation at Animal Services Unit, University of Bristol for four weeks after.

3.2.1.1 Heart extraction and perfusion

Four weeks after surgery, SHAM and LAD rats (n=5) were culled according to Schedule 1 by stunning and cervical dislocation. Hearts were extracted and immediately immersed into ice cold KH buffer. Hearts were cannulated into Langendorff apparatus and perfused with KH buffer for 5 minutes, followed by cardioplegia solution for another 5 minutes. Tissues from apex, right and left atrium were collected and immediately snap frozen in liquid nitrogen for storage at -80 °C. Perfusion was then switched to EM fixative solution for 4 minutes.

For the additional group of LAD rats, blood samples were obtained using tail cannulation prior to surgery, and 4 weeks after ligation, just before termination. Blood samples were collected into EDTA tubes kept on ice until centrifugation at 1000 g for 10 minutes. The resultant plasma was collected into 0.5 ml Eppendorf tubes and stored at -80 °C. Extracted hearts were submerged in PBS/EDTA solution prepared for OCT embedding for histology.

3.2.2 Liquid Chromatography Tandem Mass Spectrometry (LC-MS/MS)

Apical myocardial tissues from both group (n=5) were homogenised for protein extraction in RIPA buffer with protease and phosphatase inhibitors, followed by quantification using Bradford essay, and then the extracted samples were sent for Proteomics facility at University of Bristol, to be analysed using Liquid Chromatography

Tandem Mass Spectrometry (LC-MS/MS) to detect changes in proteins and phosphoproteins as described in detail in section (2.4.1).

3.2.3 High Performance Liquid Chromatography (HPLC)

Apical, right and left atrial tissues from both group (n=5) were crushed with pestle and mortar for metabolites extraction using PCA and neutralised with K_2CO_3. The tissue extract was sent for HPLC analysis to determine cardiac energetics in apex, left and right atria from each group as described in section (2.4.2).

3.2.4 Nuclear Magnetic Resonance (NMR)

Blood samples taken from rats prior to surgery and 4 weeks after LAD coronary artery ligation were collected into EDTA tubes, centrifuged at 1000 g for 10 minutes, and the plasma was transferred into Eppendorf tubes and stored in -80 °C freezer until later use. Plasma samples and tissue extracts (section 2.3.3.1) were then transferred to School of Chemistry, University of Bristol on dry ice for blood metabolites analysis using Nuclear Magnetic Resonance spectroscopy (NMR). Full method is described in section (2.4.3).

Spike-in experiment

Spike-in experiment of acetone and arginine involves injecting a small of pure metabolite sample into plasma and re-running NMR spectra. Overlapping of the spiked sample signal with the original un-spiked one at the exact chemical shift (ppm) confirms the presence of the metabolite(s). Therefore, 1.25 mM acetone and 2 mM Arginine in PBS buffer were injected separately into a pooled sample of rat plasma. Spectra of original plasma were first acquired using 700 MHz spectrometer. Then the spectra of metabolites in PBS buffer were recorded and compared against the spectra of plasma and metabolites mixture.

3.2.5 Light Microscopy

Heart tissues from LAD rats (n=4) and a group of control from healthy adult rats (n=4) were fixed and OCT embedded and prepared for cryosectioning, and staining with H&E, EVG and Masson's trichrome. Full details regarding these techniques are found in section (2.4.4).

3.2.6 Electron Microscopy

Left ventricular tissues from SHAM and LAD rats (n=5) were fixed with EM fixative solution and sent for Wolfson Bioimaging facility for processing, EPON epoxy resin embedding, sectioning, and staining with uranyl acetate and lead citrate to study post ischaemic cardiac remodelling at ultrastructural structural level. Full details regarding these techniques are found in section (2.4.5).

3.3 Results

3.3.1 Effect of LAD coronary artery ligation on gross rodent cardiac morphology

Hearts extracted from rats in SHAM and LAD groups were perfused in the Langendorff mode to flush out blood and restore physiological condition prior to tissue collection and storage. Unlike SHAM group, hearts in LAD group exhibit a remarkable whitish scar area distal to surgical tie site (figure 3.1).

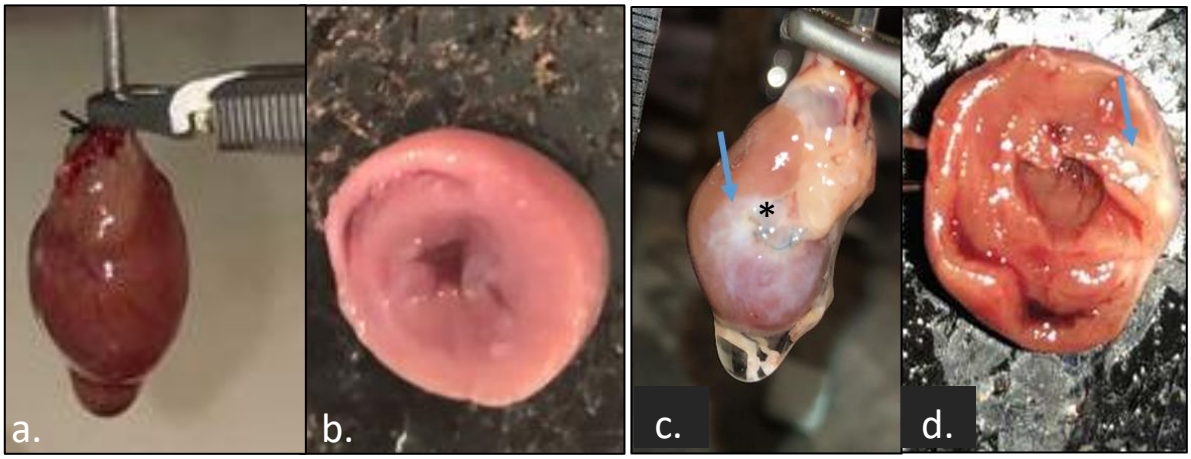

Figure 3.1 Extracted SHAM and LAD hearts. a. A representative SHAM heart in Langendorff perfusion. b. A cross-section of SHAM heart at the end of perfusion. c. LAD heart in Langendorff perfusion, asterisk indicates position of surgical knot. d. LAD heart cross-section. Blue arrows in (c. and d.) indicate the regional infarcted area.

Masson trichrome staining was used as a conventional method to establish a solid histological evidence of the infarcted scarred myocardium four weeks after LAD coronary artery ligation as represented in figure 3.2.

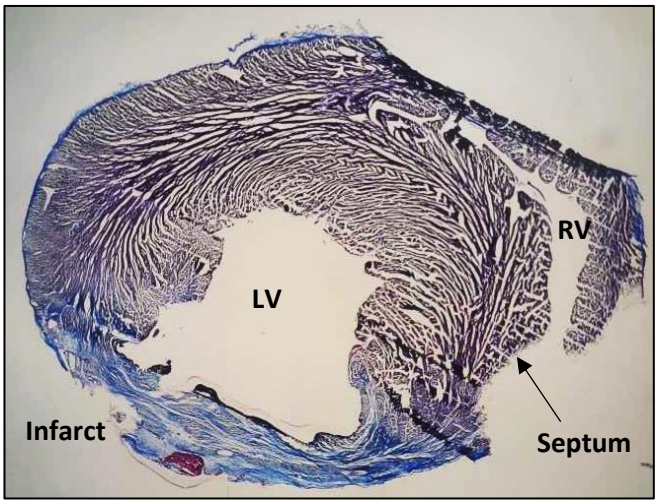

Figure 3.2 Representative section of Masson's Trichrome staining of LAD heart. Transverse section of a representative LAD coronary artery ligated heart stained with Masson's trichrome stain. Collagen dense scar, located in the infarcted free wall of left ventricle, appears in blue. LV left ventricle. RV right ventricle. image was taken with objective lens magnification x1.25.

3.3.1.1 Effect of LAD coronary artery ligation on distribution of cardiac fibrosis

For detailed microscopic examination, three distinct areas from LAD hearts (infarct, border zone and remote) were selected based on Masson trichrome stain (figure 3.3). Four weeks post infarction, the infarct area demonstrates a pattern of compact fibrosis, characterised by its collagen dense disruption and scarcity of cardiomyocytes. In the border zone, however, cardiomyocytes were interspersed with blue collagen septa (i.e., diffuse fibrosis). Remote area shows bundles of cardiomyocytes with little to no fibrosis. This stain was also used to quantify the percentage of fibrous tissue in both groups from multiple cardiac sections as shown in figure 3.4. There was significant increase in fibrosis in LAD hearts compared to control (28.2% vs. 1.8%, p <0.01).

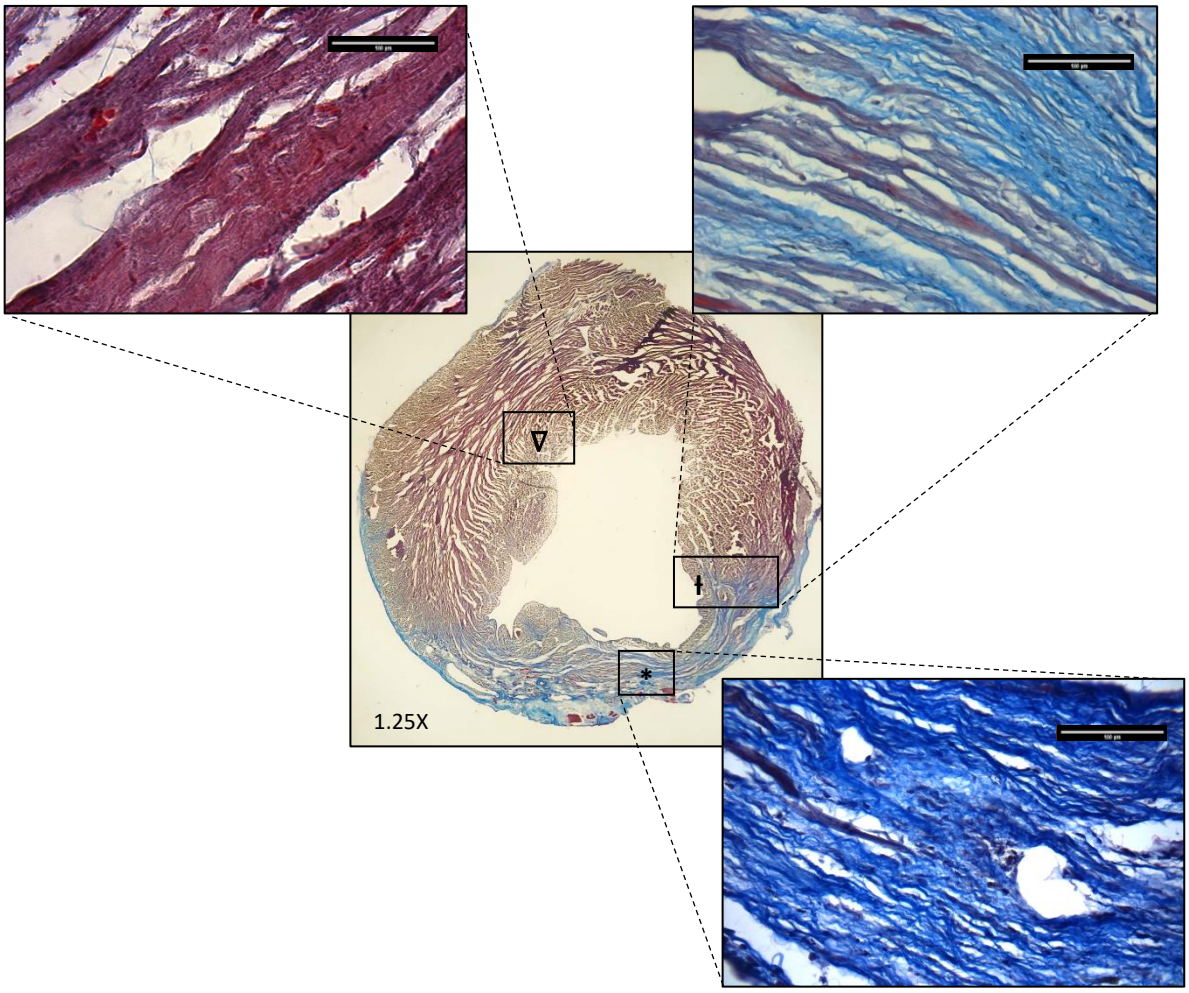

Figure3.3 Masson's trichrome staining of infarct, border zone and remote areas. Three areas in the LAD heart were selected and demarcated using Masson's trichrome stain into infarct (*), border zone (ɬ) and remote (∇). Central image was taken with objective lens magnification x1.25, and the rest with x40. Scale bar set to 100 microns.

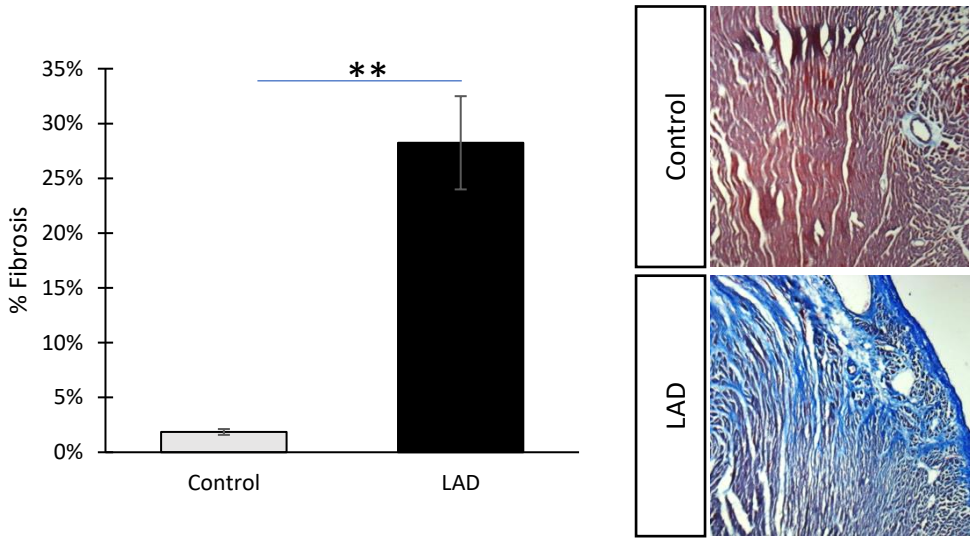

Figure 3.4 Percentage of fibrosis in control and LAD groups. Quantification of cardiac fibrosis was performed from serial cross-section from LAD and control groups. Data were analysed using unpaired student's t-test and presented as mean percentages (SEM). ** p< 0.01, n=4

3.3.1.2 Effect of LAD coronary artery ligation on elastin deposition and arteriolar wall thickness

EVG staining was used to identify elastin fibres (purple), collagen (red) in contrast to cardiomyocytes, which are stained in orange, as seen in figure 3.5. In control hearts, elastin is found in the elastic layer that connects intima to media in small arteries and arterioles. The outer layer (adventitia) is surrounded by a collagen rich matrix with occasional fibroblasts. However, infarct areas 4 weeks after LAD coronary artery ligation appear to include widespread discrete of elastin fibres bundles, in addition to collagen. Border zone exhibits interspersed collagen (diffuse fibrosis) with elastic fibres confined to the wall of arterioles, whilst no similar pattern was observed in the remote area.

EVG stain was used to detect differences in the arterial wall thickness of medium to small arterioles (20-200 micron in diameter) in infarcted area of LAD group against the control. There was significant increase in the ratio of total arteriolar wall area to total arteriolar area in LAD group, indicating an increased thickening of arteriolar wall as seen in figure 3.6.

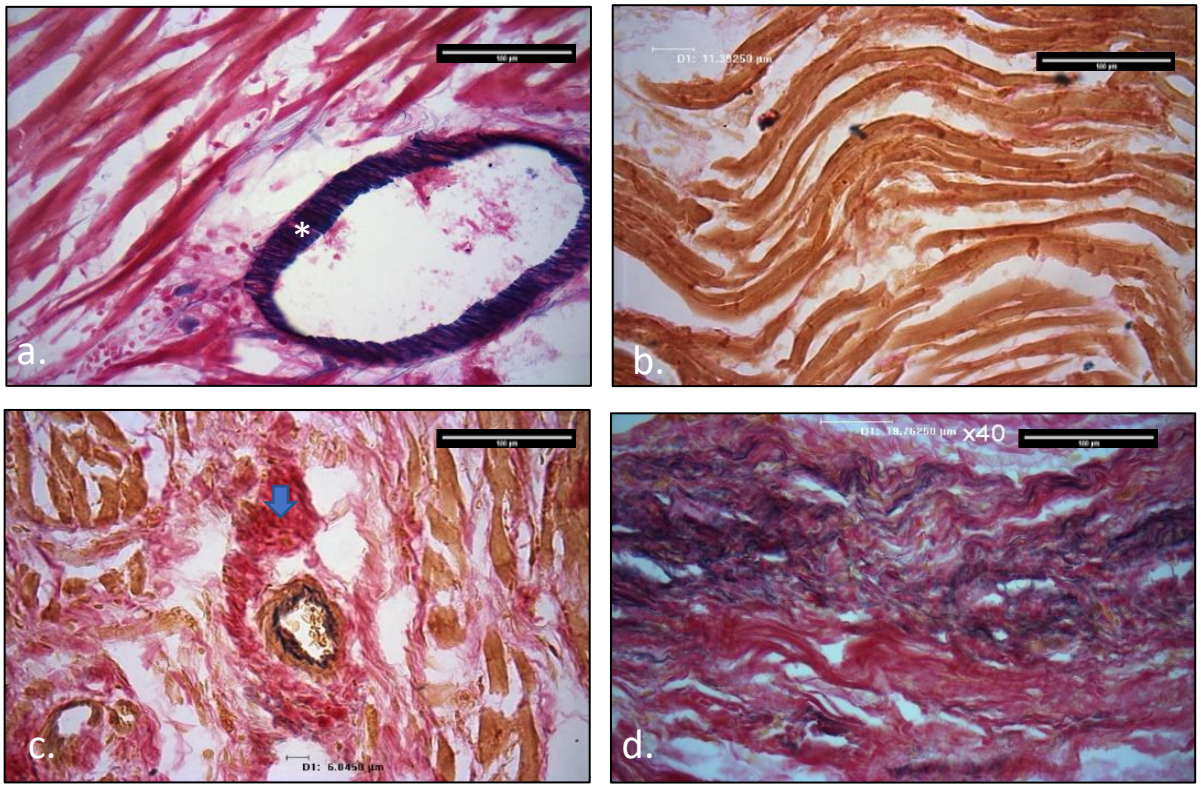

Figure 3.5 Representative EVG staining of control and LAD heart sections. a. Control heart, b. remote area, **c.** border zone and d. infarct area. Elastin is stained in purple (white asterisks in a), collagen in red (blue arrow in c), and cardiomyocytes in orange. Images were taken with objective lens magnification x40. Scale bar set to 100 microns.

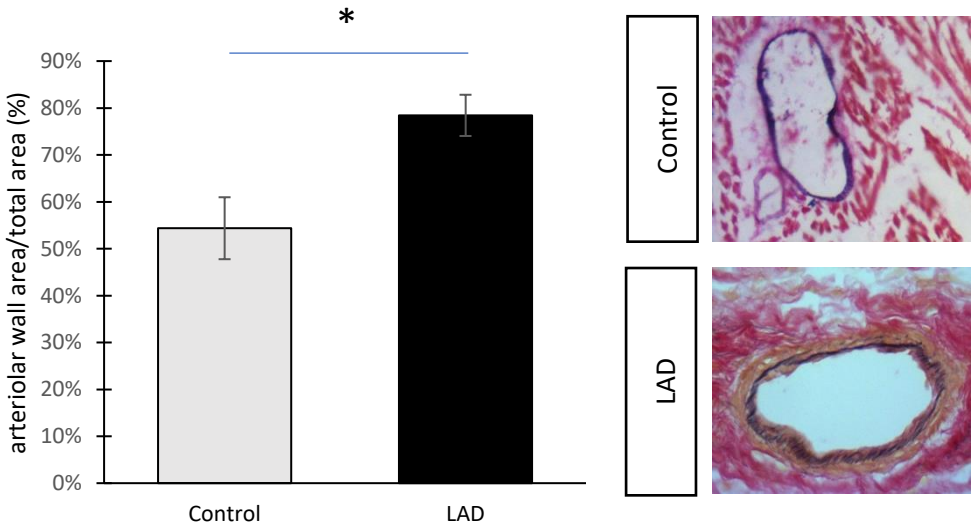

Figure 3.6 Percentage of arteriolar wall area to total arteriolar area. Percentage of artery wall area to total artery area was measured for each group, 3-4 fields were examined for each heart. Data were analysed using unpaired student's t-test and presented as mean percentages (SEM). * $p < 0.05$, n=4.

3.3.1.3 Effect of LAD coronary artery ligation on cardiac cellular infiltration

Haematoxylin &Eosin staining is used to differentiate the eosinophilic cytoplasm, which is stained in dark pink, from nuclei (blue) as shown in figure 3.7. Massive cellular infiltration is observed in the collagen dense matrix in infarct area of LAD hearts, and to a lesser extent, in the border zone. Control hearts show clear bundles of cardiomyocytes without cellular infiltration, similar appearance is noted for the remote area of LAD hearts.

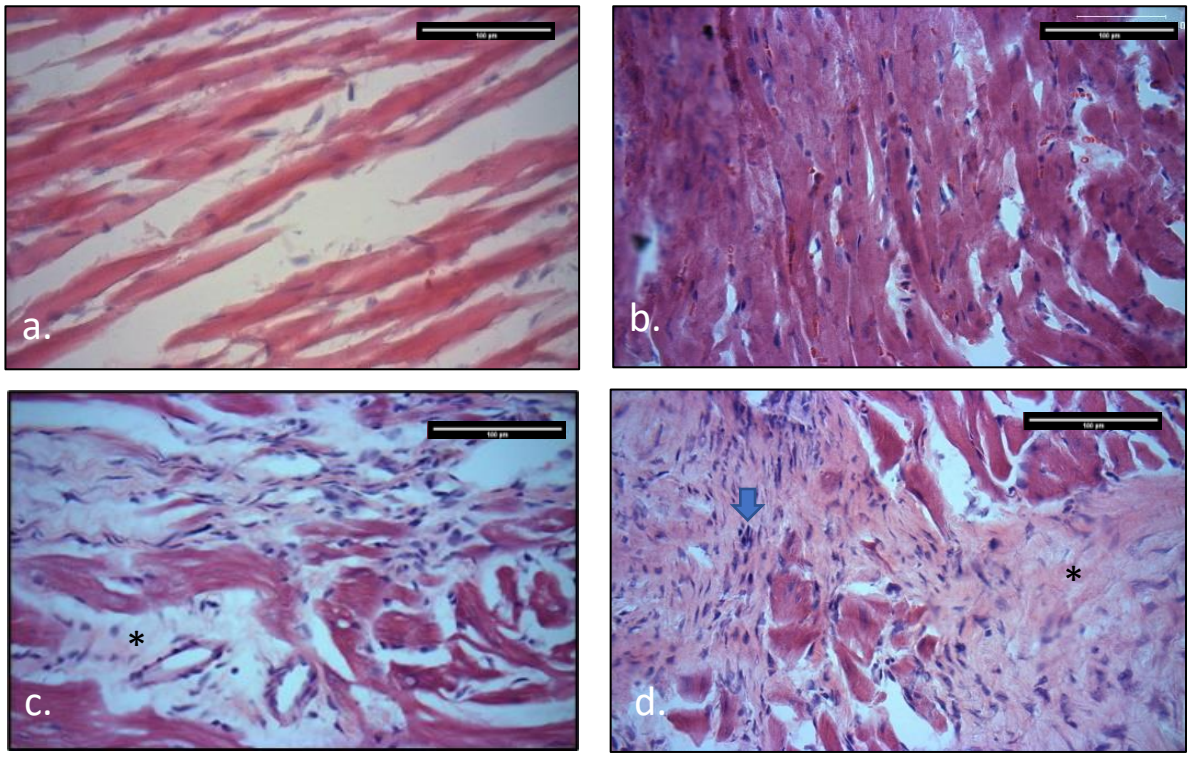

Figure 3.7 Representative H&E staining of control and LAD heart sections. a. control heart, b. remote area, **c.** border zone and d. infarct area. Cytoplasm is stained in dark pink, collagen in light pink (asterisks in c and d), and nuclei in blue (blue arrow in d). Images were taken with objective lens magnification x40. Scale bar set to 100 microns.

3.3.2 Effect of LAD coronary artery ligation on rodent cardiac ultrastructure

Transmission electron microscopy imagining (FEI TecnaiTM 12) was used to analyse structural differences observed in the infarct area of LAD hearts compared to SHAM hearts, 4 weeks after procedure. Measurements of mitochondrial morphology, distribution, cristae density and sarcomere length, along with characterisation and detection of the various elements of the interstitial architecture were performed.

Figures 3.8- 3.10 are representative examples of infarcted areas taken from LAD heart. Numerous fibroblasts, and few myofibroblast, as well as endothelial cells, are scattered in the collagen-rich matrix. Telopodes, characteristic structures of telocytes, were observed in close proximity to the sarcolemma.

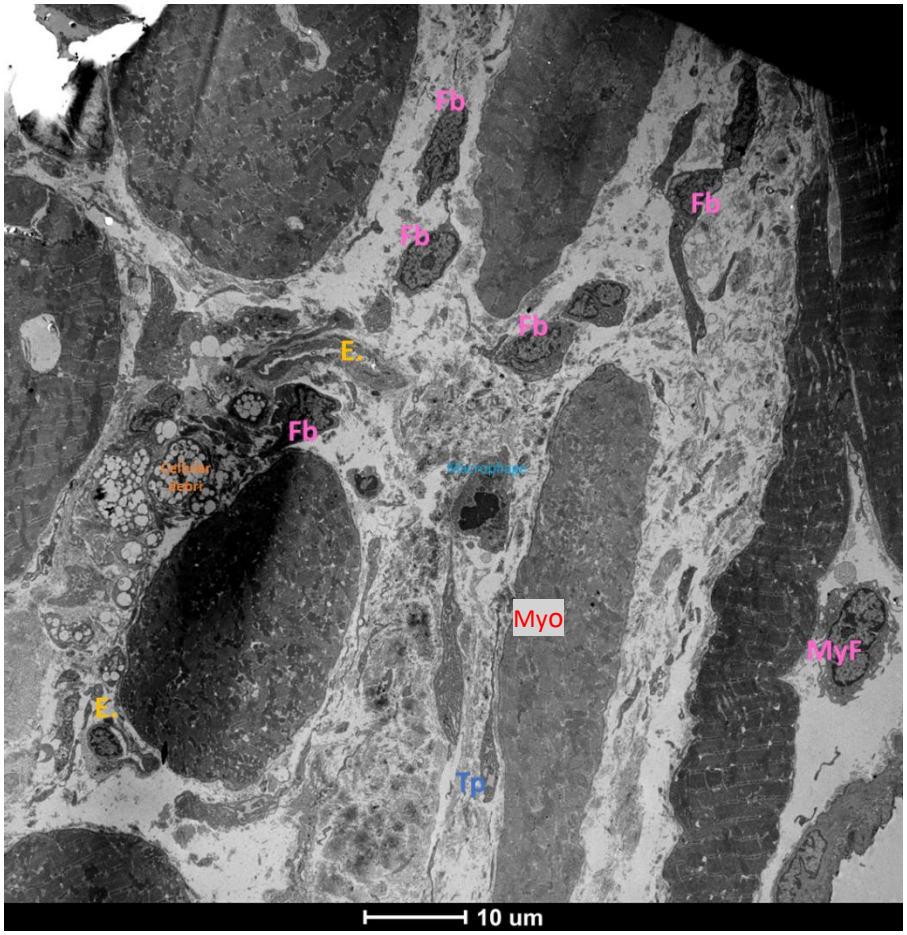

Figure 3.8 TEM micrograph from a representative LAD ligated left ventricle. E. endothelial cell, cl. Collagen, MyF myofibroblast, Fb, fibroblast, Tp, telopode, Myo, cadriomyocyte

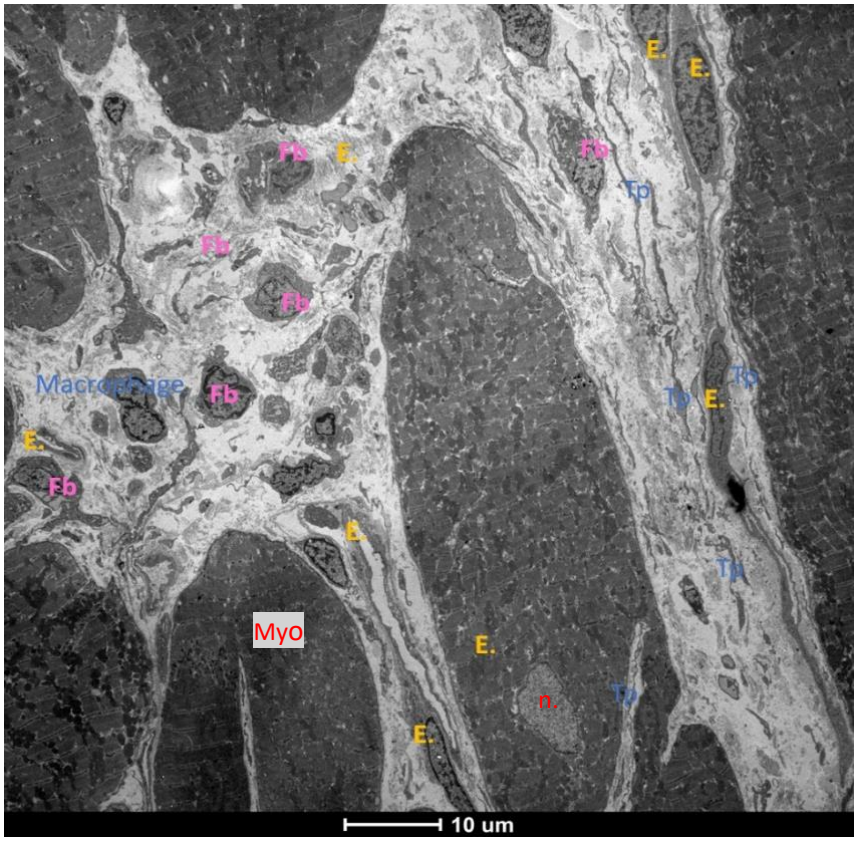

A

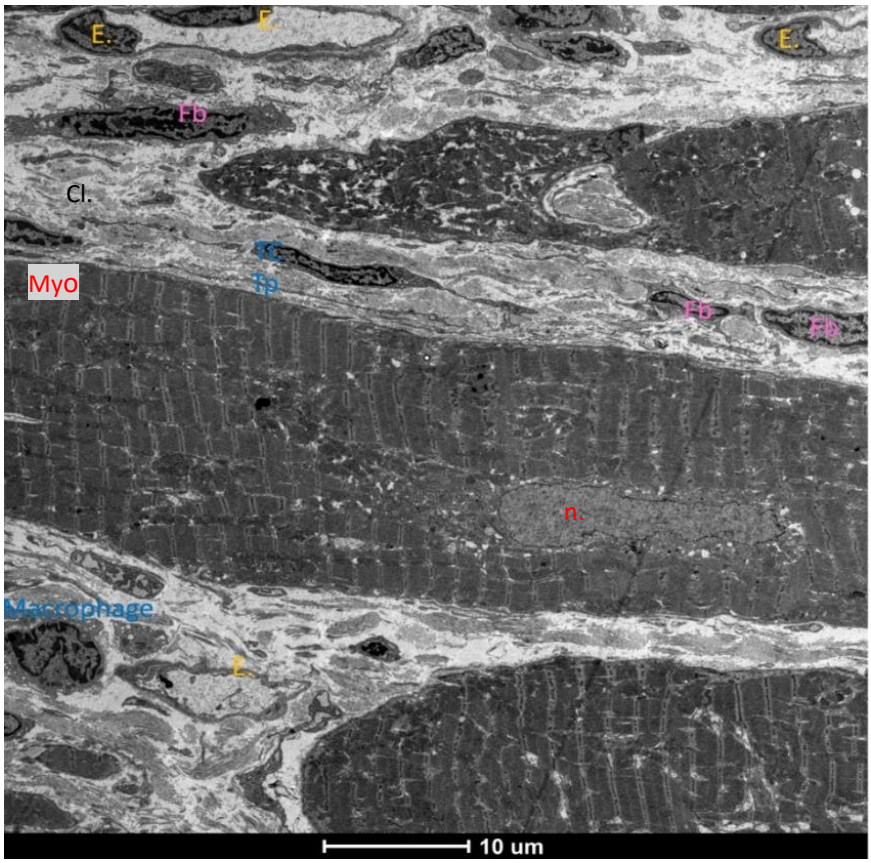

B

Figure 3.9 A and B: Distribution of matrix cellular components in between cardiomyocytes in from representative LAD hearts. E. endothelial cell, cl. Collagen, MyF myofibroblast, Fb, fibroblast, TC, telocyte, Tp, telopode, Myo, cardiomyocyte, n. nucleus.

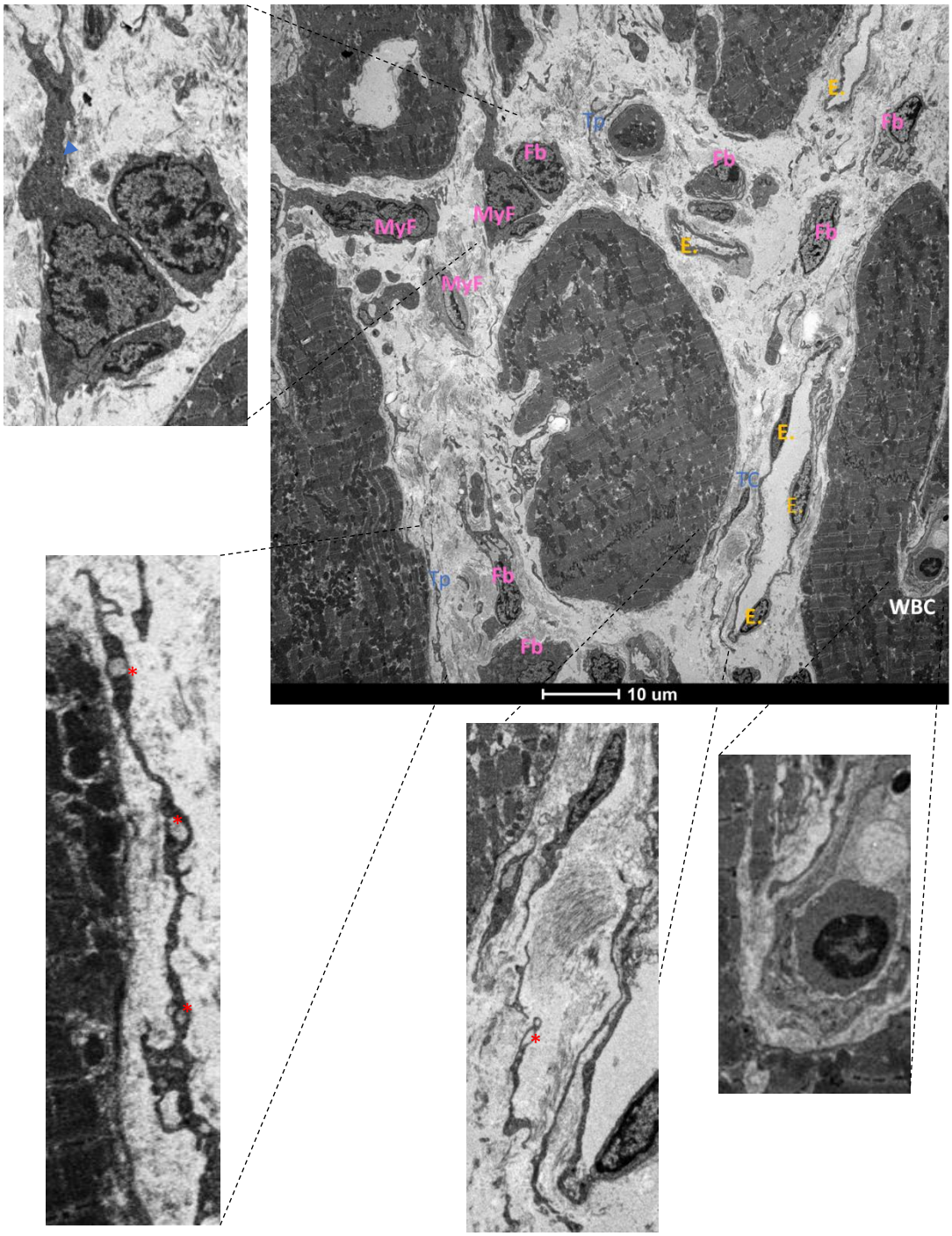

Figure 3.10 TEM micrographs of white blood cell, telocyte and fibroblasts in LAD ligated left ventricle. E. endothelial cell, MyF myofibroblast, Fb, fibroblast, Tp, telopode, WBC, white blood cell. Blue arrow heads pointed to stress fibers in myofiberoblast, red asterisks vacuolations in telopodes.

3.3.2.1 Mitochondrial cristae density, subpopulation distribution and morphometry

Based on their location and distribution, there are three subpopulations of mitochondria in cardiomyocytes: Interfibrillar (IF), subsarcolemmal (SS) and perinuclear (PN). First, cardiomyocytes total area was measured for each group (figure 3.11A), and then the distribution of each subpopulation was measured and compared for both groups, as shown in figure 3.11B. Cardiomyocytes in LAD group had slightly insignificant increase in total area. Interfibrillar mitochondrial distribution tend to be decreased in LAD group ($p > 0.05$), and other subpopulations did not significantly differ from SHAM.

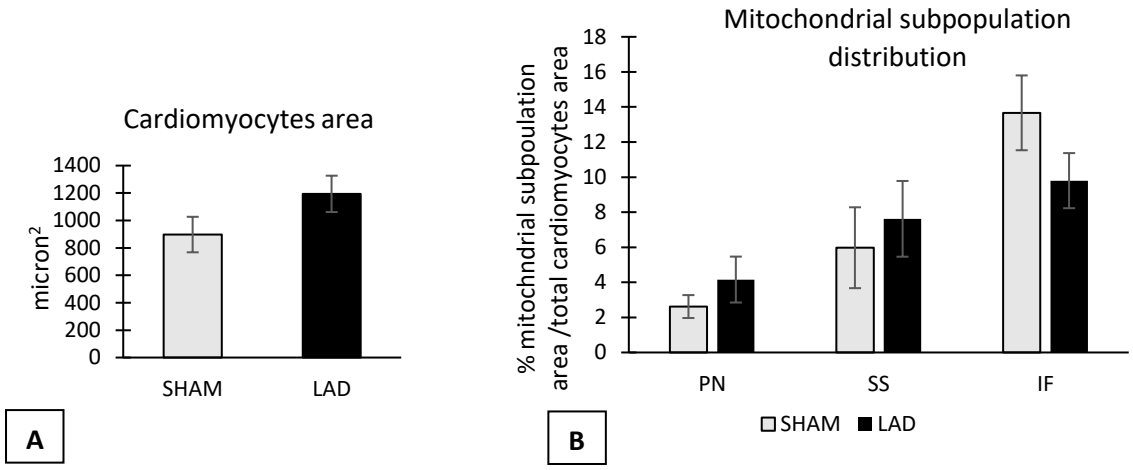

Figure 3.11 Mitochondrial distribution in rats A) Average cardiomyocyte area in each group, 3-4 fields containing longitudinal cardiomyocytes were examined for each heart. B) Percentage of mitochondrial subpopulations areas to total cardiomyocytes area. Mitochondrial subpopulation area that occupies selected area within cardiomyocyte was measured, and the ratio was calculated to total cardiomyocyte area. Data are presented as mean ± SEM, and analysed using unpaired student's t-test. n=5. IF interfibrillar, PN perinuclear and SS subsarcolemmal.

Mitochondrial cristae density, which is inversely correlated to the ratio of intercristae space to the mitochondrion area, reflects the degree of cristae separation and mitochondrial swelling, was analysed for each group. In LAD group, there was significant increase in ratio of intercristae space area to total mitochondrial area compared to SHAM, reflecting a decrease in mitochondrial cristae density as seen in figure 3.12.

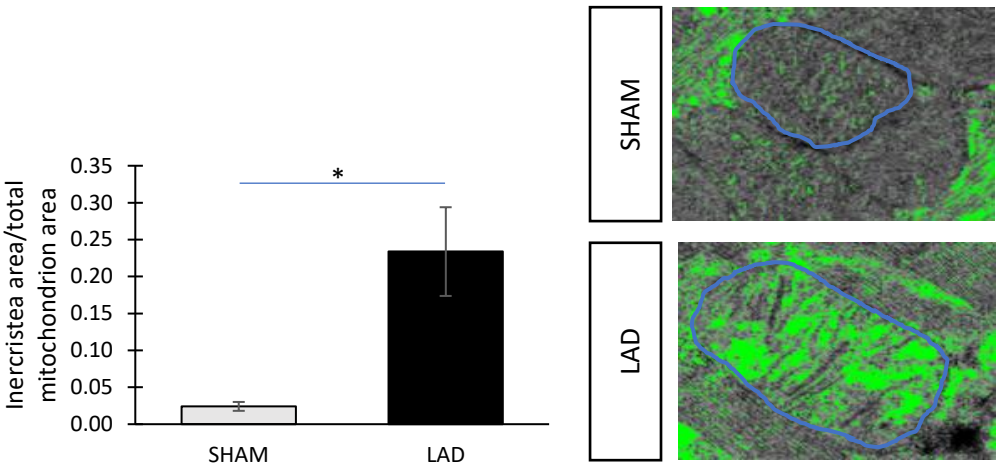

Figure 3.12 Mitochondrial density in SHAM and LAD group. Bars charts represent the ratio of intercristae area to total mitochondrion area in each group. Data are presented as mean ± SEM and analysed using unpaired t-test. Images were analysed using ImageJ software through automatic threshold level detection for each mitochondrial (green filter, within blue border, covers intercristae area). n =5, 3-4 fields were examined for each heart, total mitochondrial count =50, * $p < 0.05$

In addition to subpopulation distribution and cristae density analysis, morphometric measurements for all mitochondrial subpopulations were measured for each group, followed by a comparison of each subtype between the two groups.

3.3.2.1.1 Mitochondrial subpopulations morphometry in SHAM group

Perinuclear and subsarcolemmal mitochondria showed a significant decrease in length when compared to interfibrillar counterpart (PN $p = 0.028$, SS $p = 0.017$ vs. IF). Similarly, subsarcolemmal mitochondria were also significantly decreased in size ($p = 0.049$ vs. IF). The perimeter and roundness of perinuclear mitochondria were significantly decreased compared to interfibrillar mitochondria. However, the remaining mitochondrial measurements did not significantly change between the three subtypes (figure 3.13).

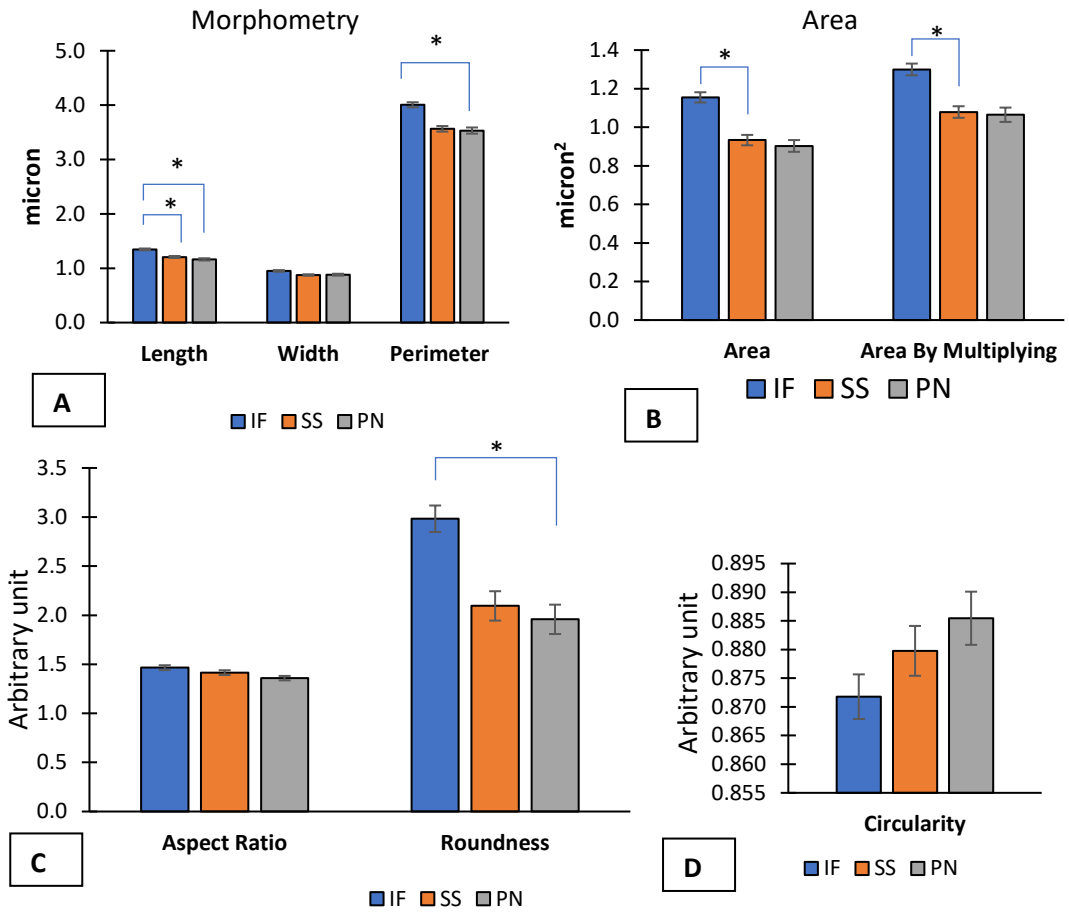

Figure 3.13 Mitochondrial morphometry of SHAM group. A) Length, width, and perimeter B) Area by size and multiplication (L*W) C) Aspect ratio, roundness, and D) Circularity. Data are presented as mean ± SEM, and analysed using one-way ANOVA followed by the Bonferroni and Games-Howell post-hoc tests. * $p < 0.05$ vs. IF. n=5, 3-4 fields were examined for each heart. Total mitochondrial count = 200 (IF), 198 (SS) and 180 (PN). IF interfibrillar, PN perinuclear and SS subsarcolemmal.

3.3.2.1.2 Mitochondrial subpopulations morphometry in LAD group

In LAD hearts, perinuclear mitochondria exhibited only significant changes in circularity and aspect ratio compared to interfibrillar mitochondria as seen in figure 3.14. This subtype had increased in circularity but decreased in aspect ratio. Unlike SHAM group, length and other morphometric measurement did not change significantly between the three subpopulations.

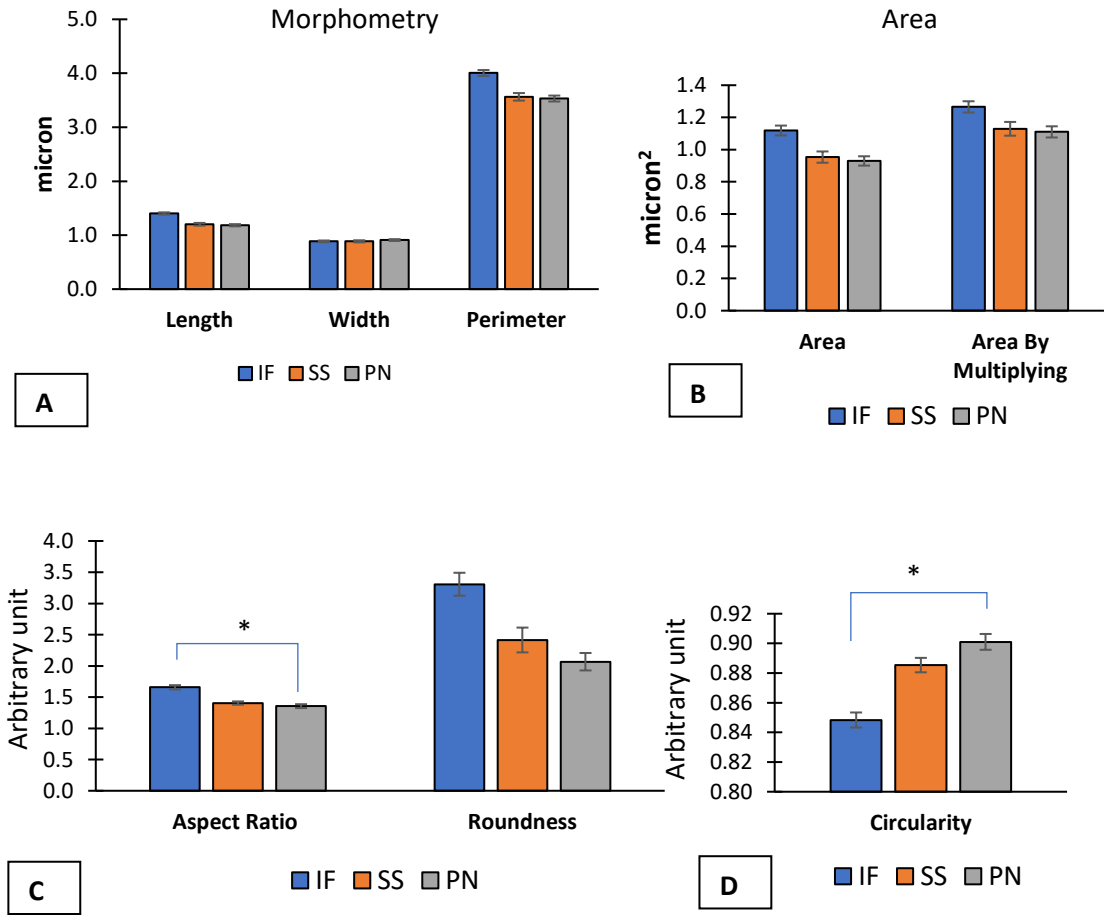

Figure 3.14 Mitochondrial morphometry of LAD group. A) Length, width, and perimeter B) Area by size and multiplication (L*W) C) Aspect ratio, roundness, and D) Circularity. Data are presented as mean ± SEM, and analysed using one-way ANOVA followed by the Bonferroni and Games-Howell post-hoc tests. * $p < 0.05$ vs. IF. n=5, 3-4 fields were examined for each heart. Total mitochondrial count = 200 (IF), 189 (SS) and 192 (SS). IF interfibrillar, PN perinuclear and SS subsarcolemmal.

3.3.2.1.3 Comparison of mitochondrial morphometry for each subtype between SHAM and LAD groups

Interfibrillar Mitochondria

Interfibrillar mitochondria of LAD hearts had a significant increase in aspect ratio (L:W) when compared to SHAM group ($p = 0.024$). IF mitochondria in LAD group appeared more rounded and decreased in size, however, these changes were not statistically significant. Other morphometric measurements did not significantly differ between the two groups (figure 3.15).

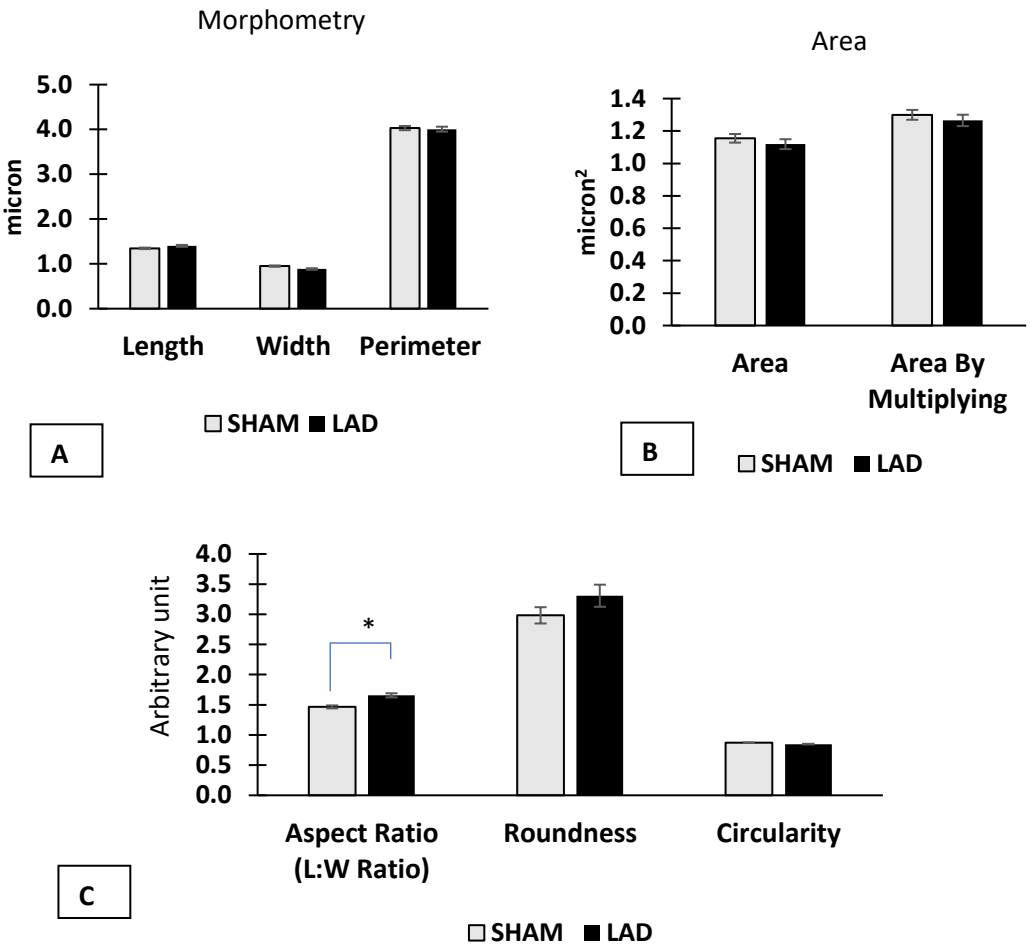

Figure 3.15 Interfibrillar mitochondrial morphometry of SHAM and LAD groups. A) Length, width, and perimeter B) Area by size and multiplication (L*W) C) Aspect ratio, roundness, and circularity. Data are presented as mean ± SEM, and analysed using unpaired student's t-test. n=5, 3-4 fields were examined for each heart. Total mitochondrial count per group = 200.

Perinuclear Mitochondria

Perinuclear mitochondria morphometric measurements showed a slight increase in area and roundness in LAD group compared to SHAM, however, these changes were not significantly different between the two groups as seen in figure 3.16.

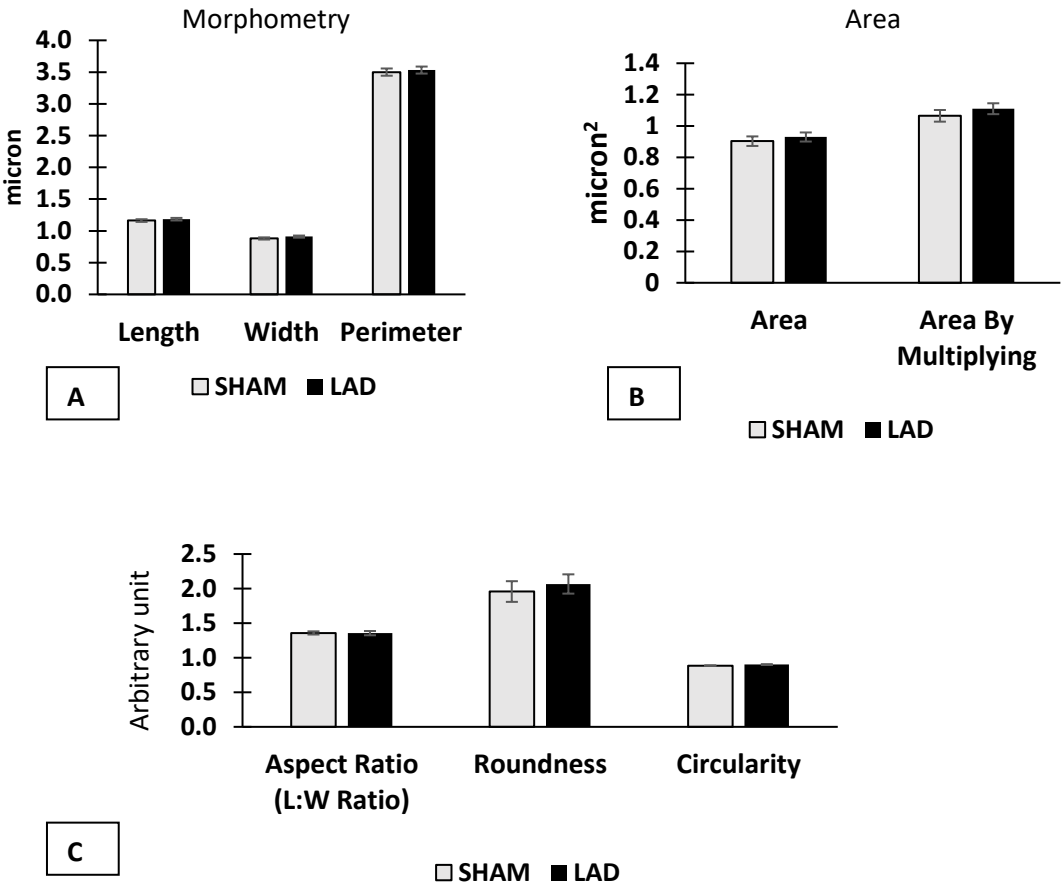

Figure 3.16 Perinuclear mitochondrial morphometry of SHAM and LAD groups. A) Length, width, and perimeter B) Area by size and multiplication (L*W) C) Aspect ratio, roundness, and circularity. Data are presented as mean ± SEM, and analysed using unpaired student's t-test, n=5, 3-4 fields were examined for each heart. Total mitochondrial count per group ≥ 180.

Subsarcolemmal mitochondria

Similarly, morphometric measurements of subsarcolemmal mitochondria were not significantly different between LAD and SHAM group as illustrated figure 3.17.

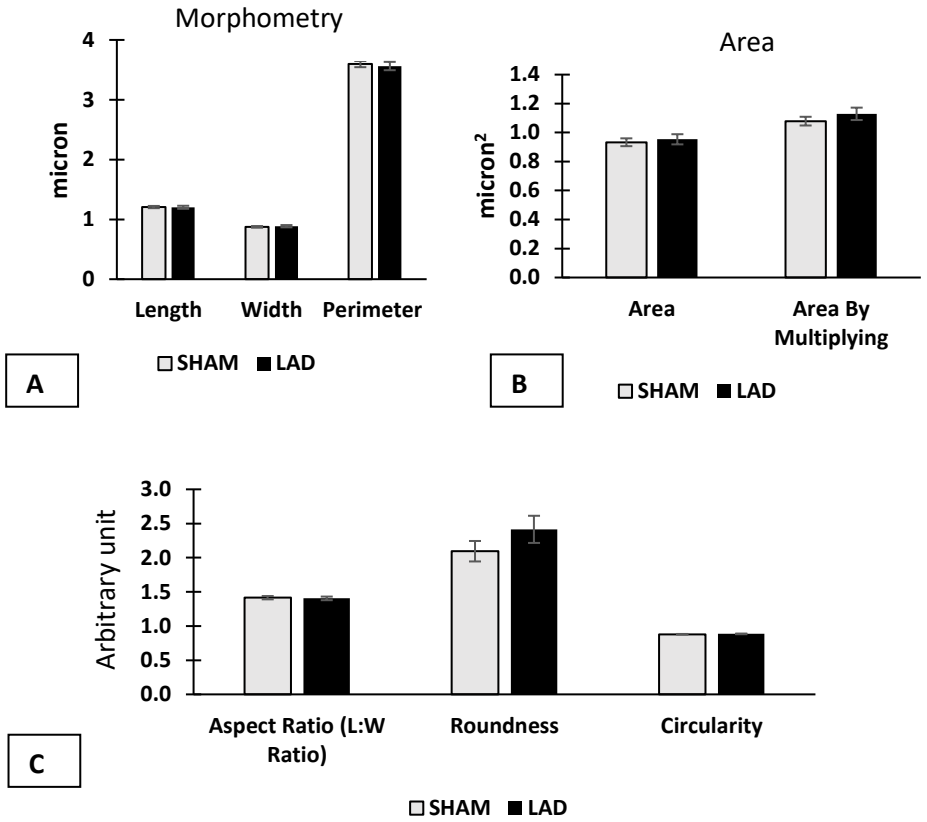

Figure 3.17 Subsarcolemmal mitochondrial morphometry of SHAM and LAD groups. A) Length, width, and perimeter B) Area by size and multiplication (L*W) C) Aspect ratio, roundness, and circularity. Data are presented as mean ± SEM, and analysed using unpaired student's t-test. n=5, 3-4 fields were examined for each heart. Total mitochondrial count per group ⩾ 189.

3.3.2.2 Sarcomere length

Diastolic sarcomere length (measured from one end of the sarcomere to the other) did not significantly vary between SHAM (1.6 ± 0.1 µm) and LAD group (1.8 ± 0.1 µm) as illustrated in figure 3.18.

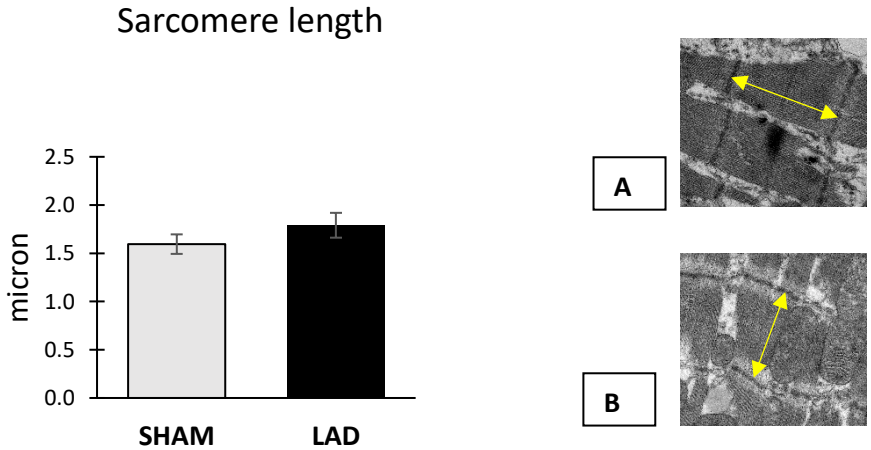

Figure 3.18 Sarcomere length in SHAM and LAD hearts**.** Data presented as mean ± SEM. Representative EM images of sarcomere length measurements in SHAM (A) and LAD group (B) with sarcomere length defined (yellow arrows). Data were analysed using unpaired t-test. n=5, 3-4 fields were examined for each heart. Total sarcomere count per heart =40.

3.3.3 Effect of LAD coronary artery ligation on rodent cardiac proteins

3.3.3.1 Total proteins

In total, 4786 proteins were detectable in both LAD and SHAM groups, of which, 321 proteins were significantly changed 4 weeks after LAD coronary artery ligation (p value < 0.05). Figure 3.19 shows a volcano plot for total proteins. There were 114 significantly different protein that had increased expression with LAD coronary artery ligation (FC > 1.3), compared to 69 proteins with decreased fold change (FC < 0.8).

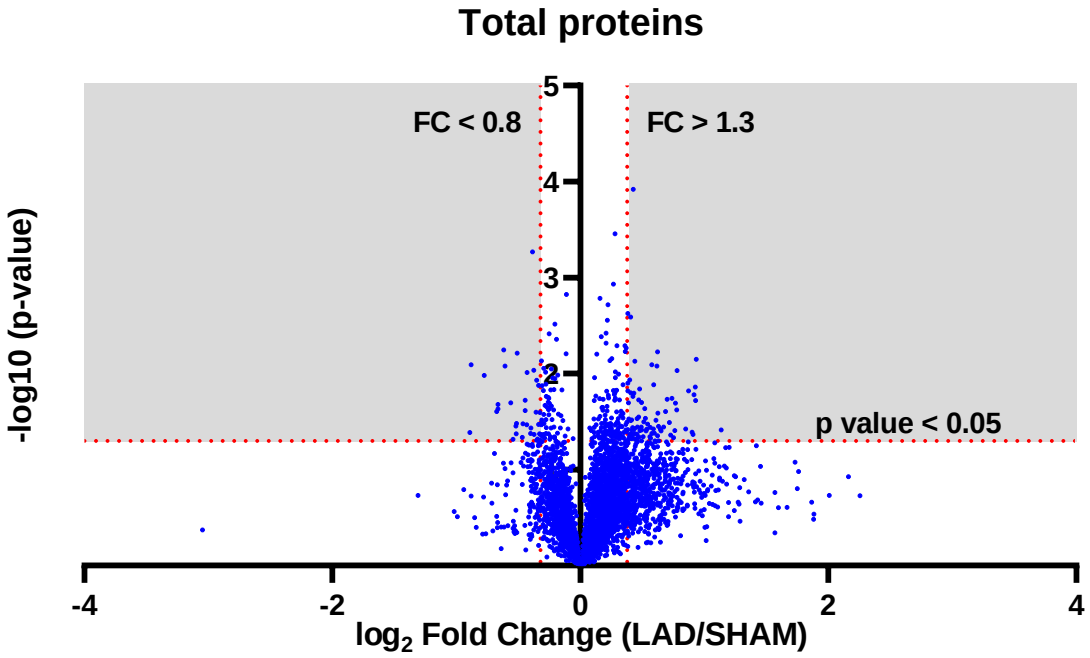

Figure 3.19 Logarithmic (volcano) plot of fold change of total proteins identified in LAD group compared to SHAM. P- value calculated using unpaired student's t-test. Reference lines indicate fold change < 0.8 or >1.3 on the x- axis, and p- value < 0.05 on the y- axis. n=5, total proteins count= 4786

A breakdown of total proteins classification into molecular and biological functions in addition to proteins class using Panther Database classification system is shown in figure 3.20. Expression heatmap of significantly different proteins (p value < 0.05) between SHAM and LAD groups was generated using heatmapper online tool as demonstrated in figure 3.21.

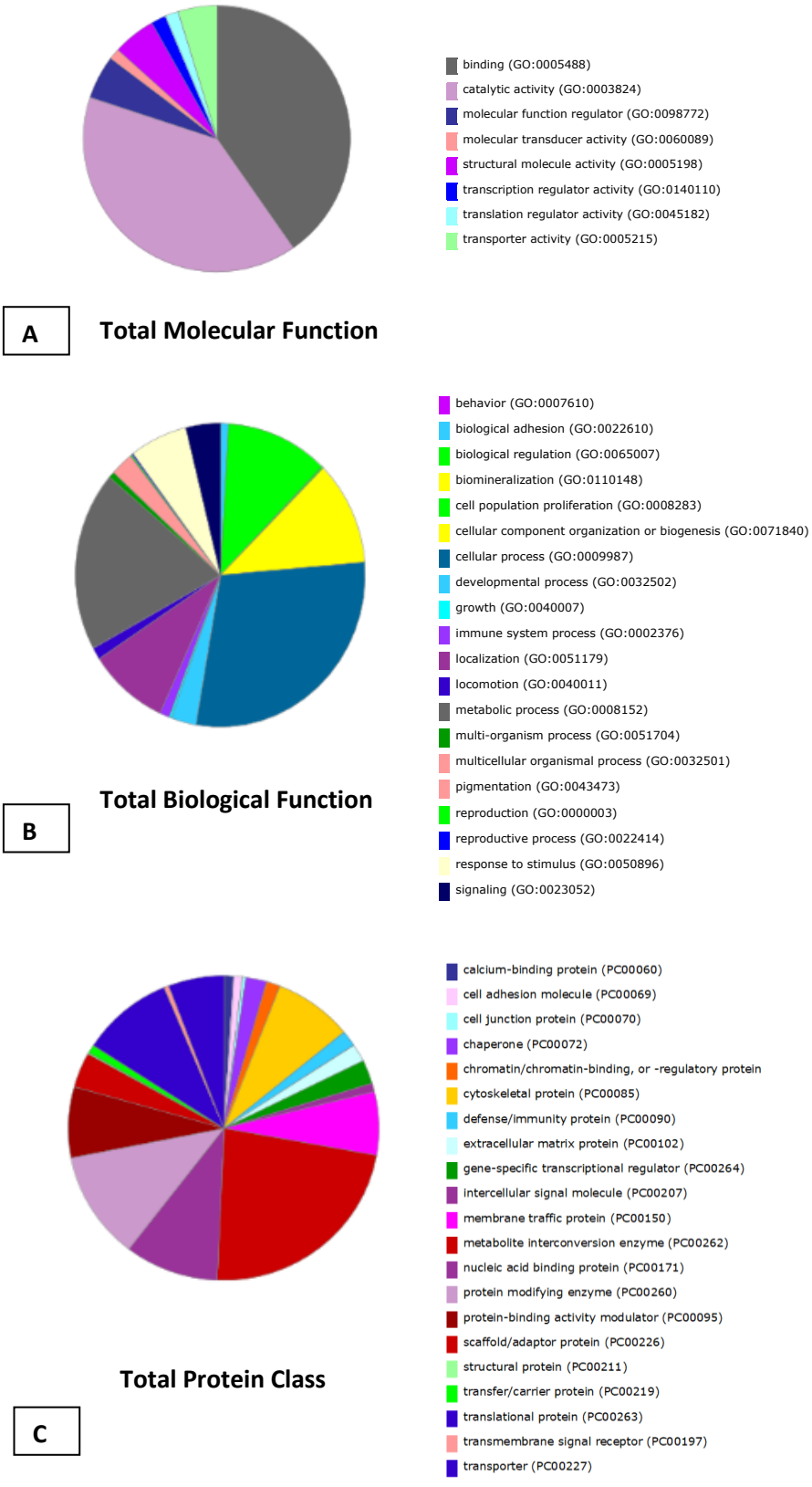

Figure 3.20 Classification of total proteins between SHAM and LAD groups using the PANTHER classification system. Proteins are classified according to molecular function (A) and biological processes (B) and protein class (C). n = 4786

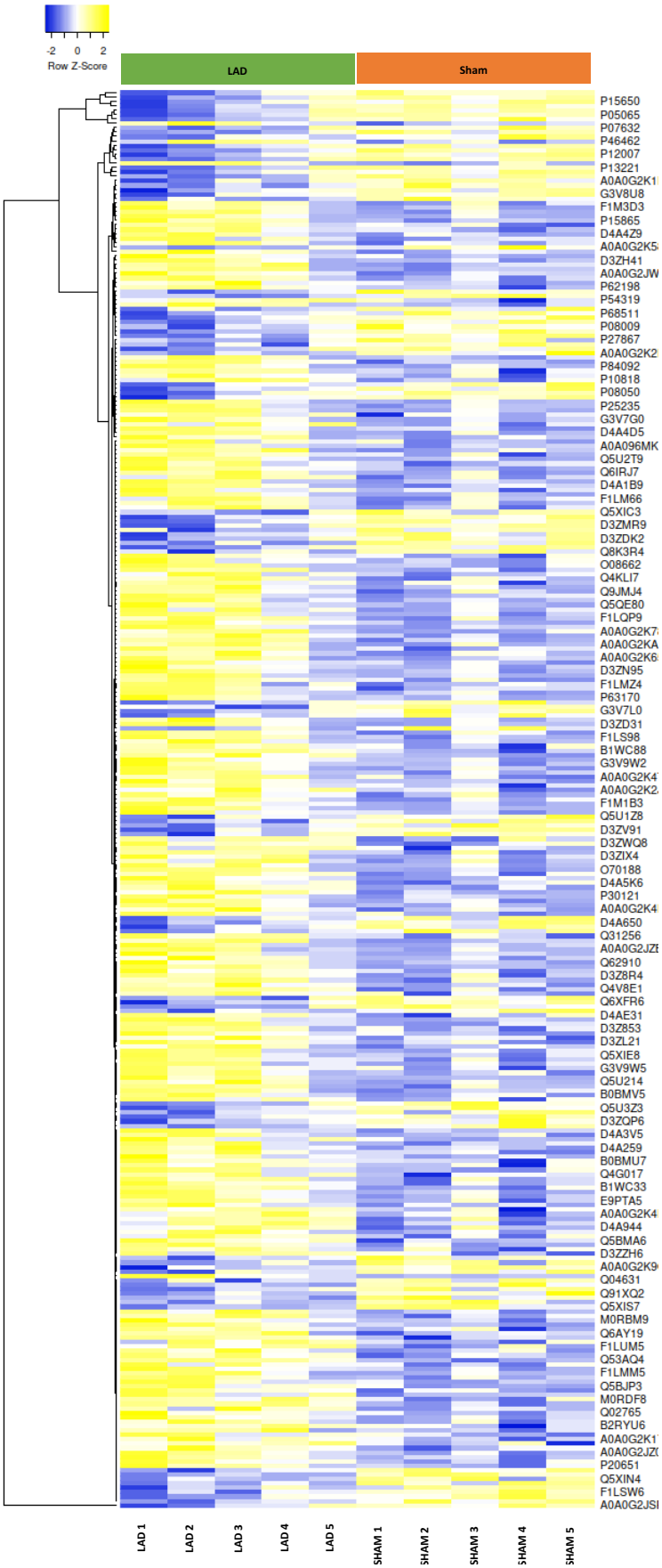

Figure 3.21 Expression heatmap of significantly different proteins ($p < 0.05$) between SHAM and LAD groups. Heatmap was created using online tool (http://www.heatmapper.ca/expression/). n = 5, total significant proteins count = 321.

Significantly different proteins were further categorised into high or low expression (fold change (LAD/SHAM) >1.3 or < 0.8, respectively). Panther database classification system was also used to breakdown protein of high and low categories according to molecular and biological functions, and protein class. Figure 3.22 shows these reported categories of significantly different proteins characterised by substantial decreased or increased fold change. Highly expressed proteins were predominantly involved in binding and catalytic activities. Proteins with low expression were classified mainly as catalytic, followed by binding and transporter activities. Interestingly, metabolites interconversion enzymes constitute a substantial class in proteins significantly decreased four weeks after LAD coronary artery ligation.

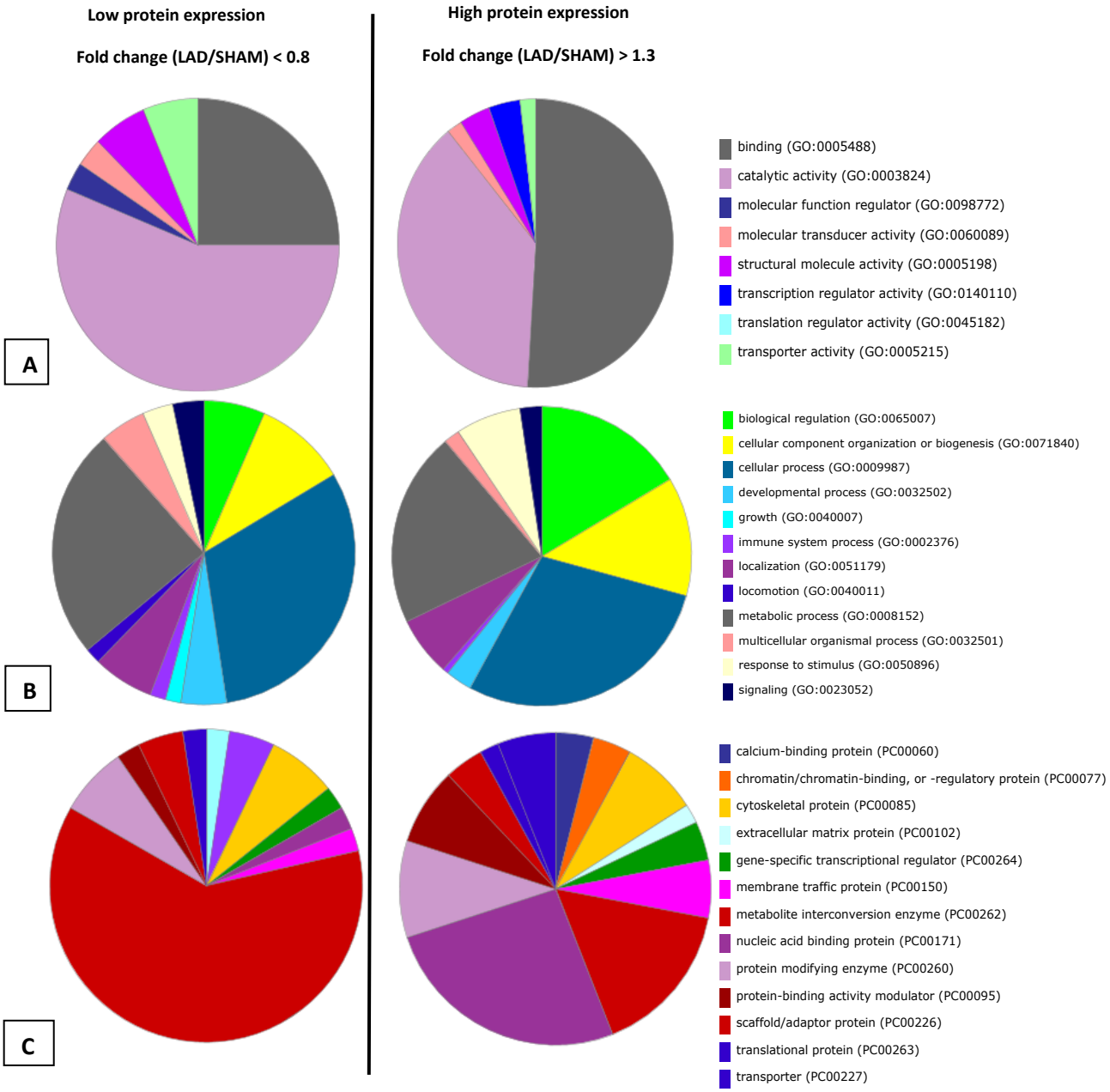

Figure 3.22 Classification of significantly different proteins between SHAM and LAD groups using the PANTHER classification system. Proteins are classified according to increased and decreased expression into molecular function (A) and biological processes (B) and protein class (C). FC fold change (LAD/SHAM), n = 5.

3.3.3.1.1 Mitochondrial proteins

A total of 357 mitochondrial proteins were detected and shown in a volcano plot (figure 3.23). Approximately 4% (n=14) of mitochondrial proteins had significant difference (p- value < 0.05) between SHAM and LAD groups.

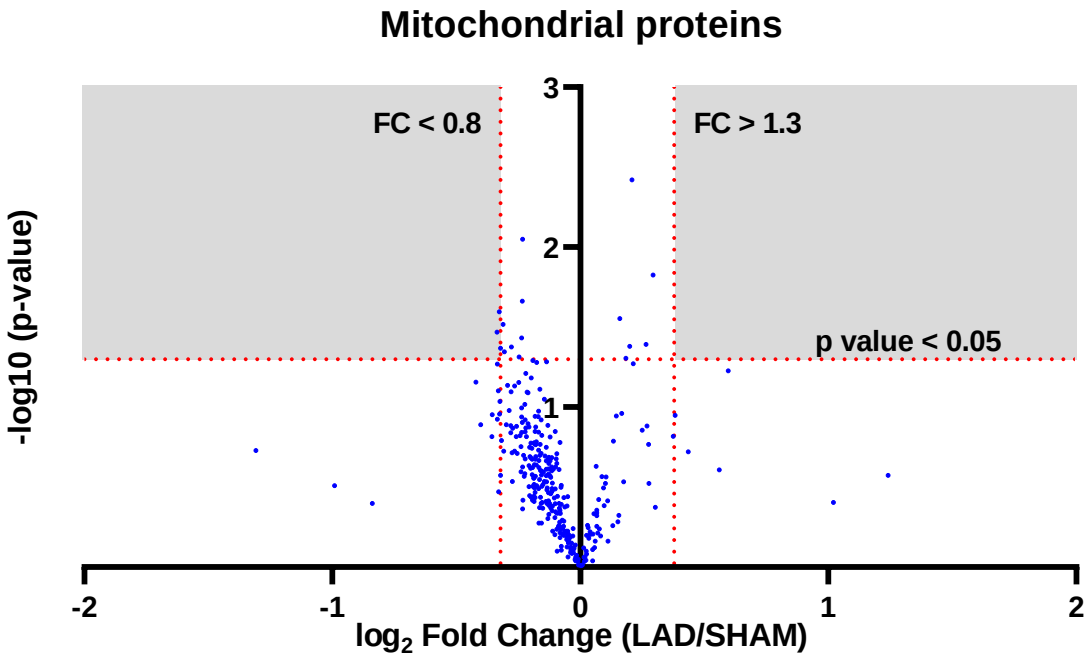

Figure 3.23 Logarithmic (volcano) plot of fold change for total mitochondrial proteins identified in LAD group compared to SHAM. P- value calculated using unpaired student's t-test. Reference lines indicate fold change < 0.8 or >1.3 on the x- axis, and p- value < 0.05 on the y- axis. n =5, total mitochondrial proteins count=357

These mitochondrial proteins are presented in figure 3.24. Highly expressed mitochondrial proteins involved in mitochondrial electron transport chain (Cytochrome c oxidase subunit 6A1, Atypical kinase COQ8B), and amino acids metabolism (Ornithine aminotransferase, Glutaminase kidney isoform). Proteins related to fatty acids metabolism (Long-chain specific acyl-CoA dehydrogenase, Short/branched chain-specific acyl-CoA dehydrogenase and Enoyl-CoA hydratase) were significantly decreased in LAD group.

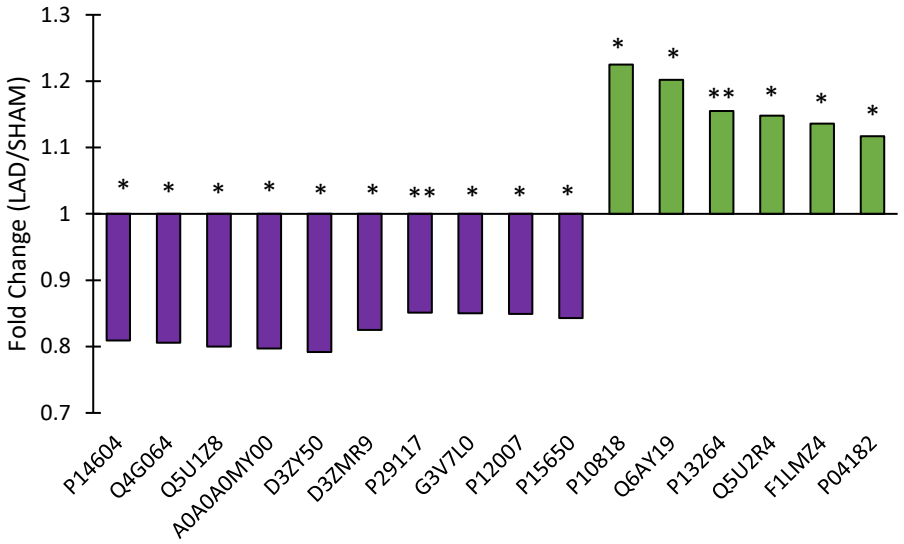

Figure 3.24 Mitochondrial proteins. **P14604**; Enoyl-CoA hydratase, **Q4G064**; 2-methoxy-6-polyprenyl-1,4-benzoquinol methylase, **Q5U1Z8**; Protein preY, **A0A0A0MY00**; Short/branched chain-specific acyl-CoA dehydrogenase, **D3ZY50**; ATP synthase mitochondrial F1 complex assembly factor 1, **D3ZMR9**; Mitochondrial ribosomal protein L21, **P29117**; Peptidyl-prolyl cis-trans isomerase F, **G3V7L0**; Adrenodoxin, **P12007**; Isovaleryl-CoA dehydrogenase, **P15650**; Long-chain specific acyl-CoA dehydrogenase, **P10818**; Cytochrome c oxidase subunit 6A1, **Q6AY19**; Atypical kinase COQ8B, **P13264**; Glutaminase kidney isoform, **Q5U2R4**; Mitochondrial ribonuclease P protein 1, **F1LMZ4**; Ribosome-releasing factor 2, **P04182**; Ornithine aminotransferase. Data were analysed using the unpaired student's t-test. * $p < 0.05$, ** $p < 0.01$, n=5

3.3.3.1.2 Kinase proteins

Nine protein kinases were increased in LAD group such as protein kinase C and tyrosine protein kinase, while three kinase proteins were downregulated (figure 3.25). These were pantothenate kinase 1 (coenzyme A biosynthesis), adenylate kinase isoenzyme 1 (De novo purine biosynthesis), and creatine kinase M-type (regulation of ATP and creatine phosphate phosphorylation).

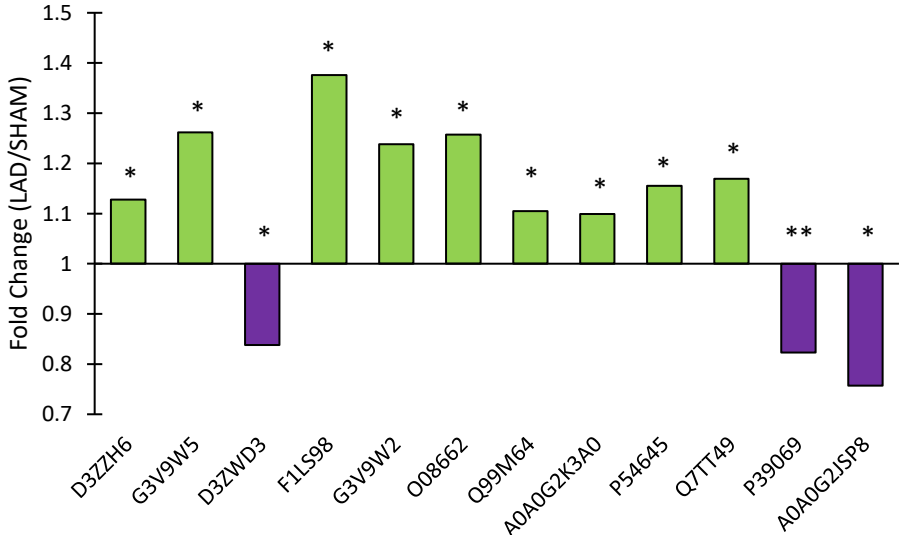

Figure 3.25 Protein kinases. **D3ZZH6**; Mitogen-activated protein kinase kinase kinase 5, **G3V9W5**; Phosphatidylinositol 5-phosphate 4-kinase type-2 gamma, **D3ZWD3**; Pantothenate kinase 1, **F1LS98**; Protein kinase C, **G3V9W2**; Tyrosine-protein kinase, **O08662**; Phosphatidylinositol 4-kinase alpha, **Q99M64** ; Phosphatidylinositol 4-kinase type 2-alpha, **A0A0G2K3A0**; Serine/threonine-protein kinase WNK1, **P54645**; 5'-AMP-activated protein kinase catalytic subunit alpha-1, **Q7TT49**; Serine/threonine-protein kinase MRCK beta, **P39069**; Adenylate kinase isoenzyme 1, **A0A0G2JSP8**; Creatine kinase M-type. Data were analysed using unpaired t-test. * $p < 0.05$, ** $p < 0.01$, n=5

3.3.3.1.3 Phosphatase proteins

Only inositol monophosphatase 2 and serine/threonine-protein phosphatase 2B catalytic subunit beta isoform and were significantly different between LAD group and SHAM (figure 3.26). The later plays an important role in Ca^{2+} mediated signal transduction, including activation of transcription factor NFATC1.

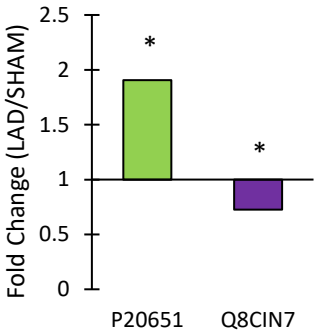

Figure 3.26 Protein Phosphatases. **P20651;** Serine/threonine-protein phosphatase 2B catalytic subunit beta isoform**, Q8CIN7;** Inositol monophosphatase 2. Data were analysed using unpaired t-test. * $p < 0.05$, n=5

3.3.3.1.4 Oxidoreductase proteins

Figure 3.27 shows the oxidases and reductases proteins that significantly changed four weeks after LAD coronary artery ligation. Aldehyde oxidase 3, which is involved in superoxide generation, was almost doubled in LAD group (FC = 2.2), whereas methionine sulfoxide reductase B3, which reduces oxidised methionine, was significantly decreased in LAD hearts.

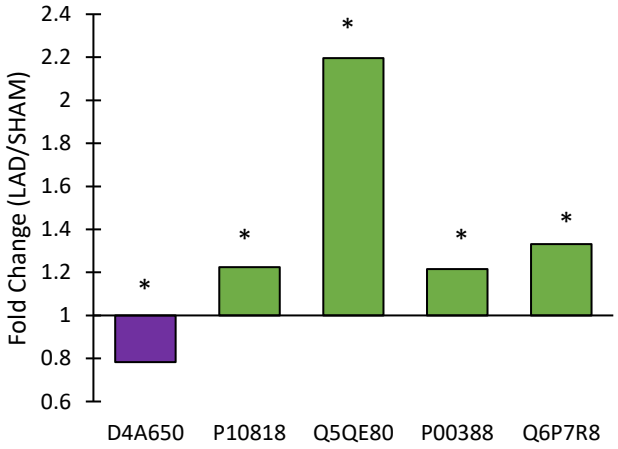

Figure 3.27 Oxidoreductase proteins. **D4A650;** Methionine sulfoxide reductase B3, **P10818;** Cytochrome c oxidase subunit 6A1, mitochondrial, **Q5QE80;** Aldehyde oxidase 3, **P00388;** NADPH-cytochrome P450 reductase, **Q6P7R8**; Very-long-chain 3-oxoacyl-CoA reductase. Data were analysed using unpaired student's t-test. * $p < 0.05$, n=5

3.3.3.1.5 Antioxidant related proteins

Significantly different antioxidant proteins such as superoxide dismutase [Cu-Zn] and glutathione peroxidase were decreased in LAD hearts compared to SHAM as seen in figure 3.28. Other major antioxidants proteins like catalase (not shown), were not differentially changed between the two groups.

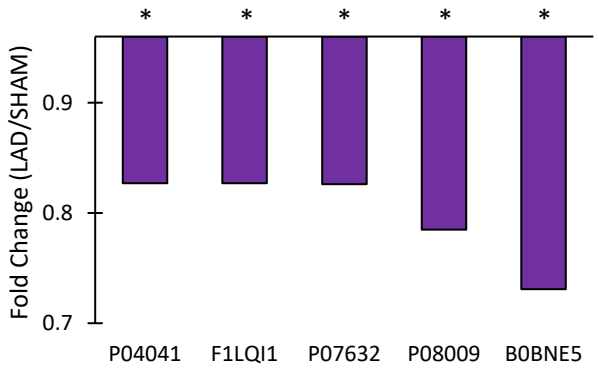

Figure 3.28 Antioxidant related proteins. **P04041**; Glutathione peroxidase 1, **F1LQI1**; Hydroxyacyl glutathione hydrolase, **P07632**; Superoxide dismutase [Cu-Zn], **P08009**; Glutathione S-transferase Yb-3, **B0BNE5**; S-formylglutathione hydrolase. Data were analysed using unpaired student's t-test. * $p < 0.05$, ** $p < 0.01$, n=5

3.3.3.1.6 Inflammation related proteins

Proteins involved in various inflammatory pathways, such as T cell activation (CD48 antigen), response to chemotaxis (lymphocyte specific 1, isoform CRA_a), macrophage and monocytes activation, (macrophage activation 2 like, CD163 antigen), and mast cell activation (tryptase), were all significantly upregulated in LAD group (figure 3.29).

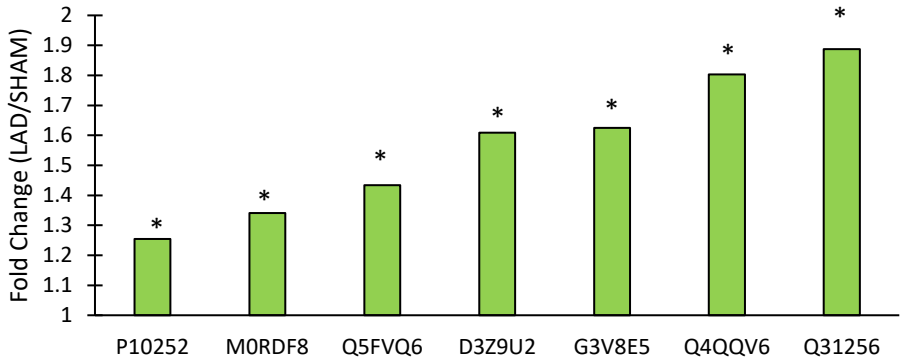

Figure 3.29 Inflammation related proteins. **P10252,** CD48 antigen**, M0RDF8;** Macrophage activation 2 like, **Q5FVQ6;** Interferon-gamma-inducible GTPase Ifgga3 protein**, D3Z9U2;** CD163 antigen, **G3V8E5;** Tryptase, **Q4QQV6;** Lymphocyte specific 1, isoform CRA a, **Q31256;** MHC class I RT1.Au heavy chain, **A0A0G2JVZ6;** Integrin subunit alpha V. Data were analysed using unpaired t-test. * $p < 0.05$, n=5

3.3.3.1.7 Ions transport proteins

Three ions transport proteins were significantly upregulated 4 weeks after LAD coronary artery ligation as shown in figure 3.30. Calcium channel voltage-dependent, alpha 2/delta subunit 2 and voltage-dependent L-type calcium channel subunit alpha mediates Ca^{2+} entry to the cell to further calcium release from the sarcoplasmic reticulum during EC coupling, while sodium/potassium-transporting ATPase subunit beta-3 is an integral membrane protein that establishes and maintain electrochemical gradient across cell membrane.

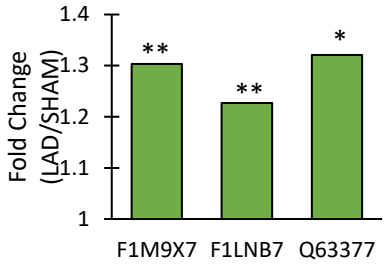

Figure 3.30 Ion transport proteins. **F1M9X7**; Calcium channel voltage-dependent, alpha 2/delta subunit 2, **F1LNB7**; Voltage-dependent L-type calcium channel subunit alpha, **Q63377**; Sodium/potassium-transporting ATPase subunit beta-3. Data were analysed using unpaired student's t-test. * $p < 0.05$, ** $p < 0.01$, n=5

3.3.3.1.8 Extracellular matrix proteins

Several extracellular proteins were either upregulated or downregulated four weeks after LAD coronary artery ligation as listed in figure 3.31. Although many collagen subunits/chains were identified with increased fold change, none were statistically significant. However, other matrix proteins such fibronectin 1, heparan sulfate proteoglycan 2, in addition to ECM enzymes like cathepsin S, and metalloproteinase inhibitor 2 were significantly changed LAD group. There is a significant increase of cathepsin S, a protease that degrades matrix proteins, including heparan sulfate proteoglycan 2, that had decreased expression in LAD group. Nevertheless, metalloproteinase inhibitor 2 acts by regulating the activity of several MMPs is increased four weeks in the intervention group (LAD).

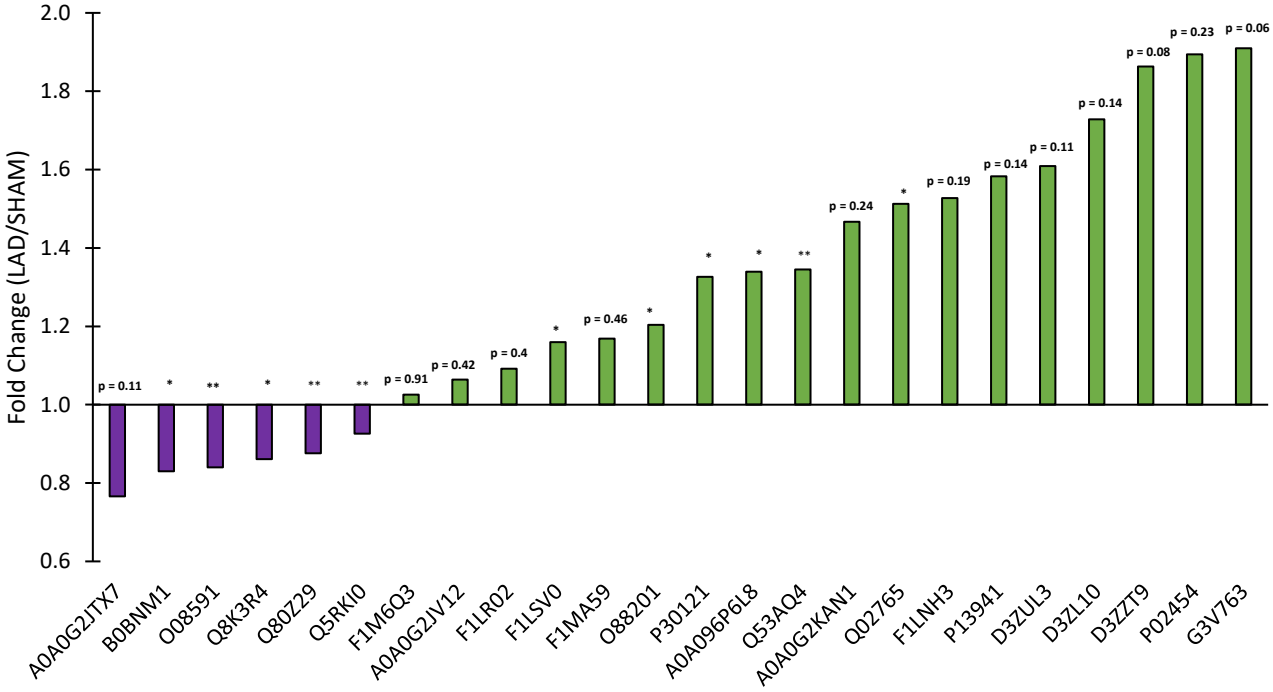

Figure 3.31 ECM proteins. **A0A0G2JTX7;** Collagen type VI alpha 5 chain, **B0BNM1;** NAD(P)HX epimerase, **O08591;** heparan sulfate proteoglycan 2, **Q8K3R4;** adiponectin C1Q and collagen domain containing, **Q80Z29;** nicotinamide phosphoribosyltransferase, **Q5RKI0;** WD repeat domain 1, **F1M6Q3;** Collagen type IV alpha 2 chain, **A0A0G2JV12;** Collagen type XV alpha 1 chain, **F1LR02;** Collagen type XVIII alpha 1 chain, **F1LSV0;** Semaphorin 4B, **F1MA59;** Collagen type IV alpha 1 chain, **O88201;** C-type lectin domain containing 11A, **P30121;** Metalloproteinase inhibitor 2, **A0A096P6L8;** fibronectin 1, **Q53AQ4;** transmembrane and ubiquitin like domain containing 1, **A0A0G2KAN1;** Collagen alpha-2(I) chain, **Q02765;** Cathepsin S, **F1LNH3;** Collagen type VI alpha 2 chain, **P13941;** Collagen alpha-1(III) chain, **D3ZUL3;** Collagen type VI alpha 1 chain, **D3ZL10;** Collagen type VI alpha 6 chain, **D3ZZT9;** Collagen type XIV alpha 1 chain, **P02454;** Collagen alpha-1(I) chain, **G3V763;** Collagen alpha-1(V) chain. Data were analysed using unpaired student's t-test. * $p < 0.05$, ** $p < 0.01$, n=5

3.3.3.1.9 Cytoskeletal proteins

Except for Myomesin 3 and Tubulin polymerization-promoting protein, all significantly different cytoskeletal proteins were upregulated in LAD group compared to SHAM. Such proteins included tubulin alpha chain, a major component of microtubules, and cytoskeleton-associated protein 4, as shown in figure 3.32. Fold change of myomesin 3, a component of M band in the sarcomere, was significantly reduced in in LAD hearts.

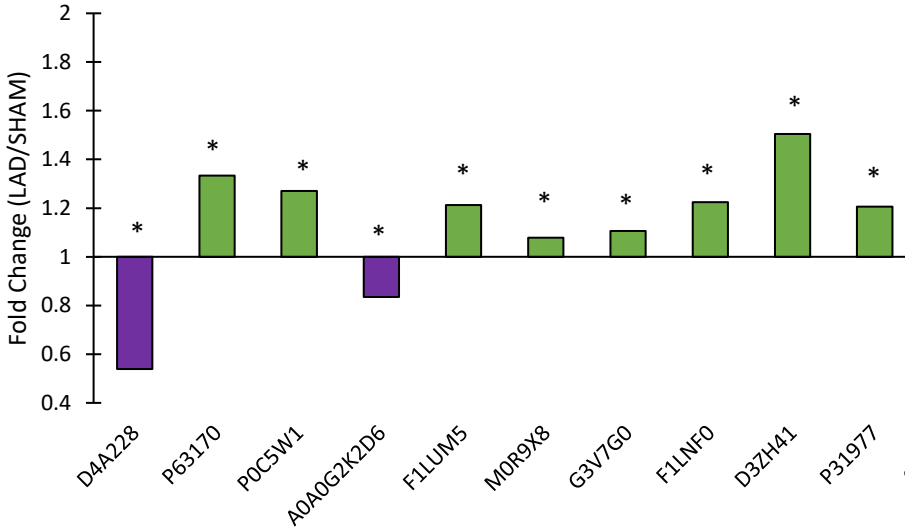

Figure 3.32 Cytoskeletal proteins. **D4A228;** Myomesin 3**, P63170;** Dynein light chain 1, cytoplasmic, **P0C5W1;** Microtubule-associated protein 1S, **A0A0G2K2D6;** Tubulin polymerization-promoting protein, **F1LUM5;** Tubulin alpha chain, **M0R9X8;** Cytoplasmic dynein 1 heavy chain 1, **G3V7G0;** Cytoplasmic dynein 1 light intermediate chain 1, **F1LNF0;** Myosin heavy chain 14, **D3ZH41;** Cytoskeleton-associated protein 4, **P31977;** Ezrin. Data were analysed using unpaired student's t-test. * $p < 0.05$, n=5

3.3.3.1.10 Z disc and junctional proteins

Five z disc related proteins were identified and significantly increased four weeks in LAD group (figure 3.33). Spectrin alpha chain non-erythrocytic 1, or alpha II-spectrin, which is localised to z disc in cardiomyocytes, but also found in cardiac fibroblasts, was almost doubled in LAD group in comparison to SHAM (FC=1.9). However, gap junction alpha-1 protein (connexin 43), a constituent of gap junction formation, was decreased in LAD group.

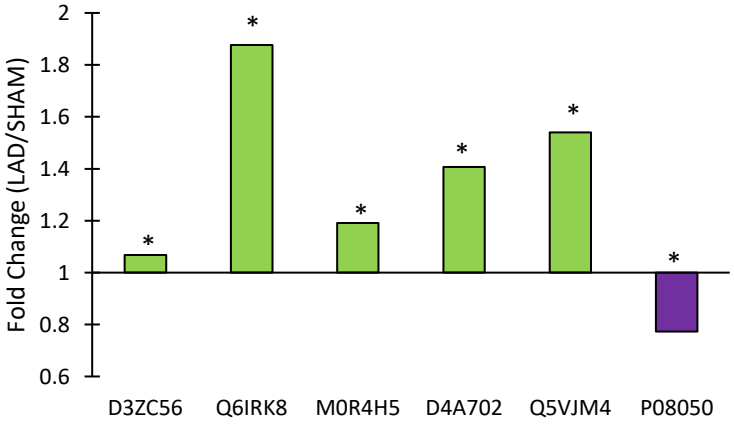

Figure 3.33 Z disc and junctional proteins. **D3ZC56;** Dystonin, **Q6IRK8;** Spectrin alpha chain, non-erythrocytic 1, **M0R4H5;** PDZ and LIM domain protein 4, **D4A702;** Synaptopodin-2, **Q5VJM4;** Cardiac titin fetal N2BA PEVK isoform (Fragment), **P08050;** Gap junction alpha-1 protein. Data were analysed using unpaired student's t-test. * $p < 0.05$, n=5

3.3.3.1.11 Metabolism proteins and enzymes

All significantly different proteins involved in cardiac metabolism were decreased in LAD groups (figure 3.34). These proteins are part of several metabolic pathways, including glycolysis (pyruvate kinase PKM, glyceraldehyde-3-phosphate dehydrogenases), fructose metabolism (fructose-bisphosphate aldolase A), as well as amino acids (kynurenine-oxoglutarate transaminase 3, branched chain amino acid aminotransferase) and fatty acids metabolism (acetyl-CoA carboxylase beta and mitochondrial enoyl-CoA hydratase).

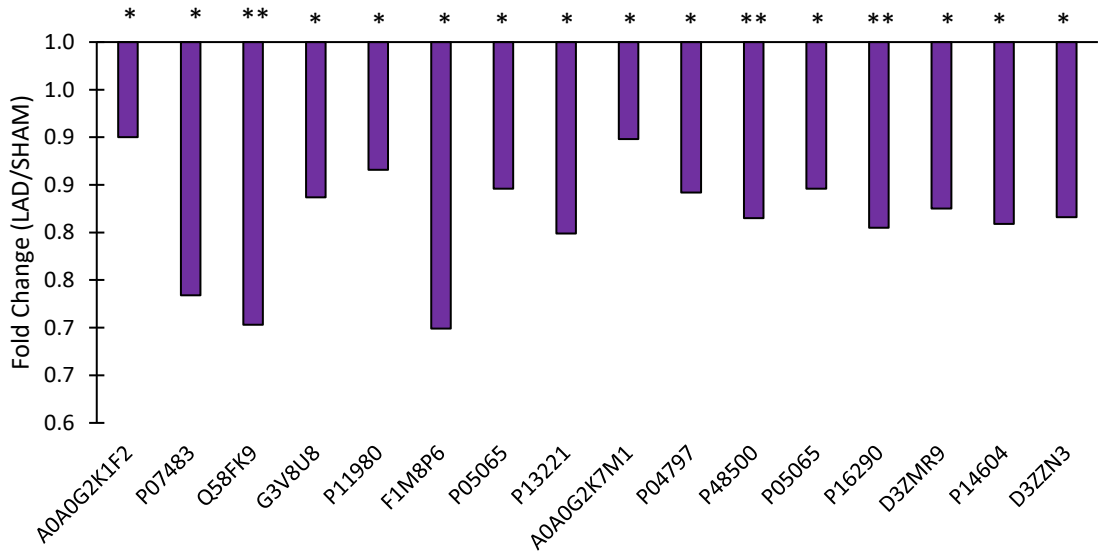

Figure 3.34 Metabolism proteins and enzymes**. A0A0G2K1F2,** Acetyl-CoA carboxylase beta, **P07483;** Fatty acid-binding protein, heart, **Q58FK9;** Kynurenine-oxoglutarate transaminase 3, **G3V8U8;** Branched-chain-amino-acid aminotransferase, **P11980;** Pyruvate kinase PKM, **F1M8P6;** Glyceraldehyde-3-phosphate dehydrogenase SV=2, **P05065;** Fructose-bisphosphate aldolase A, **P13221;** Aspartate aminotransferase, cytoplasmic, **A0A0G2K7M1;** Glyceraldehyde-3-phosphate dehydrogenase SV=1, **P04797;** Glyceraldehyde-3-phosphate dehydrogenase SV=3, **P48500;** Triosephosphate isomerase, **P05065** Fructose-bisphosphate aldolase A, **P16290;** Phosphoglycerate mutase 2, **D3ZMR9;** Mitochondrial ribosomal protein L21, **P14604;** Enoyl-CoA hydratase, mitochondrial, **D3ZZN3;** Acetyl-coenzyme A synthetase. Data were analysed using unpaired student's t-test. * $p < 0.05$, ** $p < 0.01$, n=5

3.3.3.2 Pathway analysis

The proteome output was further analysed using Ingenuity Pathway Analysis software IPA (Qiagen, Germany). Instead of proteins selection that is based on their shared functional or structural similarities, IPA software provides in depth assessment of data to identify main signalling pathways that were significantly different four weeks after LAD coronary artery ligation in rats. Figure 3.35 shows the top three signalling pathways that were changed based on the p value and fold change of components for each pathway. This is indicated by z score, a statistical measure reflecting the match between the expected relationship direction and the observed gene expression. These pathways are protein kinase A signalling, G beta gamma and phospholipase C signalling pathways.

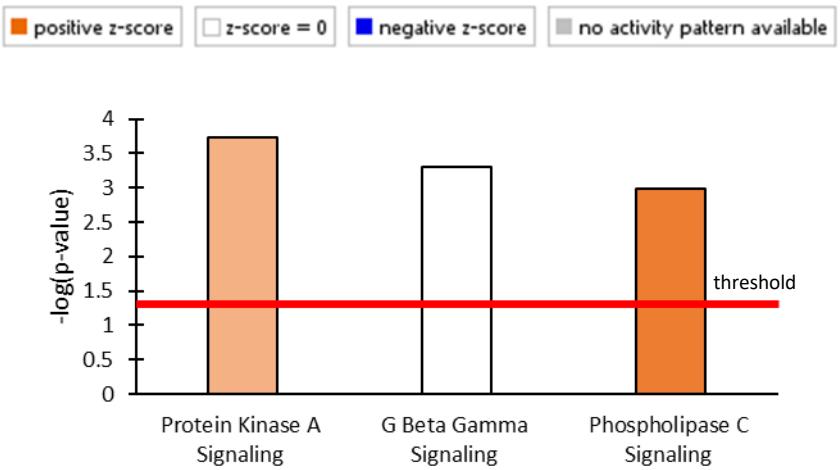

Figure 3.35 Top signalling pathways in LAD and SHAM proteome output. y- axis shows level of significance for each pathway (red horizontal line represents threshold, corresponding to $p < 0.05$). The direction of change in colour, represents z-score; positive scores represent relatively higher results in LAD group. Figure is reproduced from Ingenuity Pathway Analysis software, Qiagen, Germany.

Figures 3.36-3.38 are illustrations of these signalling pathways, with fold change of the significantly different proteins components.

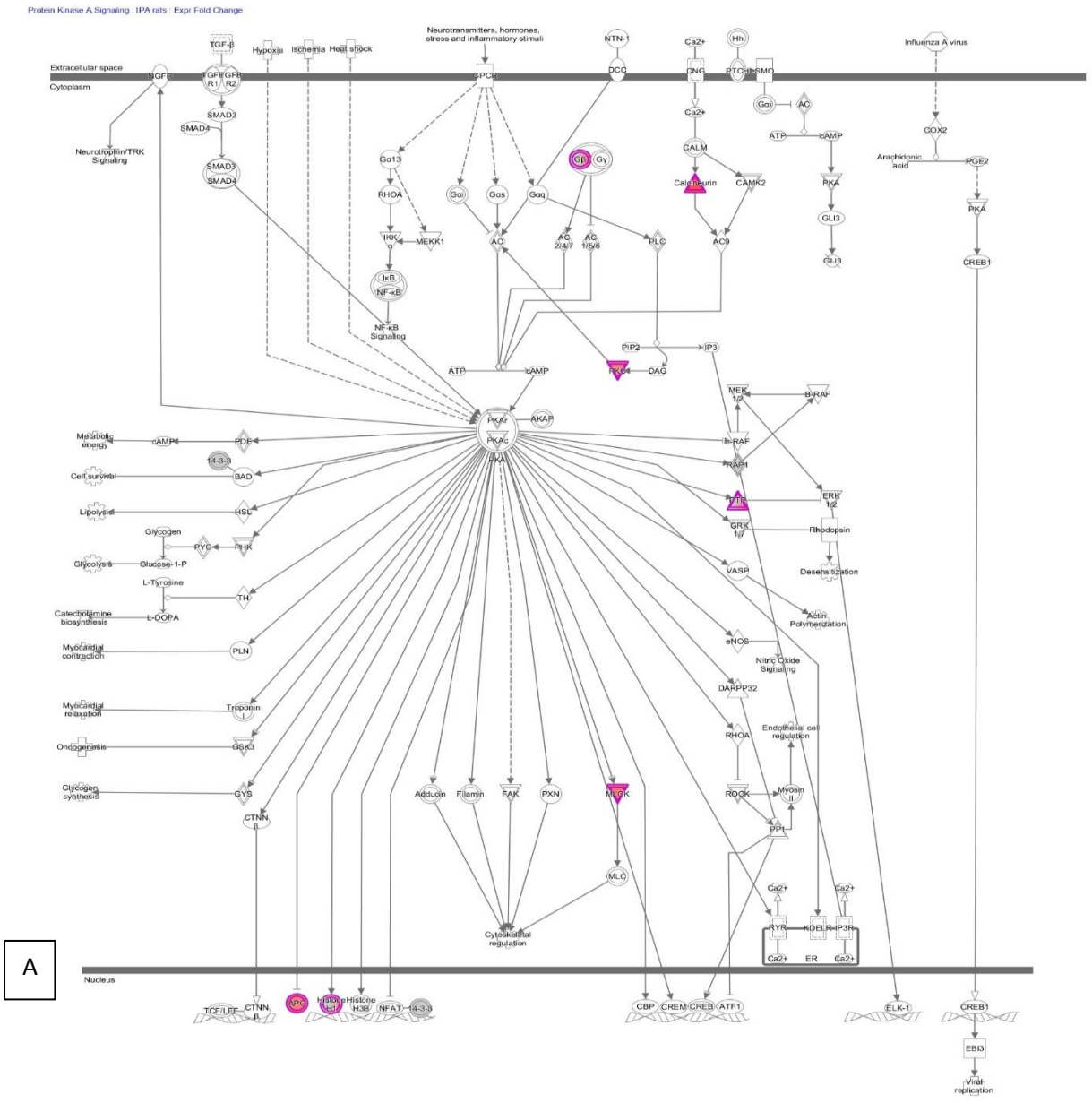

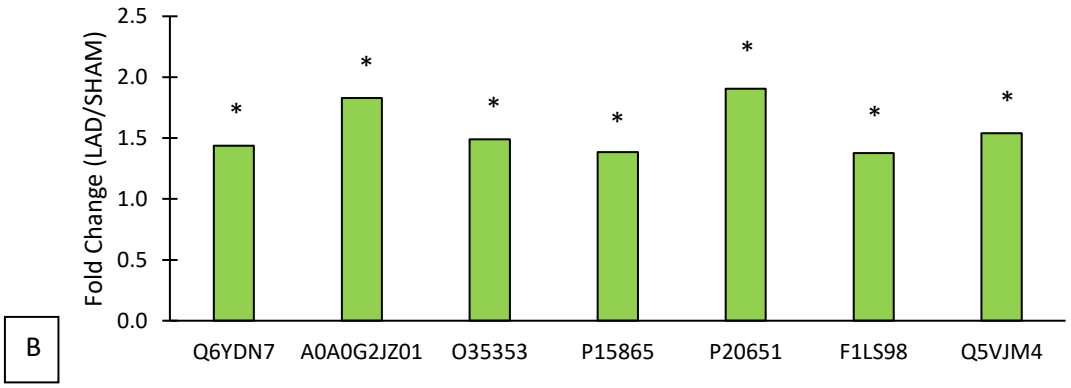

Figure 3.36 Protein kinase A signalling pathway (A) pathway illustration, and fold change of component proteins in (B). **Q6YDN7;** cell division cycle 26, **A0A0G2JZ01;** EYA transcriptional coactivator and phosphatase 3, **O35353;** G protein subunit beta 4, **P15865;** histone cluster 1, H1e, **P20651;** protein phosphatase 3 catalytic subunit beta, **F1LS98;** protein kinase C alpha, **Q5VJM4;** titin. Data were analysed using unpaired student's t-test. * $p < 0.05$, n=5

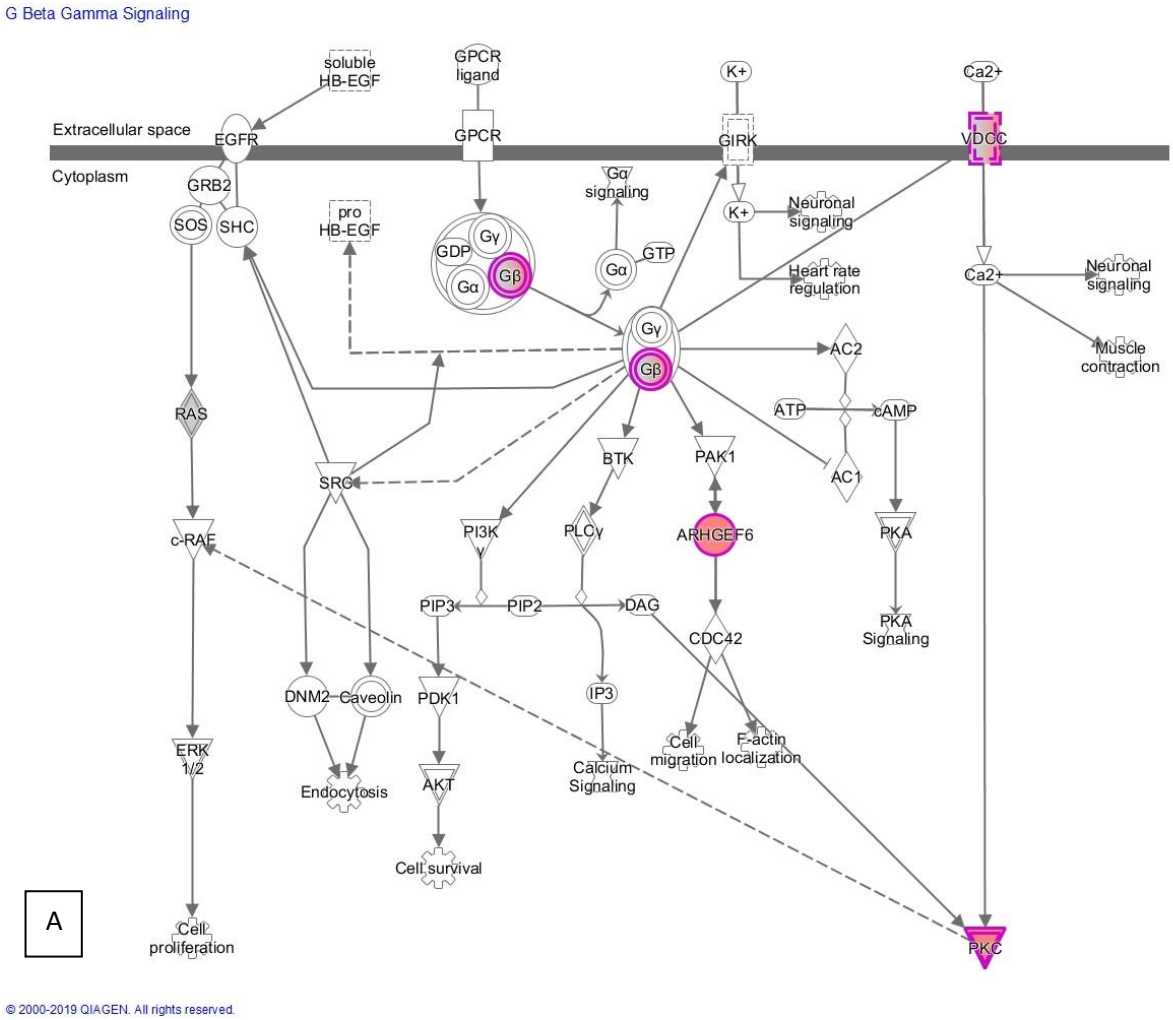

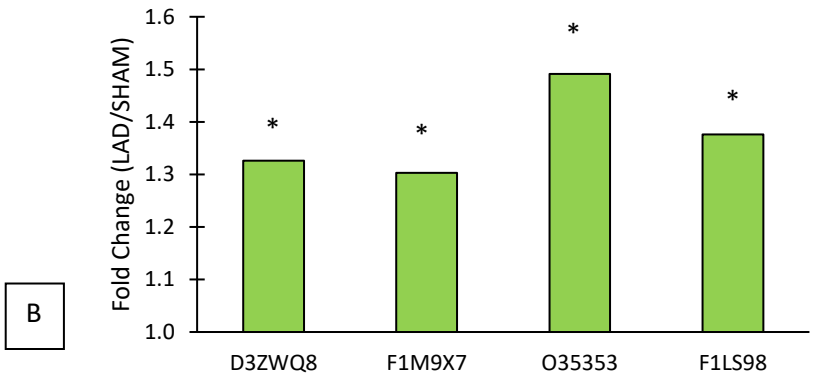

Figure 3.37 G beta gamma signalling pathway (A) pathway illustration, and fold change of component proteins (B). **D3ZWQ8;** Rho guanine nucleotide exchange factor 6, **F1M9X7;** Calcium channel, voltage-dependent, alpha 2/delta subunit 2, **O35353;** Guanine nucleotide-binding protein subunit beta-4, **F1LS98;** Protein kinase C. Data were analysed using unpaired student's t-test. * $p < 0.05$, n=5

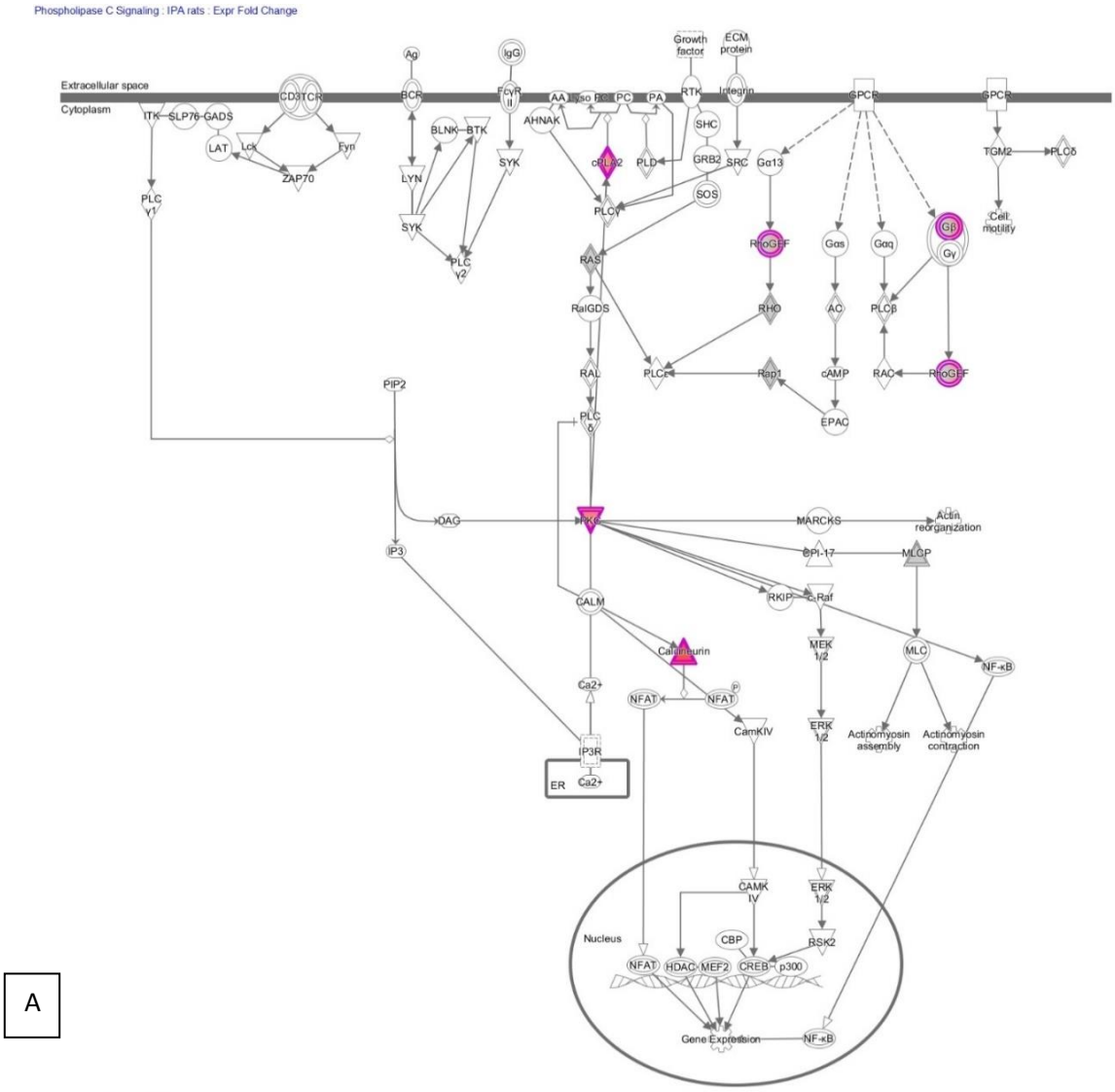

A

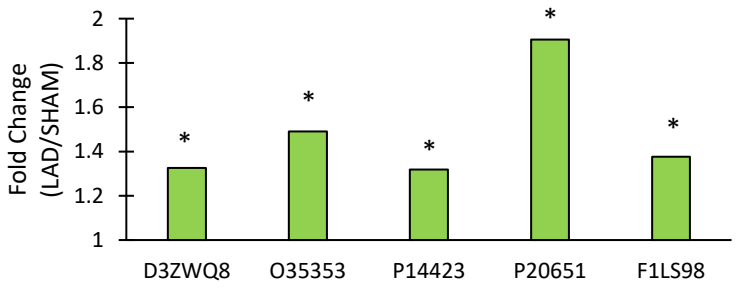

B

Figure 3.38 PLC signalling pathway (A) pathway illustration, and fold change of component proteins in (B). **D3ZWQ8;** Rho guanine nucleotide exchange factor 6, **O35353;** Guanine nucleotide-binding protein subunit beta-4, **P14423;** Phospholipase A2, membrane associated, **P20651;** Serine/threonine-protein phosphatase 2B catalytic subunit beta isoform, **F1LS98;** Protein kinase C. Data were analysed using unpaired student's t-test. * $p < 0.05$, n=5

3.3.3.3 Effect of LAD coronary artery ligation on cardiac phosphoproteins

A total of 990 phosphoproteins were detected in LAD and SHAM groups, of which 210 were significantly different ($p < 0.05$). Phosphosites of total detected phosphoproteins are shown in figure 3.39.

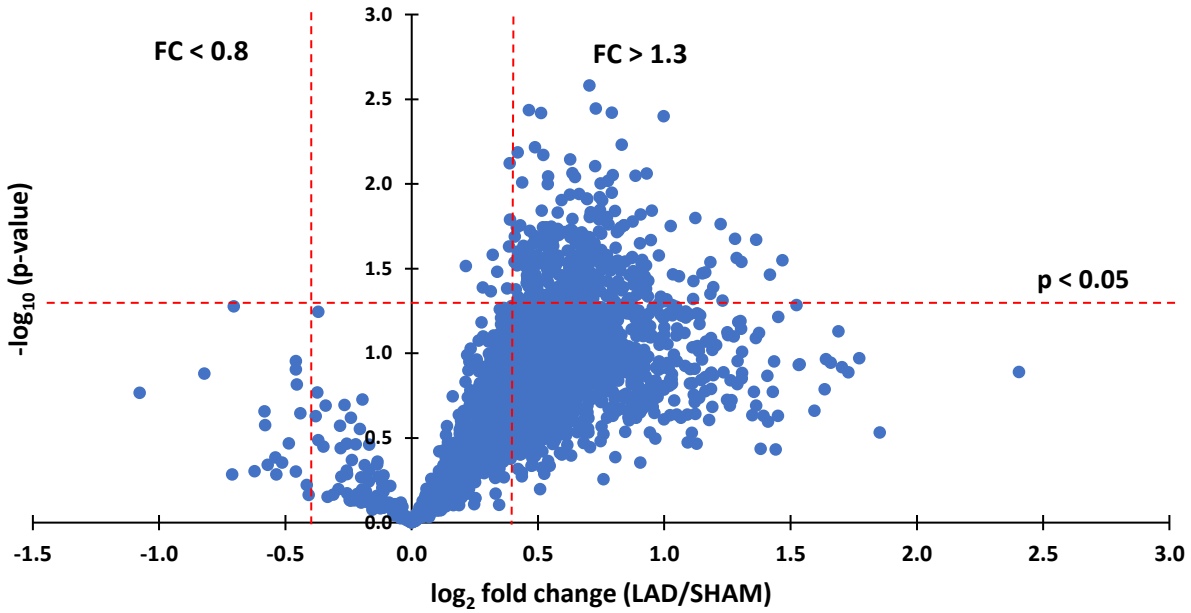

Figure 3.39 Logarithmic (volcano) plot of fold change for total detected phosphosites in LAD group compared to SHAM. Reference perpendicular dotted red lines indicate fold change < 0.8 or >1.3. Horizontal dotted red line indicates statistical significance at p- value < 0.05 as calculated using unpaired student's t-test. FC: fold change. n=5. Total phosphosite count=2264.

These phosphoproteins, which were different in LAD compared to SHAM, are mainly involved in the molecular binding activity, followed by catalytic and transporter activities based on Panther database classification system (figure 3.40).

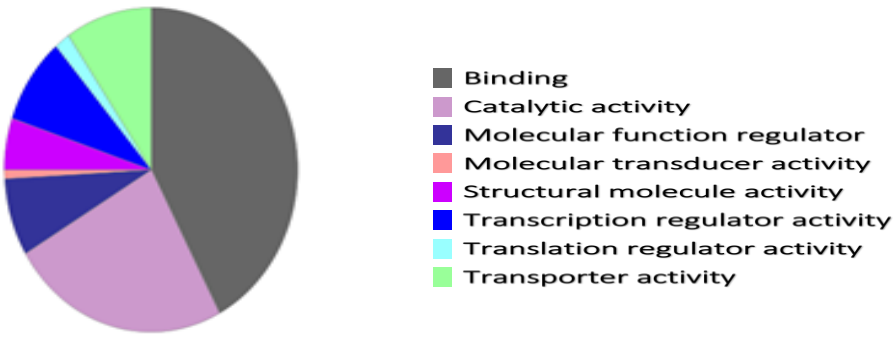

Figure 3.40 Molecular function of significantly different phosphoproteins. Panther Go-Slim molecular function of significant phosphoproteins. ($p < 0.05$) using protein accession numbers. Phosphoproteins count=210

A selection of significantly different phosphorylation sites (serine and threonine) is shown in table 3.1. There is an increased phosphorylation of phosphosites in cellular signalling proteins, including Heat Shock Protein 90 alpha, catenin alpha 1, in addition to ion transporters, i.e., L-type Ca+2 channel subunit alpha 2 and ryanodine receptor 2. These effects are also seen in sarcomere structural proteins such as Myosin-binding protein C, cardiac-type and z-disc related proteins, for example, myomesin 2, obscurin, vinculin and nexilin, as well as tight junction proteins (tight junction protein 2, tensin 2).

Table 3.1 Changes in phosphoproteins in LAD and SHAM groups ($p < 0.05$). Data were analysed using unpaired student's t-test. n = 5 S; serine, T; threonine.

Protein	Accession Number	Phosphorylation site(s)	FC (LAD/SHAM)	p-value
Ion transporters				
Voltage-dependent L-type calcium channel subunit alpha	Q71QJ6	S1700	1.3	0.03
Ryanodine receptor 2	B0LPN4	S2358	1.3	0.02
Sodium/potassium-transporting ATPase subunit alpha-1	P06685	S40	1.3	0.03
Sodium/hydrogen exchanger 1	P26431	S790	1.5	0.045
Sodium channel protein	A0A0G2JWG8	S224	1.6	0.02
Sarcoplasmic/endoplasmic reticulum calcium ATPase 2	P11507	S38 T376 S663	1.3 1.4 1.4	0.02 0.04 0.03
Electrogenic sodium bicarbonate cotransporter 1	Q9JI66	S1026 S262	1.8 1.7	0.04 0.03
Structural proteins				
Vinculin	A0A0G2K8V2	S721 S290 S346	1.6 1.5 1.6	0.01 0.03 0.02

Protein	Accession Number	Phosphorylation site(s)	FC (LAD/SHAM)	p-value
Structural proteins (cont.)				
Tight junction protein 2	Q3ZB99	S1132	1.4	0.01
Tensin 2	M0R671	S1086	1.5	0.04
Spectrin β chain	A0A0G2K8W9	S2132	1.3	
Taxilin beta	A0A0G2K2T1	S477	1.3	0.04
Synaptopodin	D3ZZ68	S596	1.5	0.02
Syntrophin, basic 1	D3ZWC6	T215	1.4	0.03
Pinin, desmosome-associated protein	D3ZAY8	S100	1.8	0.01
Obscurin, cytoskeletal calmodulin and titin-interacting RhoGEF	A0A0G2JUP3	S6445	1.6	0.01
Nexilin (Fragment)	C5H4P9	S80	1.4	0.03
Myosin-binding protein C, cardiac-type	P56741	S427	1.9	0.04
Desmin	P48675	S28	1.7	0.045
Myomesin 2	G3V7K1	S76	1.4	0.02
Myosin regulatory light chain 2, ventricular/cardiac muscle isoform	P08733	S15	2	0.03
Microtubule-associated protein 1B	F1LRL9	S904	1.4	0.04
Junctophilin-2	Q2PS20	S479 S462	1.3 1.4	0.004 0.02
A-kinase anchor protein 6	Q9WVC7	S1568	1.6	0.01

Protein	Accession Number	Phosphorylation site(s)	FC (LAD/SHAM)	p-value
Structural proteins (cont.)				
A-kinase anchor protein 12	Q5QD51	S350	2.2	0.03
A-kinase anchor protein 13	F1M3G7	S765	1.4	0.03
Actin-binding LIM protein 1	A0A0G2JW01	S480 S467	1.6 1.5	0.03 0.03
Signalling proteins				
Heat shock protein HSP 90-alpha	P82995	S263	1.5	0.04
Catenin (Cadherin associated protein), alpha 1	Q5U302	T660	1.5	0.02
Enzymes				
Dual-specificity phosphatase 27, atypical	D3ZRM0	S559	1.8	0.04
ATP synthase subunit beta	G3V6D3	S415	1.5	0.02
Striated muscle-specific serine/threonine-protein kinase	Q63638	S1177	1.4	0.04
SRSF protein kinase 3	A0A0G2KAH6	S73	1.4	0.04
Inositol-trisphosphate 3-kinase B	P42335	S202	1.6	0.03
Apoptosis related				
BCL2-associated transcription factor 1	B1WC16	S385 S397 S496	1.6 1.6 1.6	0.03 0.03 0.04
Cyclin Y	F1MA89	S73	1.5	0.04
Cell cycle and apoptosis regulator 2	F1LM55	S298	2.1	0.04

3.3.4 Effect of LAD coronary artery ligation on cardiac energetics

All cellular metabolites were measured using HPLC apparatus from apical, right and left atrial tissues of LAD and SHAM hearts 4 weeks after surgical procedure, data were compared regionally between the two groups.

3.3.4.1 Apical energetic profile

Table 3.2 lists different metabolites levels as taken from apical region in LAD and SHAM groups. In general, metabolites levels were slightly decreased in LAD group. However, none of these metabolites were significantly different compared to SHAM.

Table 3.2 Apical energy metabolites in LAD and SHAM hearts. Data are presented as mean ± SEM. Data were analysed using unpaired student's t -test. n=5

Metabolite	SHAM (nmol/mg)	LAD (nmol/mg)	p value
GTP	0.12 ± 0.01	0.13 ± 0.04	0.75
GDP	0.11 ± 0.03	0.10 ± 0.01	0.70
GMP	0.06 ± 0.02	0.05 ± 0.02	0.64
IMP	0.22 ± 0.13	0.10 ± 0.03	0.11
ATP	1.45 ± 0.25	1.25 ± 0.43	0.51
ADP	1.43 ± 0.28	1.31 ± 0.36	0.81
Hypoxanthine	0.2 ± 0.02	0.2 ± 0.07	0.59
Xanthine	0.07± 0.01	0.07± 0.02	0.99
AMP	1.38 ± 0.31	1.14 ± 0.19	0.74
B-NAD	0.47 ± 0.10	0.41 ± 0.08	0.75
Inosine	0.31 ± 0.14	0.39 ± 0.14	0.73
Adenosine	0.47 ± 0.21	0.33 ± 0.07	0.52

Phosphorylation ratios of guanosine and adenine metabolites were calculated and showed no significant difference in phosphorylation potential between the two groups. Adenine metabolites pool (summation of ATP, ADP, and AMP levels), and energy charge ([ATP+0.5*ADP]/total adenine pool) were slightly decreased in LAD group, however, this change was not statically significant (figure 3.41)

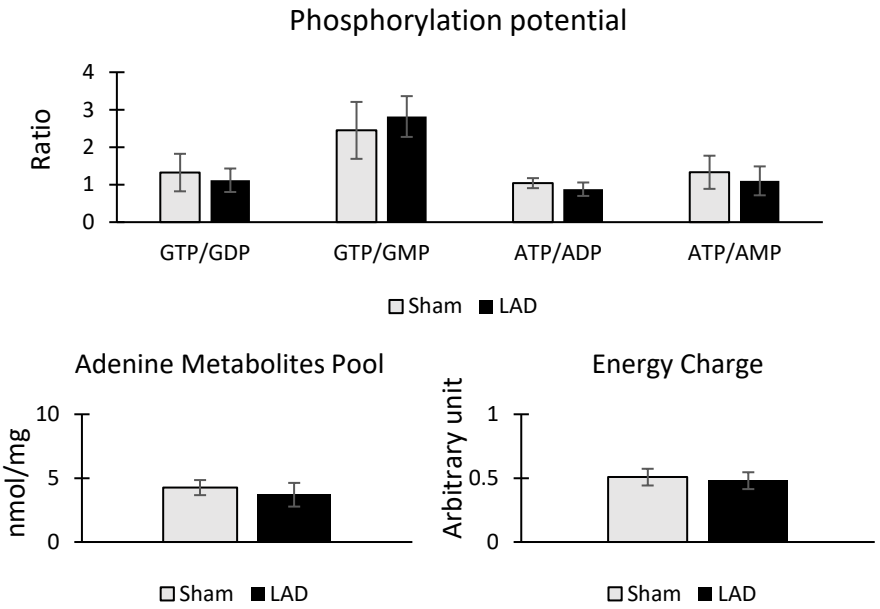

Figure 3.41 Phosphorylation potential, energy charge, and adenine metabolites pool of apex in LAD and SHAM groups. Data are presented as mean ± SEM and analysed using unpaired student's t-test. n = 5

3.3.4.2 Right atrium energetics profile

Right atrial metabolites levels in LAD and SHAM groups are listed in table 3.3. Levels of B-NAD and guanosine metabolites were generally higher in LAD group, whereas inosine was decreased. However, no statistically significant difference was noted.

Table 3.3 Right atrial energy metabolites in LAD and SHAM hearts. Data are presented as mean ± SEM, and analysed using unpaired student's t-test. n= 5

Metabolite	SHAM (nmol/mg)	LAD (nmol/mg)	p value
GTP	0.09 ± 0.02	0.38 ± 0.33	0.47
GDP	0.09 ± 0.01	0.43± 0.36	0.43
GMP	0.04 ± 0.01	1.52 ± 0.90	0.33
ATP	1.07 ± 0.26	1.03 ± 0.7	0.07
ADP	1.02 ± 0.09	1.60 ± 1.02	0.14
AMP	0.81 ± 0.08	0.69 ± 0.22	0.41
B-NAD	0.42 ± 0.09	0.80 ± 0.57	0.56
Inosine	0.24 ± 0.09	0.12 ± 0.07	0.43
Adenosine	0.31 ± 0.08	0.33 ± 0.19	0.39

However, there was a reduction in energy charge, total adenine pool and phosphorylation potential in LAD group compared to SHAM as seen in figure 3.42. Interestingly, GTP to GMP ratio was significantly reduced in LAD group.

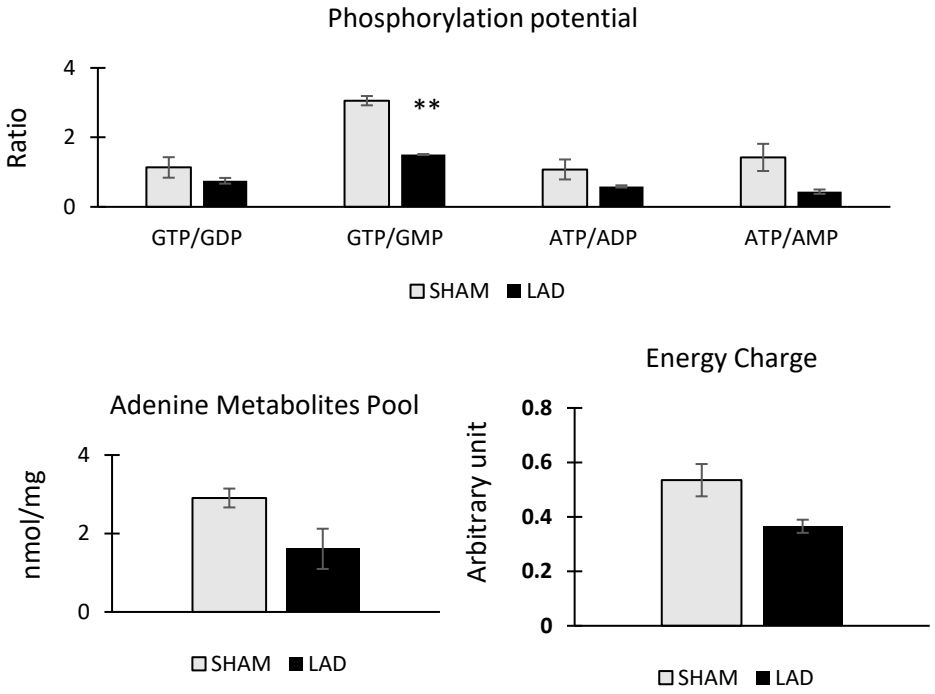

Figure 3.42 Phosphorylation potential, energy charge, and adenine metabolites pool of right atrium in LAD and SHAM groups. Data are presented as mean ± SEM and analysed using unpaired student's t-test. ** p< 0.01, n = 5

3.3.4.3 Left atrium energetics profile

Table 3.4 includes all left atrial energy metabolites levels from LAD and SHAM groups. Similar to right atrial profile, there was no significant difference between the two groups. Nevertheless, phosphorylation potential and energy charge were slightly increased in LAD group (figure 3.43).

Table 3.4 Left atrial energy metabolites in LAD and SHAM groups. Data are presented as mean ± SEM, and were analysed using unpaired student's t-test. n = 5

Metabolite	SHAM (nmol/mg)	LAD (nmol/mg)	p value
GTP	0.14 ± 0.03	0.14 ± 0.06	0.91
GDP	0.17 ± 0.06	0.10 ± 0.04	0.42
GMP	0.06 ± 0.01	0.10 ± 0.08	0.71
IMP	0.33 ± 0.13	0.39 ± 0.31	0.87
ATP	1.36 ± 0.30	1.52 ± 0.60	0.82

Metabolite (cont.)	SHAM (nmol/mg)	LAD (nmol/mg)	p value
ADP	1.48 ± 0.39	1.45 ± 0.76	0.98
Hypoxanthine	0.19 ± 0.02	0.31 ± 0.17	0.56
AMP	2.08 ± 0.93	1.17 ± 0.76	0.47
B-NAD	0.68 ± 0.18	0.47 ± 0.24	0.52
Inosine	0.50 ± 0.15	0.60 ± 0.41	0.82
Adenosine	0.82 ± 0.41	0.47 ± 0.23	0.46

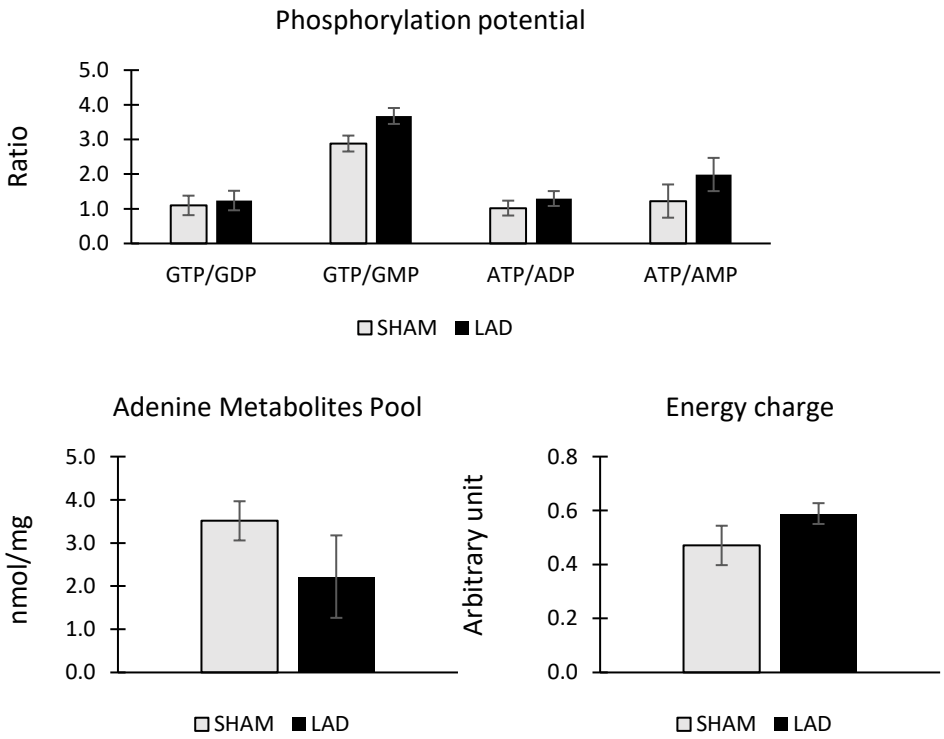

Figure 3.43 Phosphorylation potential, energy charge, and adenine metabolites pool of left atrium in LAD and SHAM groups. Data are presented as mean ± SEM, and were analysed using unpaired student's t-test. n= 5

3.3.5 Effect of LAD coronary artery ligation on cardiac metabolites

Using 1H-NMR spectral analysis of PCA extracted cardiac tissues from rat apical region, 16 metabolites were detected in both groups as seen in figure 3.44. Excluding cardiac energetics, these metabolites included amino acids, glucose, lactate, and lipids. However, none of these metabolites were statically significant between SHAM and LAD groups.

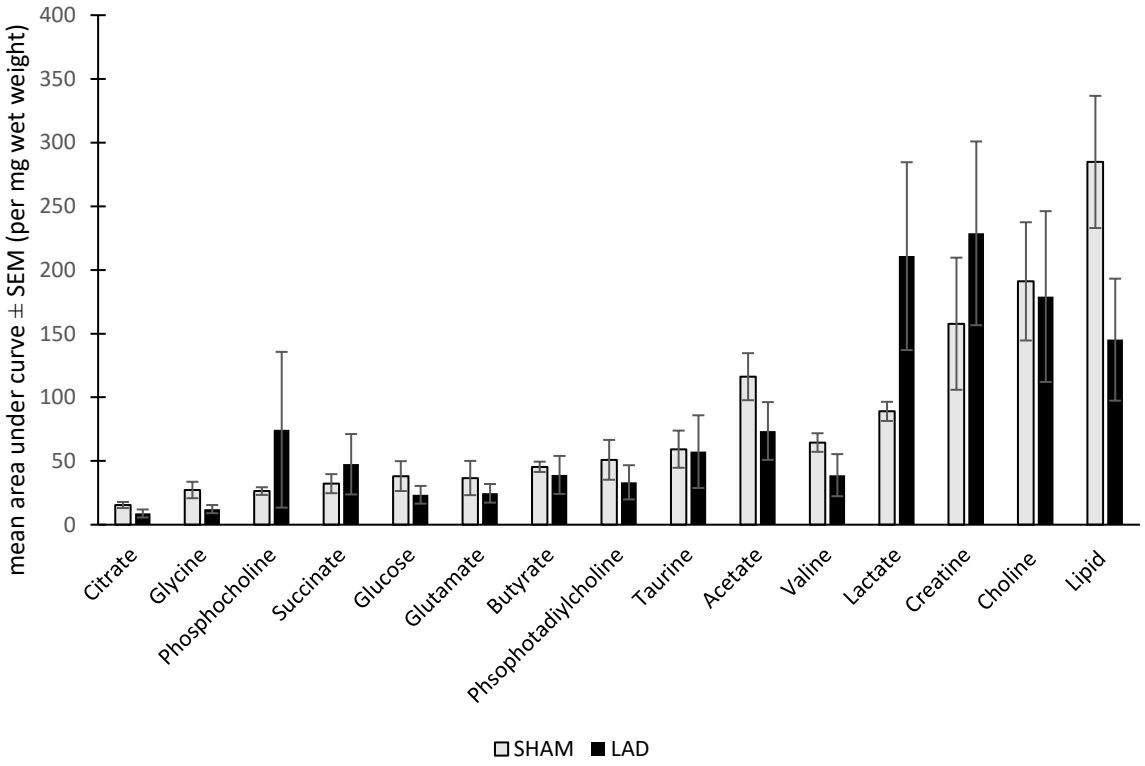

Figure 3.44 Rat apical cardiac metabolites. Metabolites in cardiac extract samples as collected from apex for LAD and SHAM groups. Data are presented as mean ± SEM, and were analysed using unpaired student's t-test. n = 4

3.3.6 Effect of LAD coronary artery ligation on blood metabolites

1H- NMR spectroscopy analysis was used to measure blood metabolites of LAD group before surgery (baseline) and four weeks after LAD coronary artery ligation. There were 24 metabolites that were annotated from NMR spectra (figures 3.45). These included TCA cycle intermediates, ketone bodies, amino acids and carbohydrates as seen in figure 3.46. However, only arginine and acetone were found to be statistically significantly different ($p < 0.05$) with an increased fold change (1.6 increase in acetone and 1.2 for arginine) as shown in figure 3.45.

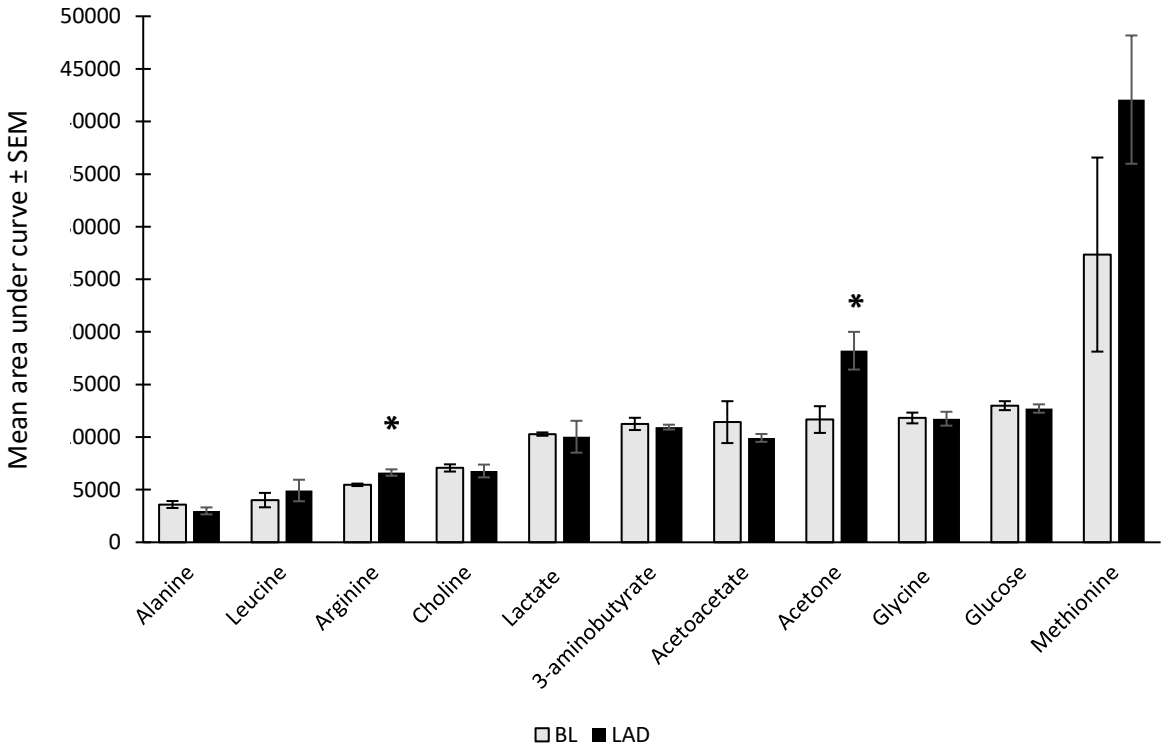

Figure 3.45 Rat blood metabolites. Metabolites in blood samples collected at baseline level (BL) and after 4 weeks LAD coronary artery ligation. Data are presented as mean ± SEM and were analysed using paired student's t-test. * $p < 0.05$, n = 4

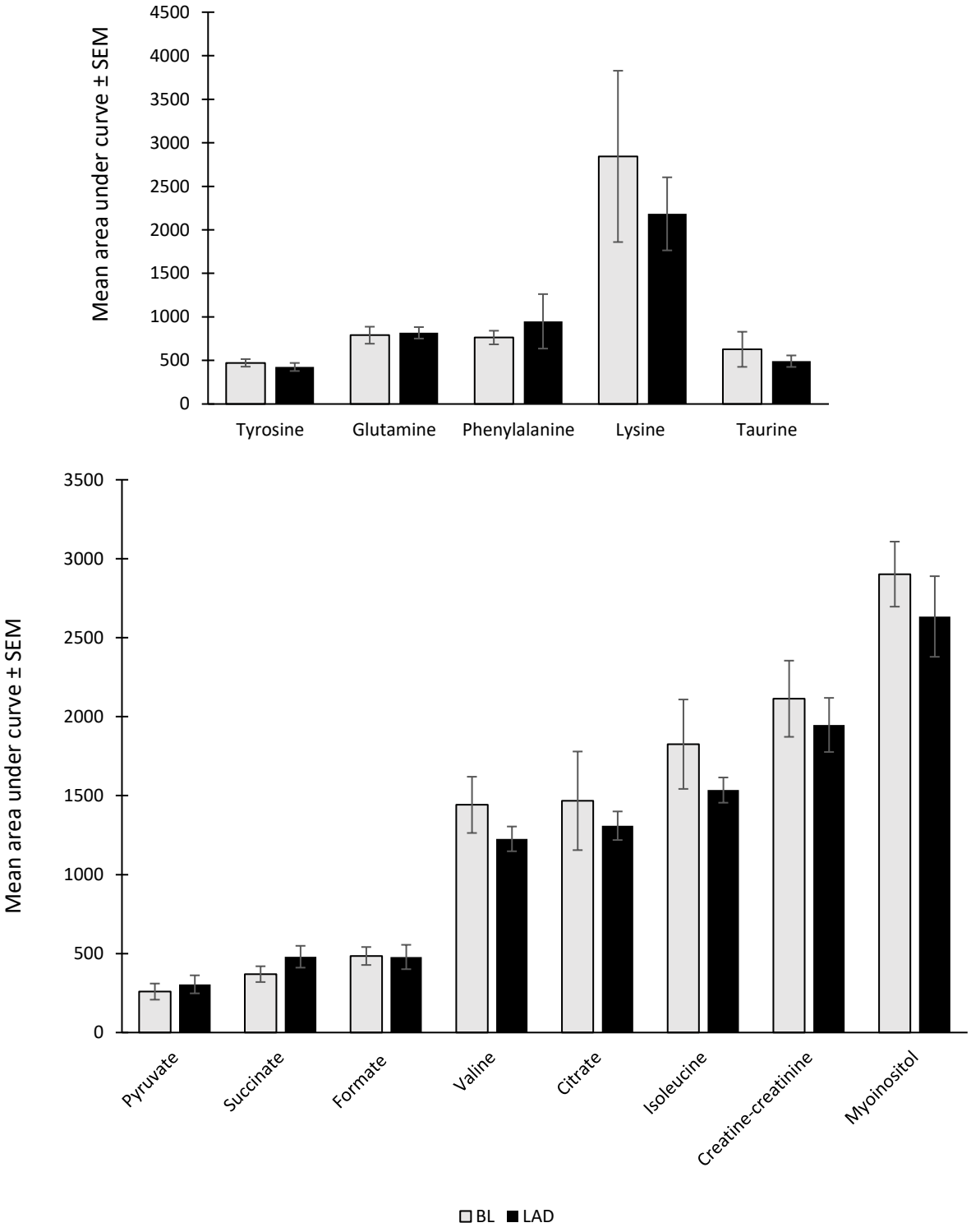

Figure 3.46 (above and below) Rat blood metabolites (cont.). Metabolites in blood samples collected at baseline level (BL) and after 4 weeks LAD coronary artery ligation. Data are presented as mean ± SEM and were analysed using paired student's t-test. n = 4

3.3.6.1 Spiked-in experiment

Spike-in experiment of arginine and acetone were done using 1H-NMR spectroscopy and buffers for both metabolites that were mixed to a pooled rat plasma. Addition of a certain metabolite to the pooled plasma must result in an enhanced signal at the exact frequency (ppm). However, acetone spiking resulted in one clear peak proved to exist in the samples (figure 3.47), while the spectra did not align perfectly with spiked arginine, suggesting possible interference of another metabolite(s) (figure 3.48).

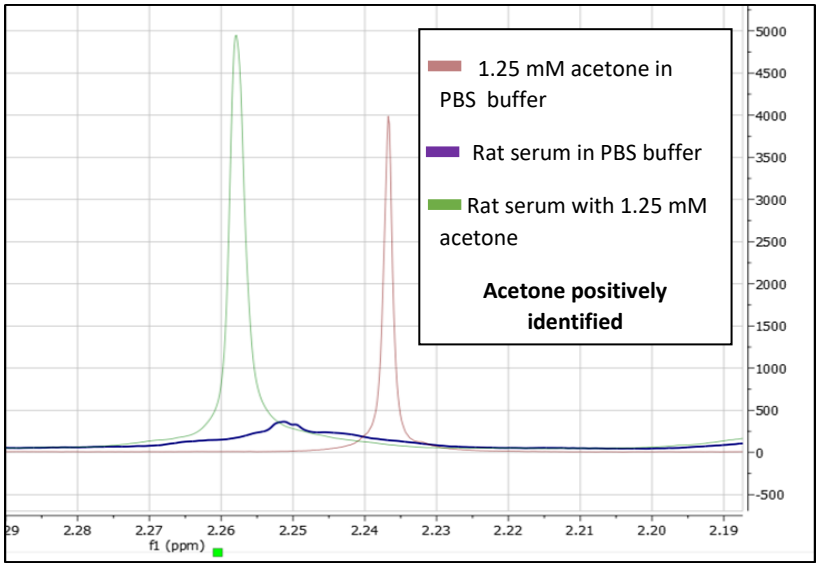

Figure 3.47 1H-NMR spectra for acetone spiked-in experiment. Spectra shown for 1.25 mM acetone in PBS buffer (in red), pooled rat plasma (purple) and rat plasma mixed with acetone (green).

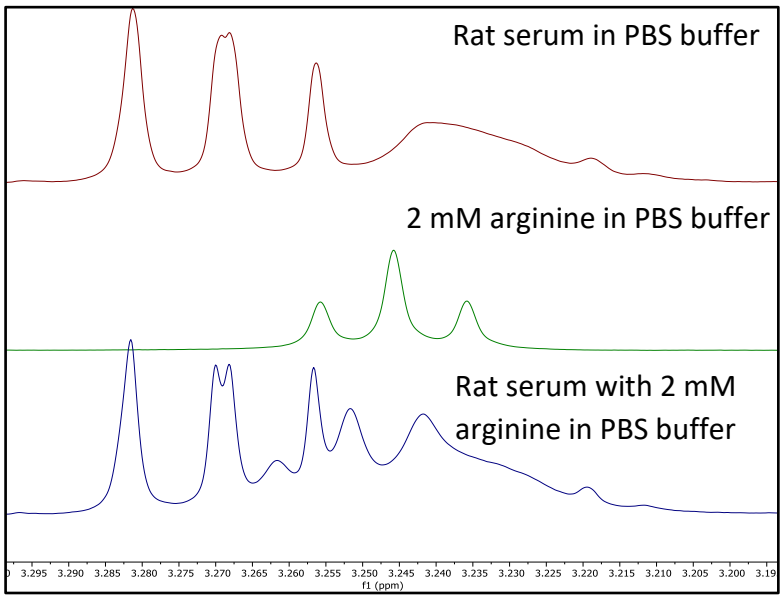

Figure 3.48 1H-NMR spectra for arginine spiked-in experiment. Spectrum of rat plasma is shown in red, 2mM arginine in PBS buffer spectrum in green, and rat plasma mixed with 2 mM arginine (purple).

3.4 Discussion

In this work, a rodent model of *in-vivo* permanent LAD coronary artery ligation in adult heart was used to investigate post ischaemic cardiac remodelling, four weeks after the infarction. Key findings in this chapter are concluded as the following:

- Post ischaemic cardiac remodelling is associated with distinctive pattens of fibrosis and structural disorganisation of extracellular matrix.
- Remodelling was associated with significant changes in mitochondrial morphometry and density and structural integrity.
- Decrease in antioxidant related cardiac proteins, and metabolic enzymes related to fatty acid and amino acids metabolic pathways.
- Upregulation of cellular calcium handling proteins were significantly upregulated and modified by phosphorylation (as in post translational modification) in remodelled hearts.
- Post ischaemic cardiac remodelling is associated with differential expression of certain cytoskeletal, ECM and z disc and junctional proteins, in addition to increased phosphorylation at multiple phosphorylation sites.
- Key signalling pathways activities include protein kinase A, Phospholipase C (PLC), and Gamma G beta protein signalling pathways.
- Blood metabolomic profiling showed significant increase in acetone and arginine with post ischaemic cardiac remodelling.

3.4.1 Post ischaemic cardiac remodelling is associated with disruption to ECM structure and proteins

Infracted areas in LAD hearts sections revealed patten of compact fibrosis, in which the collagen is deposited in a large dense area with a scarcity of cardiomyocytes, while in the border zone, collagen distribution appears rather diffuse, i.e., septa of collagen intersperse living cardiomyocytes (figure 3.3). Some of these features have been described in human myocardium post MI (Rog-Zielinska, Norris et al. 2016). Moreover, as seen in electron micrographs, the infarcted area is heavily populated with nonmyocytes, such as fibroblasts (and myofibroblast), endothelial cells, telocytes, and macrophages, etc. all of which are crucial for ongoing infract remodelling and matrix reorganisation (Sun and Weber 2000, Fomovsky and Holmes 2010).

Tissue fibrosis is driven by fibroblasts which mediate tissue-repair, angiogenesis and biological responses that result in scar formation (Rog-Zielinska, Norris et al. 2016). Fibroblasts were noted in various stages of differentiation and activation (figures 3.8 -3.10). In response to tissue injury and TGF-β release, fibroblasts become activated and differentiate into myofibroblasts that are extensively involved in continuous *de novo* synthesis of fibrillar collagen (type III and I) and degradation (Fu, Khalil et al. 2018), as well as deposition of ECM components such as proteoglycans, glycoproteins (Czubryt 2012), and as identified in our work, cathpesin S and heparan sulfate, and in addition to activation of angiogenesis and release proinflammatory cytokines (Lindner, Zietsch et al. 2014).

Electron micrographs showed infiltrating immune cells such as macrophages into ECM (figures 3.9 and 3.10). Proteomics data showed that proteins involved in immune response activation were all increased in LAD group, even after four weeks of cardiac injury. One of these proteins is tryptase, which is contained in mast cells, therefore, it is as a marker for mast cell activation (Vanderslice, Ballinger et al. 1990). Tryptase, which is increased significantly in LAD group, triggers *in-vitro* rat cardiac fibroblasts proliferation and conversion to myofibroblast phenotype, favouring collagen deposition (Janicki, Brower et al. 2015) In this regards, there has been an evolving evidence demonstrating that cardiac mast cell plays a substantial role in adverse remodelling and several cardiovascular disorders (Janicki, Brower et al. 2015). Nevertheless, Chancy et. al showed that cardiac mast cells, which store and release biologically active substances and mediators such as tumour necrosis factor-α (TNF-α) and proteases like chymase and tryptase, are involved in MMPs activation in volume-overloaded hearts (Brower, Chancey et al. 2002). Whether mast cells predominately mediate pro-inflammatory or pro-proliferative response in the ischaemic myocardium is not yet fully understood.

In addition, CD 48 antigen, increased in LAD group, is involved in both innate and adaptive immune responses, such as granulocyte and lymphocytes activation and proliferation, through its interaction with CD244 receptor on cytotoxic T cell as well as Natural Killer cells(NK)(McArdel, Terhorst et al. 2016). Experimental small and large animal models provided evidence for both T and B lymphocytes infiltrate into the infarct zone following acute MI (Yan, Anzai et al. 2013). For example, cytotoxic T lymphocytes (CD8) increased one week following ischaemia, and when collected from rats subjected to acute MI, they had a deleterious effect on healthy cardiomyocytes (Ong, Hernández-Reséndiz et al. 2018)

Nonetheless, telocytes, characterised by their small cell body and thin long telopodes (10-30 um) (Bei, Wang et al. 2015), are involved in neovascularization and tissue regeneration (Zhao, Liao et al. 2014). In the myocardium, telocytes are believed to form cardiac network of interstitial cells with cardiomyocytes through cellular junctions, this helps mediating intercellular signalling (Gherghiceanu and Popescu 2012). Recent evidence argues that cardiac telocytes may play an important role in the maintenance of the structural and functional integrity of the myocardium (Nour, Sarhan et al. 2017). Our work data showed different alterations compared to Zhao et. al, who documented undetectable levels of telocytes in the infarcted area 28 days post MI in murine heart (Zhao, Chen et al. 2013). We have identified several telocytes that were in close proximity to cardiomyocytes in EM images of the infract area (figures 3.8 -3.10). This could be explained by the species-related differences, since mice achieve scar maturity faster than rats, in addition to extensive and large transmural infract after LAD ligation (Yang, Liu et al. 2002), or alternatively the stage at which telocytes are examined. In our work, it is evident that the infracted area has remaining cellular elements from late proliferative phase, hence the quantification of telocytes at later stage of remodelling could possibly result in massive decrease in telocytes density in the myocardium, as most cells undergo apoptosis to leave collagen rich scar. Interestingly, telocytes in LAD group were marked by cytoplasmic vacuolation and shrinkage of their telopodes, suggesting continuous degeneration and cell stress (figure 3.10), similar findings were observed by Richter et. al in failing human myocardium (Richter and Kostin 2015).

Finally, remodelling of arteriolar wall was evident with post ischaemic remodelling, in which the ratio of wall area to total area was increased (figure 3.6). This could be explained by disruption of endothelial cells and excessive vascular smooth muscle cells proliferation and turnover in tunica media, possibly as a result of inflammation, ROS release and induction of hypoxia signalling pathway in VSMC leading to vascular remodelling (Zhuge, Zhang et al. 2020).

3.4.2 Changes in mitochondrial morphology and molecular content and metabolism

This work has provided evidence of disruption to mitochondrial morphology, proteome and function which is maintained 4 weeks after cardiac injury. These changes are selective and linked to different mitochondrial subpopulations. Interfibrillar mitochondria had a significantly increased aspect ratio (length to width) in LAD hearts compared to SHAM, i.e., appeared more elongated, which indicates a tendency towards mitochondrial fusion. Work by Sun et al. showed that mitochondria tend towards fusion in isolated rat heart after short periods of hypoxia (3-5 min) (Sun, Dhalla et al. 1969). Likewise, others have observed marked elongation of interfibrillar mitochondria in patients with ischaemic cardiomyopathies (Tandler, Dunlap et al. 2002, Kanzaki, Terasaki et al. 2010). It is possible that mitochondrial fusion could emerge as an adaptive pro survival mechanism to mitigate cellular stress and damage and increase the oxidative phosphorylation capacity and to compensate for partially damaged mitochondria (Tondera, Grandemange et al. 2009, Youle and van der Bliek 2012). Mitochondria in cardiomyocytes are spatially distributed into three main subpopulations; interfibrillar subpopulation serve to provide ATP necessary for myofibril contraction, while subsarcolemmal and perinuclear subpopulation provide the needed energy for sarcolemmal ion pumps and nucleus, respectively (Hollander, Thapa et al. 2014). While mitochondrial subpopulation distribution did not significantly vary between the two groups, mitochondrial

cristae density, however, was significantly decreased in LAD hearts (figure 3.12). This is shown as a separation of intercristae spaces, and these changes are linked to the disruptive metabolic status of the mitochondria (Logan 2006).

As detected in proteomic data from the rodent model, several mitochondrial proteins that were diminished are related to ATP synthesis and ECT (figure 3.24). Moreover, LAD hearts were decreased in key mitochondrial enzymes involved in amino acids and fatty acids metabolism. For instance, branched chain amino acid aminotransferase 2 (BCAT2), which catalyses reversible transamination reaction of branched chain amino acids BCAA (valine, leucine and isoleucine) to produce branched chain keto acids (Holeček 2018). Defect in BCAA catabolism was found in failing hearts of mice and patients, which alters cardiac contractile function and redox homeostasis (Sun, Olson et al. 2016, Uddin, Zhang et al. 2019). Moreover, impairment of fatty acids oxidation, through reduction of the pathway rate limiting enzyme acetyl-CoA carboxylase beta (ACACB) and mitochondrial enoyl-CoA hydratase (ECHS1), indicate a loss of the metabolic flexibility in heart failure (Neubauer 2007, Karwi, Uddin et al. 2018), which results in a drop of mitochondrial oxidation rates by 30-40% (Fillmore, Mori et al. 2014). This reduction in oxidation rate is associated with decrease in fatty acids and glucose metabolism, which is inefficient in energy production needed for contraction and ionic homeostasis.

Moreover, oxidative stress mediates mitochondrial damage through increased production of ROS, and/or decreased antioxidant defence mechanisms. In this regard, our work has shown significant decrease of antioxidant enzymes levels in LAD hearts, for instance, glutathione peroxidase 1 (GSHPx-1), superoxide dismutase SOD [Cu-Zn] and several other glutathione s-transferases/hydrolases. Glutathione peroxidase 1 (GSHPx-1) reduces lipid hydroperoxides, while superoxide dismutase [Cu-Zn] catalyses the conversion of superoxide radicals into molecular oxygen or hydrogen peroxide (Krishnamurthy 2012). Other studies have also provided evidence of progressive decrease in SOD and GSHPx activities in the infarcted myocardium, followed by the non-infarcted region in rodents (Sun 2009). The depletion of antioxidant enzymes content in infarcted hearts can indirectly reflect the continuous state of oxidative stress, which leads to extensive proteins and lipid peroxidation, and cellular damage. This is also consistent with the continuous presence of debris including evidence of macrophages and leukocyte in electron micrographs of LAD hearts (figure 3.9-3.10).

Additionally, blood acetone, the smallest of ketone bodies that is formed by spontaneous decarboxylation of acetoacetate in mitochondria (Sass 2012), was significantly increased four weeks after LAD coronary artery ligation as concluded from NMR results. While data regarding metabolic profiling of animal models with post ischaemic cardiac remodelling are still lacking, there have been reported evidence concerning ketone bodies in clinical studies of patients with heart failure. Both Du Z and Tenori L et. al showed modulation of ketone bodies metabolism and reported marked increase in acetone and β-hydroxybutyrate levels in blood of HF patients with mildly to severely reduced EF in comparison to healthy control (Tenori, Hu et al. 2013, Du, Shen et al. 2014). At the level of heart itself, a study showed that myocardium maintains ketone bodies extraction in heart failure (Janardhan, Chen et al. 2011), while other studies concluded that in diseases, such as hypertrophic and dilated cardiomyopathies, ketone bodies utilisation is elevated (Cotter, Schugar et al. 2013).

3.4.3 Sarcomere proteins with post ischaemic cardiac remodelling

Sarcomere length is one the main determinants of cardiac contractile strength, based on Frank-Starling relationship, it directly affects the contraction and relaxation of myofibrils, and eventually cardiac function.

The sarcomere length, as measured using EM imaging four weeks after LAD coronary artery ligation, was slightly elongated in LAD group but did not significantly change compared to SHAM hearts. Nonetheless, passive myocardial stiffening, which determines stretching, is affected by expression of titin isoforms (Neagoe, Kulke et al. 2002). Titin, a giant protein which connects z disc to M line, is normally present in N2B isoform, but during ischaemia, an increase of N2BA isoform expression, which is also seen in rats proteomic data, is linked to reduced sarcomere stiffness and increased compliance (Warren, Jordan et al. 2003). Differences in sarcomere length after ischaemia are also time dependant, as shown by Crozatier et al, in which sarcomere length was increased 15 minutes after ischaemia, as measured from the infarct area of open-chest LAD coronary artery ligated canine heart, due to overstretching from rapid loss of cardiomyocytes. Moreover, there was a prominent time dependant variation in sarcomere lengths as measured 45 minutes to 2 hours afterwards (Crozatier, Ashraf et al. 1977).

However, z disc, which is found at the border between two adjacent sarcomeres, is not only involved in maintaining the structural integrity of sarcomere, but it also plays an active role in cell signalling in cardiomyocytes (Knöll, Buyandelger et al. 2011). Proteomics data from LAD and SHAM groups demonstrated differential overexpression of many structural elements in z disc such spectrin alpha chain, non-erythrocytic 1, PDZ and LIM domain protein 4, Synaptopodin-2. However, little is known about the effect of ischaemia and chronic remodelling on z-disc structures. For instance, synaptopodin-2 regulates intracellular signalling between z disc and nucleus in cardiomyocytes, along with other proteins like A-kinase anchoring protein (AKAP), Calcineurin and CaMKII (Faul, Dhume et al. 2007). While PDZ-LIM domain protein interacts with α-actinin proteins and Protein Kinase C to mediate its translocation to z disc (Zheng, Cheng et al. 2010, Maturana, Nakagawa et al. 2011). All these results demonstrate the dynamic response of z disc that could be implicated in pathophysiology of post ischaemic remodelling.

Not only proteins expression that changes with post ischaemic cardiac remodelling, but also protein post-translational modification (including phosphorylation), results in alteration and vast diversity of proteins activities. Whether these changes occur acutely and continue for four weeks after cardiac injury, or manifest only at later stage of cardiac remodelling is unknown. These included A-kinase anchoring protein (AKAP)-12 (pS350), Spectrin β chain (pS2132), Heat Shock Protein (HSP) α (pS263), catenin-α1 (pT660) and nexilin (pS80). Catenin-α1 is located in intercalated discs in cardiomyocytes and plays an important role in anchoring cytoskeleton to sarcolemma (Jamora and Fuchs 2002). Interestingly, phosphorylation of threonine phospho-linker in actin-binding domain of this protein promotes intercellular adhesions in drosophila, mice and human cells (Escobar, Desai et al. 2015). Moreover, AKAP-12, a cytoskeletal scaffold protein that is involved in signal transduction of PKC and PKA. Upon its phosphorylation by PKC, AKAP-12 translocates from plasma membrane to mediate actin cytoskeleton reorganization (Akakura and Gelman 2012). Nevertheless, how these responses are linked to post ischaemic remodelling is still to be elucidated.

3.4.3 Effect of post ischaemic remodelling on cellular calcium handling proteins

Defective calcium homeostasis is a distinguished feature of heart failure, which results in disruption to cardiac contraction and relaxation and LV function. Some calcium handling protein such as calcium channel voltage-dependent, alpha 2/delta subunit 2 and voltage-dependent L-type calcium channel subunit alpha were upregulated in LAD group, whereas sarcoplasmic/endoplasmic reticulum calcium ATPase 2 (SERCA2) and Ryanodine receptor 2 (RyR2) were subjected to increased phosphorylation. In particular, there was increased phosphorylation of SERCA2 in LAD group at several phosphorylation sites, including serine 38, which is shown to increase Vmax of calcium transport by Ca^{2+}/calmodulin-dependent protein kinase CaMK (Toyofuku, Curotto Kurzydlowski et al. 1994). Other unique unreported sites were T376 and S663. However, RyR2 had increased phosphorylation at S2358. It is known that with increased adrenergic stimulation during heart failure, there is increased phosphorylation of RyR2 by several kinases, such as PKA, at different phosphorylation sites, including S2809 and S2030 (Jiang, Lokuta et al. 2002, Xiao, Jiang et al. 2005). It is important to take in consideration that slight variations in phosphorylation sites are species dependant. Nonetheless, hyperphosphorylation of RyR2 enhances its Ca^{2+} sensitivity, which may lead to increased diastolic sarcoplasmic reticulum calcium leak (Bers 2006), and with loss of synchronous sarcoplasmic reticulum Ca^{2+} release, this consequently triggers cardiac arrhythmia as seen in rabbit HF model rabbit using coronary artery ligation (Fowler, Wang et al. 2020). However, data regarding effects of these posttranslational modification on cardiac contractility and performance are still limited.

3.4.4 PKC signalling in post ischaemic cardiac remodelling

IPA analysis highlighted the role of three main signalling pathway in post ischaemic cardiac remodelling in rodent model. All of these pathways included PKC to initiate downstream signalling for multiple cellular targets. PKC, specifically subunit alpha, exerts regulatory effects on cardiac contractility and hypertrophic response (Dorn and Force 2005, Steinberg 2012), and it modulates cardiac response in IRI (Kang, Zhang et al. 2010) . PKC mediated activation of PKA through adenylate cyclase results in phosphorylation of many proteins such as myosin light chain kinase (MLCK), leading to cytoskeletal regulation and titin, which ultimately reduce myofibrillar passive tension (Krüger and Linke 2006). PKC activation in G beta gamma signalling pathway activates extracellular signal–regulated kinase1/2 (ERK1/2), which promotes cardiac hypertrophy and growth (Braz, Bueno et al. 2002). Moreover, PKC mediates pathological maladaptive hypertrophy via activation of calcineurin, which mediates dephosphorylation of nuclear factor of activated T cells (NFAT), allowing its translocation to nucleus to activate transcription of hypertrophic response genes (Dorn and Force 2005) as seen PLC pathway (figure 3.38).

In summary, using a rat model of sustained ischaemia after permanent LAD coronary artery ligation, this work highlighted, amongst several changes, the complicity of mitochondrial morphological disruption as evident by decreased cristae density, in addition to oxidative stress, through decreased expression of antioxidant related proteins in post ischaemic cardiac remodelling. Moreover, z disc proteins appear to play significant role in

pathophysiological processes following acute sustained myocardial injury, as they provide not only structural support to sarcomere, but also initiation of various cellular signalling pathways.

Chapter 4

Post ischaemic cardiac remodelling in porcine model of Ischaemia reperfusion injury

4.1 Introduction

The study in chapter 3 focused on cardiac remodelling after acute MI in rodent model. Rodent hearts are excellent for initial investigations given their low cost and their longevity. Nonetheless, rodents do not easily develop coronary disease, and they have different action potential profile and heart rate reaching 450 bpm. Therefore, it is important to compare data obtained from rat with a clinically relevant large animal model. Although the dog was considered as the closest to human (e.g., similar collaterals), its use in cardiovascular clinical studies has markedly reduced largely due to ethical issues.

The use of porcine model in cardiovascular research has gained wide acclaim due to the anatomical and physiological similarities between human and pig hearts (Spannbauer, Traxler et al. 2019). This great advantage facilitated the translation of numerous therapeutic interventions and devices from small animal models to patients. Nonetheless, high costs, labour intensive care, and the lack of developed collateral coronary circulation in pigs remain major limitations that challenge the use of this model as a substitute to human heart to study ischaemic heart diseases (Seiler, Stoller et al. 2013). In contrast to humans, who have the most advanced coronary collateral function after the guinea pig, the pig has the least advanced collateral function in comparison to all other relevant models of mammals (Seiler, Stoller et al. 2013). Furthermore, the high rate of mortality due to fatal arrhythmias in pigs during surgical induction of ischaemia and/or reperfusion is an issue for many research centres (Spannbauer, Traxler et al. 2019). Despite this, the porcine model of cardiovascular disease remains important for translating interventions from rodents to clinical practice. In general, *in-vivo* large animal models are divided into open or closed chest models (Kumar, Kasala et al. 2016). Percutaneous left anterior descending coronary artery occlusion in pigs is a popular model for studying heart failure after acute MI, and is used largely for investigating therapeutic interventions (Laguens, Cabeza Meckert et al. 2002, Champagne, Su et al. 2003, Jansen of Lorkeers, Gho et al. 2015, Malka, Meerkin et al. 2015, Collantes, Pelacho et al. 2017).

Studies investigating heart failure following MI tend to focus on one aspect of functional, structural and signalling changes with remodelling, and there is lack of studies that monitor other aspects of remodelling in an integrated manner. Therefore, this work aims to extend knowledge about cardiac remodelling following acute MI in a large animal model. Based on that, we decided to investigate molecular, cellular, histological changes in porcine model of post ischaemic cardiac remodelling four weeks after IRI. This model is currently being used in Bristol to test therapeutic interventions that can reduce injury and mitigate the severity of heart failure. In view of the complexity of remodelling (see different phases in section 1.4), improved knowledge will assist in interpreting outcome and in identifying pathways that can be targeted to reduce the detrimental effects of remodelling leading to heart failure.

4.2 Methods

The procedures and methods used in this chapter are fully described in detail in materials and methods chapter (chapter 2).

4.2.1 Experimental procedure

In summary, animal procedures were undertaken at the University of Bristol Translational Biomedical Research Centre (TBRC) in accordance with the United Kingdom Animal (Scientific Procedures) Act, 1986 (under PPL 7008975). Female Yorkshire pigs weighing 58-64 kg (n = 4) underwent closed-chest balloon catheter inflation to occlude the left anterior descending (LAD) coronary artery for 60 minutes, the mean pressure of occlusion was 10.6 atmospheric pressure (atm). This was followed by balloon deflation and recovery. The intervention was performed at the TBRC and carried out by Dr Tom Johnson and assisted by Dr. Domenico Bruno. As a precaution to decrease the possibility of lethal ventricular arrhythmia, both amiodarone and magnesium (300 mg and 8 mg, respectively over 4 hours) were administered at the time of MI induction through a central line. Cardiopulmonary resuscitation was performed in case of arrhythmia. Healthy adult pigs, which did not undergo any surgical intervention, were taken as a control group (n= 4). Cardiac imaging and cardiac troponin-I measurements were performed by the surgical team at selected time intervals (further explained in the appendix), after which pigs underwent termination, and cardiac tissues from the infarcted area of the left ventricle in addition to blood samples were collected. The left ventricular tissues were snap frozen in liquid nitrogen and stored at -80 °C.

Blood collection was done at the baseline (before surgery), reperfusion, and 10, 20 ,30 minutes; 1, 4 and 24 hours and at termination (4 weeks). Each sample was transferred into EDTA tube (BD Vacutainer, UK) and centrifuged at 1000 g at 4 °C for 10 minutes. The plasma was collected into Eppendorf tubes and stored at -80 °C freezers for cardiac troponin-I measurement and nuclear magnetic resonance experiments.

Tissues collected from the left ventricle of control or LAD group (four weeks after intervention) were snap frozen in liquid nitrogen and stored at -80 °C freezers for proteins extraction. Chunks of left ventricle were also placed in 4% paraformaldehyde solution, kept at 4 °C for 24 hours, and sent for tissue processing the following day.

4.2.2 Liquid Chromatography Tandem Mass Spectrometry (LC-MS/MS)

Left ventricular myocardial tissues from both groups (n= 4) were homogenised for protein extraction in RIPA buffer with protease and phosphatase inhibitors, followed by quantification using Bradford essay, and then the extracted samples were sent for Proteomics facility at University of Bristol, to be analysed using Liquid Chromatography Tandem Mass Spectrometry (LC-MS/MS) to detect changes in proteins and phosphoproteins as described in detail in section (2.4.1).

4.2.3 High Performance Liquid Chromatography (HPLC)

Left ventricular, right and left atrial tissues from both groups (n= 4) were crushed with pestle and mortar for metabolites extraction using PCA and neutralised with K_2CO_3. The tissue extract was sent for HPLC analysis to determine cardiac energetics in left ventricle, left and right atria from each group as described in section (2.4.2).

4.2.4 Nuclear Magnetic Resonance (NMR)

Blood samples taken from pigs (4 weeks after LAD coronary artery occlusion and control) were collected into EDTA tubes, centrifuged at 1000 g for 10 minutes, and the plasma was transferred into Eppendorf tubes and stored in -80 °C freezer until later use. Plasma samples in addition to PCA extracted tissues were transferred to School of Chemistry, University of Bristol on dry ice for metabolites analysis using Nuclear Magnetic Resonance spectroscopy (NMR). Full method is described in section (2.4.3).

4.2.5 Light Microscopy

Tissues from porcine hearts were fixed using 4% paraformaldehyde solution and prepared for processing, embedding, and sectioning, and staining with H&E, EVG and Masson's trichrome stains to study post ischaemic cardiac remodelling at gross structural level. Full details regarding these techniques are found in section (2.4.4).

4.2.6 Electron Microscopy

Left ventricular tissues from porcine hearts were fixed with 4% paraformaldehyde solution. Samples were sent for Wolfson Bioimaging facility for processing, EPON epoxy resin embedding, sectioning, and staining with uranyl acetate and lead citrate to study post ischaemic cardiac remodelling at ultrastructural structural level. Full details regarding these techniques are found in section (2.4.5).

4.3 Results

4.3.1 Effect of 60-minute LAD coronary artery occlusion /reperfusion on gross porcine cardiac morphology

Data regarding cardiac injury measurement and assessment of the porcine model following ischaemia reperfusion injury as used in this study are included in the appendix. This work was carried out by the TBRC team, which and includes CMR measurements (ejection fraction and infarct size) and cardiac troponin I (cTnI) results.

4.3.1.1 Effect of 60-minute LAD coronary artery occlusion /reperfusion on cardiac fibrosis

Masson trichrome staining was used to establish a histological evidence of the infarcted scarred myocardium, as observed in the septal area four weeks after LAD coronary artery balloon occlusion and reperfusion. There is an extensive deposition of collagen (in blue) in LAD group sections as seen figure 4.1. There was significant eight-fold increase in the percentage of fibrosis in LAD sections compared to control (figure 4.2).

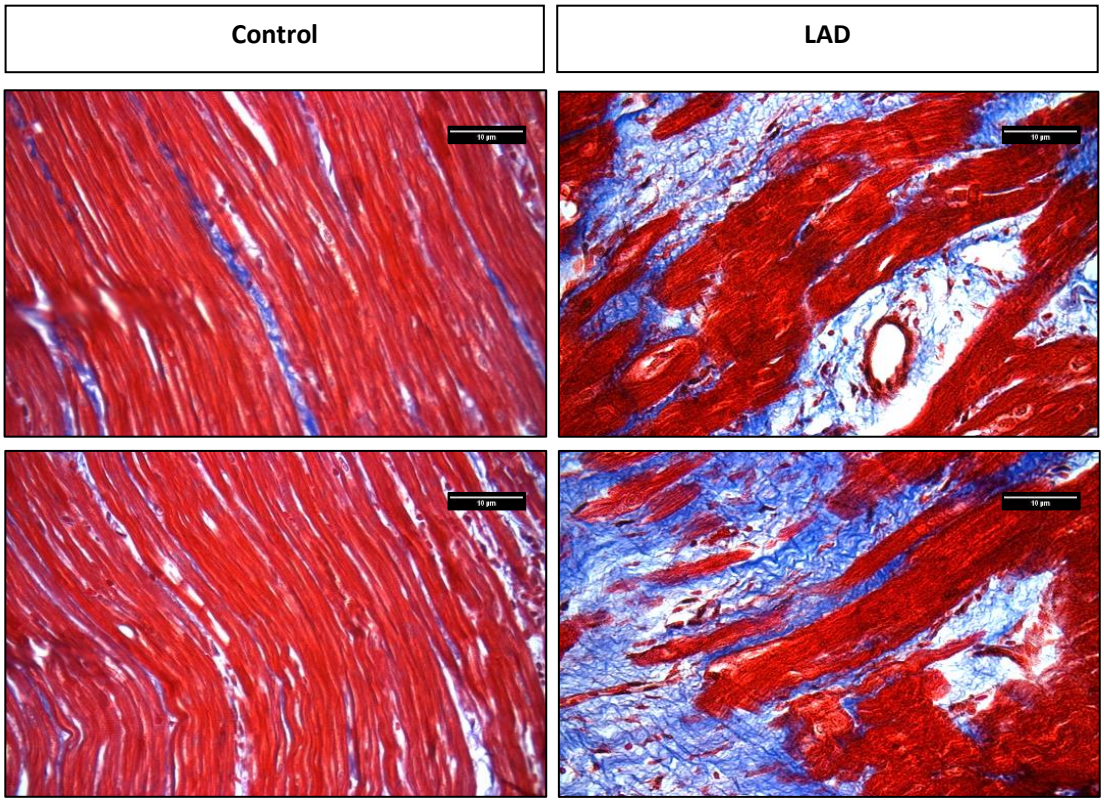

Figure 4.1 Representative Masson's trichrome staining of control and LAD cardiac sections. Sections were taken from the infarct in LAD group, and from left ventricle in control. Images were acquired with objective lens x40. Scale bar set to 100 microns. Extensive fibrosis (blue) can be seen perivascular as well as diffused in between myocytes bundles in all samples collected from LAD hearts. In contrast, there is markedly less evidence of fibrosis as seen in control group.

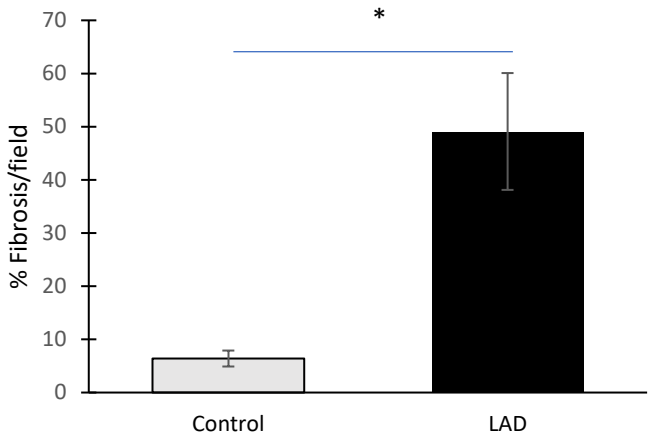

Figure 4.2 Percentage of fibrous tissue in control and LAD groups. Quantification of cardiac fibrosis was performed in the infarct area (% of area of fibrosis to total acquired field) in LAD group and corresponding LV area in control using Masson's trichrome stain. Data were analysed using unpaired student's t-test and presented as mean percentages (SEM). * $p < 0.05$, n = 4, 3-4 fields were examined for each heart.

4.3.1.2 Effect of 60-minute LAD coronary artery occlusion /reperfusion on elastin deposition and arteriolar wall thickness

Figure 4.3 shows EVG staining, which was used to identify elastin fibres (purple), collagen (red) in contrast to cardiomyocytes (orange). In addition to collagen, infarcted areas 4 weeks after LAD coronary artery occlusion and reperfusion appear to have widespread distribution of elastin in the perivascular space. Moreover, there was a significant increase in ratio of arteriolar wall area to total arteriolar area in LAD group compared to control (fold change (LAD/Control) = 1.67, $p < 0.01$) as seen in figure 4.4.

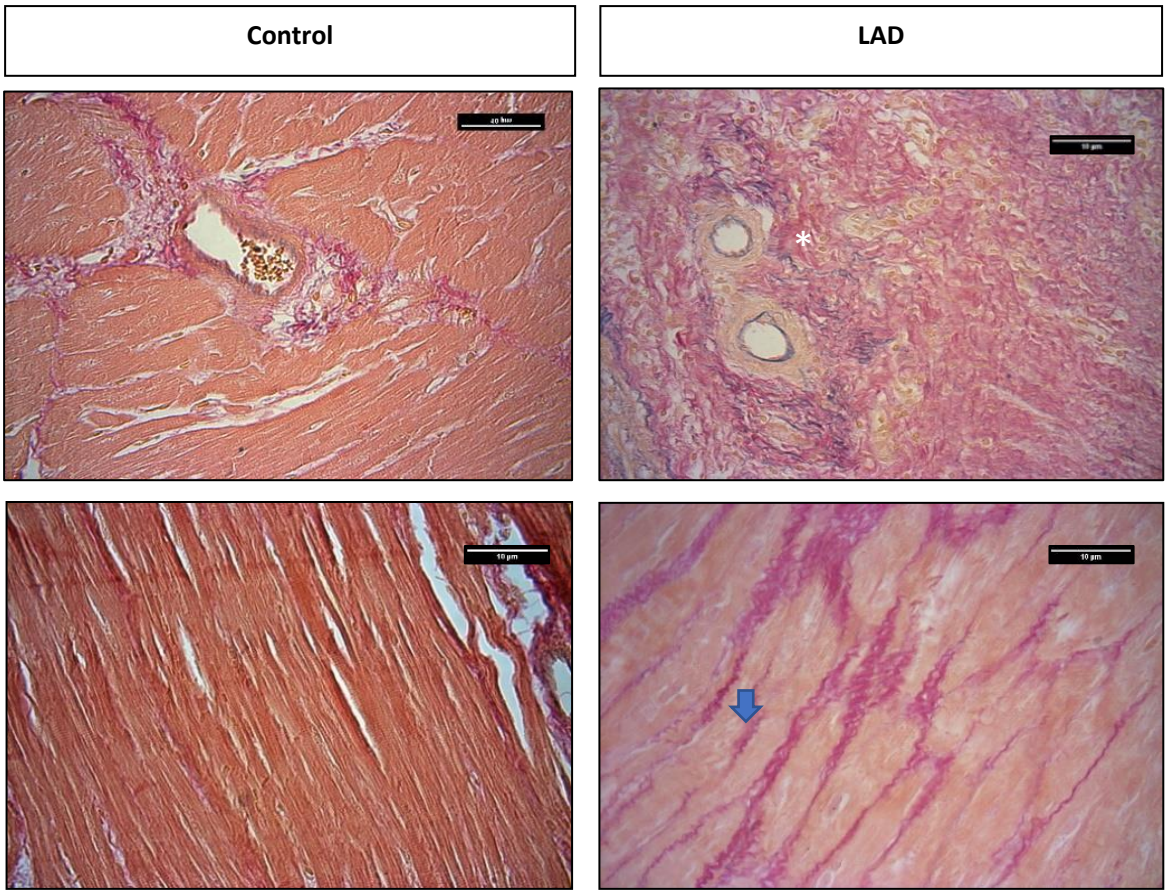

Figure 4.3 EVG staining of control and LAD heart sections. Elastin is stained in purple (blue arrow), collagen in red (white asterisks), and cardiomyocytes in orange. Images were taken with objective lens magnification x40. Scale bar set to 100 microns.

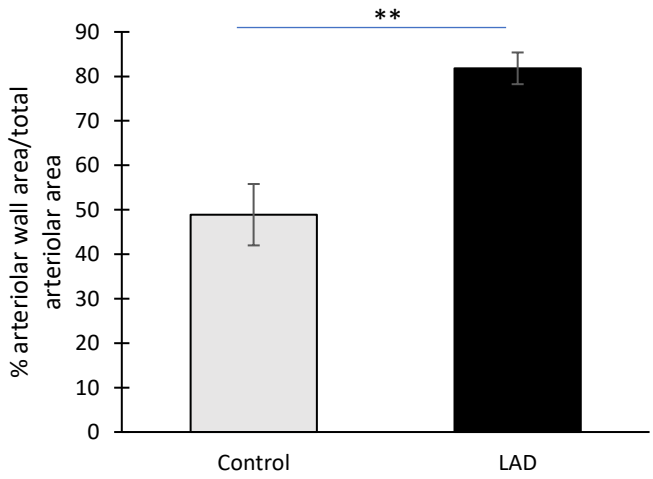

Figure 4.4 Percentage of porcine arteriolar wall area to total arteriolar area. Quantification was performed in EVG stained sections. Data are presented as mean percentages (SEM), and analysed using unpaired student's t-test. ** $p < 0.01$, $n = 4$, 3-4 fields were examined for each heart.

4.3.1.3 Effect of LAD coronary artery occlusion on cardiac cellular infiltration

Haematoxylin and eosin staining (as shown in figure 4.5) showed various interstitial infiltration of connective tissue cells (such as fibroblast and myofibroblast) in the matrix in between cardiomyocytes in LAD sections.

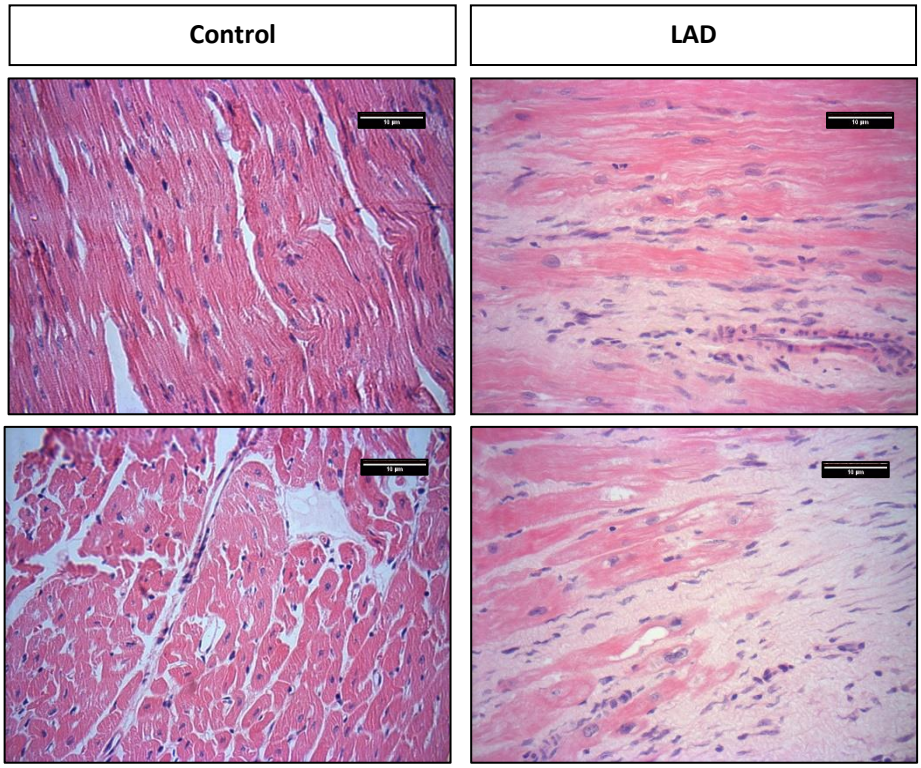

Figure 4.5 H&E staining of control and LAD heart sections. Cytoplasm is stained in dark pink, collagen in light pink, and nuclei in blue. Images were taken with objective lens magnification x40. Scale bar set to 100 microns.

4.3.2 Effect of 60-minute LAD coronary artery occlusion /reperfusion on porcine cardiac ultrastructure

Transmission electron microscopy imagining (FEI TecnaiTM 12) was used to analyse ultrastructural differences observed in the infarct area of LAD hearts 4 weeks after balloon LAD artery occlusion and reperfusion compared to control. Figures 3.6 and 3.7 are examples of infarcted areas taken from LAD heart.

Marked disruption to cardiomyocytes is noted in samples from the infract area of LAD group. Many telocytes in LAD group are characterised by cytoplasmic vacuolations and telopodes shrinkage. Moreover, there are numerous fibroblasts, endothelial and immune cells in the collagen dense matrix as seen in figures 4.6 and 4.7). In addition, measurements of porcine mitochondrial cristae density, subpopulation distribution and morphology and sarcomere length, along with characterisation and detection of the various elements of the interstitial architecture were performed.

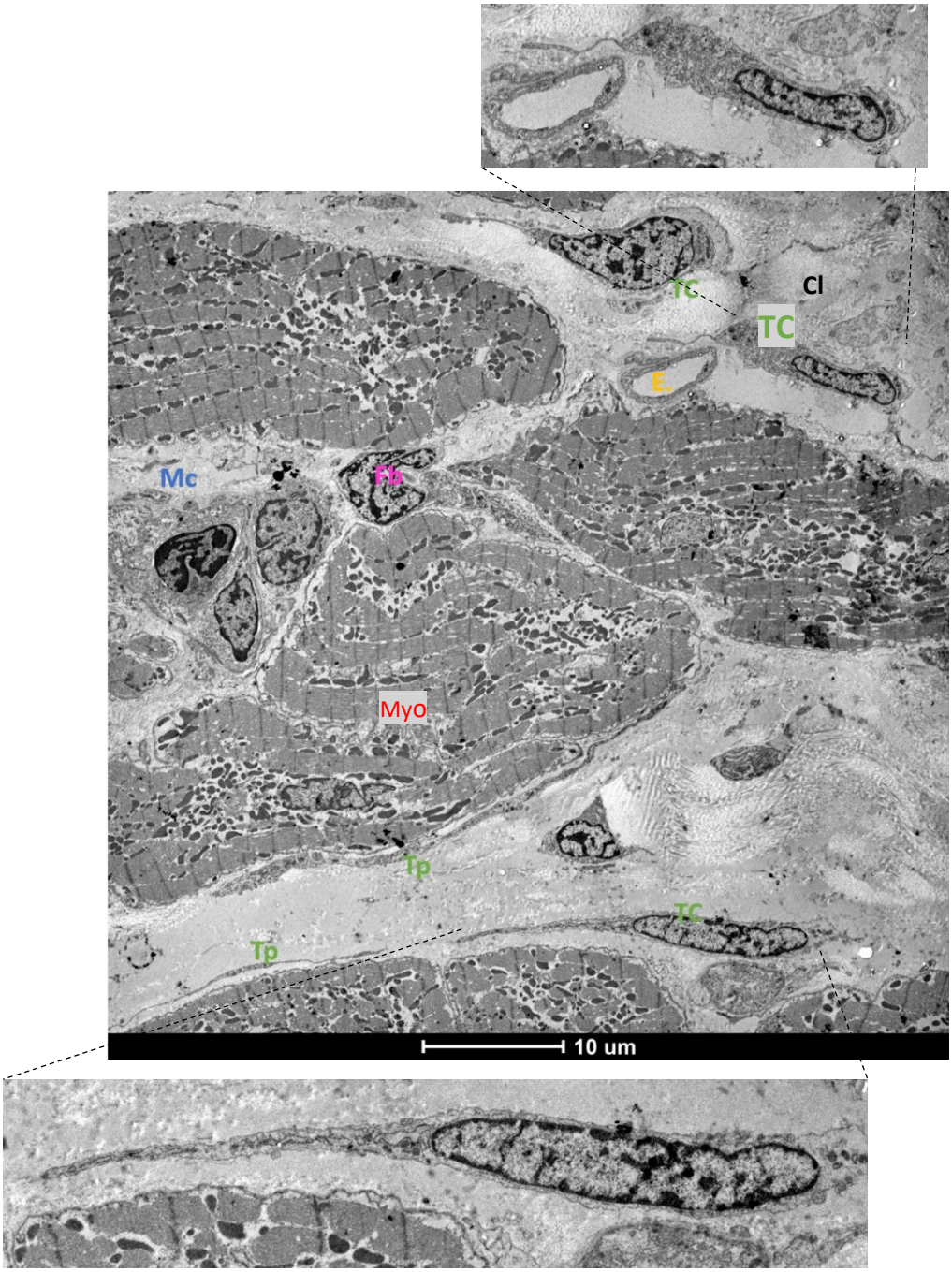

Figure 4.6 TEM micrograph from the infarct of LAD group. E. endothelial cell, cl. Collagen, Fb fibroblast, Tp telopode,TC telocyte, Myo cardiomyocyte, Mc Macrophage

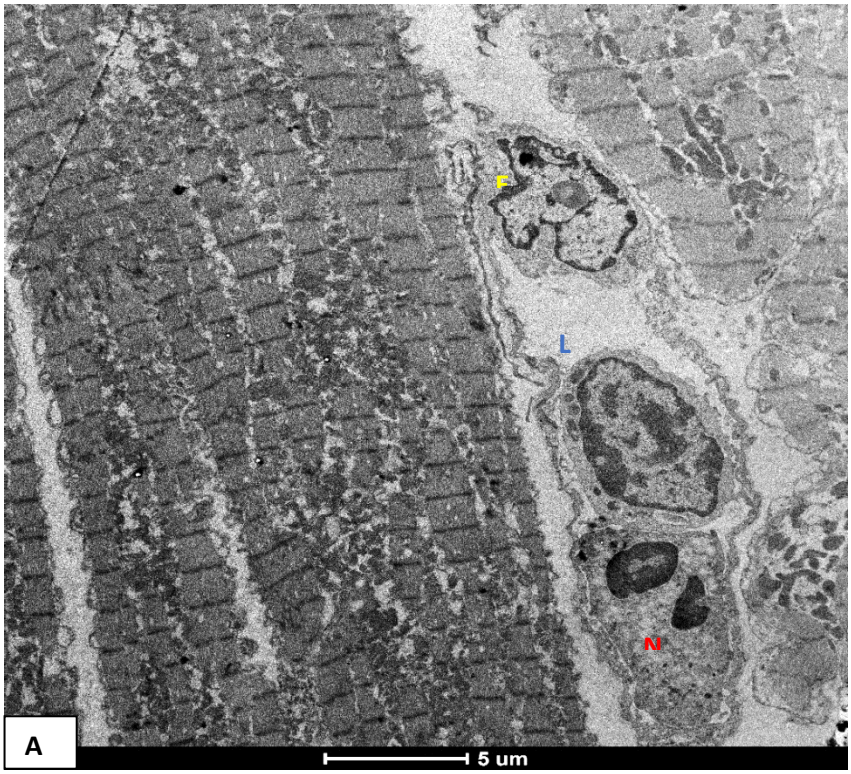

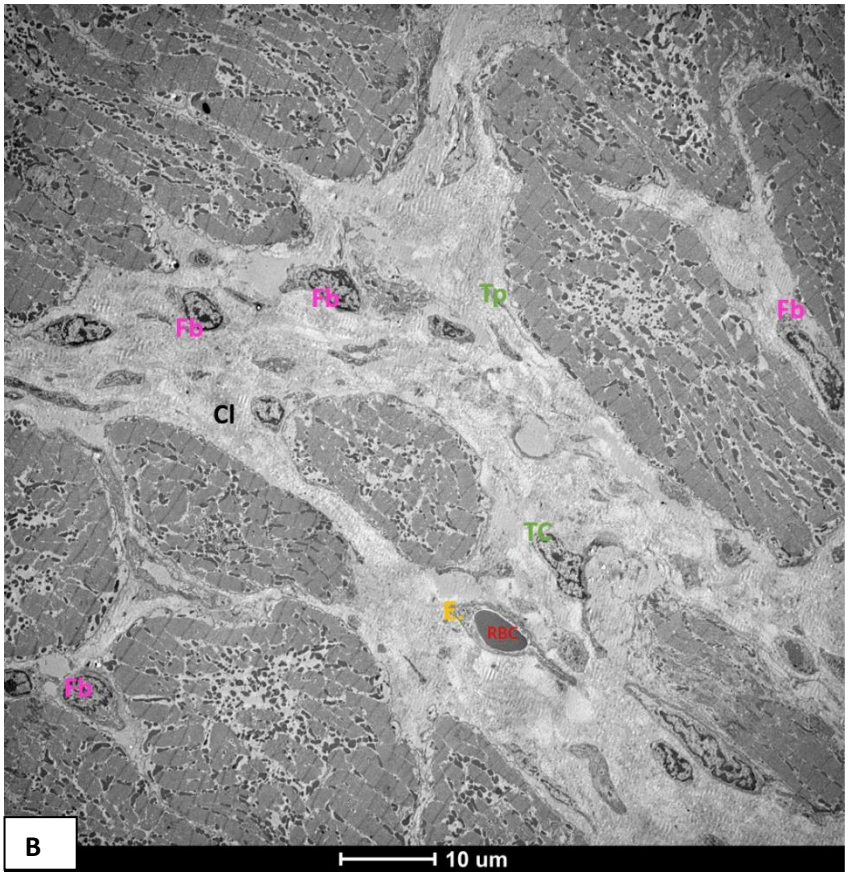

Figure 4.7 (A and B) TEM micrographs from the infarct of LAD group. E. endothelial cell, RBC, red blood cell, cl. Collagen, MyF myofibroblast, Fb fibroblast, Tp telopode,TC telocyte, , N neutrophil, L Lymphocyte .

4.3.2.1 Mitochondrial subpopulation distribution, cristae density, and morphometry

Cardiomyocytes area was measured for control and LAD groups (figure 4.8 A) and the distribution of each subpopulation was measured for each group and compared, as shown in figure 4.8 B. Cardiomyocytes area in LAD group was slightly increased ($p > 0.05$). However, there was significant decrease in interfibrillar mitochondria subpopulation distribution in LAD group compared to control ($p = 0.02$).

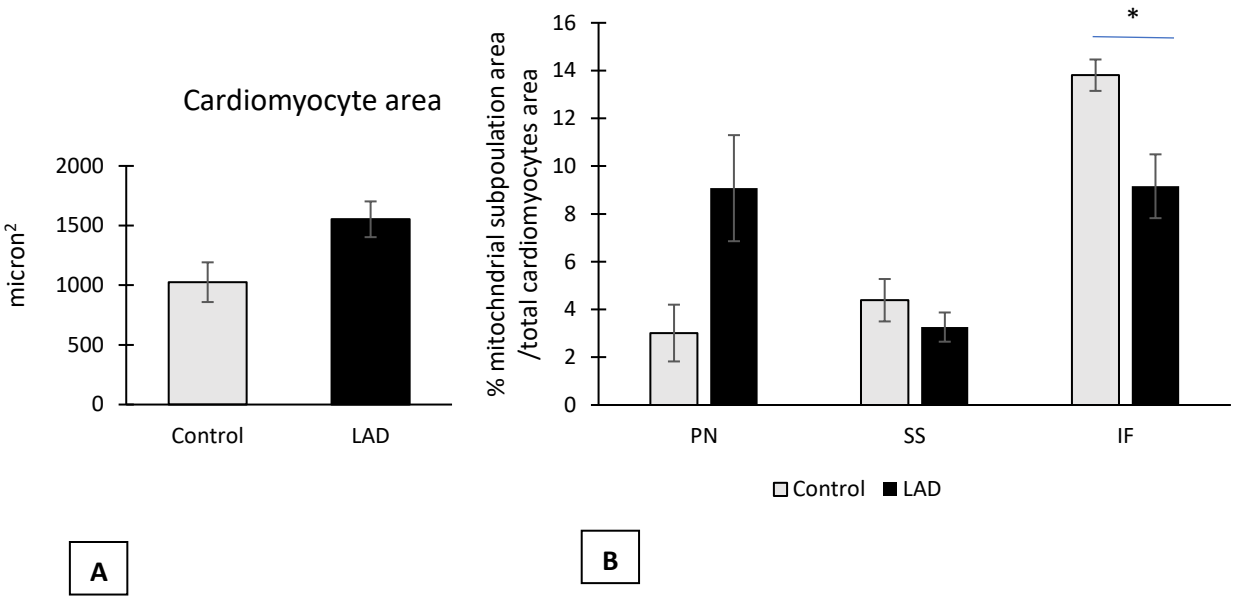

Figure 4.8 A and B Cardiomyocytes area and mitochondrial subpopulation distribution A) Average cardiomyocyte area in each group. B) Percentage of mitochondrial subpopulation area to total cardiomyocytes area. Data are presented as mean ± SEM. Data were analysed using unpaired t-test. n=4, 3-4 fields were examined for each sample. IF interfibrillar, PN perinuclear and SS subsarcolemmal.

The ratio of intercristae space area to total mitochondrial area, which reflects mitochondrial cristae density, was significantly increased in LAD group compared to control as seen in figure 4.9.

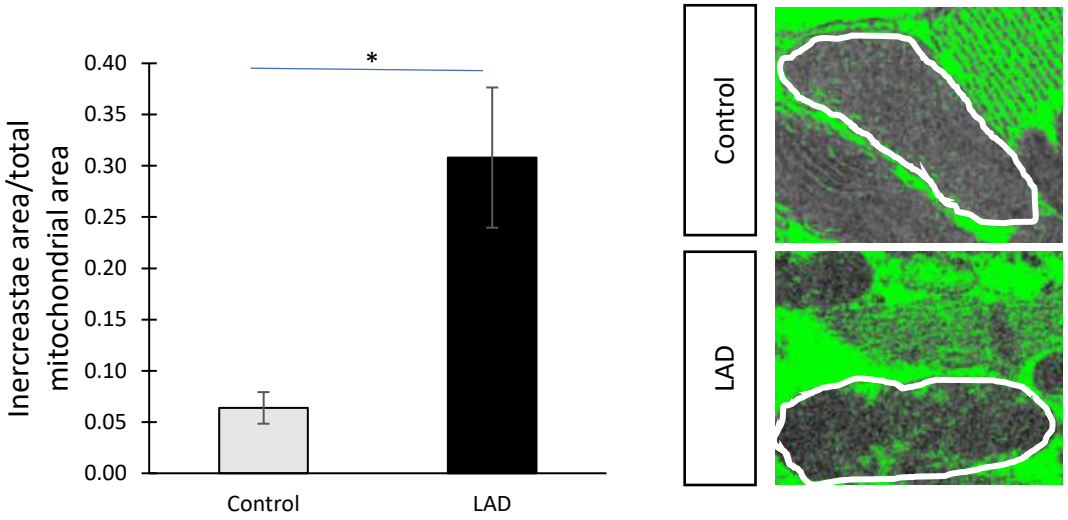

Figure 4.9 Mitochondrial density in control and LAD groups. Bar chart represents the average ratio of intercristae space area to total mitochondrion area in each group. Data are presented as mean ± SEM and analysed using unpaired student's t-test. Images were analysed using ImageJ software through automatic threshold level detection for each mitochondrial (green filter inside white border covers intercristae area). n=4, 3-4 fields were examined for each heart, total mitochondrial count = 40. * $p < 0.05$.

4.3.2.1.1 Mitochondrial subpopulations morphometry in Control group

In general, interfibrillar mitochondria appeared longer and with increased area and aspect ratio, however, no significant differences were observed amongst the three subtypes (figure 4.10).

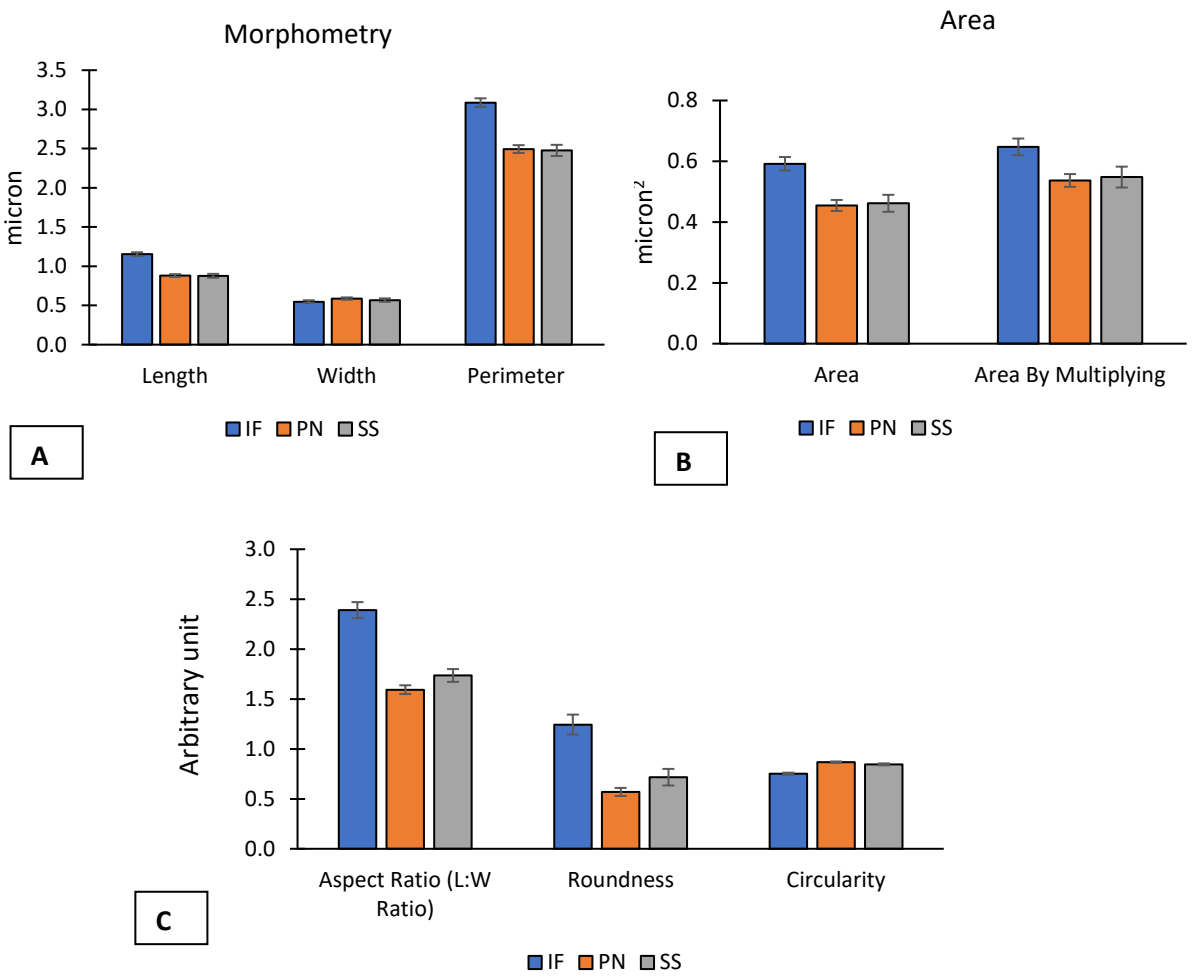

Figure 4.10 Mitochondrial morphometric measurement of control group. A) Length, width and perimeter B) Area by size and multiplication (L*W) C) Aspect ratio, roundness, and circularity. Data are presented as mean ± SEM, and were analysed using one-way ANOVA followed by the Bonferroni and Games-Howell post-hoc tests. SS subsarcolemmal, IF interfibrillar, PN perinuclear, n=4. Total mitochondrial count = 163 (IF), 143 (SS) and 159 (PN).

4.3.2.1.2 Mitochondrial subpopulations morphometry in LAD group

In LAD hearts, perinuclear mitochondria showed significant decrease in length and perimeter compared to interfibrillar mitochondria as seen in figure 4.11. This subtype had increased in circularity coupled with a decrease in aspect ratio. Unlike control group, length and other morphometric measurements did not change significantly between the three subpopulations.

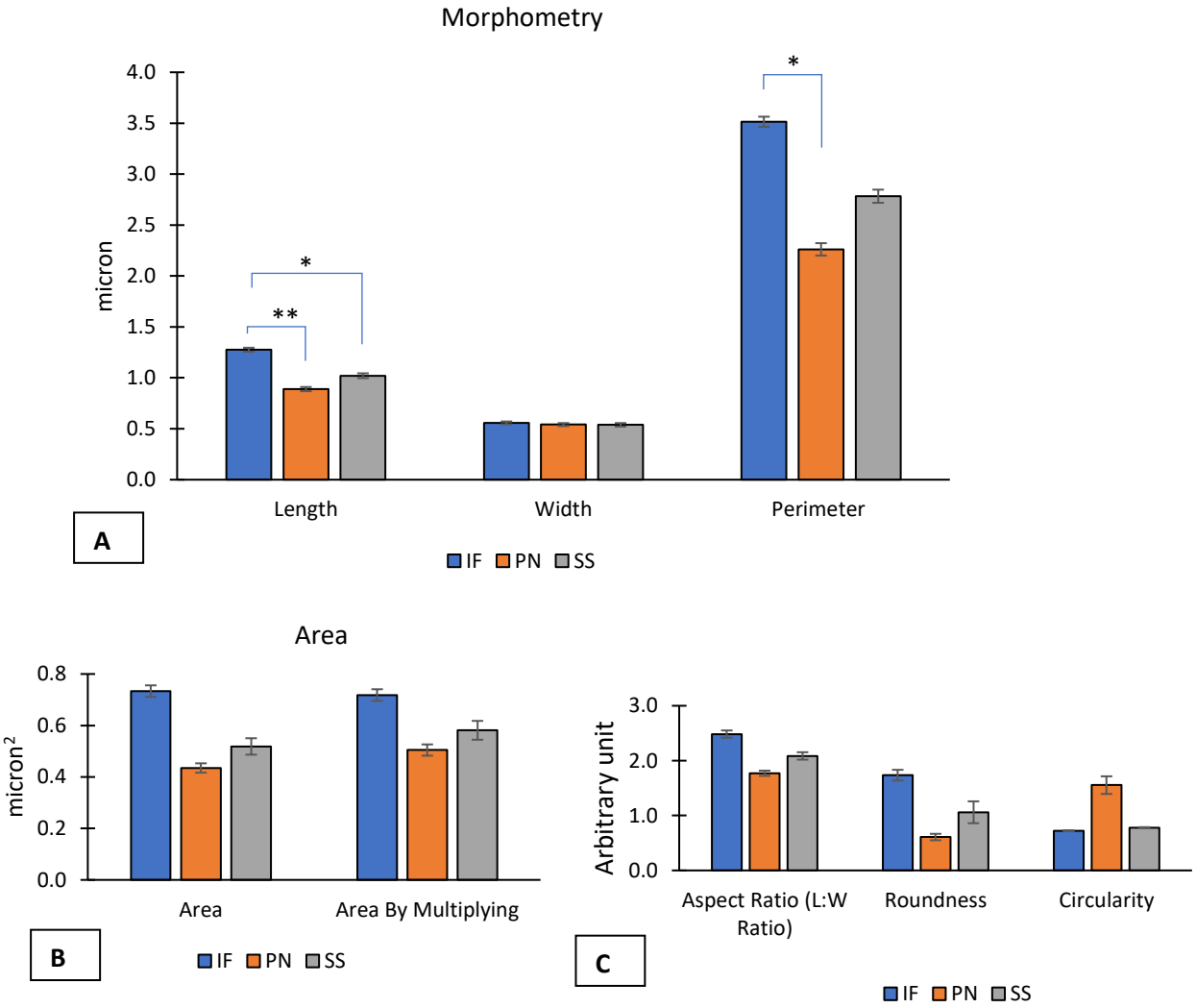

Figure 4.11 Mitochondrial morphometric measurements of LAD group. A) Length, width and perimeter B) Area by size and multiplication (L*W) C) Aspect ratio, roundness, and circularity. Data are presented as mean ± SEM. Data were analysed using one-way ANOVA followed by the Bonferroni and Games-Howell post-hoc tests. * = $p < 0.05$, **= $p < 0.01$. SS subsarcolemmal, IF interfibrillar, PN perinuclear, n=4. Total mitochondrial count = 163 (IF), 160 (SS) and 143 (PN).

4.3.2.1.3 Comparison of mitochondrial morphometric measurements between control and LAD groups

Interfibrillar mitochondria

Interfibrillar mitochondria of LAD hearts had increased length, perimeter and area, however, none of these measurements were significantly different to the control group as seen in figure 4.12.

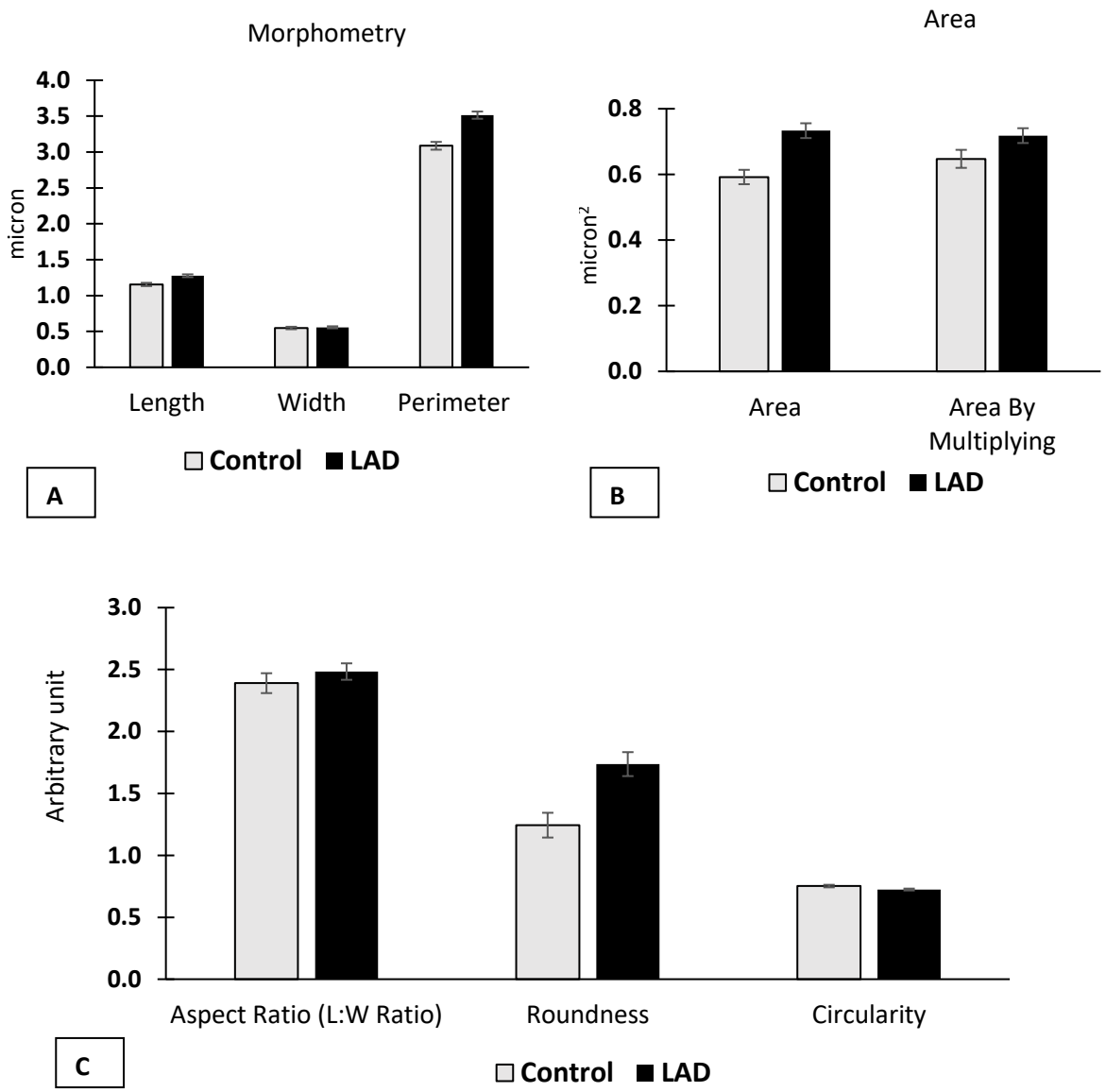

Figure 4.12 Interfibrillar mitochondrial morphometric measurements of control and LAD groups. A) Length, width and perimeter B) Area by size and multiplication (L*W) C) Aspect ratio, roundness, and circularity. Data are presented as mean ± SEM, and were analysed using unpaired student's t-test. n=4. Total mitochondrial count per group= 163.

Perinuclear Mitochondria

Perinuclear mitochondria morphometric measurements showed slight decrease in area and roundness in LAD group compared to control, however, these changes were not significantly different between the two groups as seen in figure 4.13.

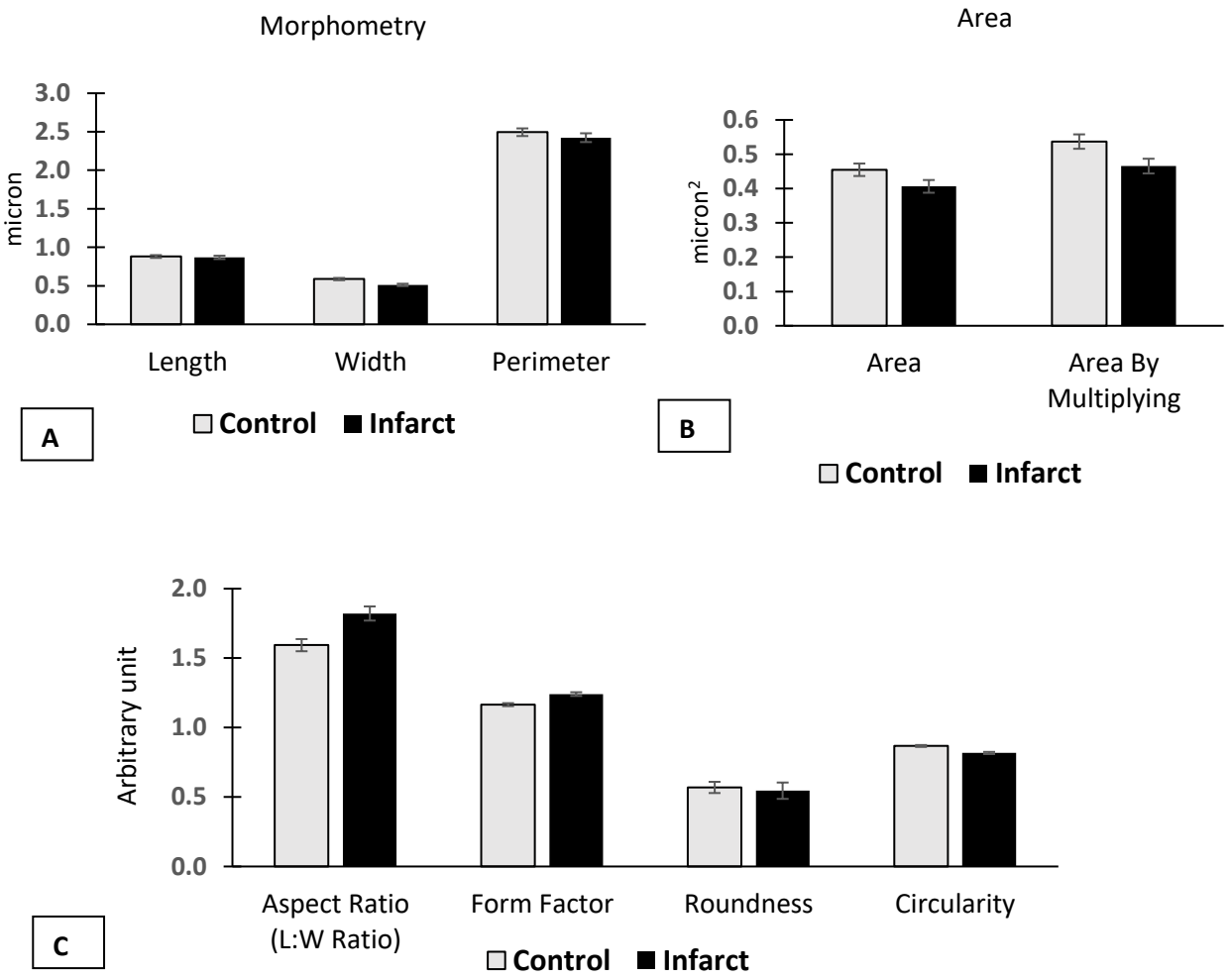

Figure 4.13 Perinuclear mitochondrial morphometry of control and LAD group. A) Length, width and perimeter B) Area by size and multiplication (L*W) C) Aspect ratio, roundness, and circularity. Data are presented as mean ± SEM, and analysed using unpaired student's t-test. n= 4. Total mitochondrial count per group ≥143.

Subsarcolemmal Mitochondria

Similarly, morphometric measurements of subsarcolemmal mitochondria were not significantly different between LAD and control groups as illustrated figure 4.14.

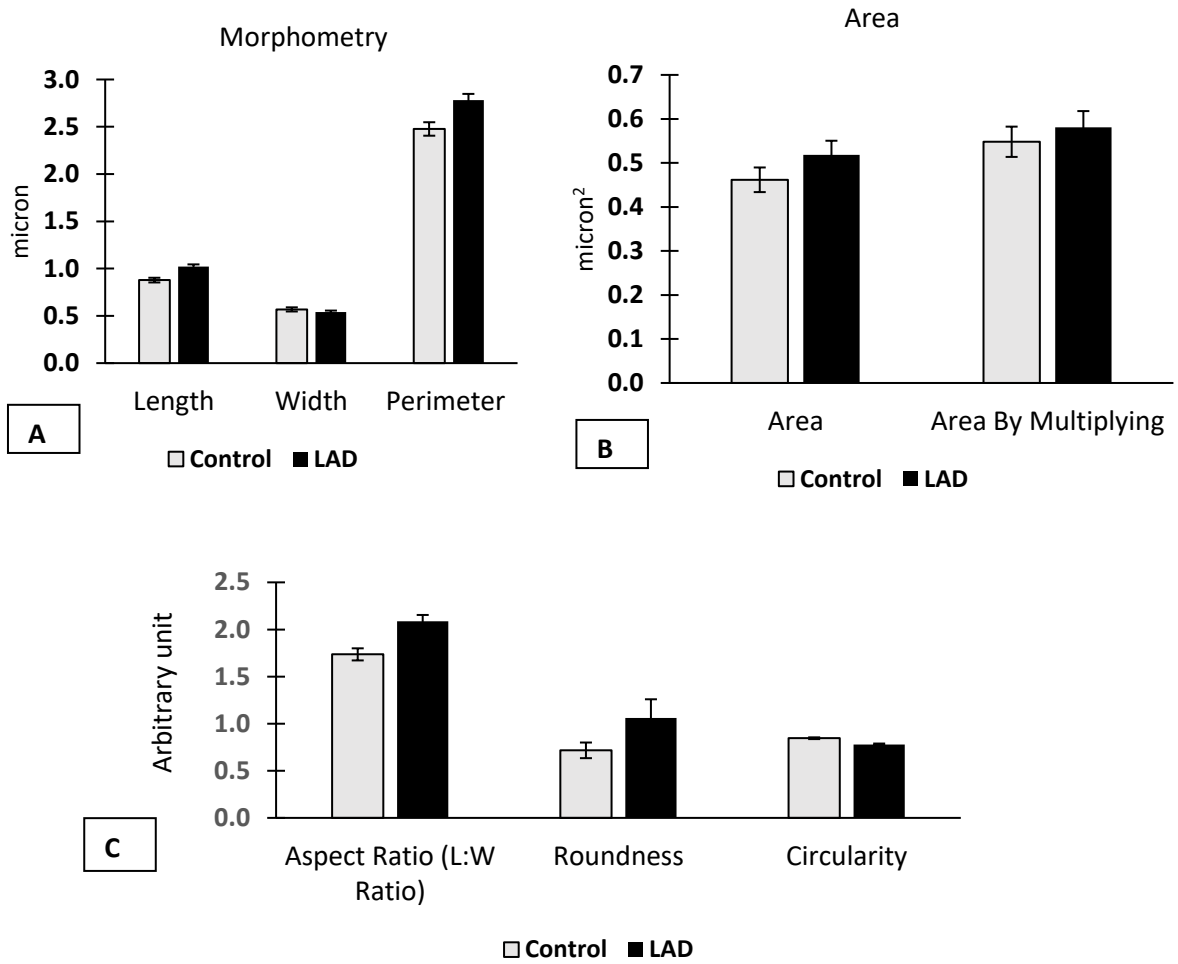

Figure 4.14 Subsarcolemmal mitochondrial morphometric measurements of control and LAD group. A) Length, width, and perimeter B) Area by size and multiplication (L*W) C) Aspect ratio, roundness, and circularity. Data are presented as mean ± SEM, and analysed using unpaired student's t-test. n = 4. Total mitochondrial count per group ⩾143.

4.3.2.2 Diastolic sarcomere length

Diastolic sarcomere length (measured from from one end of sarcomere to the other) did not significantly vary between control (1.4 ± 0.2 µm) and LAD group (1.6 ± 0.1 µm) as illustrated in figure 4.15. Sarcomere length ranged from 1.04 -1.78 micron in control group, while the range was higher for LAD group (1.4 -1.85 micron).

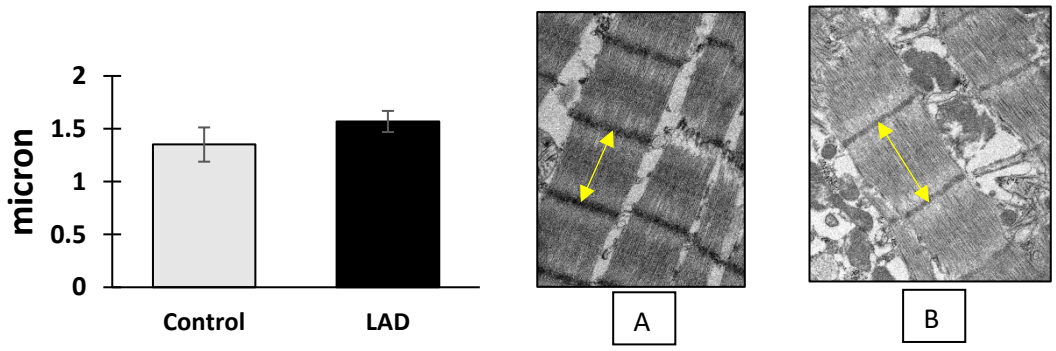

Figure 4.15 Sarcomere length in control and LAD porcine hearts**.** Data presented as mean ± SEM, and analysed using unpaired student's t-test. Measurement of 200 sarcomere from each group (50 per sample) were taken, n=4. Representative EM images of sarcomere length measurements in control (A) and LAD group (B) with sarcomere length defined (yellow arrows).

4.3.3 Effect of 60-minute LAD coronary artery occlusion /reperfusion on porcine cardiac proteomics

4.3.3.1 Total proteins

In total, 5661 proteins were detected in both LAD and control groups. Of which, 909 proteins were significantly changed 4 weeks after LAD coronary artery occlusion and reperfusion (p value < 0.05). Figure 4.16 is a volcano plot for total identified proteins. There were 272 significantly different protein that had increase in expression (FC > 1.3) in LAD group, compared to 538 proteins with decreased fold change (FC < 0.8).

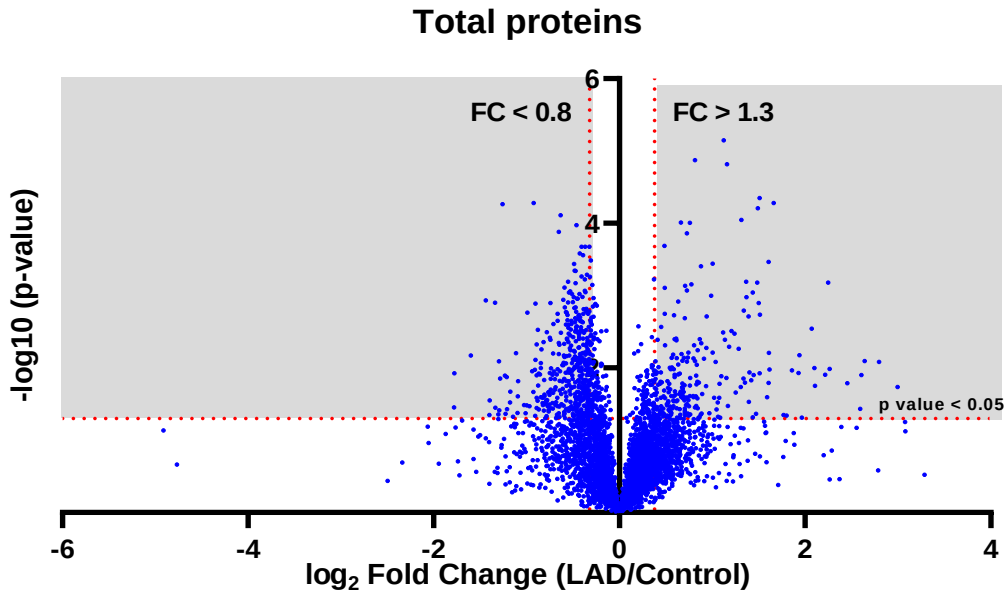

Figure 4.16 Logarithmic (volcano) plot of fold change for total proteins identified in LAD and control group. p- value calculated using unpaired student's t-test. Reference lines indicate fold change < 0.8 or >1.3 on the x- axis, and p- value < 0.05 on the y- axis. n= 4, total proteins count=5661

A breakdown of total proteins classification into molecular and biological functions in addition to proteins class, using Panther Database classification system, is shown in figure 4.17. Expression heatmap of significantly different proteins (p value < 0.05) between control and LAD groups was generated using Rstudio (PBC, USA) as demonstrated in figure 4.18.

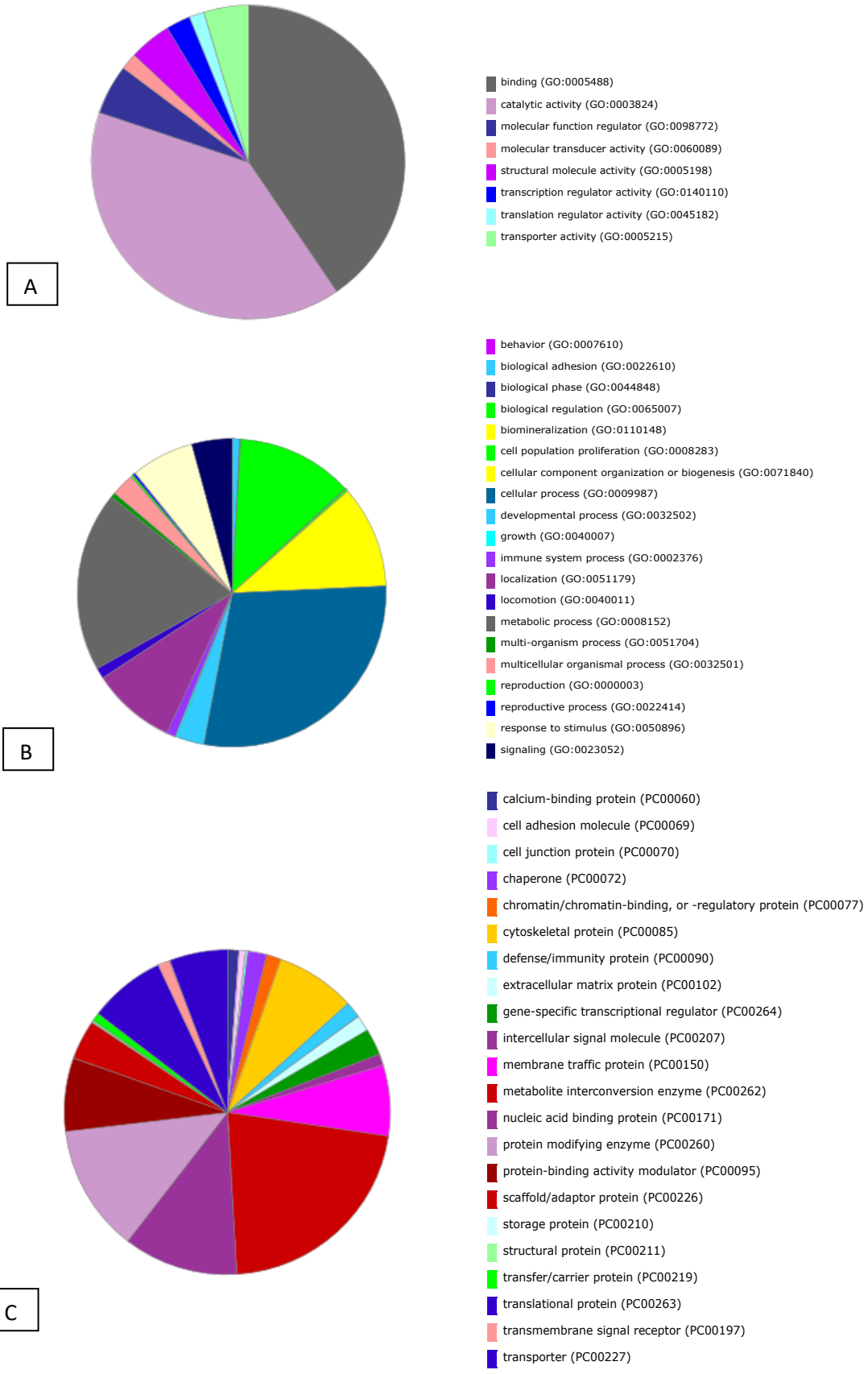

Figure 4.17 Classification of total proteins identified in control and LAD groups using the PANTHER classification system**.** Proteins are classified according to molecular function (A) and biological processes (B) and protein class (C).

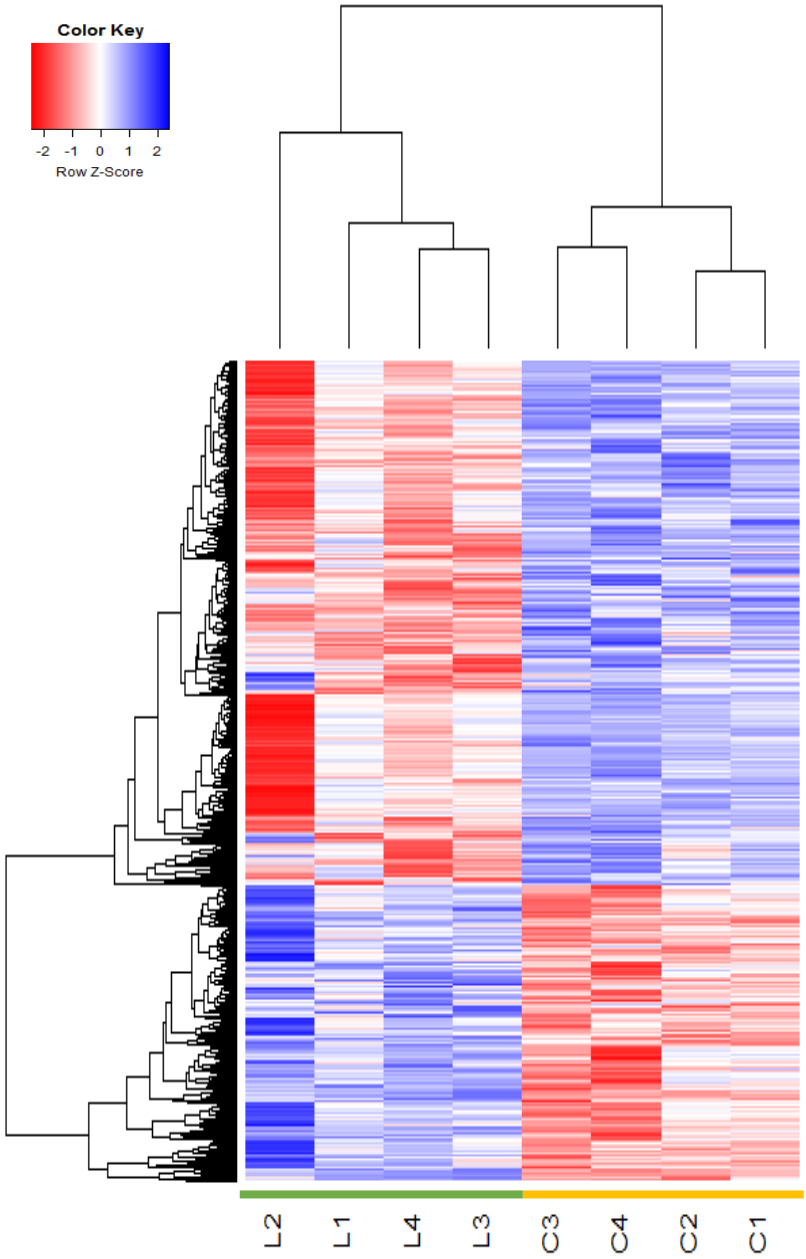

Figure 4.18 Expression heatmap of significantly different proteins (p <0.05) from porcine proteomics output. Heatmap was created using Rstudio software. n=4, total significant protein count=909. L; LAD pigs, C; control pigs.

Significantly different proteins were further categorised into high or low expression (fold change (LAD/Control) >1.3 or < 0.8, respectively). Panther database classification system was also used to breakdown protein of high and low expression into categories based on molecular functions and biological processes, and protein classes. Highly expressed proteins were predominantly involved in binding and catalytic activities. Proteins with low expression were mainly classified as catalytic, followed by binding and transporter activities. Interestingly, metabolites interconversion enzymes constitute a substantial class in significantly decreased proteins four weeks after LAD coronary artery occlusion and reperfusion (figure 4.19).

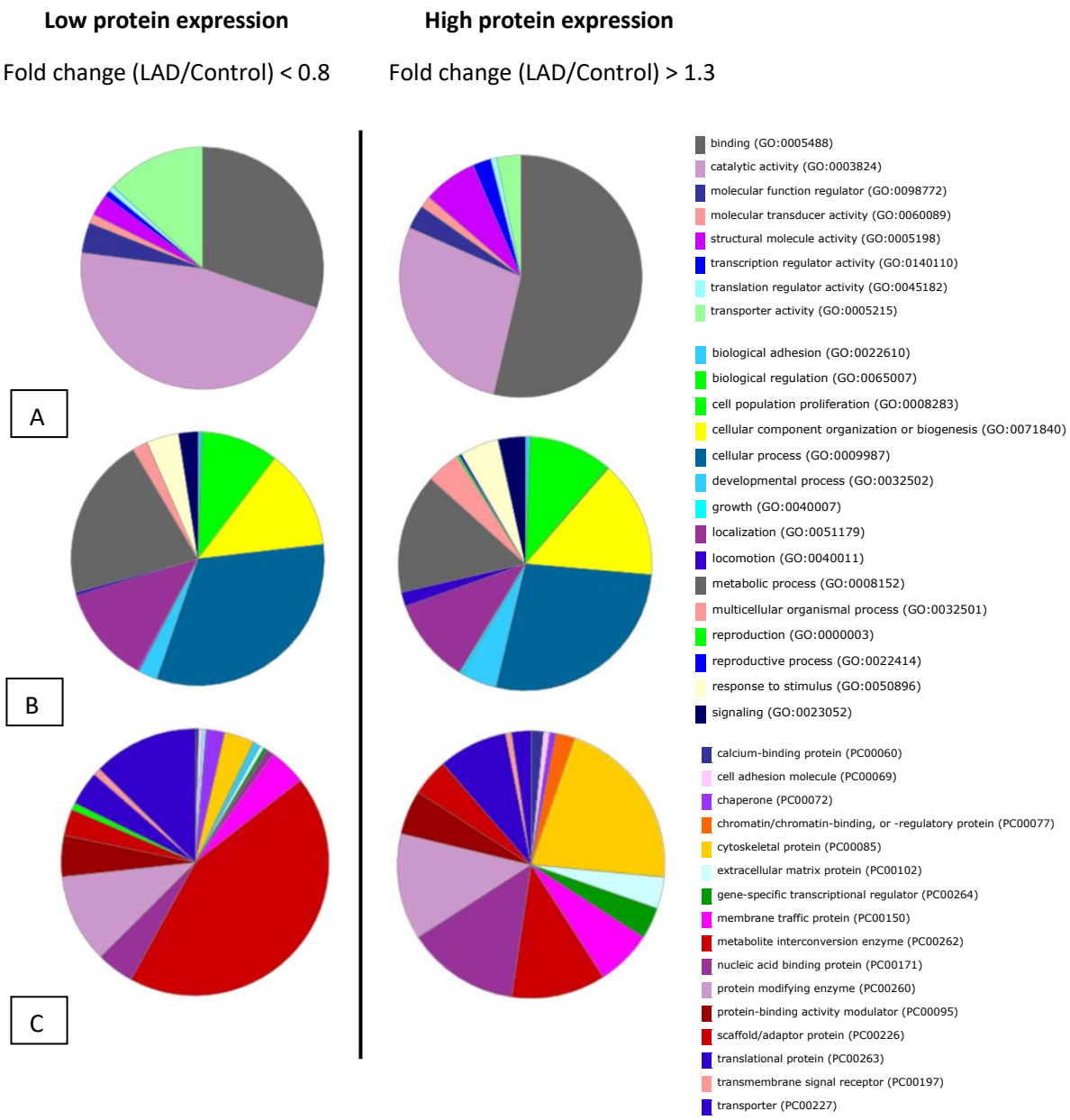

Figure 4.19 Classification of significantly different proteins identified from porcine proteomics output using the PANTHER classification system. Proteins are classified according to increased (n=272) and decreased (n= 538) expression into molecular function (A) and biological processes (B) and protein class (C).

4.3.3.1.1 Mitochondrial Proteins

A total of 403 mitochondrial proteins were detected and shown as a Volcano plot (figure 4.20). Approximately 44.6% (n = 180) of mitochondrial proteins had significant difference (p- value < 0.05) between control and LAD groups. Most of these proteins were decreased in LAD group.

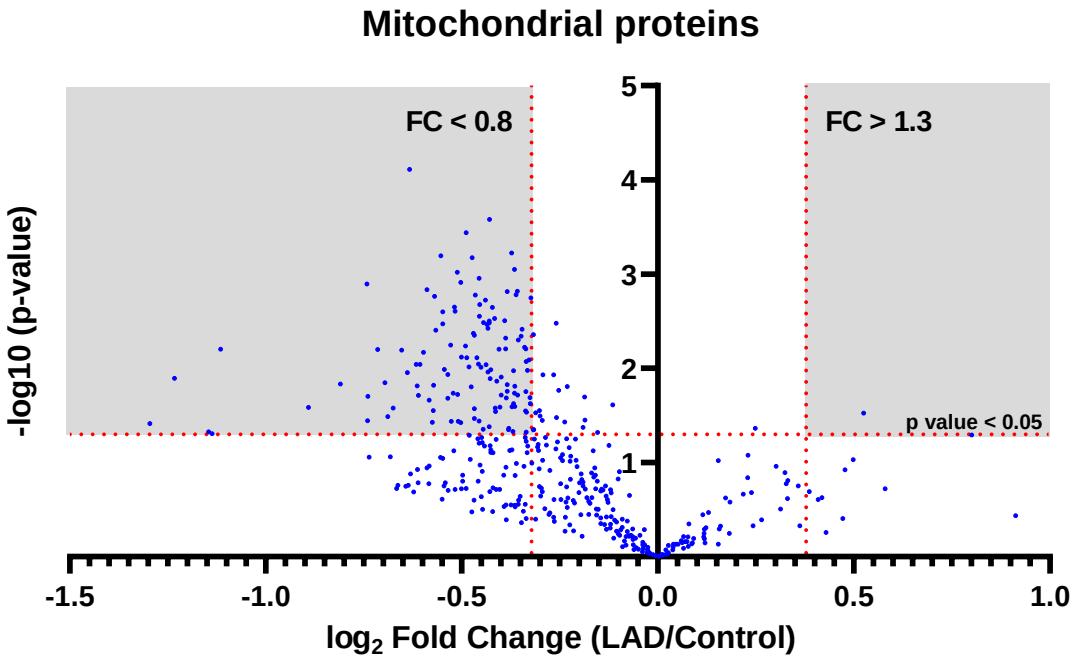

Figure 4.20 Logarithmic (volcano) plot of fold change for total mitochondrial proteins identified in LAD group compared to control. p- value calculated using unpaired student's t-test. Reference lines indicate abundance ratio (Fold change LAD/control) < 0.8 or >1.3 on the x- axis, and p- value < 0.05 on the y- axis. n= 4, total mitochondrial count=432

4.3.3.1.2 Kinase proteins

Figure 4.21 shows all the significantly increased (figure 4.21 A) and decreased (4.21 B) kinases proteins in control and LAD groups. Amongst notable kinases are glycogen synthase kinase 3 (GSK-3), adenylate Kinase Isoenzyme 1 (adenine nucleotide metabolism), mitochondrial Creatine Kinase 2 and creatine kinase M-type.

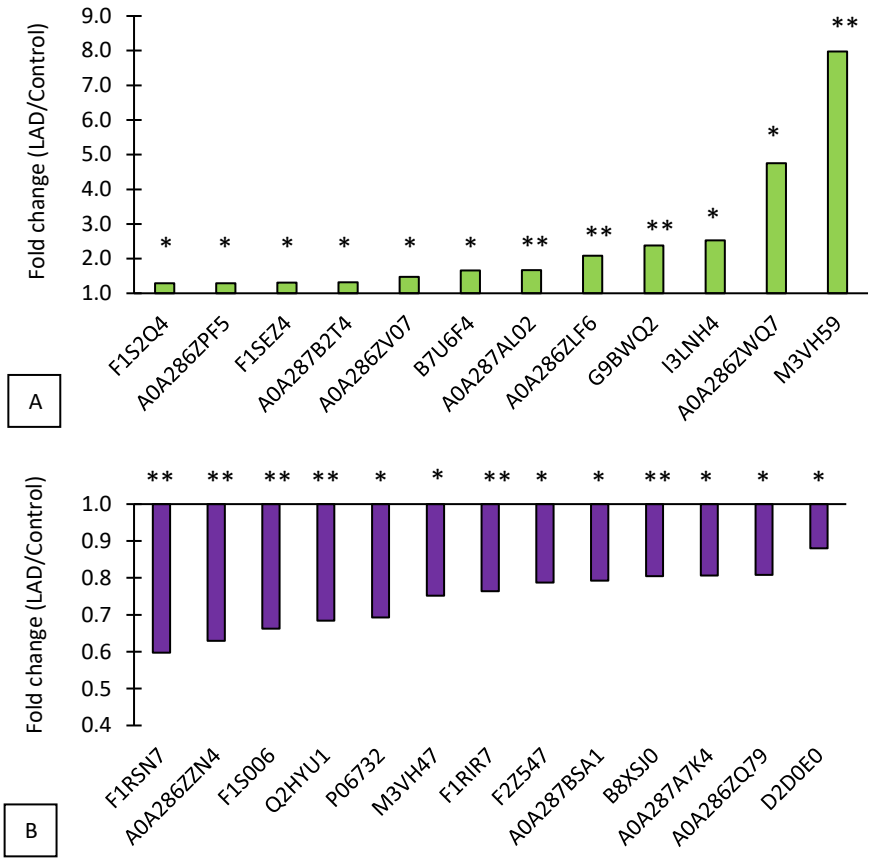

Figure 4.21 A and B Protein kinases. **I3LNH4;** Ca^{2+}/Calmodulin-Dep Prot Kinase Type 1D, **A0A286ZWQ7;** Ser/Thr-Prot Kinase DCLK1, **A0A286ZV07;** L-Fucose Kinase, M3VH47 Casein Kinase 1, Delta Tv1, **M3VH59;** Phosphatidylinositol-4-Phosphate 3-Kinase, Cat Sub Type 2 Alpha, **A0A286ZLF6;** Ser/Thr-Prot Kinase N2, **F1RSN7;** AARF Domain-Containing Kinase 5, **A0A287BD11;** Ser/Thr-Prot Kinase SMG1, **A0A287AL02;** Non-Specific Ser/Thr-Prot Kinase, **A0A287B2T4;** Ser/Thr Prot Kinase Nek3, **P06732;** Creatine Kinase M-Type, **A0A287B0J6;** Activated CDC42 Kinase 1, **F1S006;** Fructosamine-3-Kinasee, **B7U6F4;** Ser/Thr Protein Kinase MST4, **A0A286ZZN4;** GSK-3 Alpha, **G9BWQ2;** Non-Specific Ser/Thr Prot Kinase, **F1S2Q4;** Ser/Thr Prot Kinase Nek9, **F1SEZ4;** MAP Kinase-Activated Prot Kinase 2, **A0A287A7K4;** Ribokinase, **D2D0E0;** Choline/Ethanolamine Kinase, **F1RIR7;** [3-Methyl-2-Oxobutanoate Dehydrogenase [Lipoamide]] Kinase, Mito, **B8XSJ0;** Acylglycerol Kinase, **A0A287BSA1;** [Pyruvate Dehydrogenase (Acetyl-Transferring)] Kinase Isozyme 2, Mito , **A0A286ZPF5** Mitogen-Activated Protein Kinase, **A0A286ZQ79;** Adenylate Kinase Isoenzyme 1, **Q2HYU1;** Mitochondrial Creatine Kinase 2. Data were analysed using unpaired student's t-test. * $p < 0.05$, ** $p < 0.01$, n=4

4.3.3.1.3 Phosphatase proteins

Majority of significantly different phosphatases were downregulated in LAD group (figure 4.22). However, inactive dual specificity phosphatase 27 (involved in oxidative stress response) and receptor-type Tyrosine-Protein Phosphatase C (T and B cells activation) were increased in LAD group.

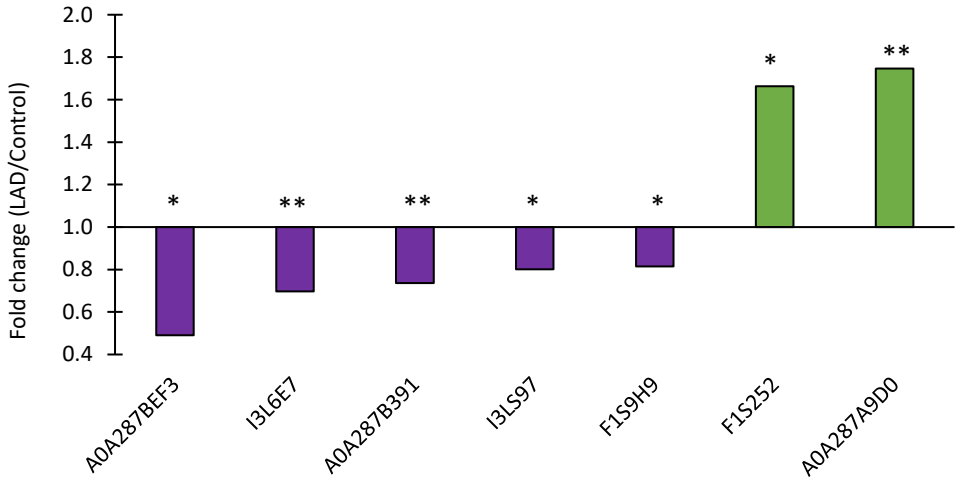

Figure 4.22 Protein Phosphatases. **A0A287BEF3;** Receptor-Type Tyrosine-Protein Phosphatase ETA, **I3L6E7;** Phosphoethanolamine/Phosphocholine Phosphatase, **A0A287B391 ;** Mg-Dep Phosphatase 1, **I3LS97 ;** Pseudouridine-5'-Phosphatase, **F1S9H9** LMW Phosphotyrosine Protein Phosphatase, **F1S252 ;** Inactive Dual Specificity Phosphatase 27, **A0A287A9D0 ;** Receptor-Type Tyrosine-Protein Phosphatase C. Data were analysed using unpaired student's t-test. * $p < 0.05$, ** $p < 0.01$, n= 4

4.3.3.1.4 ATP synthesis proteins

Various mitochondrial ATP synthase subunits and assembly factors were significantly decreased 4 weeks after LAD coronary artery occlusion and reperfusion as seen in figure 4.23.

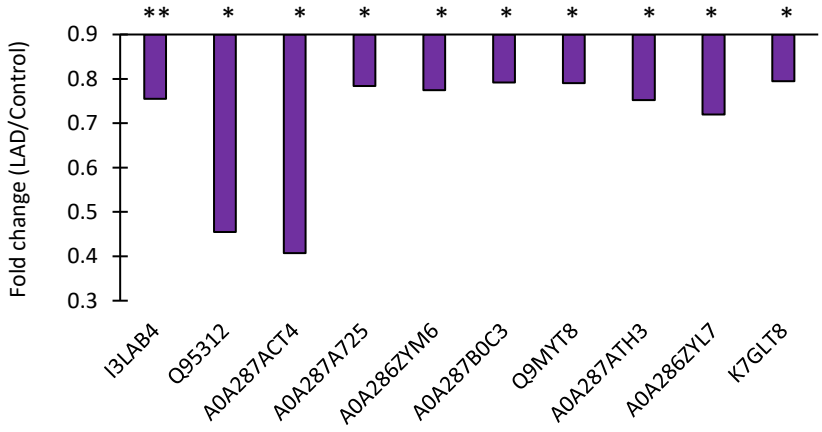

Figure 4.23 ATP synthesis proteins. **I3LAB4;** ATP Synthase Mitochondrial F1 Complex Assembly Factor 2, **Q95312;** ATP Synthase Subunit Delta, Mitochondrial, **A0A287ACT4;** ATP Synthase Subunit G 2, Mitochondrial-Related, **A0A287A725;** ATP Synthase Subunit, **A0A286ZYM6;** ATP Synthase F(0) Complex Subunit B1, Mitochondrial, **A0A287B0C3;** ATP Synthase Subunit D, Mitochondrial, **Q9MYT8;** ATP Synthase Subunit E, Mitochondrial, **A0A287ATH3;** ATP Synthase F(0) Complex Subunit C1, Mitochondrial, **A0A286ZYL7;** ATP Synthase Subunit Delta, Mitochondrial, **K7GLT8;** ATP Synthase Subunit Beta. Data were analysed using unpaired student's t-test. * $p < 0.05$,** $p < 0.01$, n=4

4.3.3.1.5 Ions transport proteins

Figure 4.24 lists ion transporters (e.g., Na^+/K^+ transporting ATPase Sub B-1) and calcium handling proteins (e.g., phospholamban and SERCA2), all of which were significantly decreased in LAD group compared to control.

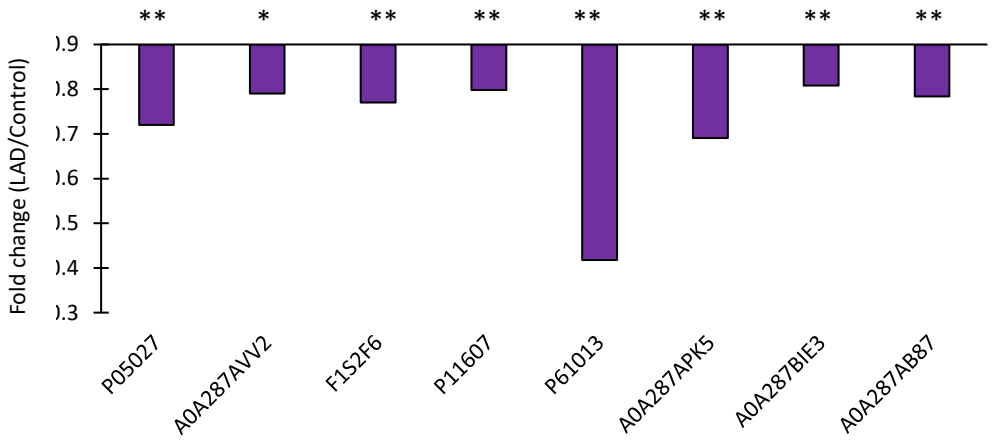

Figure 4.24 Ion transporters. **P05027;** Na/K-Transporting ATPase Sub Beta-1, **A0A287AVV2;** Voltage Dependent Anion-Selective Channel Protein 1, **F1S2F6;** Voltage dependent anion-selective Channel Protein 2, **P11607;** Sarcoplasmic/Endoplasmic Reticulum Calcium ATPase 2, **P61013;** Cardiac Phospholamban, **A0A287APK5;** Calcium-Transporting ATPase, **A0A287BIE3;** Voltage-dependent L-type Calcium Channel subunit Beta-2, **A0A287AB87;** Voltage-Dependent L-Type Calcium Channel Subunit Alpha. Data were analysed using unpaired student's t-test. * $p < 0.05$, ** $p < 0.01$, n=4

4.3.3.1.6 Antioxidant related proteins

Significantly different antioxidant proteins such as thioredoxin Reductase 2 and glutathione reductase were reduced in LAD hearts compared to control as seen in figure 4.25.

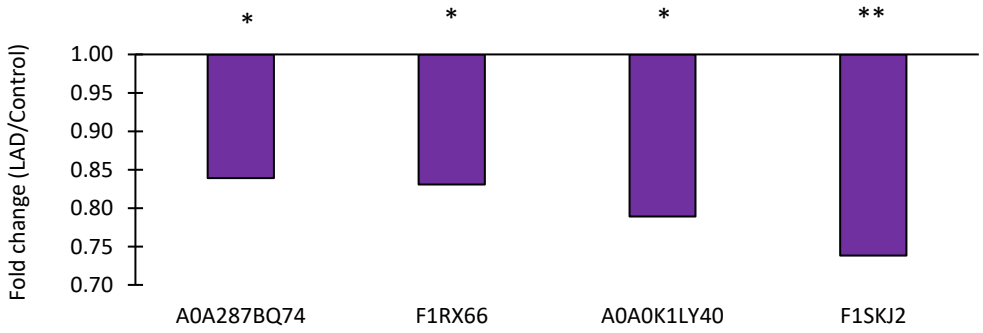

Figure 4.25 Antioxidant related proteins. **A0A287BQ74;** Thioredoxin Reductase 2, Mito, **F1RX66;** Glutathione Reductase, **A0A0K1LY40;** Peptide-Methionine (R)-S-Oxide Reductase, **F1SKJ2;** Thioredoxin, Mito. Data were analysed using unpaired student's t-test. * $p < 0.05$, ** $p < 0.01$, n=4

4.3.3.1.7 Oxidoreductase proteins

Figure 4.26 shows the oxidases and reductases proteins that significantly changed four weeks after LAD ligation. Except for NADPH-Cytochrome P450 Reductase, and Ubiquinol-Cytochrome-C Reductase Complex Assembly Factor 3, all the proteins in this class were significantly decreased in LAD hearts. Notably, NADH-Ubiquinone Oxidoreductase 75 KDA subunit, which forms the largest subunit of complex I of ETC was decreased significantly in LAD group.

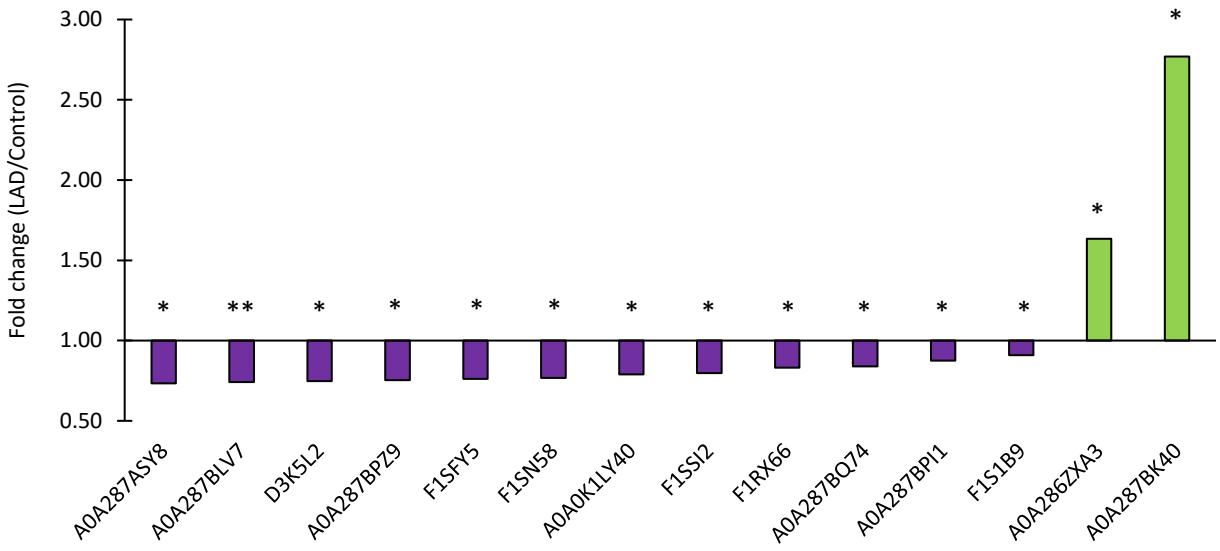

Figure 4.26 Oxidoreductase proteins. **A0A287ASY8;** NADPH:AdrenodoxinOxidoreductase, Mito, **A0A287BLV7;** NADH-Ubiquinone Oxidoreductase 75 KDA Sub, Mito , **D3K5L2;** Ubiquinol-Cytochrome C Reductase Complex Chaperone, **A0A287BPZ9;** Oxidoreductase-Like Domain-Containing Protein 1, **F1SFY5;** Oxidoreductase HTATIP2, **F1SN58;** Sulfide:Quinone Oxidoreductase, Mito, **A0A0K1LY40;** Peptide-Methionine (R)-S-Oxide Reductase, **F1SSI2;** DH/Reductase Sdr Family Member 7, **F1RX66;** Glutathione Reductase, **A0A287BQ74;** Thioredoxin Reductase 2, Mito, **A0A287BPI1;** Electron Transfer Flavoprotein-Ubiquinone Oxidoreductase, Mito, **F1S1B9;** DH/Reductase Sdr Family Member 11, **A0A286ZXA3;** NADPH-Cytochrome P450 Reductase, **A0A287BK40;** Ubiquinol-Cytochrome-C Reductase Complex Assembly Factor 3. Data were analysed using unpaired student's t-test. * $p < 0.05$, ** $p < 0.01$, n=4

4.3.3.1.8 Metabolism proteins and enzymes

Almost all significantly different proteins involved in cardiac metabolism were decreased in LAD groups (figure 4.27). These proteins are part of several metabolic pathways, including glycolysis (acetyltransferase, component of Pyruvate DH Complex), as well as amino acids (branched chain amino acid aminotransferase) and fatty acids metabolism (Malonyl-CoA-Acyl Carrier Protein Transacylase, Acyl Coenzyme A Synthetase Long-Chain 1, Very Long-Chain Specific Acyl-CoA DH and Very-Long-Chain (3r)-3-Hydroxyacyl-CoA Dehydratase).

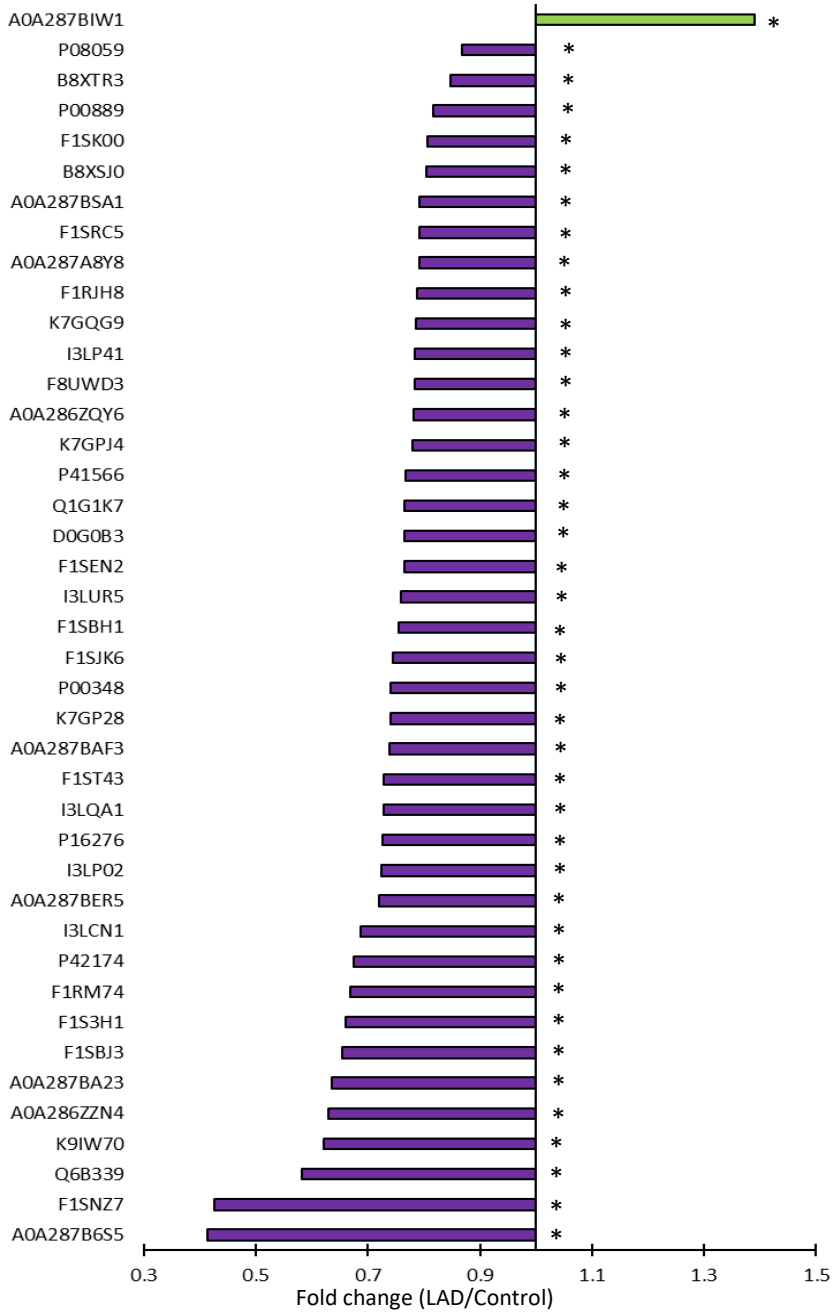

Figure 4.27 Metabolism proteins and enzymes. **A0A287B6S5;** Alpha-Enolase, **F1SNZ7;** Succinate--CoA Ligase [Adp/Gdp-Forming] Subunit Alpha, Mito ,**Q6B339;** Acyl Coenzyme A Synthetase Long-Chain 1 (Fragment), **K9IW70;** Acetyltransferase Component Of Pyruvate DH Complex, **A0A286ZZN4;** Glycogen Synthase Kinase-3 Alpha, **A0A287BA23;** Acetyl-Coenzyme A Synthetase, **F1SBJ3;** Arginine-Hydroxylase Ndufaf5, Mito, **F1S3H1;** Methylmalonate-Semialdehyde DH [Acylating], Mito, **F1RM74;** Glyceraldehyde-3-Phosphate Dehydrogenase, **P42174;** Glutamate Dehydrogenase 1, Mito (Fragments), **I3LCN1;** Gamma-Enolase, **A0A287BER5;** Branched-Chain-Amino-Acid Aminotransferase, **I3LP02;** Acetyl-CoA Acetyltransferase, Mito, **P16276;** Aconitate Hydratase, Mito, **I3LQA1;** Aldehyde Dehydrogenase Family 8 Member A1, **F1ST43;** Very Long-Chain Specific Acyl-CoA DH, Mito, **A0A287BAF3;** Adenylosuccinate Synthetase Isozyme 1, **K7GP28;** 3-Hydroxyacyl-Coa DH Type-2, **P00348;** Hydroxyacyl-Coenzyme A DH, Mito, **F1SJK6;** Very-Long-Chain (3r)-3-Hydroxyacyl-CoA Dehydratase, **F1SBH1;** D-Aminoacyl-tRNA Deacylase, **I3LUR5;** Acyl-CoA DH Family Member 9, Mito, **F1SEN2;** Glutamate Dehydrogenase 1, Mito, **D0G0B3;** Acetyl-Coenzyme A Acyltransferase 2, **Q1G1K7;** Isocitrate Dehydrogenase [NAD] Sub Mito, **P41566;** Isocitrate Dehydrogenase [NAD] Sub Gamma, Mito (Fragments), **K7GPJ4;** Acyl-Coenzyme A Thioesterase 9, Mito, **A0A286ZQY6;** Isocitrate Dehydrogenase [NAD] Sub, Mito, **F8UWD3;** Alpha-L-Fucosidase, **I3LP41;** Malate Dehydrogenase, **K7GQG9;** Malonyl-CoA-Acyl Carrier Protein Transacylase, Mito, **F1RJH8;** Argininosuccinate Lyase, **A0A287A8Y8;** Short-Chain-Specific Acyl-CoA DH, Mito, **F1SRC5;** Aconitate Hydratase, Mito, **A0A287BSA1;** [Pyruvate Dehydrogenase (Acetyl-Transferring)] Kinase Isozyme 2, Mito, **B8XSJ0;** Acylglycerol Kinase, **F1SK00;** Isocitrate Dehydrogenase [NADP], **P00889;** Citrate Synthase, Mito, **B8XTR3;** 1-Acylglycerol-3-P O-Acyltransferase 5, **P08059;** Glucose-6-Phosphate Isomerase, **A0A287BIW1**; UDP-Glucose 4-Epimerase. . Data were analysed using unpaired student's t-test. * $p < 0.05$, ** $p < 0.01$, n=4

4.3.3.1.9 Collagen subunits and chains

Several collagen types and chains were identified in porcine proteomics output, nonetheless, only five were significantly increased in LAD group. These included procollagen (proCol) α-1(V), Col α-1(I) Chain, Col α-1(XIV) Chain, proCol α-2(V) and Col α-1(III) Chain, as shown in figure 4.28.

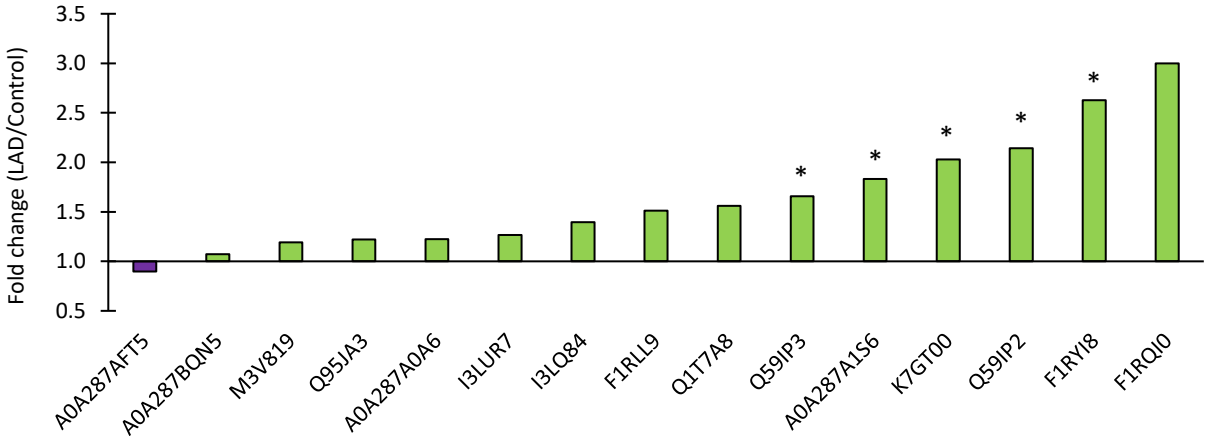

Figure 4.28 Collagen subtypes and chains. A0A287AFT5; Col α-1(Xv) Chain, **A0A287BQN5;** Col α-1(XVIII) Chain, **M3V819;** Col, Type IV, α-1, **Q95JA3;** Col Type I α-1 (Fragment), **A0A287A0A6;** Col Type VI α-6 Chain , **I3LUR7** Col α-3(VI) Chain, **I3LQ84** Col Type VI α-2 Chain, **F1RLL9;** Col α-2(Iv) Chain, **Q1T7A8;** Type VI Col α-1 Chain (Fragment), **Q59IP3;** ProCol α-1(V), **A0A287A1S6;** Col α-1(I) Chain, K7GT00 Col α-1(XIV) Chain, **Q59IP2;** ProCol α-2(V), F1RYI8 Col α-1(III) Chain, **F1RQI0;** Col α-1(XII) Chain. Data were analysed using unpaired student's t-test. * $p < 0.05$, n=4

4.3.3.1.10 Z disc proteins

Z disc proteins such as plectin and filamin C were identified and significantly increased four weeks after LAD coronary artery occlusion and reperfusion (figure 4.29). However, calsarcin 1 (myozenin 2) and neubulette were significantly decreased in LAD group.

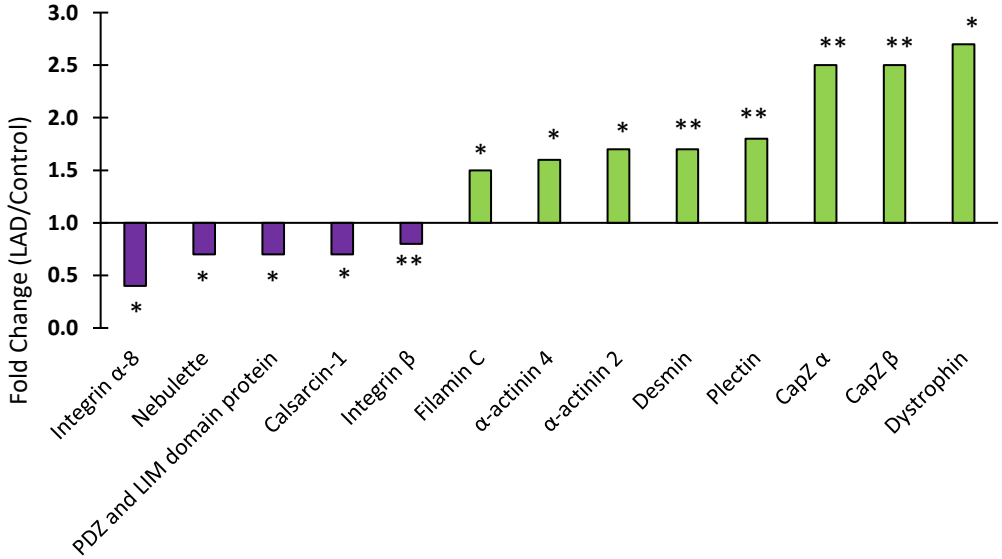

Figure 4.29 Z disc proteins. Data were analysed using unpaired student's t-test. * $p < 0.05$, ** $p < 0.01$, n=4

4.3.3.1.11 Inflammation related proteins

Inflammation related proteins were significantly upregulated in LAD group compared to control as seen in figure 4.30. Such proteins are involved in T and B cells activation (Receptor-Type Tyrosine-Protein Phosphatase C). Others such as cardiotrophin-1 (figure 4.31), which is involved in cardioprotection during ischaemia and hypertrophic response, was significantly decreased in LAD group.

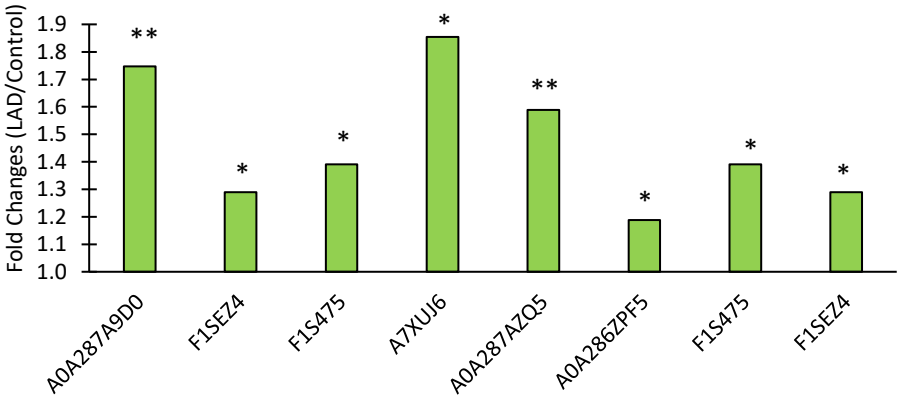

Figure 4.30 Inflammation related proteins. **A0A287A9D0;** Receptor-Type Tyrosine-Protein Phosphatase C, **F1SEZ4;** MAP Kinase-activated Protein Kinase 2, **F1S475;** 1-Phosphatidylinositol 4,5-Bisphosphate Phosphodiesterase Gamma, **A7XUJ6;** TNF Receptor-Associated Factor 6, **A0A287AZQ5;** Tumor Necrosis Factor Alpha-Induced Protein 2, **A0A286ZPF5;** Mitogen-activated protein kinase, **F1S475;** 1-phosphatidylinositol 4,5-bisphosphate phosphodiesterase ɣ, **F1SEZ4;** MAP kinase-activated protein kinase 2. Data were analysed using unpaired student's t-test. * $p < 0.05$, ** $p < 0.01$, n =4

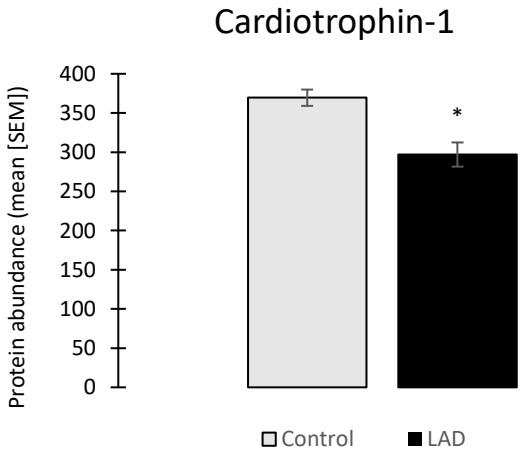

Figure 4.31 Average cardiotrophin-1 abundance in control and LAD group. Data are presented as mean (±SEM), and analysed using unpaired student's t-test. * $p < 0.05$, n =4

4.3.3.2 Pathway analysis

The proteomics output was further analysed using Ingenuity Pathway Analysis software IPA (Qiagen, Germany). Instead of proteins selection that is focused on functional or structural similarities, IPA software provides in depth assessment of data to identify main signalling pathways that were significantly different, four weeks after LAD coronary artery occlusion and reperfusion in porcine model. Figure 4.32 shows the top three signalling pathways that were changed based on their z scores, which included epithelial adherens junction signalling, actin cytoskeleton and integrin signalling. These pathways and their components are presente in figures 4.33-4.35.

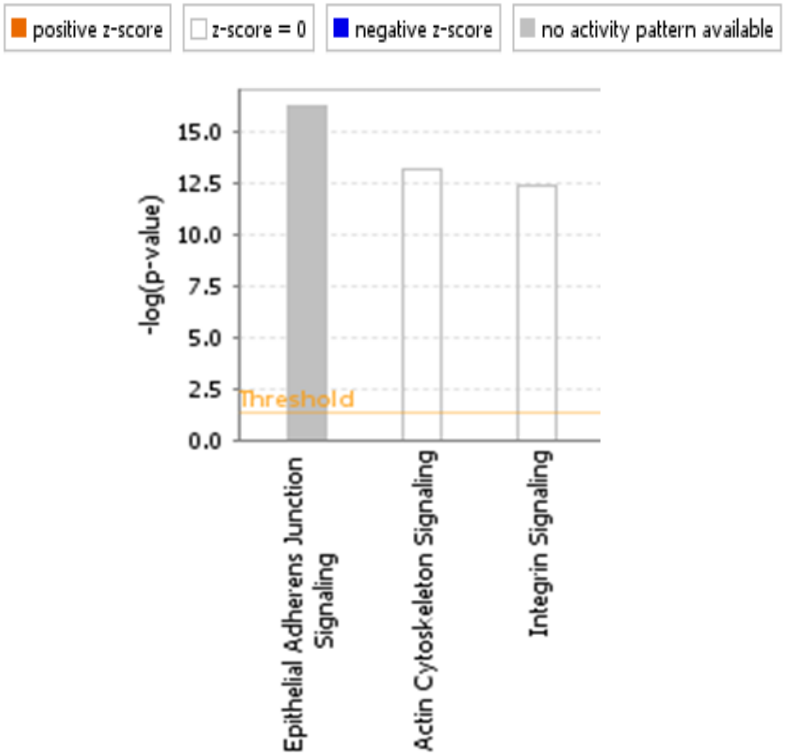

Figure 4.32 Selected top functional categories comparing LAD and control groups proteome. Threshold line represents significance value (y- axis) and direction of change in colour, represents z-score; negative scores are relatively higher results in control, whilst positive in LAD. Output adapted from Ingenuity Pathway Analysis software, Qiagen, Germany.

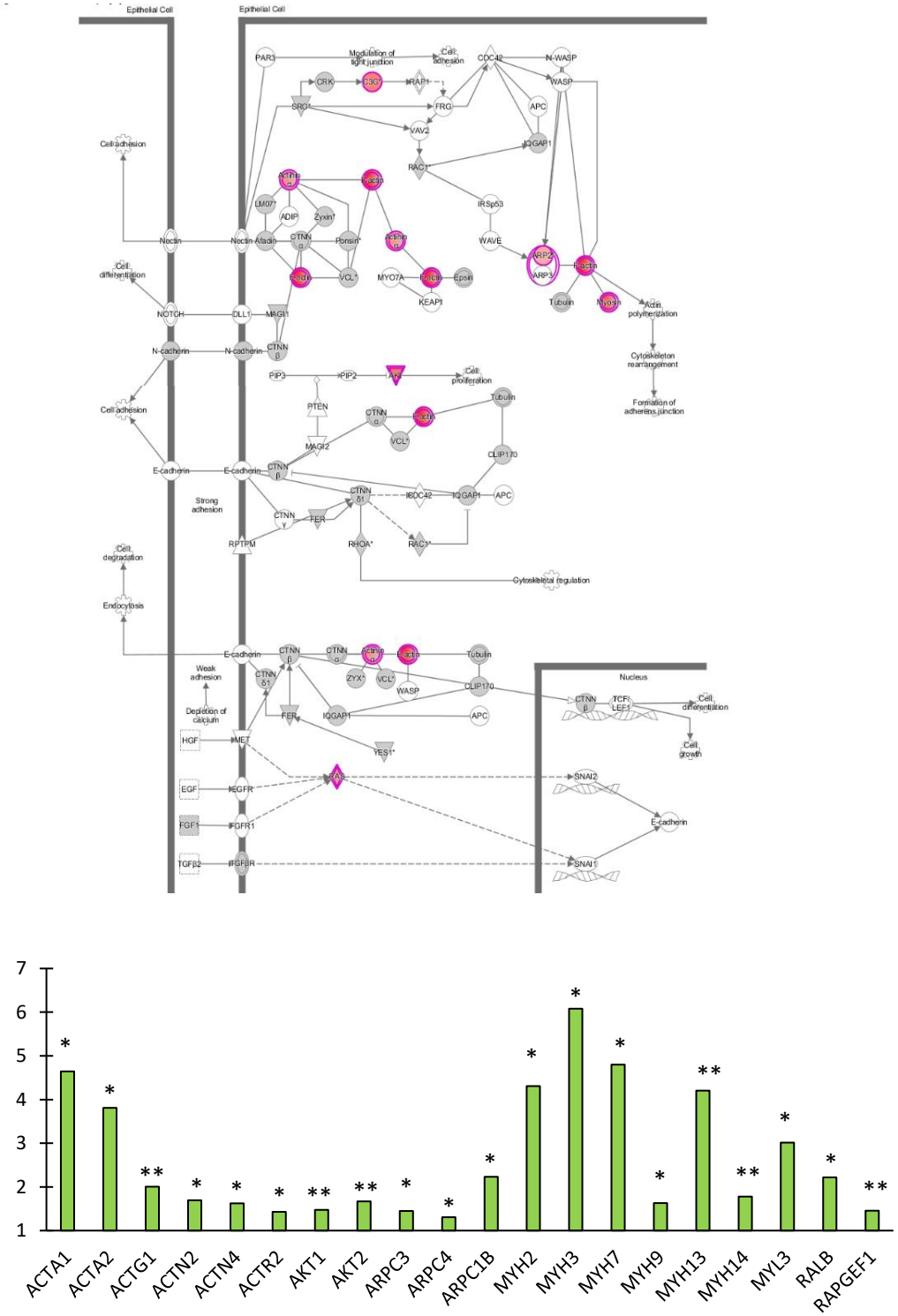

Figure 4.33 Epithelial adherens junction. **ACTA1;** actin alpha 1, skeletal muscle, **ACTA2;** actin alpha 2, smooth muscle, **ACTG1;** actin gamma 1, **ACTN2;** actinin alpha 2, **ACTN4;** actinin alpha 4, **ACTR2;** actin related protein 2, **AKT1;** AKT serine threonine kinase 1, **AKT2;** AKT serine threonine kinase 2, **ARPC3;** actin related protein 23 complex subunit 3, **ARPC4;** actin related protein 23 complex subunit 4, **ARPC1B;** actin related protein 23 complex subunit 1B, **MYH2;** myosin heavy chain 2, **MYH3;** myosin heavy chain 3, **MYH7;** myosin heavy chain 7, **MYH9;** myosin heavy chain 9, **MYH13;** myosin heavy chain 13, **MYH14;** myosin heavy chain 14, **MYL3;** myosin light chain 3, **RALB;** RAS like proto-oncogene B, **RAPGEF1;** Rap guanine nucleotide exchange factor 1, * $p < 0.05$, ** $p < 0.01$, n=4

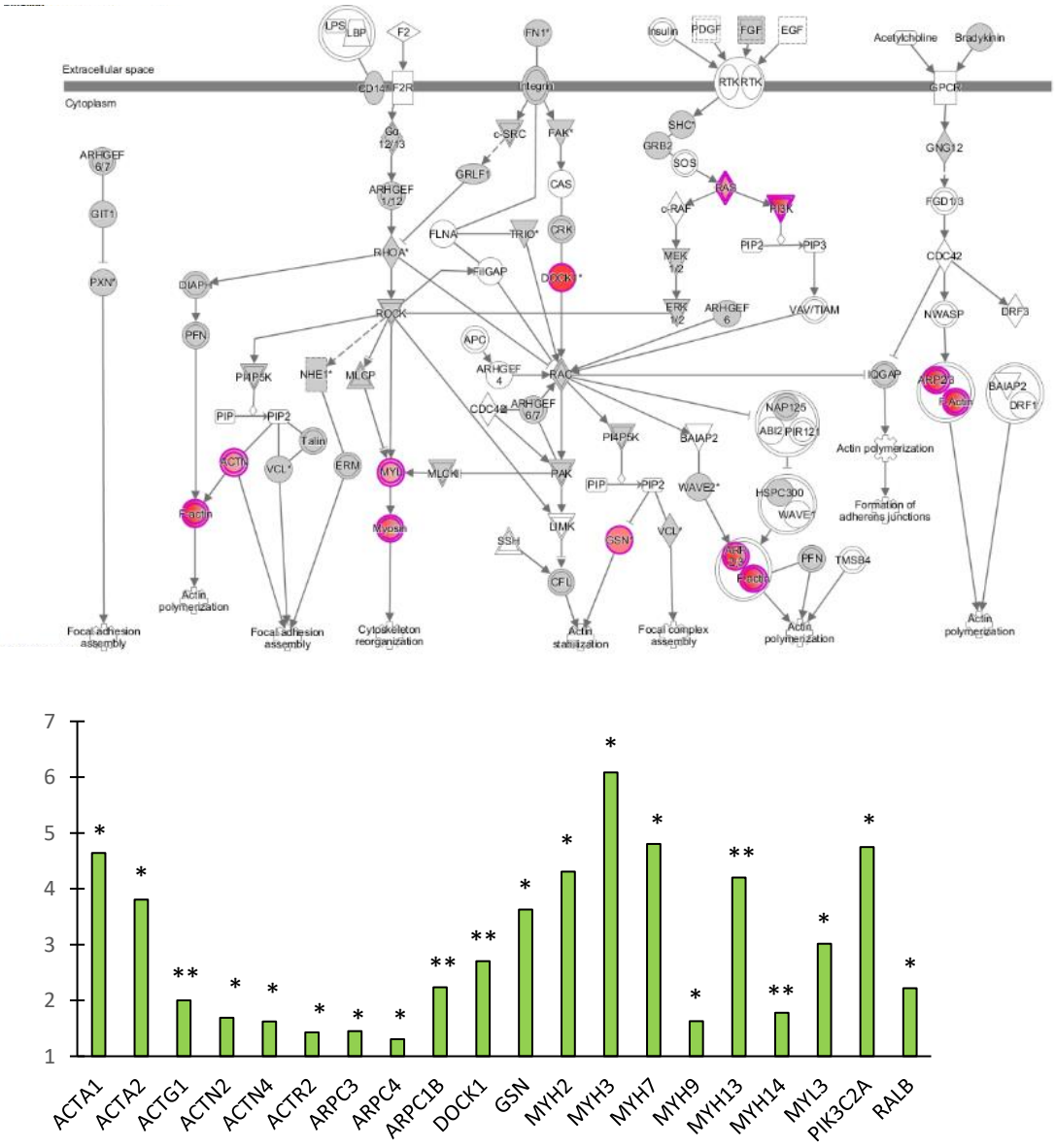

Figure 4.34 Actin cytoskeleton signalling. **ACTA1;** actin alpha 1, skeletal muscle, **ACTA2;** actin alpha 2, smooth muscle, **ACTG1;** actin gamma 1, **ACTN2;** actinin alpha 2, **ACTN4;** actinin alpha 4, **ACTR2;** actin related protein 2, **ARPC3;** actin related protein 23 complex subunit 3, **ARPC4;** actin related protein 23 complex subunit 4, **ARPC1B;** actin related protein 23 complex subunit 1B, **DOCK1;** dedicator of cytokinesis 1, **GSN;** gelsolin, **MYH2;** myosin heavy chain 2, **MYH3;** myosin heavy chain 3, **MYH7;** myosin heavy chain 7, **MYH9;** myosin heavy chain 9, **MYH13;** myosin heavy chain 13, **MYH14;** myosin heavy chain 14, **MYL3;** myosin light chain 3, **PIK3C2A;** phosphatidylinositol-4-phosphate 3-kinase catalytic subunit type 2 alpha, **RALB;** RAS like proto-oncogene B, * $p < 0.05$, ** $p < 0.01$, n=4

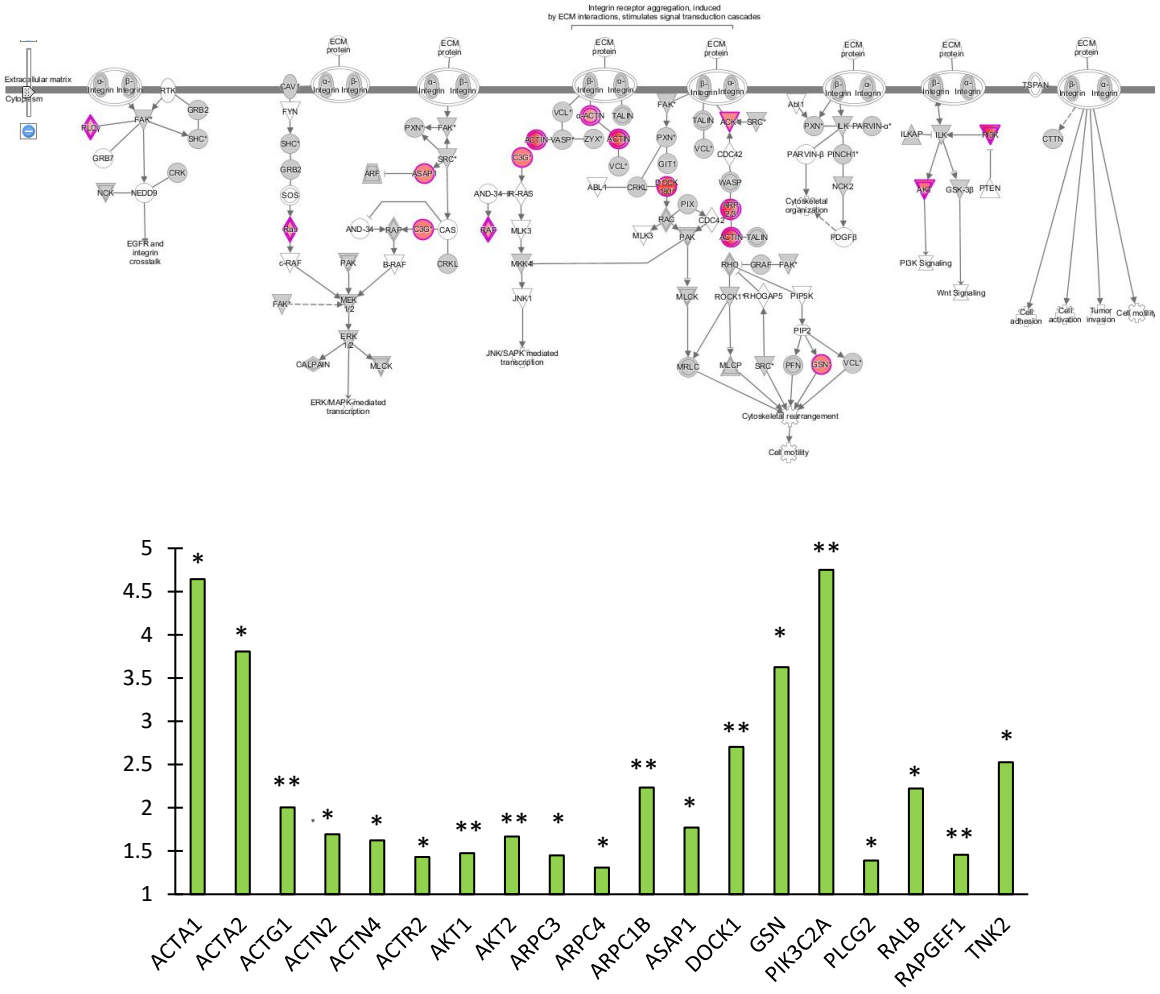

Figure 4.35 Integrin signalling proteins. **ACTA1;** actin alpha 1, skeletal muscle, **ACTA2;** actin alpha 2, smooth muscle, **ACTG1;** actin gamma 1, **ACTN2;** actinin alpha 2, **ACTN4;** actinin alpha 4, **ACTR2;** actin related protein 2, **AKT1;** AKT serinethreonine kinase 1, **AKT2;** AKT serinethreonine kinase 2, **ARPC3;** actin related protein 23 complex subunit 3, **ARPC4;** actin related protein 23 complex subunit 4, **ARPC1B;** actin related protein 23 complex subunit 1B, **ASAP1;** ArfGAP with SH3 domain, ankyrin repeat and PH domain 1, **DOCK1;** dedicator of cytokinesis 1, **GSN;** gelsolin, **PIK3C2A;** phosphatidylinositol-4-phosphate 3-kinase catalytic subunit type 2 alpha, **PLCG2;** phospholipase C gamma 2, **RALB;** RAS like proto-oncogene B, **RAPGEF1;** Rap guanine nucleotide exchange factor 1, **TNK2;** tyrosine kinase non receptor 2, * $p < 0.05$, ** $p < 0.01$, n=4

4.3.3.3 Effect of 60-minute LAD coronary artery occlusion /reperfusion on cardiac phosphoproteins

A total of 1153 phosphoproteins were detected in LAD and control groups, of which 66 were significantly different ($p < 0.05$). Phosphosites of total detected phosphoproteins are shown in figure 4.36.

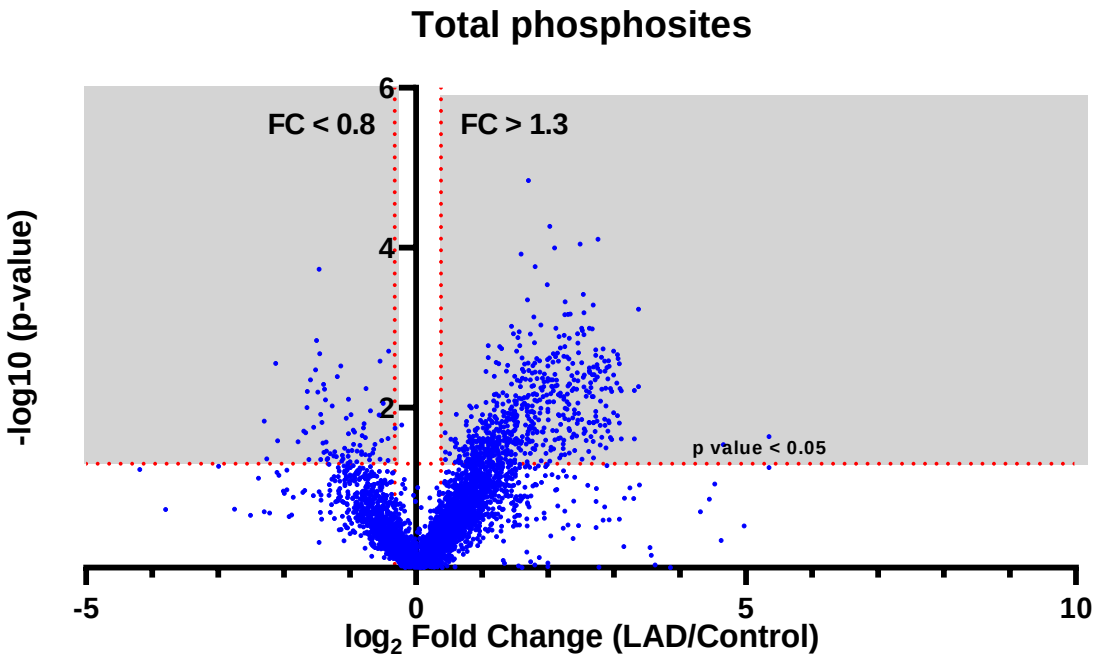

Figure 4.36 Logarithmic (volcano) plot of fold change for total detected phosphosites in porcine phosphoproteome. Reference perpendicular dotted red lines indicate fold change < 0.8 or >1.3 on y-axis. Horizontal dotted red line indicates statistical significance at p- value < 0.05. FC: fold change. n=4, total phosphosite count=1153

Phosphoproteins that are statistically different ($p < 0.05$) were mainly involved in molecular binding activity, followed by catalytic and transducer activities based on Panther database classification system (figure 4.37).

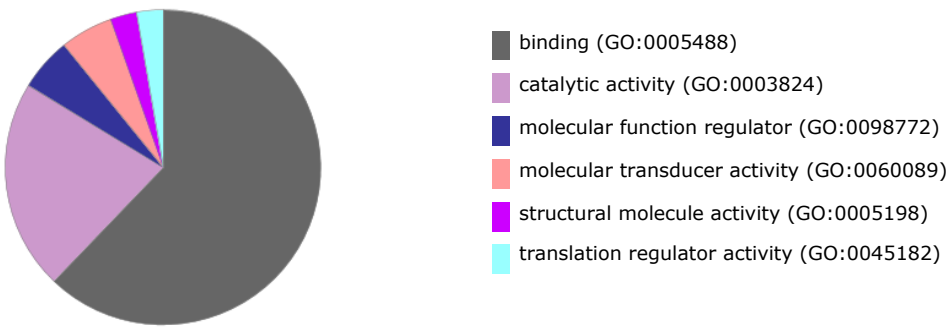

Figure 4.37 Molecular function of significantly different phosphoproteins. Panther Go-Slim molecular function of significant phosphoproteins. ($p < 0.05$) using protein accession numbers. n=4, phosphoproteins count=66

Selected significantly different phosphorylation sites (serine, threonine and tyrosine) are listed in table 4.1. There is an increased phosphorylation of phosphosites of cellular signalling proteins, including Heat Shock Protein 90 β, catenin α 1, as well as ion transporters, such as sarcoplasmic/endoplasmic reticulum calcium ATPase 2 (SERCA2). These effects are also seen in sarcomere structural proteins including spectrin β chain and Z-disc related proteins (PDZ and LIM domain protein 1) as well as tight junction proteins (gap junction protein).

Table 4.1 Changes in phosphoproteins in control and LAD groups ($p < 0.05$). Data were analysed using unpaired student t-test. n = 4. S; serine, T; threonine and Y; tyrosine

Protein	**Accession Number**	**Phosphorylation site(s)**	**FC (LAD/SHAM)**	**p-value**
Ion transporters				
Sodium/hydrogen exchanger	F1STQ3	S799	2.3	0.013
Calcium voltage-gated channel auxiliary subunit β 2	A0A287ANL1	T221	0.6	0.011
Sarcoplasmic/endoplasmic reticulum calcium ATPase 2	P11607	S50,S51	2.5	0.04
Structural proteins				
Leiomodin 2	F1SLY4	S514 S515 S518 T519 Y13 T385	1.7 3.0 4.2 4.3 2.9 4.4	0.045 0.003 0.007 0.017 0.001 0.036
Tropomyosin β chain	A0A287AN33	S283	2.3	0.007
Cardiac muscle α actin 1	B6VNT8	T55	2.8	0.011
Gap junction protein	F1SF43	S369	0.4	0.027
Nebulette;NEBL	F1RVG6	S387	2.3	0.017
		S538	4.4	0.004
Myosin heavy chain 8; MYH8	F1SS62	S1203	1.8	0.010
Actin, α skeletal muscle	P68137	Y242	2.4	0.027
Fibrillin-1	F1SN67	S2702	1.5	0.030
Spectrin β chain	A0A287BJV2	S2341	1.6	0.044
		S2169	3.2	0.019
Paxillin Paxillin	M3UZB4	S306 S85	2.1 2.2	0.03 0.04
Prelamin-A/C	F1RLQ2	S22	4.4	0.00

Protein	Accession Number	Phosphorylation site(s)	FC (LAD/SHAM)	p-value
Structural proteins (cont.)				
Myosin-1	F1SS64	S1203	1.9	0.02
		S1144	3.4	0.03
Synemin	A0A287B3V0	S418	2.5	0.02
PDZ and LIM domain protein 1	F1SC51	S158	3.8	0.02
Palmdelphin	Q2MJV9	S342	1.6	0.04
		S385	1.6	0.04
		S426	2.0	0.03
Tensin-1	K9IWG9	S911	2.0	0.04
		S1363	2.1	0.03
		T1310	2.6	0.04
		S1103	2.6	0.03
		S1289	2.7	0.04
Microtubule-associated protein	A0A287BPN0	S759	2.0	0.03
		T641	2.5	0.04
		S2169	2.7	0.02
		S1597	3.1	0.01
		S698	5.7	0.04
Signalling proteins				
Catenin α 1 (CTNNA1)	F1RGJ2	T838	1.9	0.048
Heat shock protein family A (HSP70) member 12B	F1S8C1	S29	2.7	0.047
Heat shock protein HSP 90-β	A0A286ZR68	S226	1.6	0.032
A-kinase anchoring protein 12	A0A287BE06	S1494	3.5	0.029
Nuclear factor 1	A0A287AQ42	S301	2.3	0.03
Histone deacetylase; HDAC6	I3LEZ7	T936	1.6	0.019
Enzymes				
Dual specificity phosphatase 27, atypical	F1S252	S561	1.8	0.041
		S562	2.5	0.005
		S473	2.4	0.016
A kinase 3 (ALPK3)	A0A287ABZ9	S502	3.1	0.011
		S1111	5.2	0.001

Protein	Accession Number	Phosphorylation site(s)	FC (LAD/SHAM)	p-value
Signalling proteins (cont.)				
DNA topoisomerase 2	F1RS45	S1513	2.3	0.036
		T1563	2.8	0.004
Glyceraldehyde-3-phosphate dehydrogenase	P00355	T182	0.4	0.00
Calpastatin	F6PU32	S208	0.6	0.03
Serine/threonine protein kinase MST4	B7U6F4	S300	0.4	0.03
6-phosphofructokinase	A0A286ZZL7	S795	2.6	0.01
ADP/ATP translocase 3	A0A287AVQ0	T84	0.3	0.01
ATP synthase subunit β	K7GLT8	S398	2.4	0.03
		S679, T680	2.9	0.01
Phosphodiesterase	B3TNN3	S145	1.9	0.02
		S140	2.2	0.02

4.3.4 Effect of 60-minute LAD coronary artery occlusion /reperfusion on porcine cardiac energetics

All cellular metabolites were measured using HPLC from control and LAD groups from left ventricular (or infarct), as well as right and left atrial tissues 4 weeks after LAD coronary artery occlusion and reperfusion. The data were compared regionally between the two groups.

4.3.4.1 Left ventricular energetics profile

Table 4.2 lists different metabolites levels taken from infarct region from LAD group and left ventricle from the control. None of these metabolites were significantly different.

Table 4.2 Energy metabolites of control (LV) and LAD (infarct) groups. Data are presented as mean ± SEM and analysed using unpaired student's t-test. n = 4

Metabolites	Control nmol/mg	LAD nmol/mg	p-value
GTP	0.09 ± 0.03	0.10 ± 0.03	0.87
GDP	0.05 ± 0.02	0.12 ± 0.04	0.16
GMP	0.02 ± 0.01	0.04 ± 0.01	0.26
IMP	0.03 ± 0.00	0.09 ± 0.03	0.17
ATP	1.54 ± 0.62	1.65 ± 0.89	0.93
ADP	0.95 ± 0.17	2.17 ± 0.78	0.22
Hypoxanthine	0.30 ± 0.12	0.05 ± 0.01	0.13
AMP	0.44 ± 0.16	0.97 ± 0.48	0.34
B-NAD	0.48 ± 0.02	0.55 ± 0.14	0.64
Inosine	1.52 ± 0.50	0.20 ± 0.06	0.08
Adenosine	0.36 ± 0.18	0.06 ± 0.02	0.19

Total adenine metabolites pool was significantly increased in LAD group, mainly due to an increase in AMP and ADP content (nearly doubled). Nonetheless, phosphorylation ratios of guanosine and adenine metabolites were calculated and showed no significant difference in phosphorylation potential. Energy charge was slightly decreased in LAD group; however, this change was not statistically significant (figure 4.38).

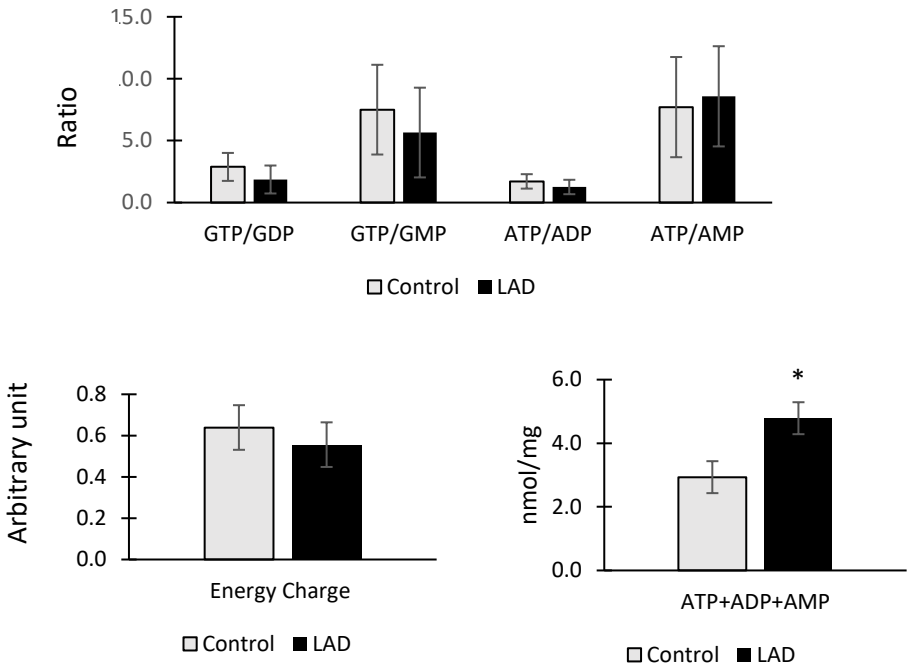

Figure 4.38 Phosphorylation potential, energy charge, and adenine metabolites pool of LAD (infarct) and control (LV) hearts. Data are presented as mean ± SEM and analysed using unpaired student's t-test. * $p < 0.05$, n = 4

4.3.4.2 Right atrium energetics profile

Right atrial metabolites levels from LAD and control groups are listed in table 4.3. Similarly, none of these metabolites levels were significantly different was noted.

Table 4.3 Right atrium (RA) energy metabolites in control and LAD groups. Data are presented as mean ± SEM and analysed using the unpaired student t-test. n = 4

Metabolites RA	Control nmol/mg	LAD nmol/mg	p-value
GTP	0.09 ± 0.03	0.10 ± 0.02	0.95
GDP	0.06 ± 0.03	0.03 ± 0.01	0.55
GMP	0.03 ± 0.01	0.02 ± 0.00	0.50
IMP	0.03 ± 0.02	0.02 ± 0.01	0.52
ATP	0.59 ± 0.27	1.11 ± 0.19	0.20
ADP	0.91 ± 0.48	0.62 ± 0.09	0.62
HYPO	0.31 ± 0.11	0.12 ± 0.01	0.23
AMP	0.49 ± 0.24	0.28 ± 0.02	0.48
B-NAD	0.23 ± 0.07	0.21 ± 0.04	0.79
Inosine	0.78 ± 0.23	0.52 ± 0.17	0.42
Adenosine	0.17 ± 0.08	0.38 ± 0.16	0.30

There were increase of ATP to ADP and AMP ratios, respectively in LAD group compared to control as seen in figure 4.39, but none were reported as significantly different between the two groups.

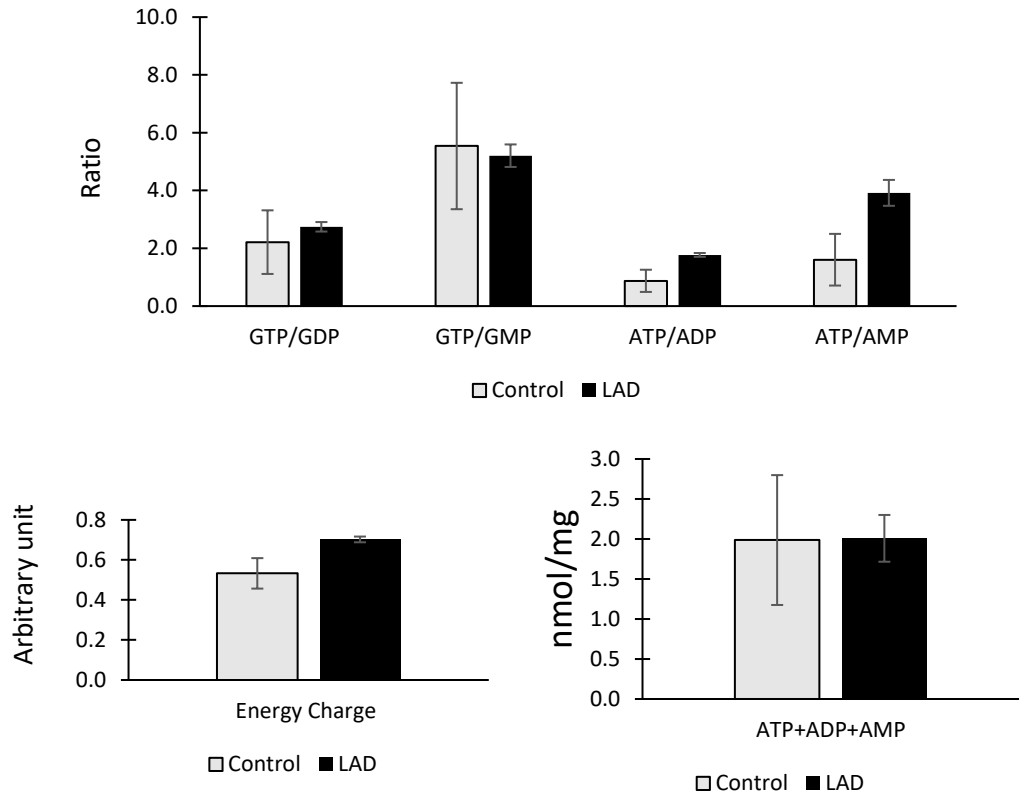

Figure 4.39 Phosphorylation potential, energy charge, and adenine metabolites pool of right atrium in LAD and control hearts. Data are presented as mean ± SEM and were analysed using unpaired student's t-test. ** p< 0.01, n = 4

4.3.4.3 Left atrium energetics profile

Table 4.4 includes left atrial metabolites levels from LAD and control groups. Only hypoxanthine and AMP levels were significantly reduced in LAD group.

Nevertheless, energy charge and GTP/GDP, ATP/ADP and ATP/AMP ratios were significantly increased in LAD group compared to control (figure 4.40).

Table 4.4 Left atrium (LA) energy metabolites in control and LAD groups. Data are presented as mean ± SEM and analysed using the unpaired student's t-test. n = 4

Metabolites LA	Control nmol/mg	LAD nmol/mg	p-value
GTP	0.11 ± 0.00	0.12 ± 0.01	0.39
GDP	0.03 ± 0.00	0.02 ± 0.00	0.07
GMP	0.01 ± 0.00	0.01 ± 0.00	0.12
IMP	0.03 ± 0.01	0.03 ± 0.01	0.84
ATP	1.51 ± 0.19	1.99 ± 0.14	0.11
ADP	0.54 ± 0.03	0.40 ± 0.04	0.05
Hyoxanthine	0.19 ± 0.02	0.01 ± 0.00	0.00
AMP	0.19 ± 0.01	0.10 ± 0.02	0.02
B-NAD	0.27 ± 0.00	0.28 ± 0.03	0.90
Inosine	0.60 ± 0.12	0.22 ± 0.09	0.07
Adenosine	0.16 ± 0.05	0.03 ± 0.01	0.08

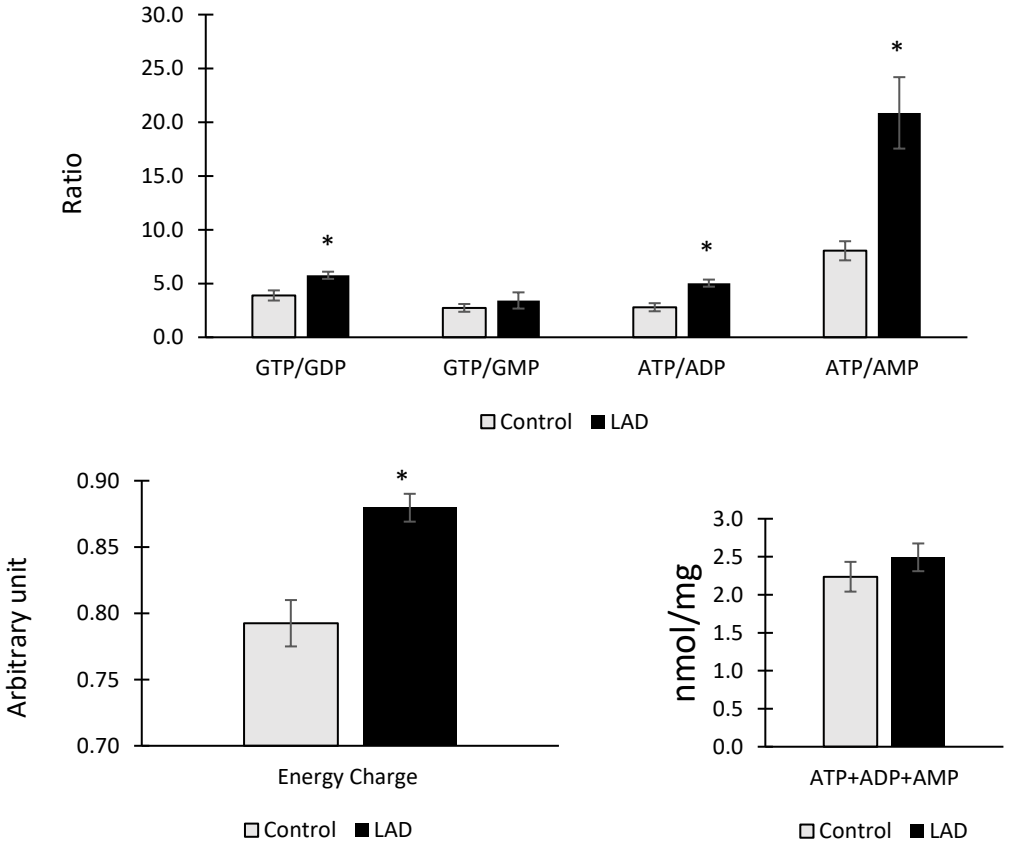

Figure 4.40 Phosphorylation potential, energy charge, and adenine metabolites pool of left atrium in LAD and control groups. Data are presented as mean ± SEM and were analysed using unpaired student's t-test. n=4

4.3.5 Effect of 60-minute LAD coronary artery occlusion /reperfusion on porcine cardiac metabolites

Using 1H-NMR spectral analysis of PCA extracted porcine cardiac tissues from left ventricle in the control and the infarct in LAD group, 16 metabolites were detected as seen in figure 4.41. These metabolites included amino acids, glucose, lactate, and lipids. Taurine was significantly increased whereas lactate was reduced in LAD group.

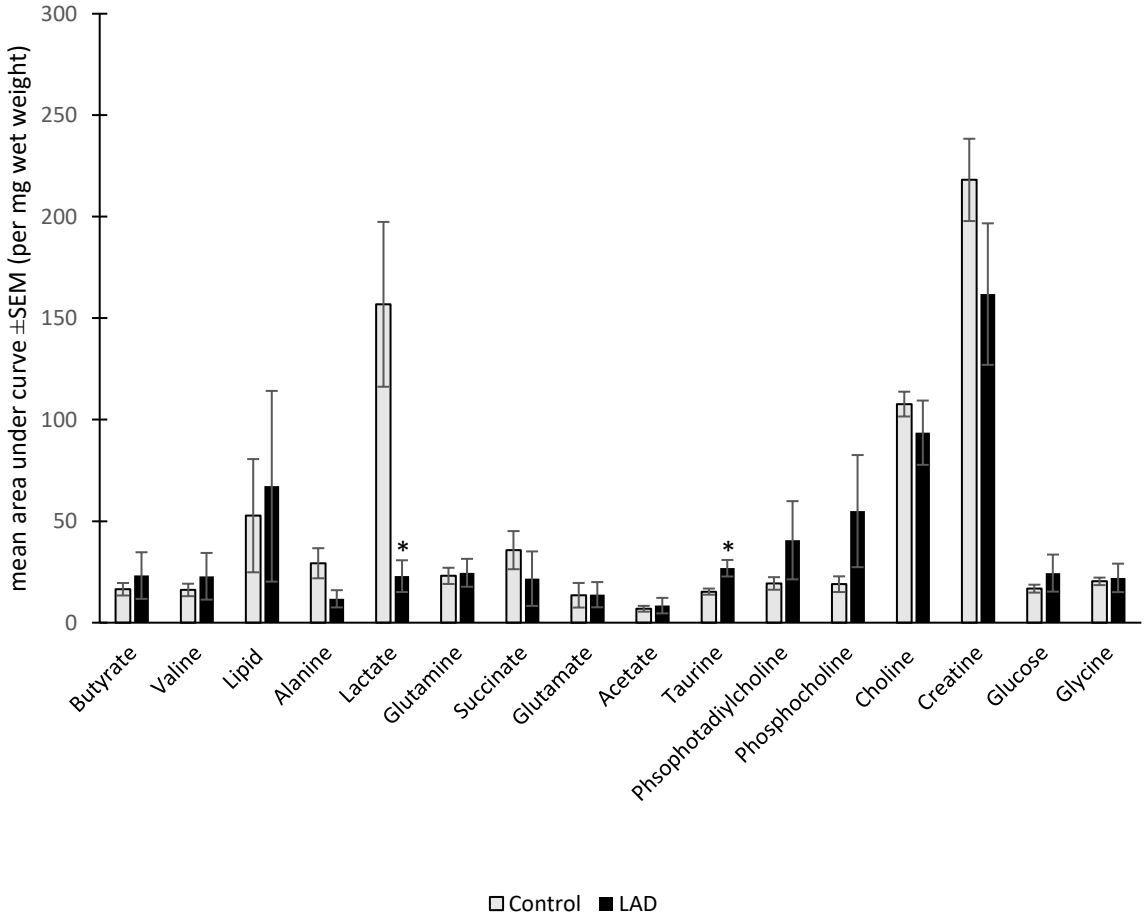

Figure 4.41 Porcine cardiac metabolites. Metabolites in cardiac extracts as collected from control and LAD group 4 weeks after LAD coronary artery occlusion and reperfusion. Data were corrected per mg of wet tissue weight and presented as mean ± SEM as analysed using unpaired student's t-test. * $p < 0.05$, $n = 4$

4.3.6 Effect of 60-minute LAD coronary artery occlusion /reperfusion on porcine blood metabolites

1H- NMR spectroscopy analysis was also used to measure blood metabolites 4 weeks after LAD occlusion and reperfusion and compared to control. In total, 24 metabolites were annotated from NMR spectra as seen in figure (4.42). Certain significantly different metabolites included TCA cycle intermediates, ketone bodies, amino acids and carbohydrates. Taurine was significantly decreased in blood from LAD group, while ketone bodies such as acetone and acetoacetate were significantly elevated.

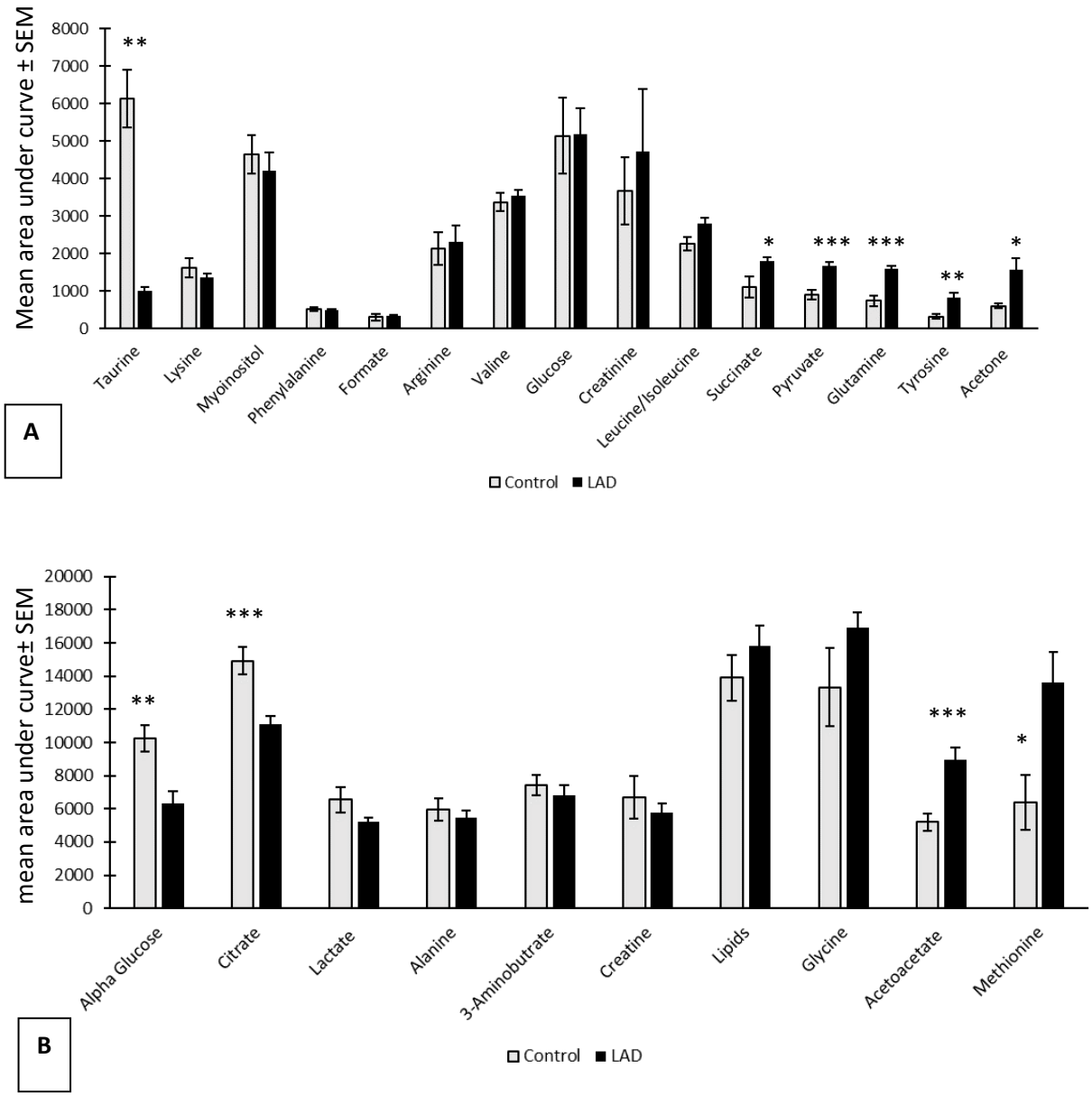

Figure 4.42 (A and B) Porcine blood metabolites. Metabolites detected in blood samples as collected from control and LAD group 4 weeks after LAD coronary artery occlusion and reperfusion. Data are presented as mean ± SEM and analysed using unpaired student's t-test. * $p < 0.05$,** $p < 0.01$,*** $p < 0.001$, n= 4

4.4 Discussion

A porcine model of *in vivo* 60-minute LAD coronary artery occlusion and reperfusion was used to investigate post ischaemic cardiac remodelling, four weeks after the infarction. The main findings are concluded as the following:

- Post ischaemic cardiac remodelling is associated with distinctive pattens of cardiac extracellular matrix fibrosis and structural disorganisation.
- Remodelling is associated with significant changes in morphometry, cristae density and subpopulation distribution of the mitochondria.
- Remodelling is associated with decreased ATP synthesis, antioxidant related cardiac proteins, fatty acid, and amino acids metabolic pathways.
- Calcium handling proteins were decreased with post ischaemic cardiac remodelling.
- There is increase in extracellular, structural, junctional and cytoskeletal proteins following post ischaemic cardiac remodelling in porcine heart.
- Main signalling pathways identified with post ischaemic cardiac remodelling in porcine model were actin cytoskeleton, integrin and tight junction signalling pathways.
- Remodelling is associated with increased levels of ketone bodies and selected amino acids in porcine blood metabolites, as well as increased cardiac taurine levels.

4.4.1 Disruption and remodelling of ECM during post MI cardiac remodelling

LAD porcine hearts sections taken from the infarct area four weeks after ischaemia reperfusion revealed patten of extensive fibrosis (eightfold increase) due to collagen deposition (figure 4.2). The infarct area is also rich in noncardiomyocytes, as seen in light and electron micrographs, which included fibroblasts (and myofibroblast), endothelial cells, telocytes, macrophages, and infiltrating leukocytes, etc. These types of cells indicate ongoing infract remodelling and scar reorganisation.

The effect of ischaemia reperfusion injury on coronary arteriolar wall thickness were marked by the substantial increase in the ratio of wall area to the total arteriolar area (figure 4.4). These arterioles (20-200 micron in diameter) play a major role in coronary resistance and blood flow regulation (Fedele, Severino et al. 2013), which contribute later to microcirculation dysfunction and deterioration of myocardial performance. The increased ROS production, with decreased NOS release, along with synthesis and release of proinflammatory mediators, and the shear stress from disruption of myocardial organisation consequently induce growth and hypertrophy of vascular smooth muscle cells SMC in tunica media (Severino, Amato et al. 2020). There is also increased in angiogenesis at this stage of cardiac remodelling, as most of the changes that occurs in coronary vasculature is secondary to endothelial dysfunction, which leads to release of vasoactive substances (such as endothlin-1)(Böhm and Pernow 2007). The increased wall thickness is an indirect measure of increased wall stress and regional myocardial intramural pressure, leading consequently to vascular remodelling (Choy and Kassab 2009). Moreover, the intercellular interaction between telocytes and other cell types such as endothelial cells and stem cells appears to be involved in mediating angiogenic response and cardiac recovery post MI (Banciu, Cretoiu et al. 2017, Liao, Chen et al. 2021). As seen in the infarct area of LAD hearts, telocytes were characteristically similar to their counterpart in patients with heart failure, in which ultrastructural alterations such as telopodes shrinkage and shortening, and cytoplasmic vacuolisation were the most prominent features, indicating incessant cellular stress and disruption to their function (Cretoiu, Cretoiu et al. 2013, Galrinho, Manole et al. 2016).

Several inflammatory cells such as macrophages and infiltrating leukocytes were seen in EM images of LAD pigs, while little to none observed in the control. At this stage of late proliferative phase, fibroblasts are extensively present in ECM, and activated myofibroblast are mediating matrix proteins and collagen synthesis. In healthy adult heart, the predominant types of collagen are type I (> 50% of total collagen), followed by type III (10–45%) (Eghbali and Weber 1990). In our work, subunits of collagen that were significantly as identified by the proteome output (figure 4.28). These included procollagen type V (α-1/2), collagen type I (α-1), collagen type III (α-1), and interestingly type XIV (α-1). Based on their mechanical properties, each subtype of collagen has different effect on scar characteristics. Work done by Asgari and Rusu et al. showed that deposition of type III and V collagen in between the stiff type I collagen appears to decrease the level of stiffness in the infract region at the end of proliferative phase (2-3 weeks), and therefore reduce the level of stretching on exerted on cardiomyocytes (Asgari, Latifi et al. 2017, Rusu, Hilse et al. 2019). Procollagen V α-1 and 2 chains, which are normally upregulated in developing hearts (Frangogiannis 2019), were also increased in post MI cardiac remodelling in porcine hearts (Barallobre-Barreiro, Didangelos et al. 2012) and in pressure overloaded myocardium in rats (Honda, Goto et al.

1993). It has been shown that procollagen V is linked to collagen fibril assembly and diameter in the myocardium (Lincoln, Florer et al. 2006). Little data is available regarding the role of collagen type XIV (α-1) during scar formation. This suntype is involved in organisation and integrating bundles of collagen, in addition to cellular adhesion to extracellular matrix, through its binding to CD44 on cell surface, and signal transduction through cytoskeleton via ankyrin protein (Schuppan, Cantaluppi et al. 1990, Ehnis, Dieterich et al. 1996, Bauer, Dieterich et al. 1997) .

4.4.2 Disruption to mitochondrial structure and molecular content in parallel with decrease in energetics in post MI hearts

Cardiac tissues collected from infarct area were used to monitor energetics and morphological, and molecular changes in the mitochondria. Morphometric measurements of different mitochondrial subpopulations did not reveal marked differences between the two groups, although, the measured areas of IF and SS mitochondria appeared larger in LAD group, possibly due to imminent swelling. There was also marked decrease in interfibrillar mitochondrial distribution in LAD porcine hearts compared to control (figure 4.8), which could be attributed to the imbalance between the energy demands and mitochondrial biogenesis as observed in decompensated HF (Rosca and Hoppel 2010). Although it is expected to observe a drop in cardiac performance (e.g. EF) in response to inadequate energy supply due to decreased IF subpopulation, the pigs used in this study had increased cardiac muscle mass, which could potentially compensate for cardiac death and loss in the infarct area (as seen in appendix). Nevertheless, mitochondrial cristae density, which reflects the degree of cristae separation, was decreased significantly in LAD group, indicating a decrease in mitochondrial respiratory rate, and therefore function (Rosca and Hoppel 2013). Similar findings were reported in patients with dilated and hypertrophic cardiomyopathies (Baandrup, Florio et al. 1981), as well as dogs with chronic ischaemic heart failure (Sharov, Goussev et al. 1998). This disruption to cristae is known to disrupt ability of mitochondria to produce ATP, which is evident in proteomic output of mitochondrial proteins, as most of these proteins had decreased expression in LAD group (figure 4.23). Mitochondrial ATP synthesis ability is known to diminish acutely after ischaemia reperfusion injury (Kuznetsov, Javadov et al. 2019), yet a persistent decrease in ATP synthesis proteins (subunits of F0/F1 complex) and creatine kinase-M type four weeks after IRI reflects the ongoing mitochondrial incapability to meet the energy demands. Similar findings were reported by Bienk et al who reported a decrease in mitochondrial ECT proteins such as complexes III and IV , 7 days after reperfusion in the ischaemic zone in the myocardium (Binek, Fernández-Jiménez et al. 2017).

These defects in oxidative phosphorylation and ETC expose mitochondria to increased level of oxidative stress weeks after infarction. In this regard, antioxidant related proteins, as identified in this work, were significantly decreased in LAD pigs. For instance, both thioredoxin reductase 2 and glutathione reductase maintain redox balance in cells through reduction of the oxidised thioredoxin and glutathione, respectively (Biterova, Turanov et al. 2005, Deponte 2013), These findings reflect a continuous chronic state of oxidative stress after ischaemia reperfusion injury.

Moreover, there was impairment of mitochondrial fatty acids oxidation (decrease in enzymes such as acetyl-coenzyme A synthetase and acetyl-coenzyme A acyltransferase 2). In heart failure, it is known that there is a 30-40% decrease in ATP levels (Beer, Seyfarth et al. 2002) in addition to shift towards foetal metabolism, which is characterised by decreased mitochondrial oxidative capacity and increased dependence on glucose oxidation (Fillmore, Mori et al. 2014). Consequently, as the heart becomes less reliant on fatty acids oxidation due to mitochondrial remodelling, and with progressive decrease in glucose oxidation possibly due to insulin resistance (Riehle and Abel 2016), other metabolites such as ketone bodies are utilised to compensate for increasingly metabolic demands during heart failure, since heart is an omnivore and would extract substrates that are present at high concentration. As concluded from NMR results, ketone bodies such as acetoacetate and acetone were both elevated in porcine blood four weeks after ischaemia reperfusion injury. Similar findings were seen in patients with ischaemic heart disease, in which levels of acetone in breath was used as marker of severity of heart failure (Marcondes-Braga, Gutz et al. 2012). However, whether this increase of ketone bodies reflects a decrease in cardiac utilisation and extraction and/or increased systemic production is yet to be determined.

Porcine blood metabolic profiling also showed a marked decrease in taurine in LAD group, while its level increased significantly in LAD cardiac tissue extracts. Taurine, a β-amino acid that is found in high levels in heart and muscle tissues, has many physiological roles including membrane stabilisation, regulation of Ca^{2+} sensitivity and contractile functions (Schaffer, Jong et al. 2010). Taurine is considered as one of the major osmolytes in cardiac tissue and it is involved in regulating sodium efflux through the action of sodium dependant taurine transporter (Suleiman, Rodrigo et al. 1992). Decrease in taurine suggests that this amino acid has been used by Na^+ to exit the myocytes, since regulation of Na^+ is important as Na^+ /Ca^{2+} exchanger can be a source of Ca^{2+}-loading and cardiomyocyte death. Therefore, cardiomyocyte ability to regulate Ca^{2+} levels can be help in cardiomyocytes protection from death by apoptosis (Lewis, Littlejohns et al. 2014). Taurine has been shown to exert cardioprotective effects during IRI, as it decreases the levels of oxidative stress and the impact of ROS on mPTP opening (Schaffer, Jong et al. 2014). Additionally, taurine is involved in activation of Akt-dependent signalling, which results in inhibition of pores formation via PKC-ε activation, all of which are crucial for survival signalling (Takatani, Takahashi et al. 2004).

Another amino acid, methionine (a sulphur containing amino acid) was markedly elevated in LAD group. This essential amino acid is involved in several metabolic processes, for example, thioredoxin and glutathione synthesis as well as proteins and polyamine metabolism (Dhar, Lysne et al. 2018). Since methionine is involved in diverse metabolic processes, it is therefore quite difficult to attribute this change to a single metabolic pathway. However, proteomics data from porcine model showed a significant decrease in mitochondrial thioredoxin and peptide-methionine (R)-S-oxide reductase. The latter is an oxidoreductase enzyme which plays a significant protective role from oxidative stress damage, caused by reactive oxygen species, through a reversible reaction to reduce the oxidized methionine to methionine using thioredoxin (Kantorow, Lee et al. 2012). It is possible that the sustained oxidative stress and mitochondrial damage in LAD pigs might be the reason behind the reduced expression of these antioxidant proteins and the increased systemic methionine. A study by Hakuno et. al showed a positive correlation between elevated plasma amino acids levels such as

methionine and HF parameters (such as EF, Blood Natriuretic Peptide, etc) in patients with stage II heart failure (Hakuno, Hamba et al. 2015).

Interestingly, taurine and methionine metabolism are linked through transulphuration pathway. Methionine is converted to homocysteine, which could be further metabolised by cystathionine β-synthase into cystathionine and later cysteine and taurine. Taurine could be also be synthesised from cysteine by the actions of cysteinesulfinic acid decarboxylase (CSD) and hypotaurine dehydrogenase (Hayes and Sturman 1981). Thus, an increase in methionine and a reduction in taurine level might be suggestive of a defect in this metabolic pathway during post ischaemic cardiac remodelling.

4.4.3 Altered actin cytoskeletal proteins and possible role in cardiomyocytes survival signalling

Measurement of sarcomeres in porcine hearts following post ischaemic cardiac remodelling did not detect significant differences in length. Similar finding was reported in patients with compensated and decompensated heart failure, in which sarcomere length was not markedly changed compared to hemodynamically normal LV function group, and did not correlate with heart failure severity (Rackley, Dalldorf et al. 1970). This could be explained by compensatory cardiac hypertrophy following ischaemia reperfusion injury, which is associated with increased number of sarcomeres (parallel addition) rather than elongation of sarcomere length (Mann and Bristow 2005). Maintenance of sarcomere structure is also linked to modifications in key sarcomere proteins such as titin, which spans the entire length of sarcomere, and mediates passive resistance through its extensible regions such as N2B subunit (Hanft, Korte et al. 2007), this protein was notably increased in LAD cardiac proteome.

Proteomics study showed overexpression of several structural elements in z disc such as α-actinin-2, Cap Z subunits and desmin. It is known that dilated and hypertrophic cardiomyopathies are linked to abnormalities in z disc proteins (Yin, Ren et al. 2015). Desmin, for example, was elevated in failing myocardium due to dilated cardiomyopathy (Heling, Zimmermann et al. 2000). Interestingly, this protein was also hyperphosphorylated in LAD pigs at different phosphorylation sites, including phosphosite S31. This phosphosite was shown to promote desmin aggregation in ischaemic HF patients and mice model of pressure-overload induced HF (Rainer Peter, Dong et al. 2018). Additionally, overexpression of CapZ β subunits in a transgenic mice resulted in hypertrophic cardiomyopathy and distorted sarcomere architecture (Sequeira, Nijenkamp et al. 2014). However, some of z disc associated signalling proteins were decreased in LAD pigs. These included calsarcin-1, which normally represses calcineurin (a Ca^{2+}-dependant phosphatase that is involved in cardiac hypertrophic signals)in cardiomyocytes (Posch, Thiemann et al. 2008).

Many of cellular signal transduction in cardiomyocytes occurs in costamere and z disc through interaction with several ECM proteins as seen in figure 4.43. (Borg, Goldsmith et al. 2000). As seen in porcine proteome output analysis using IPA software, the role of epithelial adherens junction, actin cytoskeleton reorganisation and integrin signalling provide novel aspects to understand post ischaemic remodelling in the myocardium four

weeks after IRI. The downstream cellular effect of these pathways involved in cytoskeletal rearrangement, actin polymerisation and stabilisation in addition to activation of PI3K/AKT signalling, which might be involved in cellular hypertrophy and survival in the heart (Sugden 2003). Gelsolin, another protein highly expressed in in integrin and actin cytoskeleton signalling pathways, is implicated in progression towards heart failure through its involvement in apoptosis mediated singling (Li, Shi et al. 2009). Inhibition of gelsolin through PI3K signalling appears to be protective from adverse remodelling (Patel, Zhabyeyev et al. 2018).

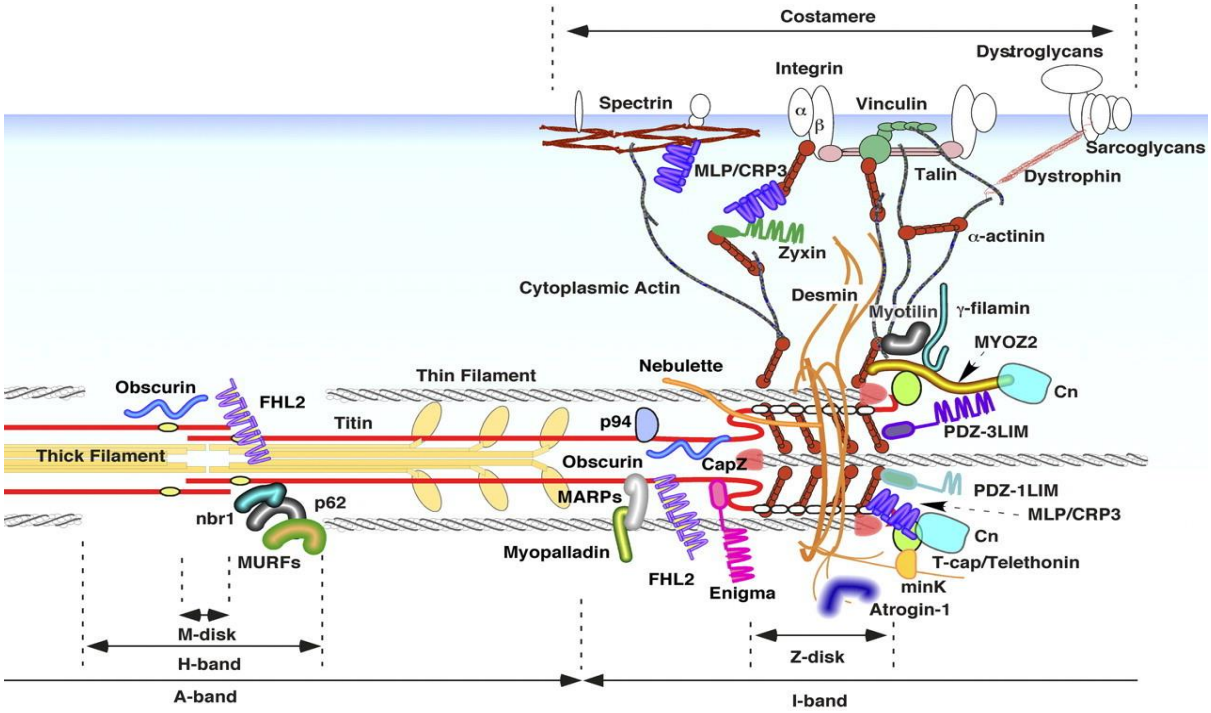

Figure 4.43 Illustration of cardiac z disc proteins. PDZ-1LIM; one-PDZ and one-LIM domain protein, MYOZ2; myozenin 2 (carsarin 1); MLP/CRP3; muscle-specific LIM protein/cysteine-rich protein 3, Cn; calcineurin, FHL2; four-and-a-half LIM protein, 2PDZ-3LIM; one-PDZ and three-LIM domain protein, MAPRs; muscle ankyrin repeat proteins, MURFs; muscle-specific ring-finger proteins. From (Hoshijima 2006)

4.4.4 Disruption to EC coupling, ionic cyclic proteins, and functional impairment

Sarcoplasmic reticulum calcium uptake and cardiac contractile function are affected by SERCA2 expression levels in the heart (Periasamy and Huke 2001). The abnormal Ca^{2+} cycling, and decreased SR calcium content are observed with decreased expression of SERCA2. As measured from proteomic output, SERCA2 and its regulatory proteins, such as phospholamban were all downregulated in LAD group. Clinical and experimental studies have shown that deficient calcium uptake by SR is associated with decreased SERCA2a levels, which leads to impaired contractility as observed in heart failure (Kawase and Hajjar 2008, Lipskaia, Chemaly et al. 2010). Additionally, phosphoproteomics analysis showed 2.5-fold increase in SERCA2 phosphorylation at two novel consecutive sites (S50 and 51), however, the role of post translational modification on these sites and its effect SERCA2 activity are yet to be determined.

In summary, work on porcine model identified significant changes to mitochondria cristae density and interfibrillar distribution, in addition to identification of novel subtypes of collagen such as collagen XIV that were increased in ECM four weeks post IRI. Antioxidant related proteins and ATP synthesis proteins were decreased with post ischaemic cardiac remodelling, while cytoskeleton and z disc area appear to be heavily involved in cardiac response post MI, through upregulation and increased phosphorylation of certain proteins. Metabolomics data showed, amongst others, a decrease in taurine levels in blood with increased cardiac content. Certain aspects in this work are similar to rat model of permanent LAD coronary artery ligation, while others are distinctive. These differences and similarities are further explained and compared in chapter 5.

Chapter 5

General discussion

5.1 Key similarities and differences between rodent and porcine model of cardiac injury

Studies using animal models of coronary artery disease have massively contributed in the expansion of understanding to pathophysiological mechanisms that are implicated in myocardial injury and repair or protection, in addition to identification of several cellular targets such as inflammation, ROS, mitochondrial damage and calcium overload (Chorro, Such-Belenguer et al. 2009). Yet, little is known regarding long term manifestation of post ischaemic cardiac remodelling leading to heart failure across different species used in cardiovascular research at multiple cellular and systemic levels.

This chapter presents the main features of post ischaemic cardiac remodelling in rodent and porcine models, focusing on key similarities and differences four weeks after myocardial injury. Although there are major distinctions between rats and pigs with regards to modality of cardiac injury, age and species-specific cardiac healing periods (i.e., being faster in small animals), the goal of this comparison is to highlight potential targets that seem to be involved in cardiac remodelling in hearts subjected to myocardial injury in two invaluable models. Based on these shared features, further experimental work could be performed to assess their significance in clinically relevant settings. However, there must be careful interpretation and comparison of data presented in chapters 3 and 4 as the aim is to provide distinct assessment of cardiac remodeling in two disparate experimental models. As explained in chapter 3, rodents are the first step used to study pathophysiology of cardiac disease and evaluate therapeutic interventions, due to a variety of reasons including cost and longevity, whereas the pig model is closer to human structurally and physiologically and has solid translational potential.

It is important to consider the fundamental differences between the two models, as listed in table 5.1. In addition to differences in cardiac structure, the mode of cardiac injury induction, i.e., reperfusion injury, was only introduced in porcine model but not in rats, as permanent ligation of the LAD coronary artery occurred. Moreover, the area used for proteomic, metabolomic and energetic analyses in rats was taken from the apical region, distal to the site of injury, whereas in pigs, the myocardial tissues were taken from the infarcted area. Since scars post MI mature faster in small animals like rodent in comparison to pigs, therefore deriving results from the exact same area in rodent heart could falsely include collagen-rich, hypcelleularised myocardial tissue that could potentially interfere with proteomics and NMR outputs. Furthermore, it is important to note that the hearts in both models were normal, non-diseased hearts.

Table 5.1 Main differences between rodent and porcine hearts.

	Rodent heart	Porcine heart	References
Heart rate (beats per minute)	330-480	70-180	(Milani-Nejad and Janssen 2014) researchservices.umn.edu
Systolic blood pressure (mm Hg)	124	> 90	researchservices.umn.edu (Gangwar, Kumar et al. 2014)
Collateral blood flow	More advanced collateral circulation, but less than humans.	Poor collateral circulation.	(Unger 2001) (Seiler, Stoller et al. 2013)
Action potential	Short action potential, lacks a plateau phase.	Similar to human action potential.	(de Boer and Stengl 2017)
Coronary circulation	Different from humans, e.g., Left Coronary Artery (LCA) has few branches.	Analogous to humans.	(h-Ici, Jeuthe et al. 2015)
Calcium cycling	Calcium removal is less dependent on Na^{+}/Ca^{2+-} exchanger activity	Calcium cycling shares similar characterises to humans.	(Hasenfuss 1998) (Johnson and Camelliti 2018)

Structural remodelling in rodent and porcine models of cardiac injury

Structural remodelling in rodent and porcine models four weeks after cardiac injury showed cellular changes that were characterised by disruption of ECM architecture, in addition to presence of several infiltrating noncardiomyocytes such as fibroblasts and telcoytes, as observed in EM images. Both models showed disruption to mitochondrial cristae density, by which there was increased ratio of intercristea area to the total mitochondrion area, which indicates disruption to mitochondrial respiration and function four weeks after injury. Similar findings of decreased mitochondrial matrix density were observed in canine model of chronic heart failure and clinically in patients with hypertrophic cardiomyopathies (Baandrup, Florio et al. 1981, Sharov, Goussev et al. 1998, Rosca and Hoppel 2013). Table 5.2 lists comparisons of key structural and ultrastructural changes based on rodent and porcine data.

Table 5.2 Comparison of structural and ultrastructural measurements as taken from infarcted and left ventricular myocardium in rodent and porcine models of cardiac injury 4 weeks after intervention (Rat: LAD coronary artery ligation, pigs: LAD coronary artery occlusion and reperfusion). Direction of change reflects measurement in LAD group compared to control or SHAM. — equal or no significant change.

	Rodent model	Porcine model
Gross structural measurements (LM)		
Cardiac fibrosis	↑	↑
Arteriolar wall thickness	↑	↑
Ultrastructural measurements (EM)		
Cardiomyocyte area	—	—
Mitochondrial cristae density	↑	↑
Mitochondrial subpopulation distribution	—	↓ (Interfibrillar subpopulation)
Mitochondrial morphometric measurement	↑ in aspect ratio (length/width)	—
Sarcomere length	—	—

Molecular remodelling in rodent and porcine models of cardiac injury

Although there are differences in proteome outputs between the two species, there were, however, selected categories in which proteins could be classified and compared amongst rats and pigs. Molecular alterations in rodent and porcine models reflected the state of mitochondrial dysfunction, as both models exhibited significant degree of mitochondrial damage. For examples, proteins involved in mitochondrial ATP synthesis and respiration were diminished. It has been shown that the inability of mitochondria to meet energy demands during remodelling leads to disease progression towards heart failure, known as energy starvation hypothesis (Zhou and Tian 2018). ATP synthesis machinery in mitochondria is disrupted by decrease in expression of ATP synthase subunits and cofactors. Pigs had several components the ATP synthesis machinery down regulated unlike the rat, which only had on significantly downregulated component (ATP synthase mitochondrial F1 assembly factor). Moreover, antioxidant related proteins were decreased reflects dysregulation in redox homeostasis and increased oxidative stress four weeks after injury.

Molecular remodeling involved many of structural proteins that were overexpressed in LAD group in rats and pigs. These proteins are located at several location such as z-disc and cytoskeleton. For example, spectrin α chain, non-erthrocytic 1 (encoded by SPTAN1), which is found in z disc and sarcolemma, is upregulated with cardiac injury. Gap junction proteins (connexins) are critical in intercellular connection and synchronized cardiac contraction, and as shown in rats and pigs proteome outputs, it had decreased expression four weeks after cardiac injury. This comparison emphasises on the role of z-disc and costamere area, as it is not only restricted

as structural components of sarcomeres, but rather a location for cellular signalling, which might be related to cardiac contractility and performance, as many of z-disc proteins translocate to cytoskeleton in response to pathological stressor (Frank and Frey 2011).

Finally, there was increased phosphorylation at different phosphorylation sites in rodent and porcine data While there are several phosphoproteins exhibited increased phosphorylation, only selected phosphoproteins were shared in both models. These included catenin α, HSP 90, AKAP12 and nexilin/nebulette. Table 5.3 summarises key changes between rodent and porcine models.

Table 5.3 Comparison of proteomic and phosphprotemics selected data, as taken from infarcted and left ventricular myocardium in rodent and porcine models of cardiac injury 4 weeks after intervention (Rat: LAD coronary artery ligation, pigs: LAD coronary artery occlusion and reperfusion). Direction of change reflects measurement in LAD group compared to control or SHAM. ND, not detectable, ═ equal or no significant change.

	Rodent model	**Porcine model**
Proteomics (with proteins examples)		
ATP synthesis proteins	↓ (ATP synthase F1 complex assembly factor 1)	↓↓ (ATP Synthase F(0) Complex Subunit B1)
Antioxidant related proteins	↓ (glutathione peroxidase 1)	↓↓ (Thioredoxin Reductase 2)
Z disc proteins	↑↑ (Spectrin alpha chain, non-erythrocytic 1)	↑ (Plectin)
Ion transport proteins	↑ (Voltage dependent L type calcium channel subunit alpha)	↓ (Voltage dependent L type Calcium Channel subunit Beta 2)
Phosphoproteomics (with phosphosites examples)		
Calcium cycling	↑ (Ryanodine receptor 2, S1700)	↑ (SERCA2, S50&S51)
Structural proteins	↑ (Tight junction protein 2, S1132)	↑ (Tensin-1, S911, S1363,T1310)
Signalling proteins	↑ (Heat shock protein HSP 90-alpha, S263)	↑ (Heat shock protein HSP 90-beta, S226)

Metabolic remodelling in rodent and porcine models of cardiac injury

As presented in table 5.4, metabolomics analysis using NMR spectroscopy revealed significant increase in blood acetone level in rats (compared to baseline levels) and pigs (in comparison to control). In addition, blood from porcine LAD group had increased level of acetoacetate (another ketone body). Despite differences and timing in collection, ketone bodies, where significantly increased in blood samples in both models. Ketone bodies metabolism in post ischaemic cardiac remodelling needs to be further explored in animal models, since it is extremely difficult to separate patients with CAD from underlying metabolic syndrome that could potentially ameliorate systemic production and utilisation of ketone bodies. Furthermore, another metabolite which is taurine only decreased in blood from porcine LAD group and elevated in porcine cardiac extract. Rodent taurine levels in blood and cardiac extract were not significantly change. As for cardiac energetics, only porcine LAD group had significant increase in total adenine pool, due to increased AMP levels.

Table 5.4 Selected blood and cardiac metabolomics, and cardiac energetics measurements in rodent and porcine models of cardiac injury 4 weeks after intervention (Rat: LAD coronary artery ligation, pigs: LAD coronary artery occlusion and reperfusion). Direction of change reflects metabolites/energetics abundance in LAD group compared to control (or SHAM). — equal or no significant change.

	Rodent model		**Porcine model**	
Metabolomics (NMR)				
Metabolite	**Blood**	**Cardiac extract**	**Blood**	**Cardiac extract**
Taurine	—	—	↓	↑
Lactate	—	—	ND	↓
Acetone	↑	ND	↑	ND
Acetoacetate	—		↑	
Arginine	↑		—	
Left ventricular/apical energetics (HPLC)				
Energy charge	—		—	
Total adenine metabolites	—		↑	

5.2 Conclusion

Post ischaemic cardiac remodelling following acute infarction is associated with alterations at the molecular, metabolic, and structural levels. In this work, animal models of cardiac injury following acute myocardial infarction were adopted using *in vivo* LAD coronary artery ligation in rodents, and balloon occlusion (inflation) and deflation in LAD coronary artery porcine hearts. Histological, proteomics, and metabolomic studies, in the myocardium and blood, were performed to detect permutations that are associated with post ischaemic cardiac remodelling in those models.

In the rodent model of chronic sustained ischaemia, there was significant decrease in cardiac antioxidant proteins in the as well as fatty acids and amino acids metabolism enzymes. While calcium handling proteins were significantly upregulated. Key signalling pathways identified in this model involved Protein Kinase A, Phospholipase C (PLC), and Gamma G beta protein signalling pathways. Metabolomics analysis showed accumulation of blood acetone four weeks after cardiac injury. Cardiac morphometric analysis showed increase in mitochondrial cristae separation, in addition to aspect ratio of interfibrillar mitochondria in infarct group, but no significant changes in sarcomere length was noted in comparison to SHAM group.

In the porcine model of ischaemia reperfusion injury, there was significant decrease in cardiac ATP synthesis, antioxidant cardiac proteins, fatty acid, and amino acids metabolic proteins. Main signalling pathways identified with post ischaemic cardiac remodelling in this model were actin cytoskeleton, integrin and tight junction signalling pathways. Metabolomics analysis revealed increased ketone bodies levels in porcine blood four weeks after the cardiac injury, and taurine in porcine cardiac extracts. Morphometric analysis showed decreased interfibrillar mitochondrial distribution, increase in mitochondrial cristae separation in the infarcted group, but no detected differences with regards to sarcomere length.

Translational aspects

As presented in this work, ketone bodies such as acetone and acetoacetate were identified markedly in blood following myocardial injury. Therefore, blood ketone bodies could be targeted as potential biomarker in CAD patients and correlated to adverse cardiac remodeling. Nonetheless, cardioprotective effects of taurine and whether a decreased in blood taurine subjects those patients to increased risk of heart failure remain critical aspects for further investigation.

As discussed in previous chapters, it is known that z disc and cytoskeleton are massively changed with dilated and hypertrophic cardiomyopathies, however, the role of ischaemia and ischaemia reperfusion injury in modulating cytoskeletal rearrangement, modification of z disc proteins expression or phosphorylation in patients with HF failure (with reduced or preserved ejection fraction), remains relatively unknown. The main signaling pathways in rodent and porcine models provided different perspective to identify potential targets in human myocardium, such as PKC/NFAT and ERK1/2 signalling, in addition to integrin and actin cytoskeleton signalling pathways.

5.3 Limitations

Animal models

Probably the most notable limitation present in this work is the inability to apply the same surgical procedures to both models. The rodent model involved chronic cardiac remodelling following sustained ischaemic injury (as in coronary artery ligation) with no reperfusion (permanent ligation). In both models, the cardiac injury was done on healthy hearts with no apparent systemic vascular or metabolic diseases, which excludes the cellular and molecular changes due to diseased coronary vasculature, as seen in progressive atherosclerotic plaque build-up in CAD patients. In rodent model, however, the cardiac injury did not precisely reflect the pathophysiological mechanisms of post-MI remodelling attributed to ischaemia reperfusion injury, as the procedure only included chronic sustained ischaemic insult without reperfusion.

Infarct healing is also different between small animals like mice and rats compared to large models. There are inconsistencies reported in literature with regards to the exact point by which scar maturity is thought to occur, as different phases of cardiac remodelling overlap over time after injury. In mice, scar healing is thought to be complete 21 days post MI, while in rats it averages around 3 weeks, and later (6 weeks onwards) in porcine and canine models (Jugdutt, Joljart et al. 1996, Yang, Liu et al. 2002, Wu, Yin et al. 2011, Houser, Margulies et al. 2012, Aronsen, Espe et al. 2017). Therefore, 4 weeks in rodent and porcine models are related to chronic stages of cardiac remodelling (late proliferative and early maturation). Ideally, assessment of cardiac remodelling at different stages would assist in better understanding and characterisation of pathophysiological mechanisms involved.

Sex differences between species is also a limitation, since male Wistar rats were only used in the rodent model of cardiac injury, it was not possible to assess the variation in cardiac remodelling in females compared to male rats. Additionally, it should be taken in consideration that male rats were compared against female pigs in selected molecular and metabolic aspects. It is known that susceptibility to cardiovascular disease in human is lower in females, which is a similarity that is shared across other species as well (Patten 2007).

Tissue collection

It was an obstacle to obtain all blood and cardiac tissues from a single set of rats, so many were outsourced from separate group of LAD rats following same surgical procedure, and these were compared against either their baseline levels (blood metabolomics) or healthy control (cardiac tissues for light microscopy). OCT embedding of cardiac tissues was not the best option to study the structure of cardiac tissue as desired, since processing (sectioning and staining) resulted occasionally in samples loss, inadequate stain uptake, thus there has been several troubleshooting efforts to obtain best quality of images.

Sample size and characteristics

This study used the minimum required number of animals (n=5 in rats, and 4 in pigs, per group) in accordance with the 3 R's rule (Refinement, Reduction and Replacement). However, increased sample size that facilitate collection of tissues over days or weeks for both models, in addition to implementation of diseased experimental models (e.g., atherosclerosis or diabetes) or with co-morbidities to investigate the vulnerability to IRI and cardioplegic arrest, and test cardioprotective interventions would assist in detection of early changes in biomarkers that could predict adverse cardiac remodelling after extended periods.

NMR spectroscopy

NMR intrinsic insensitivity is a major issue and drawback to this technique, in which many of the metabolites were not detected or distinguished from other noise in the spectra. Unlike other methods such as gas or mass spectroscopy. Despite this, there are continuous efforts to enhance the technique sensitivity to detect wide range of metabolites. Metabolomics identification and annotation were challenging task since little or underdeveloped databases are available for those species, unlike human metabolome.

Proteomics

With porcine proteome, the lack of available databases with completed and integrated porcine proteome database made it difficult to characterise several proteins without relying on human database as reference. Therefore, proteomics results were generated based on human proteome, a step which is necessarily performed to decrease the number of uncharacterized proteins in porcine data, even though there are advances in porcine gene entries, they are not yet fully completed. Phosphorylation sites databases are not also fully developed for porcine phosphoproteome.

Electron Microscopy

Due to inability to perfuse a porcine heart with EM fixative, cardiac samples that were sent for EM processing and embedding have been fixed with conventional fixation. It resulted to samples loss in many cases or a decrease in contract sometimes.

Covid-19 impact

This work should have included patients data, as a project grant was given to metabolomics study to assess metabolomic profile in STEMI patients and compare these results with pigs and rat. However, since the pandemic, ethical approval was halted as non-covid related clinical trials were stopped during pandemic.

5.4 Future direction

Based on data from this work, it is planned to continue metabolomics study on patients with coronary artery disease to detect metabolic profiles after MI and during cardiac remodelling. Moreover, for porcine and rodent models, future work would be inclusive to molecular and metabolic profiles from borderzone and nonischaemic areas of the heart and compare it accordingly with infarcted region in both models. Additionally, measurement of certain proteins such as collagen XIV and z disc proteins using Western Blot from

infarcted areas in rodent and porcine hearts to validate their significance in post ischaemic cardiac remodelling. Taurine and ketone bodies levels will be assessed at their baseline levels and after myocardial injury, to monitor their fluctuations in blood and cardiac tissues. Moreover, collection of blood samples at several time points to ensure the detection of early blood metabolites that are altered in accordance with functional parameters and cardiac enzymes release. A comparative study could be also drawn using *ex-vivo* Langendorff perfusion of whole rat heart to identify acute changes at selected time points that are manifested at the functional and molecular levels following ischaemia reperfusion injury and/or sustained ischaemia by LAD coronary artery ligation or occlusion.

References

Websites

Slideshare.net

https://www.researchservices.umn.edu/services-name/research-animal-resources

https://www.thermofisher.com/uk/en/home.html

https://medicine.yale.edu/labmed/

https://www.sciencephoto.com/

http://heatmapper.ca/

https://courses.lumenlearning.com/wm-biology2/chapter/structure-of-the-heart/.

Abdul-Ghani, S., K. J. Heesom, G. D. Angelini and M.-S. Suleiman (2014). "Cardiac Phosphoproteomics during Remote Ischemic Preconditioning: A Role for the Sarcomeric Z-Disk Proteins %J BioMed Research International." **2014**: 11.

Abel, E. D. (2004). "Glucose transport in the heart." Front Biosci **9**: 201-215.

Adler, N., L. L. Camin and P. Shulkin (1976). "Rat model for acute myocardial infarction: application to technetium-labeled glucoheptonate, tetracycline, and polyphosphate." Journal of nuclear medicine: official publication, Society of Nuclear Medicine **17**(3): 203-207.

Akakura, S. and I. H. Gelman (2012). "Pivotal Role of AKAP12 in the Regulation of Cellular Adhesion Dynamics: Control of Cytoskeletal Architecture, Cell Migration, and Mitogenic Signaling %J Journal of Signal Transduction." **2012**: 7.

Armstrong, S., J. M. Downey and C. E. Ganote (1994). "Preconditioning of isolated rabbit cardiomyocytes: induction by metabolic stress and blockade by the adenosine antagonist SPT and calphostin C, a protein kinase C inhibitor." Cardiovasc Res **28**(1): 72-77.

Aronsen, J. M., E. K. S. Espe, K. Skårdal, A. Hasic, L. Zhang and I. Sjaastad (2017). "Noninvasive stratification of postinfarction rats based on the degree of cardiac dysfunction using magnetic resonance imaging and echocardiography." American Journal of Physiology-Heart and Circulatory Physiology **312**(5): H932-H942.

Asgari, M., N. Latifi, H. K. Heris, H. Vali and L. Mongeau (2017). "In vitro fibrillogenesis of tropocollagen type III in collagen type I affects its relative fibrillar topology and mechanics." Sci Rep **7**(1): 1392.

Avkiran, M. and M. S. Marber (2002). "Na(+)/H(+) exchange inhibitors for cardioprotective therapy: progress, problems and prospects." J Am Coll Cardiol **39**(5): 747-753.

Baandrup, U., R. A. Florio, F. Roters and E. G. Olsen (1981). "Electron microscopic investigation of endomyocardial biopsy samples in hypertrophy and cardiomyopathy. A semiquantitative study in 48 patients." Circulation **63**(6): 1289-1298.

Baandrup, U., R. A. Florio, F. Roters and E. G. Olsen (1981). "Electron microscopic investigation of endomyocardial biopsy samples in hypertrophy and cardiomyopathy. A semiquantitative study in 48 patients." Circulation **63**(6): 1289-1298.

Bai, H., K. Sun, J.-H. Wu, Z.-H. Zhong, S.-L. Xu, H.-R. Zhang, Y.-H. Gu and S.-F. Lu (2020). "Proteomic and metabolomic characterization of cardiac tissue in acute myocardial ischemia injury rats." PLOS ONE **15**(5): e0231797.

Banciu, D., D. Cretoiu, S. Cretoiu and A. Banciu (2017). "Telocytes involvement in recovery after myocardial infarction." JOURNAL OF SHANGHAI UNIVERSITY (NATURAL SCIENCE) **23**: 155.

Barallobre-Barreiro, J., A. Didangelos, F. A. Schoendube, I. Drozdov, X. Yin, M. Fernández-Caggiano, P. Willeit, V. O. Puntmann, G. Aldama-López, A. M. Shah, N. Doménech and M. Mayr (2012).

"Proteomics Analysis of Cardiac Extracellular Matrix Remodeling in a Porcine Model of Ischemia/Reperfusion Injury." Circulation **125**(6): 789-802.
Barba, I., M. Andres and D. Garcia-Dorado (2019). "Metabolomics and Heart Diseases: From Basic to Clinical Approach." Curr Med Chem **26**(1): 46-59.
Basak, T., S. Varshney, S. Akhtar and S. Sengupta (2015). "Understanding different facets of cardiovascular diseases based on model systems to human studies: A proteomic and metabolomic perspective." Journal of Proteomics **127**: 50-60.
Bauer, M., W. Dieterich, T. Ehnis and D. Schuppan (1997). "Complete primary structure of human collagen type XIV (Undulin)1DNA-sequences reported in this paper have been submitted to the EMBL/GenBank Data Libraries with accession numbers Y11709, Y11710 and Y11711.1." Biochimica et Biophysica Acta (BBA) - Gene Structure and Expression **1354**(3): 183-188.
Baum, J. and H. S. Duffy (2011). "Fibroblasts and myofibroblasts: what are we talking about?" Journal of cardiovascular pharmacology **57**(4): 376-379.
Beer, M., T. Seyfarth, J. Sandstede, W. Landschütz, C. Lipke, H. Köstler, M. von Kienlin, K. Harre, D. Hahn and S. Neubauer (2002). "Absolute concentrations of high-energy phosphate metabolites in normal, hypertrophied, and failing human myocardium measured noninvasively with (31)P-SLOOP magnetic resonance spectroscopy." J Am Coll Cardiol **40**(7): 1267-1274.
Bei, Y., F. Wang, C. Yang and J. Xiao (2015). "Telocytes in regenerative medicine." Journal of Cellular and Molecular Medicine **19**(7): 1441-1454.
Berg, J. M., J. L. Tymoczko and L. Stryer (2010). Biochemistry, W. H. Freeman.
Bers, D. M. (2002). "Cardiac excitation-contraction coupling." Nature **415**(6868): 198-205.
Bers, D. M. (2006). "Cardiac ryanodine receptor phosphorylation: target sites and functional consequences." The Biochemical journal **396**(1): e1-e3.
Bers, D. M., W. J. Lederer and J. R. Berlin (1990). "Intracellular Ca transients in rat cardiac myocytes: role of Na-Ca exchange in excitation-contraction coupling." Am J Physiol **258**(5 Pt 1): C944-954.
Beyersdorf, F. (2009). "The use of controlled reperfusion strategies in cardiac surgery to minimize ischaemia/reperfusion damage." Cardiovascular Research **83**(2): 262-268.
Binek, A., R. Fernández-Jiménez, I. Jorge, E. Camafeita, J. A. López, N. Bagwan, C. Galán-Arriola, A. Pun, J. Agüero, V. Fuster, B. Ibanez and J. Vázquez (2017). "Proteomic footprint of myocardial ischemia/reperfusion injury: Longitudinal study of the at-risk and remote regions in the pig model." Scientific Reports **7**(1): 12343.
Binek, A., R. Fernández-Jiménez, I. Jorge, E. Camafeita, J. A. López, N. Bagwan, C. Galán-Arriola, A. Pun, J. Agüero, V. Fuster, B. Ibanez and J. Vázquez (2017). "Proteomic footprint of myocardial ischemia/reperfusion injury: Longitudinal study of the at-risk and remote regions in the pig model." Scientific reports **7**(1): 12343-12343.
Bing, W., I. D. Fraser and S. B. Marston (1997). "Troponin I and troponin T interact with troponin C to produce different Ca2+-dependent effects on actin-tropomyosin filament motility." The Biochemical journal **327 (Pt 2)**(Pt 2): 335-340.
Birdsall, H. H., D. M. Green, J. Trial, K. A. Youker, A. R. Burns, C. R. MacKay, G. J. LaRosa, H. K. Hawkins, C. W. Smith, L. H. Michael, M. L. Entman and R. D. Rossen (1997). "Complement C5a, TGF-beta 1, and MCP-1, in sequence, induce migration of monocytes into ischemic canine myocardium within the first one to five hours after reperfusion." Circulation **95**(3): 684-692.
Biterova, E. I., A. A. Turanov, V. N. Gladyshev and J. J. Barycki (2005). "Crystal structures of oxidized and reduced mitochondrial thioredoxin reductase provide molecular details of the reaction mechanism." Proc Natl Acad Sci U S A **102**(42): 15018-15023.
Böhm, F. and J. Pernow (2007). "The importance of endothelin-1 for vascular dysfunction in cardiovascular disease." Cardiovascular Research **76**(1): 8-18.
Borg, T. K., E. C. Goldsmith, R. Price, W. Carver, L. Terracio and A. M. Samarel (2000). "Specialization at the Z line of cardiac myocytes." Cardiovasc Res **46**(2): 277-285.

Braz, J. C., O. F. Bueno, L. J. De Windt and J. D. Molkentin (2002). "PKC alpha regulates the hypertrophic growth of cardiomyocytes through extracellular signal-regulated kinase1/2 (ERK1/2)." The Journal of cell biology **156**(5): 905-919.
Briston, T., M. Roberts, S. Lewis, B. Powney, J. M. Staddon, G. Szabadkai and M. R. Duchen (2017). "Mitochondrial permeability transition pore: sensitivity to opening and mechanistic dependence on substrate availability." Scientific Reports **7**(1): 10492.
Brower, G. L., A. L. Chancey, S. Thanigaraj, B. B. Matsubara and J. S. Janicki (2002). "Cause and effect relationship between myocardial mast cell number and matrix metalloproteinase activity." Am J Physiol Heart Circ Physiol **283**(2): H518-525.
Byrne, J. A., D. J. Grieve, A. C. Cave and A. M. Shah (2003). "Oxidative stress and heart failure." Arch Mal Coeur Vaiss **96**(3): 214-221.
Camacho, P., H. Fan, Z. Liu and J. Q. He (2016). "Large Mammalian Animal Models of Heart Disease." J Cardiovasc Dev Dis **3**(4).
Champagne, S., J. B. Su, T. Unterseeh, S. Elamine, N. Elbaz, P. Garot, J. L. Dubois-Rande, P. Merlet, L. Hittinger and E. Teiger (2003). "[Electromechanical mapping of myocardial ischemia in coronary occlusion in the pig]." Arch Mal Coeur Vaiss **96**(4): 332-338.
Chase, A. (2007). Cardiac vulnerability to insult studied in a mouse model of coronary artery disease.
Chen, L., J. Song and S. Hu (2019). "Metabolic remodeling of substrate utilization during heart failure progression." Heart Fail Rev **24**(1): 143-154.
Chen, W. and N. G. Frangogiannis (2013). "Fibroblasts in post-infarction inflammation and cardiac repair." Biochim Biophys Acta **1833**(4): 945-953.
Cheng, A., T. C. Nguyen, M. Malinowski, F. Langer, D. Liang, G. T. Daughters, N. B. Ingels, Jr. and D. C. Miller (2006). "Passive ventricular constraint prevents transmural shear strain progression in left ventricle remodeling." Circulation **114**(1 Suppl): I79-86.
Cheng, J. P. X., C. Mendoza-Topaz, G. Howard, J. Chadwick, E. Shvets, A. S. Cowburn, B. J. Dunmore, A. Crosby, N. W. Morrell and B. J. Nichols (2015). "Caveolae protect endothelial cells from membrane rupture during increased cardiac output." Journal of Cell Biology **211**(1): 53-61.
Cheung, P.-Y., W. Wang and R. Schulz (2000). "Glutathione protects against myocardial ischemia–reperfusion injury by detoxifying peroxynitrite." Journal of molecular and cellular cardiology **32**(9): 1669-1678.
Chorro, F. J., L. Such-Belenguer and V. López-Merino (2009). "Animal Models of Cardiovascular Disease." Revista Española de Cardiología (English Edition) **62**(1): 69-84.
Choy, J. S. and G. S. Kassab (2009). "Wall thickness of coronary vessels varies transmurally in the LV but not the RV: implications for local stress distribution." American journal of physiology. Heart and circulatory physiology **297**(2): H750-H758.
Clarke, S. J., G. P. McStay and A. P. Halestrap (2002). "Sanglifehrin A acts as a potent inhibitor of the mitochondrial permeability transition and reperfusion injury of the heart by binding to cyclophilin-D at a different site from cyclosporin A." J Biol Chem **277**(38): 34793-34799.
Cohn, J. N., R. Ferrari and N. Sharpe (2000). "Cardiac remodeling--concepts and clinical implications: a consensus paper from an international forum on cardiac remodeling. Behalf of an International Forum on Cardiac Remodeling." J Am Coll Cardiol **35**(3): 569-582.
Collantes, M., B. Pelacho, M. J. Garcia-Velloso, J. J. Gavira, G. Abizanda, I. Palacios, L. Rodriguez-Borlado, V. Alvarez, E. Prieto, M. Ecay, E. Larequi, I. Penuelas and F. Prosper (2017). "Non-invasive in vivo imaging of cardiac stem/progenitor cell biodistribution and retention after intracoronary and intramyocardial delivery in a swine model of chronic ischemia reperfusion injury." J Transl Med **15**(1): 56.
Cotter, D. G., R. C. Schugar and P. A. Crawford (2013). "Ketone body metabolism and cardiovascular disease." American Journal of Physiology-Heart and Circulatory Physiology **304**(8): H1060-H1076.
Cresci, S., N. L. Pereira, F. Ahmad, M. Byku, L. de Las Fuentes, D. E. Lanfear, C. M. Reilly, A. T. Owens, M. J. Wolf, G. American Heart Association Council on, M. Precision, C. Council on, N. Stroke, C. Council on Quality of and R. Outcomes (2019). "Heart Failure in the Era of Precision Medicine: A

Scientific Statement From the American Heart Association." Circ Genom Precis Med: HCG0000000000000058.
Cretoiu, S. M., D. Cretoiu, A. Marin, B. M. Radu and L. M. Popescu (2013). "Telocytes: ultrastructural, immunohistochemical and electrophysiological characteristics in human myometrium." Reproduction **145**(4): 357-370.
Crompton, M. (1999). "The mitochondrial permeability transition pore and its role in cell death." Biochem J **341 (Pt 2)**(Pt 2): 233-249.
Crozatier, B., M. Ashraf, D. Franklin, J. Ross, L. Nimmo and D. McKown (1977). "Sarcomere length in experimental myocardial infarction: Evidence for sarcomere overstretch in dyskinetic ventricular regions." Journal of Molecular and Cellular Cardiology **9**(10): 785-797.
Curello, S., C. Ceconi, C. Bigoli, R. Ferrari, A. Albertini and C. Guarnieri (1985). "Changes in the cardiac glutathione status after ischemia and reperfusion." Experientia **41**(1): 42-43.
Curello, S., C. Ceconi, A. Cargnoni, A. Cornacchiari, R. Ferrari and A. Albertini (1987). "Improved procedure for determining glutathione in plasma as an index of myocardial oxidative stress." Clin Chem **33**(8): 1448-1449.
Czubryt, M. P. (2012). "Common threads in cardiac fibrosis, infarct scar formation, and wound healing." Fibrogenesis & Tissue Repair **5**(1): 19.
Dampney, R. A. L. (2016). "Central neural control of the cardiovascular system: current perspectives." **40**(3): 283-296.
de Boer, T. P. and M. Stengl (2017). "Action potential contour and inter-species differences." EP Europace **20**(9): 1395-1396.
Delmar, M. (2004). "The intercalated disk as a single functional unit." Heart Rhythm **1**(1): 12-13.
Deponte, M. (2013). "Glutathione catalysis and the reaction mechanisms of glutathione-dependent enzymes." Biochim Biophys Acta **1830**(5): 3217-3266.
Des Rosiers, C., F. Labarthe, S. G. Lloyd and J. C. Chatham (2011). "Cardiac anaplerosis in health and disease: food for thought." Cardiovasc Res **90**(2): 210-219.
Dhalla, N. S., R. M. Temsah and T. Netticadan (2000). "Role of oxidative stress in cardiovascular diseases." J Hypertens **18**(6): 655-673.
Dhalla, N. S., R. M. Temsah and T. Netticadan (2000). "Role of oxidative stress in cardiovascular diseases." Journal of Hypertension **18**(6).
Dhar, I., V. Lysne, R. Seifert, G. F. T. Svingen, P. M. Ueland and O. K. Nygård (2018). "Plasma methionine and risk of acute myocardial infarction: Effect modification by established risk factors." Atherosclerosis **272**: 175-181.
Doenst, T., T. D. Nguyen and E. D. Abel (2013). "Cardiac metabolism in heart failure: implications beyond ATP production." Circulation research **113**(6): 709-724.
Dong, W.-J., J. J. Jayasundar, J. An, J. Xing and H. C. Cheung (2007). "Effects of PKA Phosphorylation of Cardiac Troponin I and Strong Crossbridge on Conformational Transitions of the N-Domain of Cardiac Troponin C in Regulated Thin Filaments." Biochemistry **46**(34): 9752-9761.
Dorn, G. W., 2nd and T. Force (2005). "Protein kinase cascades in the regulation of cardiac hypertrophy." The Journal of clinical investigation **115**(3): 527-537.
Drake, K. J., V. Y. Sidorov, O. P. McGuinness, D. H. Wasserman and J. P. Wikswo (2012). "Amino acids as metabolic substrates during cardiac ischemia." Experimental biology and medicine (Maywood, N.J.) **237**(12): 1369-1378.
Droge, W. (2002). "Free radicals in the physiological control of cell function." Physiological reviews **82**(1): 47-95.
Du, Z., A. Shen, Y. Huang, L. Su, W. Lai, P. Wang, Z. Xie, Z. Xie, Q. Zeng, H. Ren and D. Xu (2014). "1H-NMR-based metabolic analysis of human serum reveals novel markers of myocardial energy expenditure in heart failure patients." PLoS One **9**(2): e88102.
Eghbali, M. and K. T. Weber (1990). "Collagen and the myocardium: fibrillar structure, biosynthesis and degradation in relation to hypertrophy and its regression." Mol Cell Biochem **96**(1): 1-14.

Ehnis, T., W. Dieterich, M. Bauer, B. v. Lampe and D. Schuppan (1996). "A Chondroitin/Dermatan Sulfate Form of CD44 Is a Receptor for Collagen XIV (Undulin)." Experimental Cell Research **229**(2): 388-397.
Escobar, D. J., R. Desai, N. Ishiyama, S. S. Folmsbee, M. N. Novak, A. S. Flozak, R. L. Daugherty, R. Mo, D. Nanavati, R. Sarpal, D. Leckband, M. Ikura, U. Tepass and C. J. Gottardi (2015). "alpha-Catenin phosphorylation promotes intercellular adhesion through a dual-kinase mechanism." J Cell Sci **128**(6): 1150-1165.
Esper, R. J., R. A. Nordaby, J. O. Vilariño, A. Paragano, J. L. Cacharrón and R. A. Machado (2006). "Endothelial dysfunction: a comprehensive appraisal." Cardiovascular Diabetology **5**(1): 4.
Fabiato, A. and F. Fabiato (1975). "Contractions induced by a calcium‐triggered release of calcium from the sarcoplasmic reticulum of single skinned cardiac cells." The Journal of Physiology **249**(3): 469-495.
Farah, C. S. and F. C. Reinach (1995). "The troponin complex and regulation of muscle contraction." The FASEB Journal **9**(9): 755-767.
Faul, C., A. Dhume, A. D. Schecter and P. Mundel (2007). "Protein kinase A, Ca2+/calmodulin-dependent kinase II, and calcineurin regulate the intracellular trafficking of myopodin between the Z-disc and the nucleus of cardiac myocytes." Molecular and cellular biology **27**(23): 8215-8227.
Fedele, F., P. Severino, N. Bruno, R. Stio, C. Caira, A. D'Ambrosi, B. Brasolin, V. Ohanyan and M. Mancone (2013). "Role of ion channels in coronary microcirculation: a review of the literature." Future Cardiol **9**(6): 897-905.
Fillmore, N., J. Mori and G. D. Lopaschuk (2014). "Mitochondrial fatty acid oxidation alterations in heart failure, ischaemic heart disease and diabetic cardiomyopathy." British Journal of Pharmacology **171**(8): 2080-2090.
Fischer, Y., J. Thomas, L. Sevilla, P. Muñoz, C. Becker, G. Holman, I. J. Kozka, M. Palacín, X. Testar, H. Kammermeier and A. Zorzano (1997). "Insulin-induced recruitment of glucose transporter 4 (GLUT4) and GLUT1 in isolated rat cardiac myocytes. Evidence of the existence of different intracellular GLUT4 vesicle populations." J Biol Chem **272**(11): 7085-7092.
Fomovsky, G. M. and J. W. Holmes (2010). "Evolution of scar structure, mechanics, and ventricular function after myocardial infarction in the rat." American Journal of Physiology-Heart and Circulatory Physiology **298**(1): H221-H228.
Foundation, B. H.
Fowler, E. D., N. Wang, M. Hezzell, G. Chanoit, J. C. Hancox and M. B. Cannell (2020). "Arrhythmogenic late Ca²⁺ sparks in failing heart cells and their control by action potential configuration." Proceedings of the National Academy of Sciences **117**(5): 2687-2692.
Frangogiannis, N. G. (2007). "Chemokines in ischemia and reperfusion." Thrombosis and Haemostasis **97**(5): 738-747.
Frangogiannis, N. G. (2008). "The immune system and cardiac repair." Pharmacol Res **58**(2): 88-111.
Frangogiannis, N. G. (2019). "The Extracellular Matrix in Ischemic and Nonischemic Heart Failure." Circulation Research **125**(1): 117-146.
Frank, D. and N. Frey (2011). "Cardiac Z-disc signaling network." The Journal of biological chemistry **286**(12): 9897-9904.
Frantz, S., J. Bauersachs and G. Ertl (2009). "Post-infarct remodelling: contribution of wound healing and inflammation." Cardiovascular research **81**(3): 474-481.
Freeman, B. A. and J. D. Crapo (1982). "Biology of disease: free radicals and tissue injury." Lab Invest **47**(5): 412-426.
French, B. A. and C. M. Kramer (2007). "Mechanisms of Post-Infarct Left Ventricular Remodeling." Drug discovery today. Disease mechanisms **4**(3): 185-196.
Fu, X., H. Khalil, O. Kanisicak, J. G. Boyer, R. J. Vagnozzi, B. D. Maliken, M. A. Sargent, V. Prasad, I. Valiente-Alandi, B. C. Blaxall and J. D. Molkentin (2018). "Specialized fibroblast differentiated states underlie scar formation in the infarcted mouse heart." The Journal of clinical investigation **128**(5): 2127-2143.

Galrinho, R. D., C. G. Manole and D. Vinereanu (2016). "Telocytes - a Hope for Cardiac Repair after Myocardial Infarction." Maedica **11**(4): 325-329.
Gangwar, A., P. Kumar, A. Rawat and S. Tiwari (2014). "Noninvasive measurement of systolic blood pressure in rats: a novel technique." Indian journal of pharmacology **46**(3): 351-352.
Gao, X.-M., Y. Liu, D. White, Y. Su, B. G. Drew, C. R. Bruce, H. Kiriazis, Q. Xu, N. Jennings, A. Bobik, M. A. Febbraio, B. A. Kingwell, R. Bucala, G. Fingerle-Rowson, A. M. Dart, E. F. Morand and X.-J. Du (2011). "Deletion of macrophage migration inhibitory factor protects the heart from severe ischemia–reperfusion injury: A predominant role of anti-inflammation." Journal of Molecular and Cellular Cardiology **50**(6): 991-999.
Garcia-Dorado, D., M. Andres-Villarreal, M. Ruiz-Meana, J. Inserte and I. Barba (2012). "Myocardial edema: A translational view." Journal of Molecular and Cellular Cardiology **52**(5): 931-939.
Gherghiceanu, M. and L. M. Popescu (2012). "Cardiac telocytes - their junctions and functional implications." Cell and tissue research **348**(2): 265-279.
Gho, B. C., R. G. Schoemaker, M. A. van den Doel, D. J. Duncker and P. D. Verdouw (1996). "Myocardial protection by brief ischemia in noncardiac tissue." Circulation **94**(9): 2193-2200.
Goldman, S. and T. E. Raya (1995). "Rat infarct model of myocardial infarction and heart failure." Journal of Cardiac Failure **1**(2): 169-177.
Goulart, V. A. M., A. K. Santos, V. C. Sandrim, J. M. Batista, M. C. X. Pinto, L. C. Cameron and R. R. Resende (2019). "Metabolic Disturbances Identified in Plasma Samples from ST-Segment Elevation Myocardial Infarction Patients." Dis Markers **2019**: 7676189.
Grieve, D. J. and A. M. Shah (2003). "Oxidative stress in heart failure. More than just damage." Eur Heart J **24**(24): 2161-2163.
Griffiths, E. J. and A. P. Halestrap (1995). "Mitochondrial non-specific pores remain closed during cardiac ischaemia, but open upon reperfusion." The Biochemical journal **307 (Pt 1)**(Pt 1): 93-98.
h-Ici, D. O., S. Jeuthe, T. Dietrich, F. Berger, T. Kuehne, S. Kozerke and D. R. Messroghli (2015). "Closed-chest small animal model to study myocardial infarction in an MRI environment in real time." Int J Cardiovasc Imaging **31**(1): 115-121.
Hakuno, D., Y. Hamba, T. Toya and T. Adachi (2015). "Plasma Amino Acid Profiling Identifies Specific Amino Acid Associations with Cardiovascular Function in Patients with Systolic Heart Failure." PLOS ONE **10**(2): e0117325.
Halestrap, A. P. (2009). "What is the mitochondrial permeability transition pore?" J Mol Cell Cardiol **46**(6): 821-831.
Hamirani, Y. S., A. Wong, C. M. Kramer and M. Salerno (2014). "Effect of Microvascular Obstruction and Intramyocardial Hemorrhage by CMR on LV Remodeling and Outcomes After Myocardial Infarction: A Systematic Review and Meta-Analysis." JACC: Cardiovascular Imaging **7**(9): 940-952.
Hanft, L. M., F. S. Korte and K. S. McDonald (2007). "Cardiac function and modulation of sarcomeric function by length." Cardiovascular Research **77**(4): 627-636.
Hanschmann, E.-M., J. R. Godoy, C. Berndt, C. Hudemann and C. H. Lillig (2013). "Thioredoxins, glutaredoxins, and peroxiredoxins--molecular mechanisms and health significance: from cofactors to antioxidants to redox signaling." Antioxidants & redox signaling **19**(13): 1539-1605.
Hasenfuss, G. (1998). "Animal models of human cardiovascular disease, heart failure and hypertrophy." Cardiovascular Research **39**(1): 60-76.
Hausenloy, D. J., M. R. Duchen and D. M. Yellon (2003). "Inhibiting mitochondrial permeability transition pore opening at reperfusion protects against ischaemia-reperfusion injury." Cardiovasc Res **60**(3): 617-625.
Hausenloy, D. J., A. Tsang, M. M. Mocanu and D. M. Yellon (2005). "Ischemic preconditioning protects by activating prosurvival kinases at reperfusion." Am J Physiol Heart Circ Physiol **288**(2): H971-976.
Hausenloy, D. J. and D. M. Yellon (2013). "Myocardial ischemia-reperfusion injury: a neglected therapeutic target." The Journal of Clinical Investigation **123**(1): 92-100.

Hausenloy, D. J. and D. M. Yellon (2013). "Myocardial ischemia-reperfusion injury: a neglected therapeutic target." J Clin Invest **123**(1): 92-100.
Hauton, D., M. J. Bennett and R. D. Evans (2001). "Utilisation of triacylglycerol and non-esterified fatty acid by the working rat heart: myocardial lipid substrate preference." Biochim Biophys Acta **1533**(2): 99-109.
Haworth, R. A. and D. R. Hunter (1979). "The Ca2+-induced membrane transition in mitochondria. II. Nature of the Ca2+ trigger site." Arch Biochem Biophys **195**(2): 460-467.
Hayes, K. and J. J. A. r. o. n. Sturman (1981). "Taurine in metabolism." **1**(1): 401-425.
Hearse, D. J. and A. Tosaki (1987). "Free radicals and reperfusion-induced arrhythmias: protection by spin trap agent PBN in the rat heart." Circulation research **60**(3): 375-383.
Heling, A., R. Zimmermann, S. Kostin, Y. Maeno, S. Hein, B. Devaux, E. Bauer, W. P. Klövekorn, M. Schlepper, W. Schaper and J. Schaper (2000). "Increased expression of cytoskeletal, linkage, and extracellular proteins in failing human myocardium." Circulation Research **86**(8): 846-853.
Henderson, C., C. Gomez, S. Novak, L. Mi-Mi and C. Gregorio (2017). Overview of the Muscle Cytoskeleton. **7:** 891-944.
Hernandez-Resendiz, S., M. Buelna, F. Correa and C. Zazueta (2012). Oxidative Stress and Mitochondrial Dysfunction in Cardiovascular Diseases.
Hinglais, N., D. Heudes, A. Nicoletti, C. Mandet, M. Laurent, J. Bariety and J. Michel (1994). "Colocalization of myocardial fibrosis and inflammatory cells in rats." Laboratory investigation; a journal of technical methods and pathology **70**(2): 286.
Holeček, M. (2018). "Branched-chain amino acids in health and disease: metabolism, alterations in blood plasma, and as supplements." Nutrition & metabolism **15**: 33-33.
Hollander, J. M., D. Thapa and D. L. Shepherd (2014). "Physiological and structural differences in spatially distinct subpopulations of cardiac mitochondria: influence of cardiac pathologies." American Journal of Physiology-Heart and Circulatory Physiology **307**(1): H1-H14.
Holness, M. and M. Sugden (2003). "Regulation of pyruvate dehydrogenase complex activity by reversible phosphorylation." Biochemical Society Transactions **31**(6): 1143-1151.
Honda, M., Y. Goto, H. Kuzuo, S. Ishikawa, S. Morioka, Y. Yamori and K. Moriyama (1993). "Biochemical remodeling of collagen in the heart of spontaneously hypertensive rats--prominent increase in type V collagen." Jpn Circ J **57**(5): 434-441.
Hoshijima, M. (2006). "Mechanical stress-strain sensors embedded in cardiac cytoskeleton: Z disk, titin, and associated structures." Am J Physiol Heart Circ Physiol **290**(4): H1313-1325.
Houser, S. R., K. B. Margulies, A. M. Murphy, F. G. Spinale, G. S. Francis, S. D. Prabhu, H. A. Rockman, D. A. Kass, J. D. Molkentin, M. A. Sussman and W. J. Koch (2012). "Animal Models of Heart Failure." Circulation Research **111**(1): 131-150.
Huxley, H. and J. Hanson (1954). "Changes in the cross-striations of muscle during contraction and stretch and their structural interpretation." Nature **173**(4412): 973-976.
Jamora, C. and E. Fuchs (2002). "Intercellular adhesion, signalling and the cytoskeleton." Nature Cell Biology **4**(4): E101-E108.
Janardhan, A., J. Chen and P. A. Crawford (2011). "Altered systemic ketone body metabolism in advanced heart failure." Tex Heart Inst J **38**(5): 533-538.
Janicki, J. S., G. L. Brower and S. P. Levick (2015). "The emerging prominence of the cardiac mast cell as a potent mediator of adverse myocardial remodeling." Methods in molecular biology (Clifton, N.J.) **1220**: 121-139.
Jansen of Lorkeers, S. J., J. M. Gho, S. Koudstaal, G. P. van Hout, P. P. Zwetsloot, J. W. van Oorschot, E. C. van Eeuwijk, T. Leiner, I. E. Hoefer, M. J. Goumans, P. A. Doevendans, J. P. Sluijter and S. A. Chamuleau (2015). "Xenotransplantation of Human Cardiomyocyte Progenitor Cells Does Not Improve Cardiac Function in a Porcine Model of Chronic Ischemic Heart Failure. Results from a Randomized, Blinded, Placebo Controlled Trial." PLoS One **10**(12): e0143953.

Javadov, S. A., S. Clarke, M. Das, E. J. Griffiths, K. H. Lim and A. P. Halestrap (2003). "Ischaemic preconditioning inhibits opening of mitochondrial permeability transition pores in the reperfused rat heart." J Physiol **549**(Pt 2): 513-524.
Javadov, S. A., K. H. Lim, P. M. Kerr, M. S. Suleiman, G. D. Angelini and A. P. Halestrap (2000). "Protection of hearts from reperfusion injury by propofol is associated with inhibition of the mitochondrial permeability transition." Cardiovasc Res **45**(2): 360-369.
Jiang, M. T., A. J. Lokuta, E. F. Farrell, M. R. Wolff, R. A. Haworth and H. H. Valdivia (2002). "Abnormal Ca2+ release, but normal ryanodine receptors, in canine and human heart failure." Circ Res **91**(11): 1015-1022.
Johnson, R. and P. Camelliti (2018). "118 Development and characterisation of an ex-vivo model of porcine myocardium for preclinical research." Heart **104**(Suppl 6): A91-A91.
Jugdutt, B. I., M. J. Joljart and M. I. Khan (1996). "Rate of Collagen Deposition During Healing and Ventricular Remodeling After Myocardial Infarction in Rat and Dog Models." Circulation **94**(1): 94-101.
Kang, M. Y., Y. Zhang, S. J. Matkovich, A. Diwan, A. H. Chishti and G. W. Dorn, 2nd (2010). "Receptor-independent cardiac protein kinase Calpha activation by calpain-mediated truncation of regulatory domains." Circ Res **107**(7): 903-912.
Kantorow, M., W. Lee and D. Chauss (2012). "Focus on Molecules: methionine sulfoxide reductase A." Experimental eye research **100**: 110-111.
Kanzaki, Y., F. Terasaki, M. Okabe, K. Otsuka, T. Katashima, S. Fujita, T. Ito and Y. Kitaura (2010). "Giant Mitochondria in the Myocardium of a Patient With Mitochondrial Cardiomyopathy." Circulation **121**(6): 831-832.
Karwi, Q. G., G. M. Uddin, K. L. Ho and G. D. Lopaschuk (2018). "Loss of Metabolic Flexibility in the Failing Heart." Frontiers in Cardiovascular Medicine **5**(68).
Katzung, B. G. and A. J. Trevor (2015). Basic and Clinical Pharmacology, McGraw-Hill Education.
Kawase, Y. and R. J. Hajjar (2008). "The cardiac sarcoplasmic/endoplasmic reticulum calcium ATPase: a potent target for cardiovascular diseases." Nat Clin Pract Cardiovasc Med **5**(9): 554-565.
Khaliulin, I., S. J. Clarke, H. Lin, J. Parker, M. S. Suleiman and A. P. Halestrap (2007). "Temperature preconditioning of isolated rat hearts--a potent cardioprotective mechanism involving a reduction in oxidative stress and inhibition of the mitochondrial permeability transition pore." J Physiol **581**(Pt 3): 1147-1161.
Khaliulin, I., A. P. Halestrap, S. M. Bryant, D. J. Dudley, A. F. James and M. S. Suleiman (2014). "Clinically-relevant consecutive treatment with isoproterenol and adenosine protects the failing heart against ischaemia and reperfusion." J Transl Med **12**: 139.
Khaliulin, I., A. P. Halestrap and M. S. Suleiman (2011). "Temperature preconditioning is optimal at 26° C and confers additional protection to hypothermic cardioplegic ischemic arrest." Exp Biol Med (Maywood) **236**(6): 736-745.
Kim, N., Y. Lee, H. Kim, H. Joo, J. B. Youm, W. S. Park, M. Warda, D. V. Cuong and J. Han (2006). "Potential biomarkers for ischemic heart damage identified in mitochondrial proteins by comparative proteomics." PROTEOMICS **6**(4): 1237-1249.
Kloner, R. A., R. Bolli, E. Marban, L. Reinlib and E. Braunwald (1998). "Medical and cellular implications of stunning, hibernation, and preconditioning: an NHLBI workshop." Circulation **97**(18): 1848-1867.
Knöll, R., B. Buyandelger and M. Lab (2011). "The Sarcomeric Z-Disc and Z-Discopathies %J Journal of Biomedicine and Biotechnology." **2011**: 12.
Kohlhauer, M., S. Dawkins, A. S. H. Costa, R. Lee, T. Young, V. R. Pell, R. P. Choudhury, A. P. Banning, R. K. Kharbanda, S. Oxford Acute Myocardial Infarction, K. Saeb-Parsy, M. P. Murphy, C. Frezza, T. Krieg and K. M. Channon (2018). "Metabolomic Profiling in Acute ST-Segment-Elevation Myocardial Infarction Identifies Succinate as an Early Marker of Human Ischemia-Reperfusion Injury." J Am Heart Assoc **7**(8).

Konstam, M. A., D. G. Kramer, A. R. Patel, M. S. Maron and J. E. Udelson (2011). "Left Ventricular Remodeling in Heart Failure." Current Concepts in Clinical Significance and Assessment **4**(1): 98-108.
Koppenol, W. H. (2001). "The Haber-Weiss cycle – 70 years later." Redox Report **6**(4): 229-234.
Krishnamurthy, P. (2012). Antioxidant Enzymes and Human Health.
Krug, A., W. D. M. De Rochemont and G. Korb (1966). "Blood supply of the myocardium after temporary coronary occlusion." Circulation Research **19**(1): 57-62.
Krüger, M. and W. A. Linke (2006). "Protein kinase-A phosphorylates titin in human heart muscle and reduces myofibrillar passive tension." J Muscle Res Cell Motil **27**(5-7): 435-444.
Kumar, A. G., C. M. Ballantyne, L. H. Michael, G. L. Kukielka, K. A. Youker, M. L. Lindsey, H. K. Hawkins, H. H. Birdsall, C. R. MacKay, G. J. LaRosa, R. D. Rossen, C. W. Smith and M. L. Entman (1997). "Induction of monocyte chemoattractant protein-1 in the small veins of the ischemic and reperfused canine myocardium." Circulation **95**(3): 693-700.
Kumar, M., E. R. Kasala, L. N. Bodduluru, V. Dahiya, D. Sharma, V. Kumar and M. Lahkar (2016). "Animal models of myocardial infarction: Mainstay in clinical translation." Regulatory Toxicology and Pharmacology **76**: 221-230.
Kuznetsov, A. V., S. Javadov, R. Margreiter, M. Grimm, J. Hagenbuchner and M. J. Ausserlechner (2019). "The Role of Mitochondria in the Mechanisms of Cardiac Ischemia-Reperfusion Injury." Antioxidants (Basel, Switzerland) **8**(10): 454.
Laguens, R., P. Cabeza Meckert, G. Vera Janavel, H. Del Valle, E. Lascano, J. Negroni, P. Werba, L. Cuniberti, V. Martinez, C. Melo, M. Papouchado, R. Ojeda, M. Criscuolo and A. Crottogini (2002). "Entrance in mitosis of adult cardiomyocytes in ischemic pig hearts after plasmid-mediated rhVEGF165 gene transfer." Gene Ther **9**(24): 1676-1681.
Lai, L., T. C. Leone, M. P. Keller, O. J. Martin, A. T. Broman, J. Nigro, K. Kapoor, T. R. Koves, R. Stevens, O. R. Ilkayeva, R. B. Vega, A. D. Attie, D. M. Muoio and D. P. Kelly (2014). "Energy metabolic reprogramming in the hypertrophied and early stage failing heart a multisystems approach." Circulation: Heart Failure **7**(6): 1022-1031.
Lee, D. and M. Michalak (2010). "Membrane associated Ca2+ buffers in the heart." BMB Rep **43**(3): 151-157.
Lewis, M., B. Littlejohns, H. Lin, G. D. Angelini and M. S. Suleiman (2014). "Cardiac taurine and principal amino acids in right and left ventricles of patients with either aortic valve stenosis or coronary artery disease: the importance of diabetes and gender." SpringerPlus **3**(1): 523.
Li, G. H., Y. Shi, Y. Chen, M. Sun, S. Sader, Y. Maekawa, S. Arab, F. Dawood, M. Chen, G. D. Couto, Y. Liu, M. Fukuoka, S. Yang, M. D. Shi, L. A. Kirshenbaum, C. A. McCulloch and P. Liu (2009). "Gelsolin Regulates Cardiac Remodeling After Myocardial Infarction Through DNase I–Mediated Apoptosis." Circulation Research **104**(7): 896-904.
Liao, Z., Y. Chen, C. Duan, K. Zhu, R. Huang, H. Zhao, M. Hintze, Q. Pu, Z. Yuan, L. Lv, H. Chen, B. Lai, S. Feng, X. Qi and D. Cai (2021). "Cardiac telocytes inhibit cardiac microvascular endothelial cell apoptosis through exosomal miRNA-21-5p-targeted cdip1 silencing to improve angiogenesis following myocardial infarction." Theranostics **11**(1): 268-291.
Lim, K. H., A. P. Halestrap, G. D. Angelini and M. S. Suleiman (2005). "Propofol is cardioprotective in a clinically relevant model of normothermic blood cardioplegic arrest and cardiopulmonary bypass." Exp Biol Med (Maywood) **230**(6): 413-420.
Lincoln, J., J. B. Florer, G. H. Deutsch, R. J. Wenstrup and K. E. Yutzey (2006). "ColVa1 and ColXIa1 are required for myocardial morphogenesis and heart valve development." Dev Dyn **235**(12): 3295-3305.
Lindner, D., C. Zietsch, J. Tank, S. Sossalla, N. Fluschnik, S. Hinrichs, L. Maier, W. Poller, S. Blankenberg, H.-P. Schultheiss, C. Tschöpe and D. Westermann (2014). "Cardiac fibroblasts support cardiac inflammation in heart failure." Basic Research in Cardiology **109**(5): 428.
Lipskaia, L., E. R. Chemaly, L. Hadri, A.-M. Lompre and R. J. Hajjar (2010). "Sarcoplasmic reticulum Ca(2+) ATPase as a therapeutic target for heart failure." Expert opinion on biological therapy **10**(1): 29-41.

Littlejohns, B., B. University of and B. University of (2013). The role of mitochondria in increased vulnerability to insults of hearts and cardiomyocytes isolated from mice fed a "Western style" high-fat diet.
Lodish H, B. A., Zipursky SL (2000). Muscle: A Specialized Contractile Machine. Molecular Cell Biology. New York, W. H. Freeman.
Logan, D. C. (2006). "The mitochondrial compartment." Journal of Experimental Botany **57**(6): 1225-1243.
Lopaschuk, G. D., J. R. Ussher, C. D. Folmes, J. S. Jaswal and W. C. Stanley (2010). "Myocardial fatty acid metabolism in health and disease." Physiol Rev **90**(1): 207-258.
Lopaschuk, G. D., J. R. Ussher, C. D. L. Folmes, J. S. Jaswal and W. C. Stanley (2010). "Myocardial Fatty Acid Metabolism in Health and Disease." Physiological Reviews **90**(1): 207-258.
Luo, C. H. and Y. Rudy (1994). "A dynamic model of the cardiac ventricular action potential. I. Simulations of ionic currents and concentration changes." **74**(6): 1071-1096.
Maack, C. and B. O'Rourke (2007). "Excitation-contraction coupling and mitochondrial energetics." Basic Research in Cardiology **102**(5): 369-392.
Malka, A., D. Meerkin, Y. D. Barac, E. Malits, N. Bachner-Hinenzon, S. Carasso, O. Ertracht, I. Angel, R. Shofti, M. Youdim, Z. Abassi and O. Binah (2015). "TVP1022: A Novel Cardioprotective Drug Attenuates Left Ventricular Remodeling After Ischemia/Reperfusion in Pigs." J Cardiovasc Pharmacol **66**(2): 214-222.
Mann, D. L. and M. R. Bristow (2005). "Mechanisms and models in heart failure: the biomechanical model and beyond." Circulation **111**(21): 2837-2849.
Manring, H. R., L. E. Dorn, A. Ex-Willey, F. Accornero and M. A. Ackermann (2018). "At the heart of inter- and intracellular signaling: the intercalated disc." Biophysical reviews **10**(4): 961-971.
Marcondes-Braga, F. G., I. G. R. Gutz, G. L. Batista, P. H. N. Saldiva, S. M. Ayub-Ferreira, V. S. Issa, S. Mangini, E. A. Bocchi and F. Bacal (2012). "Exhaled acetone as a new biomaker of heart failure severity." Chest **142**(2): 457-466.
Maturana, A. D., N. Nakagawa, N. Yoshimoto, K. Tatematsu, M. Hoshijima, K. Tanizawa and S. Kuroda (2011). "LIM domains regulate protein kinase C activity: a novel molecular function." Cell Signal **23**(5): 928-934.
McArdel, S. L., C. Terhorst and A. H. Sharpe (2016). "Roles of CD48 in regulating immunity and tolerance." Clinical Immunology **164**: 10-20.
McEwen, M., P. Sullivan, A. Rabchevsky and J. Springer (2011). "Targeting Mitochondrial Function for the Treatment of Acute Spinal Cord Injury." Neurotherapeutics : the journal of the American Society for Experimental NeuroTherapeutics **8**: 168-179.
McGarry, J. D., G. Mannaerts and D. W. Foster (1977). "A possible role for malonyl-CoA in the regulation of hepatic fatty acid oxidation and ketogenesis." The Journal of clinical investigation **60**(1): 265-270.
McKirnan, M. D., Y. Ichikawa, Z. Zhang, A. E. Zemljic-Harpf, S. Fan, D. K. Barupal, H. H. Patel, H. K. Hammond and D. M. Roth (2019). "Metabolomic analysis of serum and myocardium in compensated heart failure after myocardial infarction." Life Sci **221**: 212-223.
Milani-Nejad, N. and P. M. Janssen (2014). "Small and large animal models in cardiac contraction research: advantages and disadvantages." Pharmacol Ther **141**(3): 235-249.
Mootha, V. K., A. E. Arai and R. S. Balaban (1997). "Maximum oxidative phosphorylation capacity of the mammalian heart." Am J Physiol **272**(2 Pt 2): H769-775.
Moris, D., M. Spartalis, E. Spartalis, G.-S. Karachaliou, G. I. Karaolanis, G. Tsourouflis, D. I. Tsilimigras, E. Tzatzaki and S. Theocharis (2017). "The role of reactive oxygen species in the pathophysiology of cardiovascular diseases and the clinical significance of myocardial redox." Annals of translational medicine **5**(16): 326-326.
Mudge, G. H., Jr., R. M. Mills, Jr., H. Taegtmeyer, R. Gorlin and M. Lesch (1976). "Alterations of myocardial amino acid metabolism in chronic ischemic heart disease." J Clin Invest **58**(5): 1185-1192.

Muller, O. J., M. B. Heckmann, L. Ding, K. Rapti, A. Y. Rangrez, T. Gerken, N. Christiansen, U. E. E. Rennefahrt, H. Witt, S. Gonzalez Maldonado, P. Ternes, D. M. Schwab, T. Ruf, S. Hille, A. Remes, A. Jungmann, T. M. Weis, J. S. Kreusser, H. J. Grone, J. Backs, P. Schatz, H. A. Katus and N. Frey (2019). "Comprehensive plasma and tissue profiling reveals systemic metabolic alterations in cardiac hypertrophy and failure." Cardiovasc Res **115**(8): 1296-1305.
Murry, C. E., R. B. Jennings and K. A. Reimer (1986). "Preconditioning with ischemia: a delay of lethal cell injury in ischemic myocardium." Circulation **74**(5): 1124-1136.
Murthy, M. and S. Pande (1984). "Mechanism of carnitine acylcarnitine translocase-catalyzed import of acylcarnitines into mitochondria." Journal of Biological Chemistry **259**(14): 9082-9089.
Nahrendorf, M., F. K. Swirski, E. Aikawa, L. Stangenberg, T. Wurdinger, J. L. Figueiredo, P. Libby, R. Weissleder and M. J. Pittet (2007). "The healing myocardium sequentially mobilizes two monocyte subsets with divergent and complementary functions." Journal of Experimental Medicine **204**(12): 3037-3047.
Nandi, S. S. and P. Mishra (2015). "Harnessing fetal and adult genetic reprograming for therapy of heart disease." Journal of nature and science **1**.
Narula, J., M. S. Dawson, B. K. Singh, A. Amanullah, E. R. Acio, F. A. Chaudhry, R. B. Arani and A. E. Iskandrian (2000). "Noninvasive characterization of stunned, hibernating, remodeled and nonviable myocardium in ischemic cardiomyopathy." Journal of the American College of Cardiology **36**(6): 1913-1919.
National Research Council Committee for the Update of the Guide for the, C. and A. Use of Laboratory (2011). The National Academies Collection: Reports funded by National Institutes of Health. Guide for the Care and Use of Laboratory Animals. th. Washington (DC), National Academies Press (US)

National Academy of Sciences.
Neagoe, C., M. Kulke, F. d. Monte, J. K. Gwathmey, P. P. d. Tombe, R. J. Hajjar and W. A. Linke (2002). "Titin Isoform Switch in Ischemic Human Heart Disease." Circulation **106**(11): 1333-1341.
Netto, L. E. S. and F. Antunes (2016). "The Roles of Peroxiredoxin and Thioredoxin in Hydrogen Peroxide Sensing and in Signal Transduction." Molecules and cells **39**(1): 65-71.
Neubauer, S. (2007). "The failing heart—an engine out of fuel." New England Journal of Medicine **356**(11): 1140-1151.
Nour, M. S., N. R. Sarhan, S. A. Mazroa and S. A. Gawish (2017). "Histological and immunohistochemical study of cardiac telocytes in a rat model of isoproterenol-induced myocardial infarction with a reference to the effect of grape seed extract." Acta Histochemica **119**(7): 747-758.
Ong, S.-B., S. Hernández-Reséndiz, G. E. Crespo-Avilan, R. T. Mukhametshina, X.-Y. Kwek, H. A. Cabrera-Fuentes and D. J. Hausenloy (2018). "Inflammation following acute myocardial infarction: Multiple players, dynamic roles, and novel therapeutic opportunities." Pharmacology & Therapeutics **186**: 73-87.
Opie, L. H., P. J. Commerford, B. J. Gersh and M. A. Pfeffer (2006). "Controversies in ventricular remodelling." Lancet **367**(9507): 356-367.
Orkand, R. K. and R. Niedergerke (1964). "HEART ACTION POTENTIAL: DEPENDENCE ON EXTERNAL CALCIUM AND SODIUM IONS." Science **146**(3648): 1176-1177.
Parlakpınar, H., M. Örüm and M. Sagir (2013). "Pathophysiology of Myocardial Ischemia Reperfusion Injury: A Review." Medicine Science **2**: 1.
Patel, M. S. and L. G. Korotchkina (2006). "Regulation of the pyruvate dehydrogenase complex." Biochem Soc Trans **34**(Pt 2): 217-222.
Patel, V. B., P. Zhabyeyev, X. Chen, F. Wang, M. Paul, D. Fan, B. A. McLean, R. Basu, P. Zhang, S. Shah, J. F. Dawson, W. G. Pyle, M. Hazra, Z. Kassiri, S. Hazra, B. Vanhaesebroeck, C. A. McCulloch and G. Y. Oudit (2018). "PI3Kα-regulated gelsolin activity is a critical determinant of cardiac cytoskeletal remodeling and heart disease." Nature Communications **9**(1): 5390.
Patten, R. D. (2007). "Models of Gender Differences in Cardiovascular Disease." Drug discovery today. Disease models **4**(4): 227-232.

Patten, R. D. and M. R. Hall-Porter (2009). "Small Animal Models of Heart Failure." Circulation: Heart Failure **2**(2): 138-144.
Periasamy, M. and S. Huke (2001). "SERCA pump level is a critical determinant of Ca2+ homeostasis and cardiac contractility." Journal of molecular and cellular cardiology **33**(6): 1053-1063.
Pfeffer, J. M., M. A. Pfeffer and E. Braunwald (1985). "Influence of chronic captopril therapy on the infarcted left ventricle of the rat." Circ Res **57**(1): 84-95.
Pfeffer, M. A. and E. Braunwald (1990). "Ventricular remodeling after myocardial infarction. Experimental observations and clinical implications." Circulation **81**(4): 1161-1172.
Pfeffer, M. A., J. M. Pfeffer, M. C. Fishbein, P. J. Fletcher, J. Spadaro, R. A. Kloner and E. Braunwald (1979). "Myocardial infarct size and ventricular function in rats." Circulation research **44**(4): 503-512.
Posch, M. G., L. Thiemann, P. Tomasov, J. Veselka, N. Cardim, M. Garcia-Castro, E. Coto, A. Perrot, C. Geier, R. Dietz, W. Haverkamp and C. Özcelik (2008). "Sequence analysis of myozenin 2 in 438 European patients with familial hypertrophic cardiomyopathy." Medical Science Monitor **14**(7): CR372-CR374.
Pouralijan Amiri, M., M. Khoshkam, R. M. Salek, R. Madadi, G. Faghanzadeh Ganji and A. Ramazani (2019). "Metabolomics in early detection and prognosis of acute coronary syndrome." Clin Chim Acta **495**: 43-53.
Prabhu, S. D. and N. G. Frangogiannis (2016). "The Biological Basis for Cardiac Repair After Myocardial Infarction." Circulation Research **119**(1): 91-112.
Prabhu, S. D. and N. G. Frangogiannis (2016). "The Biological Basis for Cardiac Repair After Myocardial Infarction." **119**(1): 91-112.
Puchalska, P. and P. A. Crawford (2017). "Multi-dimensional roles of ketone bodies in fuel metabolism, signaling, and therapeutics." Cell metabolism **25**(2): 262-284.
Qu, Q., F. Zeng, X. Liu, Q. J. Wang and F. Deng (2016). "Fatty acid oxidation and carnitine palmitoyltransferase I: emerging therapeutic targets in cancer." Cell Death & Disease **7**(5): e2226-e2226.
Rackley, C. E., F. G. Dalldorf, W. P. Hood, Jr. and B. R. Wilcox (1970). "Sarcomere length and left ventricular function in chronic heart disease." Am J Med Sci **259**(2): 90-96.
Rainer Peter, P., P. Dong, M. Sorge, J. Fert-Bober, J. Holewinski Ronald, Y. Wang, A. Foss Catherine, S. An Steven, A. Baracca, G. Solaini, G. Glabe Charles, G. Pomper Martin, E. Van Eyk Jennifer, F. Tomaselli Gordon, N. Paolocci and G. Agnetti (2018). "Desmin Phosphorylation Triggers Preamyloid Oligomers Formation and Myocyte Dysfunction in Acquired Heart Failure." Circulation Research **122**(10): e75-e83.
Ramachandra, C. J. A., S. Hernandez-Resendiz, G. E. Crespo-Avilan, Y.-H. Lin and D. J. Hausenloy (2020). "Mitochondria in acute myocardial infarction and cardioprotection." EBioMedicine **57**: 102884.
Rasmussen, T., B. Follin, J. Kastrup, M. Brandt-Larsen, J. Madsen, T. Emil Christensen, K. Pharao Hammelev, P. Hasbak and A. Kjaer (2016). "Angiogenesis PET Tracer Uptake ((68)Ga-NODAGA-E[(cRGDyK)](2)) in Induced Myocardial Infarction in Minipigs." Diagnostics (Basel) **6**(2).
Reuter, H. and G. W. Beeler, Jr. (1969). "Sodium current in ventricular myocardial fibers." Science **163**(3865): 397-399.
Richter, M. and S. Kostin (2015). "The failing human heart is characterized by decreased numbers of telocytes as result of apoptosis and altered extracellular matrix composition." Journal of cellular and molecular medicine **19**(11): 2597-2606.
Riehle, C. and E. D. Abel (2016). "Insulin signaling and heart failure." Circulation research **118**(7): 1151-1169.
Rog-Zielinska, E. A., R. A. Norris, P. Kohl and R. Markwald (2016). "The Living Scar – Cardiac Fibroblasts and the Injured Heart." Trends in Molecular Medicine **22**(2): 99-114.
Rog-Zielinska, E. A., R. A. Norris, P. Kohl and R. Markwald (2016). "The Living Scar – Cardiac Fibroblasts and the Injured Heart." Trends in Molecular Medicine **22**(2): 99-114.

Rohr, S. (2004). "Role of gap junctions in the propagation of the cardiac action potential." Cardiovascular Research **62**(2): 309-322.
Rosa, I., C. Taverna, L. Novelli, M. Marini, L. Ibba-Manneschi and M. Manetti (2019). "Telocytes constitute a widespread interstitial meshwork in the lamina propria and underlying striated muscle of human tongue." Scientific Reports **9**(1): 5858.
Rosca, M. G. and C. L. Hoppel (2010). "Mitochondria in heart failure." Cardiovascular Research **88**(1): 40-50.
Rosca, M. G. and C. L. Hoppel (2013). "Mitochondrial dysfunction in heart failure." Heart failure reviews **18**(5): 607-622.
Rouslin, W. (1983). "Mitochondrial complexes I, II, III, IV, and V in myocardial ischemia and autolysis." American Journal of Physiology-Heart and Circulatory Physiology **244**(6): H743-H748.
Rusu, M., K. Hilse, A. Schuh, L. Martin, I. Slabu, C. Stoppe and E. A. Liehn (2019). "Biomechanical assessment of remote and postinfarction scar remodeling following myocardial infarction." Scientific Reports **9**(1): 16744.
Sansbury, B. E., A. M. DeMartino, Z. Xie, A. C. Brooks, R. E. Brainard, L. J. Watson, A. P. DeFilippis, T. D. Cummins, M. A. Harbeson, K. R. Brittian, S. D. Prabhu, A. Bhatnagar, S. P. Jones and B. G. Hill (2014). "Metabolomic analysis of pressure-overloaded and infarcted mouse hearts." Circulation: Heart Failure **7**(4): 634-642.
Saraste, M. (1999). "Oxidative phosphorylation at the fin de siècle." Science **283**(5407): 1488-1493.
Sass, J. O. (2012). "Inborn errors of ketogenesis and ketone body utilization." **35**(1): 23-28.
Schaffer, S. W., C. J. Jong, T. Ito and J. Azuma (2014). "Effect of taurine on ischemia–reperfusion injury." Amino Acids **46**(1): 21-30.
Schaffer, S. W., C. J. Jong, K. C. Ramila and J. Azuma (2010). "Physiological roles of taurine in heart and muscle." Journal of biomedical science **17 Suppl 1**(Suppl 1): S2-S2.
Schuppan, D., M. C. Cantaluppi, J. Becker, A. Veit, T. Bunte, D. Troyer, F. Schuppan, M. Schmid, R. Ackermann and E. G. Hahn (1990). "Undulin, an extracellular matrix glycoprotein associated with collagen fibrils." J Biol Chem **265**(15): 8823-8832.
Schutz, Y. (1995). "The basis of direct and indirect calorimetry and their potentials." Diabetes Metab Rev **11**(4): 383-408.
Sciencephoto.
Seiler, C., M. Stoller, B. Pitt and P. Meier (2013). "The human coronary collateral circulation: development and clinical importance." Eur Heart J **34**(34): 2674-2682.
Sequeira, V., L. L. A. M. Nijenkamp, J. A. Regan and J. van der Velden (2014). "The physiological role of cardiac cytoskeleton and its alterations in heart failure." Biochimica et Biophysica Acta (BBA) - Biomembranes **1838**(2): 700-722.
Seropian, I. M., S. Toldo, B. W. Van Tassell and A. Abbate (2014). "Anti-Inflammatory Strategies for Ventricular Remodeling Following ST-Segment Elevation Acute Myocardial Infarction." Journal of the American College of Cardiology **63**(16): 1593-1603.
Severino, P., A. Amato, M. Pucci, F. Infusino, F. Adamo, L. I. Birtolo, L. Netti, G. Montefusco, C. Chimenti, C. Lavalle, V. Maestrini, M. Mancone, W. M. Chilian and F. Fedele (2020). "Ischemic Heart Disease Pathophysiology Paradigms Overview: From Plaque Activation to Microvascular Dysfunction." International Journal of Molecular Sciences **21**(21): 8118.
Sharov, V. G., A. Goussev, M. Lesch, S. Goldstein and H. N. Sabbah (1998). "Abnormal mitochondrial function in myocardium of dogs with chronic heart failure." J Mol Cell Cardiol **30**(9): 1757-1762.
Sharov, V. G., A. Goussev, M. Lesch, S. Goldstein and H. N. Sabbah (1998). "Abnormal Mitochondrial Function in Myocardium of Dogs with Chronic Heart Failure." Journal of Molecular and Cellular Cardiology **30**(9): 1757-1762.
Slideshare.
Soininen, P., A. J. Kangas, P. Würtz, T. Tukiainen, T. Tynkkynen, R. Laatikainen, M.-R. Järvelin, M. Kähönen, T. Lehtimäki, J. Viikari, O. T. Raitakari, M. J. Savolainen and M. Ala-Korpela (2009). "High-

throughput serum NMR metabonomics for cost-effective holistic studies on systemic metabolism." Analyst **134**(9): 1781-1785.
Solaini, G. and D. A. Harris (2005). "Biochemical dysfunction in heart mitochondria exposed to ischaemia and reperfusion." The Biochemical journal **390**(Pt 2): 377-394.
Sowton, A. P., J. L. Griffin and A. J. Murray (2019). "Metabolic Profiling of the Diabetic Heart: Toward a Richer Picture." Front Physiol **10**: 639.
Spannbauer, A., D. Traxler, K. Zlabinger, A. Gugerell, J. Winkler, J. Mester-Tonczar, D. Lukovic, C. Müller, M. Riesenhuber, N. Pavo and M. Gyöngyösi (2019). "Large Animal Models of Heart Failure With Reduced Ejection Fraction (HFrEF)." **6**(117).
Stanley, W. C., F. A. Recchia and G. D. Lopaschuk (2005). "Myocardial substrate metabolism in the normal and failing heart." Physiol Rev **85**(3): 1093-1129.
Steinberg, S. F. (2012). "Cardiac actions of protein kinase C isoforms." Physiology (Bethesda, Md.) **27**(3): 130-139.
Stenemo, M., A. Ganna, S. Salihovic, C. Nowak, J. Sundstrom, V. Giedraitis, C. D. Broeckling, J. E. Prenni, P. Svensson, P. K. E. Magnusson, L. Lind, E. Ingelsson, J. Arnlov and T. Fall (2019). "The metabolites urobilin and sphingomyelin (30:1) are associated with incident heart failure in the general population." ESC Heart Fail **6**(4): 764-773.
Stevens, S. C. W., D. Terentyev, A. Kalyanasundaram, M. Periasamy and S. Györke (2009). "Intra-sarcoplasmic reticulum Ca2+ oscillations are driven by dynamic regulation of ryanodine receptor function by luminal Ca2+ in cardiomyocytes." The Journal of physiology **587**(Pt 20): 4863-4872.
Sugden, P. H. (2003). "Ras, Akt, and Mechanotransduction in the Cardiac Myocyte." Circulation Research **93**(12): 1179-1192.
Suleiman, M. d.-S., G. C. Rodrigo and R. A. Chapman (1992). "Interdependence of intracellular taurine and sodium in guinea pig heart." Cardiovascular Research **26**(9): 897-905.
Sun, C. N., N. S. Dhalla and R. E. Olson (1969). "Formation of gigantic mitochondria in hypoxic isolated perfused rat hearts." Experientia **25**(7): 763-764.
Sun, H., K. C. Olson, C. Gao, D. A. Prosdocimo, M. Zhou, Z. Wang, D. Jeyaraj, J. Y. Youn, S. Ren, Y. Liu, C. D. Rau, S. Shah, O. Ilkayeva, W. J. Gui, N. S. William, R. M. Wynn, C. B. Newgard, H. Cai, X. Xiao, D. T. Chuang, P. C. Schulze, C. Lynch, M. K. Jain and Y. Wang (2016). "Catabolic Defect of Branched-Chain Amino Acids Promotes Heart Failure." Circulation **133**(21): 2038-2049.
Sun, Y. (2009). "Myocardial repair/remodelling following infarction: roles of local factors." Cardiovascular research **81**(3): 482-490.
Sun, Y. and K. T. Weber (2000). "Infarct scar: a dynamic tissue." Cardiovascular Research **46**(2): 250-256.
Taegtmeyer, H. (1994). "Energy metabolism of the heart: from basic concepts to clinical applications." Curr Probl Cardiol **19**(2): 59-113.
Takatani, T., K. Takahashi, Y. Uozumi, T. Matsuda, T. Ito, S. W. Schaffer, Y. Fujio and J. Azuma (2004). "Taurine prevents the ischemia-induced apoptosis in cultured neonatal rat cardiomyocytes through Akt/caspase-9 pathway." Biochemical and biophysical research communications **316**(2): 484-489.
Takeda, N. and I. Manabe (2011). "Cellular Interplay between Cardiomyocytes and Nonmyocytes in Cardiac Remodeling." International Journal of Inflammation **2011**: 535241.
Talman, V. and H. Ruskoaho (2016). "Cardiac fibrosis in myocardial infarction—from repair and remodeling to regeneration." Cell and Tissue Research **365**(3): 563-581.
Tandler, B., M. Dunlap, C. L. Hoppel and M. Hassan (2002). "Giant Mitochondria in a Cardiomyopathic Heart." Ultrastructural Pathology **26**(3): 177-183.
Taverne, Y. J. H. J., A. J. J. C. Bogers, D. J. Duncker and D. Merkus (2013). "Reactive Oxygen Species and the Cardiovascular System." Oxidative Medicine and Cellular Longevity **2013**: 862423.
Tenori, L., X. Hu, P. Pantaleo, B. Alterini, G. Castelli, I. Olivotto, I. Bertini, C. Luchinat and G. F. Gensini (2013). "Metabolomic fingerprint of heart failure in humans: a nuclear magnetic resonance spectroscopy analysis." Int J Cardiol **168**(4): e113-115.

Tepass, U., K. Truong, D. Godt, M. Ikura and M. Peifer (2000). "Cadherins in embryonic and neural morphogenesis." Nature Reviews Molecular Cell Biology **1**(2): 91-100.
Thind, G. S., P. R. Agrawal, B. Hirsh, L. Saravolatz, C. Chen-Scarabelli, J. Narula and T. M. Scarabelli (2015). "Mechanisms of myocardial ischemia-reperfusion injury and the cytoprotective role of minocycline: scope and limitations." Future Cardiol **11**(1): 61-76.
Titford, M. (2005). "The long history of hematoxylin." Biotech Histochem **80**(2): 73-78.
Tondera, D., S. Grandemange, A. Jourdain, M. Karbowski, Y. Mattenberger, S. Herzig, S. Da Cruz, P. Clerc, I. Raschke, C. Merkwirth, S. Ehses, F. Krause, D. C. Chan, C. Alexander, C. Bauer, R. Youle, T. Langer and J.-C. Martinou (2009). "SLP-2 is required for stress-induced mitochondrial hyperfusion." The EMBO Journal **28**(11): 1589-1600.
Toyofuku, T., K. Curotto Kurzydlowski, N. Narayanan and D. H. MacLennan (1994). "Identification of Ser38 as the site in cardiac sarcoplasmic reticulum Ca(2+)-ATPase that is phosphorylated by Ca2+/calmodulin-dependent protein kinase." J Biol Chem **269**(42): 26492-26496.
Tran, D. H. and Z. V. Wang (2019). "Glucose Metabolism in Cardiac Hypertrophy and Heart Failure." Journal of the American Heart Association **8**(12): e012673.
Troidl, C., H. Möllmann, H. Nef, F. Masseli, S. Voss, S. Szardien, M. Willmer, A. Rolf, J. Rixe, K. Troidl, S. Kostin, C. Hamm and A. Elsässer (2009). "Classically and alternatively activated macrophages contribute to tissue remodelling after myocardial infarction." J Cell Mol Med **13**(9b): 3485-3496.
Turrens, J. F. (2003). "Mitochondrial formation of reactive oxygen species." The Journal of Physiology **552**(2): 335-344.
Uddin, G. M., L. Zhang, S. Shah, A. Fukushima, C. S. Wagg, K. Gopal, R. Al Batran, S. Pherwani, K. L. Ho, J. Boisvenue, Q. G. Karwi, T. Altamimi, D. S. Wishart, J. R. B. Dyck, J. R. Ussher, G. Y. Oudit and G. D. Lopaschuk (2019). "Impaired branched chain amino acid oxidation contributes to cardiac insulin resistance in heart failure." Cardiovascular Diabetology **18**(1): 86.
Unger, E. F. (2001). "Experimental evaluation of coronary collateral development." Cardiovascular Research **49**(3): 497-506.
University, Y.
Ussher, J. R., S. Elmariah, R. E. Gerszten and J. R. Dyck (2016). "The Emerging Role of Metabolomics in the Diagnosis and Prognosis of Cardiovascular Disease." J Am Coll Cardiol **68**(25): 2850-2870.
van der Vusse, G. J., M. van Bilsen and J. F. Glatz (2000). "Cardiac fatty acid uptake and transport in health and disease." Cardiovascular research **45**(2): 279-293.
Vanderslice, P., S. M. Ballinger, E. K. Tam, S. M. Goldstein, C. S. Craik and G. H. Caughey (1990). "Human mast cell tryptase: multiple cDNAs and genes reveal a multigene serine protease family." Proceedings of the National Academy of Sciences **87**(10): 3811.
Vedin, O., C. S. P. Lam, A. S. Koh, L. Benson, T. H. K. Teng, W. T. Tay, O. Ö. Braun, G. Savarese, U. Dahlström and L. H. Lund (2017). "Significance of Ischemic Heart Disease in Patients With Heart Failure and Preserved, Midrange, and Reduced Ejection Fraction." Circulation: Heart Failure **10**(6): e003875.
Walker, C. A. and F. G. Spinale (1999). "The structure and function of the cardiac myocyte: a review of fundamental concepts." J Thorac Cardiovasc Surg **118**(2): 375-382.
Warren, C. M., M. C. Jordan, K. P. Roos, P. R. Krzesinski and M. L. Greaser (2003). "Titin isoform expression in normal and hypertensive myocardium." Cardiovascular Research **59**(1): 86-94.
Watkins, D. W., J. M. X. Jenkins, K. J. Grayson, N. Wood, J. W. Steventon, K. K. Le Vay, M. I. Goodwin, A. S. Mullen, H. J. Bailey, M. P. Crump, F. MacMillan, A. J. Mulholland, G. Cameron, R. B. Sessions, S. Mann and J. L. R. Anderson (2017). "Construction and in vivo assembly of a catalytically proficient and hyperthermostable de novo enzyme." Nature Communications **8**(1): 358.
Wayman, N. S., M. C. McDonald, P. K. Chatterjee and C. Thiemermann (2003). "Models of coronary artery occlusion and reperfusion for the discovery of novel antiischemic and antiinflammatory drugs for the heart." Methods Mol Biol **225**: 199-208.
Wheaton, W. W. and N. S. Chandel (2011). "Hypoxia. 2. Hypoxia regulates cellular metabolism." American journal of physiology. Cell physiology **300**(3): C385-C393.

White, M. Y., S. J. Cordwell, H. C. K. McCarron, A. M. Prasan, G. Craft, B. D. Hambly and R. W. Jeremy (2005). "Proteomics of ischemia/reperfusion injury in rabbit myocardium reveals alterations to proteins of essential functional systems." PROTEOMICS **5**(5): 1395-1410.
WHO.
Willems, I. E. M. G., M. G. Havenith, J. G. R. De Mey and M. J. A. P. Daemen (1994). "The α-smooth muscle actin-positive cells in healing human myocardial scars." American Journal of Pathology **145**(4): 868-875.
Wright, S. H. (2004). "Generation of resting membrane potential." **28**(4): 139-142.
Wu, Y., X. Yin, C. Wijaya, M. H. Huang and B. K. McConnell (2011). "Acute myocardial infarction in rats." J Vis Exp(48).
Xiao, B., M. T. Jiang, M. Zhao, D. Yang, C. Sutherland, F. A. Lai, M. P. Walsh, D. C. Warltier, H. Cheng and S. R. Chen (2005). "Characterization of a novel PKA phosphorylation site, serine-2030, reveals no PKA hyperphosphorylation of the cardiac ryanodine receptor in canine heart failure." Circ Res **96**(8): 847-855.
Xie, J. R. and L. N. Yu (2007). "Cardioprotective effects of cyclosporine A in an in vivo model of myocardial ischemia and reperfusion." Acta anaesthesiologica Scandinavica **51**(7): 909-913.
Xu, L., G. Mann and G. Meissner (1996). "Regulation of cardiac Ca2+ release channel (ryanodine receptor) by Ca2+, H+, Mg2+, and adenine nucleotides under normal and simulated ischemic conditions." Circ Res **79**(6): 1100-1109.
Yan, X., A. Anzai, Y. Katsumata, T. Matsuhashi, K. Ito, J. Endo, T. Yamamoto, A. Takeshima, K. Shinmura, W. Shen, K. Fukuda and M. Sano (2013). "Temporal dynamics of cardiac immune cell accumulation following acute myocardial infarction." Journal of Molecular and Cellular Cardiology **62**: 24-35.
Yang, F., Y.-H. Liu, X.-P. Yang, J. Xu, A. Kapke and O. A. Carretero (2002). "Myocardial Infarction and Cardiac Remodelling in Mice." Experimental Physiology **87**(5): 547-555.
Yasui, B., F. Fuchs and F. N. Briggs (1968). "The Role of the Sulfhydryl Groups of Tropomyosin and Troponin in the Calcium Control of Actomyosin Contractility." Journal of Biological Chemistry **243**(4): 735-742.
Yen, C. and P. C. Hsieh "Pathology of permanent, LAD-ligation induced myocardial infarction differs across small (mice, rat) and large (pig) animal models."
Yin, Z., J. Ren and W. Guo (2015). "Sarcomeric protein isoform transitions in cardiac muscle: a journey to heart failure." Biochim Biophys Acta **1852**(1): 47-52.
Youle, R. J. and A. M. van der Bliek (2012). "Mitochondrial fission, fusion, and stress." Science (New York, N.Y.) **337**(6098): 1062-1065.
Young, M. E., P. McNulty and H. Taegtmeyer (2002). "Adaptation and maladaptation of the heart in diabetes: Part II: potential mechanisms." Circulation **105**(15): 1861-1870.
Yu, H., T. Kalogeris and R. J. Korthuis (2019). "Reactive species-induced microvascular dysfunction in ischemia/reperfusion." Free Radical Biology and Medicine **135**: 182-197.
Zbinden, G. and R. Bagdon (1963). "Isoproterenol-induced heart necrosis, an experimental model for the study of angina pectoris and myocardial infarct." Revue canadienne de biologie **22**: 257.
Zhao, B., S. Chen, J. Liu, Z. Yuan, X. Qi, J. Qin, X. Zheng, X. Shen, Y. Yu, T. J. Qnin, J. Y.-H. Chan and D. Cai (2013). "Cardiac telocytes were decreased during myocardial infarction and their therapeutic effects for ischaemic heart in rat." Journal of cellular and molecular medicine **17**(1): 123-133.
Zhao, B., Z. Liao, S. Chen, Z. Yuan, C. Yilin, K. K. H. Lee, X. Qi, X. Shen, X. Zheng, T. Quinn and D. Cai (2014). "Intramyocardial transplantation of cardiac telocytes decreases myocardial infarction and improves post-infarcted cardiac function in rats." Journal of Cellular and Molecular Medicine **18**(5): 780-789.
Zhao, Z. Q., J. S. Corvera, M. E. Halkos, F. Kerendi, N. P. Wang, R. A. Guyton and J. Vinten-Johansen (2003). "Inhibition of myocardial injury by ischemic postconditioning during reperfusion: comparison with ischemic preconditioning." Am J Physiol Heart Circ Physiol **285**(2): H579-588.

Zheng, M., H. Cheng, I. Banerjee and J. Chen (2010). "ALP/Enigma PDZ-LIM domain proteins in the heart." Journal of molecular cell biology **2**(2): 96-102.
Zhong, Z., J. Liu, Q. Zhang, W. Zhong, B. Li, C. Li, Z. Liu, M. Yang and P. Zhao (2019). "Targeted metabolomic analysis of plasma metabolites in patients with coronary heart disease in southern China." Medicine (Baltimore) **98**(7): e14309.
Zhou, B. and R. Tian (2018). "Mitochondrial dysfunction in pathophysiology of heart failure." The Journal of Clinical Investigation **128**(9): 3716-3726.
Zhou, J., L. Sun, L. Chen, S. Liu, L. Zhong and M. Cui (2019). "Comprehensive metabolomic and proteomic analyses reveal candidate biomarkers and related metabolic networks in atrial fibrillation." Metabolomics **15**(7): 96.
Zhou, P. and W. T. Pu (2016). "Recounting Cardiac Cellular Composition." Circulation research **118**(3): 368-370.
Zhu, M. R., Z. Fulati, Y. Liu, W. S. Wang, Q. Wu, Y. G. Su, H. Y. Chen and X. H. Shu (2019). "The value of serum metabolomics analysis in predicting the response to cardiac resynchronization therapy." J Geriatr Cardiol **16**(7): 529-539.
Zhuge, Y., J. Zhang, F. Qian, Z. Wen, C. Niu, K. Xu, H. Ji, X. Rong, M. Chu and C. Jia (2020). "Role of smooth muscle cells in Cardiovascular Disease." International journal of biological sciences **16**(14): 2741-2751.
Zimmer, A., A. K. Bagchi, K. Vinayak, A. Bello-Klein and P. K. Singal (2019). "Innate immune response in the pathogenesis of heart failure in survivors of myocardial infarction." Am J Physiol Heart Circ Physiol **316**(3): H435-H445.

Appendix

1- CMR measurement in porcine model

Cardiac imaging was taken 2 days and 4 weeks after surgery using multi-slice cine CMR (Siemen Healthcare Limited, Magnetom 3T PRISMA, Erlangen Germany) at the Translational Biomedical Research Centre in University of Bristol. Thirty images throughout the cardiac cycle were obtained. Cardiac contours were manually drawn and analysed by Dr. E Sammut using software package CVI42 (Calgary, Canada, V5.6.6). Full width half maximum (FWHM) method was used to measure myocardial scar weight in grams. This technique follows an initial region that extends to include pixels with a signal intensity greater of 50% of a user selected point. Then, the maximum intensity (MX) expected in the initial region is computationally calculated. Consequently, the infarcted area is measured as the total area that presents with more than 50% of the initial region's maximum intensity (Area infarcted= MX* 0.5).

Pigs undergoing closed-chest balloon LAD catheter inflation for 60 minutes and deflation had on average 21 grams of the infarct (using CMR) two days after surgery, and 8.5 grams at termination after weeks (Figure 10). No major difference in the percentage of left ventricular ejection fraction was observed (Δ %EF = 9.67%) as shown in figures 1 and 2.

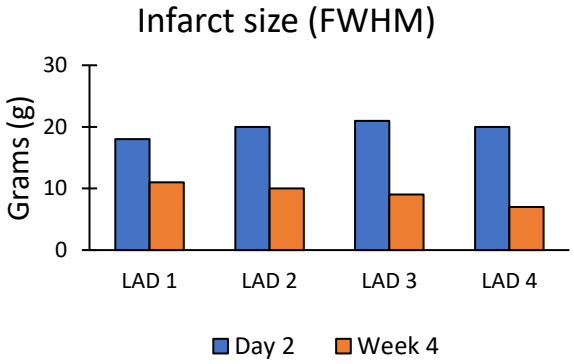

Figure A.1 Time-dependent changes in infarct size in pigs. Bar chart demonstrating infarct size (g) in pigs 2 days and 4 weeks after I/R injury. FWHM: Full Width at Half Maximum

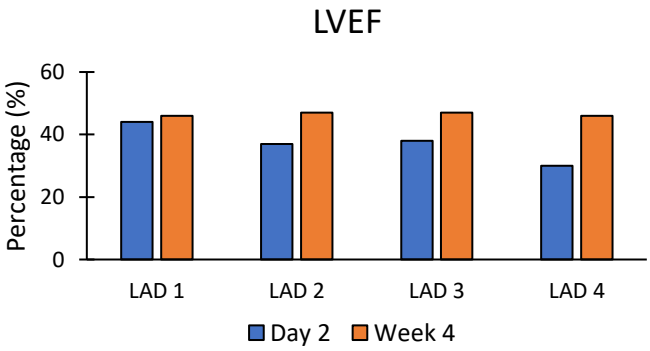

Figure A.2 Change in ejection fraction in pigs after IRI. Bar chart demonstrating the percentage of Left Ventricular Ejection Fraction (LVEF) in pigs 2 days and 4 weeks after I/R injury.

2- Cardiac Troponin I measurement

Cardiac troponin-I (c-TnI) assay was measured by Mr. D Lopez using an ultra-sensitive pig cardiac troponin enzyme-linked immunosorbent assay (CTNI-9-US Life Diagnostics, PA). Samples were diluted following manufacturer instruction and each of the plasma sample was analysed in duplicates.

This method uses a rabbit anti-TnI polyclonal antibody for the solid phase on the microfilter plate that binds to the Troponin-I in the sample. When a goat anti-cTnI peptide specific polyclonal antibody conjugated to horseradish peroxidase (HRP) is added to the plate, Troponin I becomes sandwiched between the two antibodies. Detection of cTnI concentration is achieved through the addition of Tetramethylbenzidine (TMB reagent) which binds to HRP, resulting in the development of a blue colour, which is later stopped by a stop solution (HCl), turning the reaction into yellow. Absorbance is then read at 450 nm using a 96-microplate reader (Opsys MR™, DYNEX Technologies, Inc. VA) and the concentration is derived from the standard curve.

High sensitivity cardiac Troponin I measurement from plasma samples showed peaked levels at four hours after reperfusion (balloon deflation), as illustrated in figure 3.

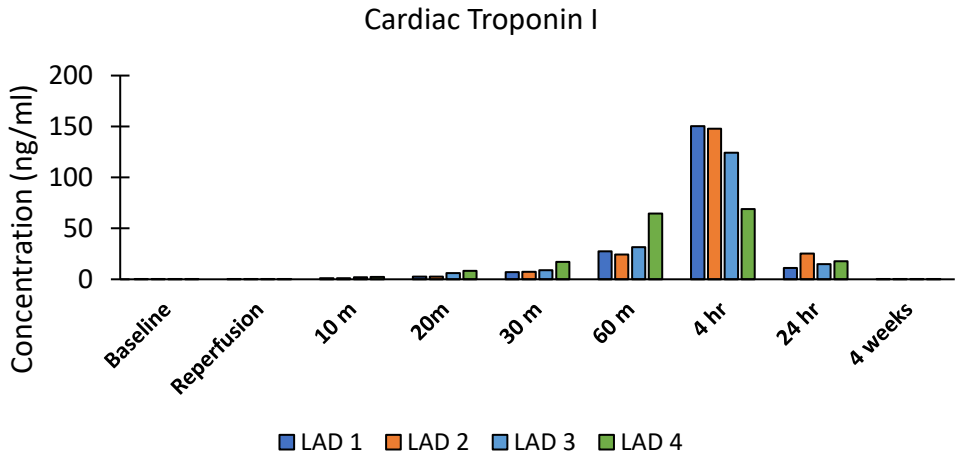

Figure A.3 Cardiac injury following acute MI. Serial Troponin I measurements taken at baseline (before ischaemia), at reperfusion and selected time intervals.

3- Grant submitted to and awarded by David Telling Charitable Trust for a pilot study of metabolic profile in STEMI patients

Study protocol and ethics application were approved by NHS University Hospitals Bristol and Weston

Changes in cardiac function and blood metabolites following acute infarction and during remodelling into heart failure: an exploratory study to inform design of a future larger study

Details of Sponsor:

University Hospitals Bristol NHS Foundation Trust,

Research and Innovation,

Level 3,

UH Bristol Education Centre,

Upper Maudlin Street,

Bristol,

BS2 8AE

Tel: 0117 342 0233

CI and Research Team Contact Details

Chief/Principal Investigator:

Dr Tom Johnson

Consultant Cardiologist

Bristol Heart Institute

University Hospitals Bristol NHS Foundation Trust
Bristol Royal Infirmary
Bristol
BS2 8HW

Investigator:

Dr Eva Sammut

NIHR Academic Clinical Lecturer, Cardiology Registrar

Bristol Heart Institute

University Hospitals Bristol NHS Foundation Trust
Bristol Royal Infirmary
BS2 8HW

Investigator:

Dr Georgia May Connolly
NIHR Academic Clinical Fellow, Cardiology Registrar
Bristol Heart Institute

University Hospitals Bristol NHS Foundation Trust
Bristol Royal Infirmary
Bristol
BS2 8HW

Investigator:

Professor Saadeh Suleiman

Professor of Cardiac Physiology

University of Bristol

Research Floor Level 7

Bristol Roya Infirmary

Upper Maudlin Street

Bristol

BS2 8HW

Investigator:

Dr Lujain Alsadder

PhD Student

University of Bristol

Research Floor Level 7

Bristol Roya Infirmary

Upper Maudlin Street

Bristol

BS2 8HW

IRAS Project ID: 27174

PROTOCOL VERSION NUMBER AND DATE:

Summary

Sufficient pump function of the heart is essential to ensure delivery of oxygenated blood to heart muscle and to other organs.

Severe coronary artery disease results in acute reduction of blood (ischaemia) to the heart, which, if not treated promptly can lead to death of heart muscle cells (infarction). However, re-introducing blood to an ischaemic area (via the placement of stents in coronary arteries called angioplasty) can further augment the ischaemic damage (reperfusion injury). Unlike other muscle types, cardiac muscle cannot generate new heart cells to replace the dead ones. Subsequently, the infarcted areas undergo gradual change involving metabolic, molecular and structural alterations which eventually can lead to a varying degree of impaired pumping function of the heart (heart failure). Heart failure leaves patients prone to dangerous heart rhythms, fluid overload, repeated hospital admissions and ultimately death. Therefore, it is important *to understand the systemic and cardiac changes that are associated with remodelling into heart failure in order to identify early biomarkers of cardiac impairment so that appropriate therapeutic interventions can be designed*.

Recent work in Bristol using experimental models of heart failure (rodent & pig) following acute ischaemia have shown interesting changes in selected blood metabolites when measured immediately after infarction (before heart failure) and after the onset of heart failure. Work is underway to establish if the changes in any of these metabolites can predict the severity/incidence of heart failure. Furthermore, identifying metabolic pathways implicated in the development of heart failure will help in the design of targeted therapeutic interventions.

We plan to extend the work on experimental models to patients with ST elevation myocardial infarction to identify metabolites that change from acute infarction to failure and correlate with the function of a failing heart. The information obtained from this exploratory focused study will be used to inform design of a future larger study. Blood samples will be collected to monitor metabolites and markers of cardiac injury and inflammation. Patients will also have an echocardiogram – an ultrasound which assesses the pumping of the heart - within 48hrs of the heart attack and at 6-8 weeks according to standard care.

Background and rationale

Coronary heart disease is the most common cause of myocardial infarction (MI). With modern treatments, most patients now survive the acute episode. However, a significant proportion of patients will develop heart failure post MI due to cell death and adverse myocardial remodelling. The British Heart Foundation estimate that there are currently approximately 900,000 people living with heart failure in the UK. This leads to a significant deterioration in quality of life, repeated admissions to hospital, increased incidence of arrhythmia and sudden cardiac death and high mortality rates.

MI is typically a consequence of atherosclerosis where there is progressive narrowing of a coronary artery leading to a demand and supply imbalance which renders areas of the myocardium ischaemic. During ischaemia, sustained cardiomyocyte deprivation of oxygen and metabolites results in disruption of intracellular metabolic and ionic homeostasis, leading to calcium loading and cardiomyocyte death. Timely reperfusion of the ischaemic zone via primary percutaneous coronary intervention (PPCI) can salvage some of the myocardium but can cause reperfusion injury, and as cardiomyocytes are terminally differentiated, regeneration of infarcted tissue is limited. Damaged myocardium undergoes a state of cleaning and repair via apoptosis and the migration of inflammatory cells to the infarcted area [1]. The inflammatory response (systemic and innate) plays a central role in cardiac remodelling post MI. These inflammatory changes are also likely to be reflected in changes in blood metabolites. These may vary depending on the stage and severity of remodelling from acute (ischaemia/reperfusion) to chronic disease (heart failure). Remodelling involves a number of metabolic, molecular and cellular alterations [2, 3] which lead to fibrosis and ultimately impaired ability of the heart to meet its intensive functional demands [4].

There is heterogeneity in the degree of adverse remodelling between patients, and there is currently no way of predicting which patients will be most affected.

Although the mechanisms underlying acute ischaemia and reperfusion injury are well understood, we know little about the chronic processes leading to subsequent heart failure as a result of adverse remodelling. Importantly, *the link between acute injury and characteristics of heart failure is not known*. Understanding and identifying the underlying triggers of heart failure after an ischaemic injury will help in design of therapeutic interventions. Since both acute injury and chronic remodelling involve metabolic alterations, metabolites are an emerging area of research to investigate the progression of heart failure and to guide therapeutic strategies [5, 6]. In particular these biomarkers are likely to improve heart failure prognostication [7] and early targeting of heart failure treatments.

Recent clinical trials have investigated alterations in blood metabolome in cardiovascular diseases including hypertrophy, coronary disease, diabetic cardiomyopathy, heart failure, atrial fibrillation and cardiac resynchronization therapy [7-14]. Recent studies have also reported changes in the metabolome in ST-segment elevation myocardial infarction (STEMI) patients [15, 16]. However, little work has been done to investigate the changes in the metabolome following acute MI and during progression in heart failure [17]. Furthermore, most

studies tend to include a heterogenous population of patients (gender, age etc) with comorbidities which are known to have a metabolic impact (e.g. diabetes and kidney disease). Researchers at Bristol have recently developed experimental models (rodent and pig) of MI with subsequent remodelling and heart failure to address this issue. The large animal model of acute MI has been established by Dr Tom Johnson (the Principal Investigator) at the Translational Biomedical Research Centre, University of Bristol. In this porcine model, four weeks post *in-vivo* LAD balloon induced MI, structural, molecular (proteins and phosphoproteins), metabolic (circulatory metabolites levels in blood) profiles were observed. Key findings involved detrimental modulation of Z-disc and cytoskeletal proteins, reduction of mitochondrial and antioxidant enzymes, and elevation of blood ketone bodies and methionine and reduction of taurine (unpublished data). Moreover, similar changes observed in rats four weeks after acute LAD ligation, included increased phosphorylation of Z-disc proteins and an increase in blood acetone. Therefore, this exploratory study has been designed to see if these findings translate to a STEMI patient population. The porcine model of MI is based on a population of animals with healthy hearts, it is unclear if these changes will be observed in a population of patients with coronary artery disease.

It is evident that there is a need to investigate changes in patients' metabolites acutely post MI and also during remodelling into heart failure. This will allow discovery of any metabolomic alterations that correlate with cardiac impairment and maladaptation, and aid identification of molecular pathways that could be targeted to aid the design of therapeutic interventions. Given the issue of heterogeneity in patients, it is important that in the first instance a focused small group of patients are selected to monitor changes in cardiac function and blood metabolites following acute infarction and during remodelling into heart failure. The aim of this exploratory study to inform design of a future larger study.

Aims

This exploratory study aims to monitor alterations in cardiac function, blood metabolites and markers of cardiac injury and inflammation in a selected group of STEMI patients (n=30) both acutely post MI and following remodelling into heart failure.

Hypothesis

1- A distinct metabolomic profile will be observed in STEMI patients who develop severe left ventricular adverse remodelling compared to STEMI patients that do not develop adverse remodelling, compared to controls.

2- A distinct profile of markers of inflammation / oxidative stress will correlate with the degree of left ventricular adverse remodelling in a group of STEMI patients, compared to a group of age-matched healthy controls.

Assessment and risk

Patients will only be included in the study if they meet the inclusion criteria, do not fulfil any of the exclusion criteria and once they are deemed clinically stable by their clinical team.

Standard care of patients after with STEMI includes:

- Blood samples taken at the time of primary percutaneous coronary intervention (PPCI)
- Blood samples taken 24 to 48hrs following admission
- Echocardiogram within 48hrs of admission
- If significant left ventricular impairment, an echocardiogram 6-8 weeks following discharge from hospital
- Clinic appointment 4-6 weeks following admission

The only additional test required for this study will be 1 additional venepuncture taken at the time of the follow up clinic appointment 6-8 weeks following PPCI.

Objectives

1) **Primary** objective**:** Observation of metabolomic profile acutely post MI and during remodelling into heart failure to identify ones that correlate with left ventricular negative remodelling.

Sample size

As this is an exploratory study to inform design of a future larger study, no formal power calculation has been performed. However, previous work within the group using a large animal model of MI and from relevant literature review, it was concluded that 30 patients and 10 controls would be adequate to obtain preliminary meaningful answers.

Patient selection

Inclusion criteria:

1. Male patients
2. Anterior STEMI (due to occlusion of left anterior descending artery (LAD))
3. Age 40-75 years

Exclusion criteria:

1. Congenital heart disease
2. Pre-existing pacing device (pacemaker or ICD).
3. Atrial fibrillation
4. Bystander coronary disease requiring intervention
5. Co-existent comorbidities such as diabetes, disease of the kidney, liver and peripheral vasculature, or chronic inflammatory conditions.

Selection of control participants:

1. Must not meet exclusion criteria mentioned above.
2. No history of cardiac disease, therefore normal LV function will be assumed. They will not undergo echocardiography.

Consent/ screening

Potentially eligible patients will be identified by screening emergency STEMI admissions. All patients admitted with an anterior STEMI will have 1 extra blood sample taken at the time of the primary percutaneous coronary intervention (PPCI) which will be stored.

Within 48hrs of their admission, a member of the research team will approach eligible patients providing them with a patient information leaflet containing full details of the study, discuss the study with them, and answer any questions they may have. Patients will be given as much time as necessary to consider their participation in the study. Informed consent will be obtained by a member of the research team. If patients are deemed to be ineligible or if they do not consent, the stored sample will be disposed of in accordance with local policy.

Method

As part of clinical routine care, STEMI patients attending the Bristol Heart Institute will be treated as follows:

1. Upon arrival, blood tests will be performed to measure troponin T, C-reactive protein, full blood count, renal and liver function, clotting screen & lipid profile.
2. At 24-48 hours post admission, blood will be collected again to measure injury and stress markers including troponin T, brain natriuretic peptide & C-reactive protein.
3. Trans-thoracic echocardiogram at 24-48 hours post admission (following angioplasty and prior to discharge)
4. Follow up appointment 4-6 weeks post discharge which will include a repeat trans-thoracic echocardiogram if there is significant left ventricular impairment on their echocardiogram during admission.

In addition to standard care described above, we propose to additional blood samples as follows:

5. Additional 5ml blood taken on arrival (at time of standard venepuncture)
6. Additional 5ml blood taken at 24-48 hours (at time of standard venepuncture)
7. Additional 5ml blood taken at 4-6 week follow up appointment (additional venepuncture).

Withdrawal criteria

Patients will be consented prior to discharge, if they withdraw consent then their data will not be used, and all samples stored will be disposed of.

Data storage and analysis

Data will be collected and retained in accordance with the Data Protection Act 1998.

Data will be pseudo-anonymised, stored on a secure NHS server as well as a secure University of Bristol server and will only be accessible to the research team.

All other data collected will be pseudo-anonymised and held on a password protected database stored on a secure NHS server accessible only to the research team.

A secure electronic 'key' with a unique participant identifier, and key personal identifiers (e.g. name, date of birth and NHS number) will be password protected and held on a secure NHS server.

Study documents will be retained in a locked cabinet in a locked office in The Bristol Heart Institute, only accessible to the research team, during and after the trial has finished. All source documents will be retained for a period of five years following the end of the study.

Statistical analysis will be performed by the group who have experience in analysing metabolomic data.

Costs

This study has secured the full total amount of funding required from the David Telling Charitable Trust (£9800).

Safety Reporting

Adverse events will be recorded and reported in accordance with University Hospitals Bristol's Research Safety Reporting SOP.

Adverse events will be recorded from the beginning of cardiac pacing until the end of the cardiac pacing procedure.

An adverse event, is defined as serious if it:

(a) results in death,

(b) is life-threatening,

(c) requires hospitalisation or prolongation of existing hospitalisation,

(d) results in persistent or significant disability or incapacity,

(e) consists of a congenital anomaly or birth defect.

Monitoring and Audit

The study will be monitored in accordance with University Hospitals Bristol's Monitoring and Oversight of Research Activity SOP. All trial related documents will be made available on request for monitoring and audit by UH Bristol, the relevant Research Ethics Committee and any other licensing bodies as applicable.

Quality Control

Where applicable, a random sample of 10% of CRFs will be checked, by the trial Research Team or R&I monitor, against entries within the database and with the source data for quality purposes. The percentage checked will be increased if a significant error rate is found.

Data Handling and Protection

The database will be designed so as to protect patient information in line with the Data Protection Act 1998. Trial staff will ensure that the participants' confidentiality is maintained through protective and secure handling and storage of patient information at the trial centres (as relevant). All documents will be stored securely and only accessible by trial staff and authorised personnel. Data will be collected and retained in accordance with the Data Protection Act 1998.

Storage of records

Study documents (paper and electronic) will be retained in a secure location during and after the trial has finished. All essential documents, including patient records and other source documents will be retained for a period of 5 years following the end of the study. Where trial related information is documented in the hard copy medical records – those records will be identified by a 'Do not destroy before dd/mm/yyyy' label where date is 5 years after the last patient last visit. Where electronic records are in use, trust policy will be followed.

Indemnity

This is an NHS-sponsored research study. For NHS sponsored research HSG(96)48 reference no. 2 refers. If there is negligent harm during the clinical trial when the NHS body owes a duty of care to the person harmed, NHS Indemnity covers NHS staff, medical academic staff with honorary contracts, and those conducting the trial. NHS Indemnity does not offer no-fault compensation and is unable to agree in advance to pay compensation for non-negligent harm. Ex-gratia payments may be considered in the case of a claim.

Authorisations

The study will be performed subject to favourable opinion/ authorisation/permission or equivalent from all necessary regulatory and other bodies. This includes but is not limited to REC, MHRA, HRA, NHS trusts.

Research Governance Statement

This study will be conducted in accordance with:

- International Conference for Harmonisation of Good Clinical Practice (ICH GCP) guidelines.
- UK Policy Framework for Health and Social Care

References

1. Zimmer, A., et al., Innate immune response in the pathogenesis of heart failure in survivors of myocardial infarction. Am J Physiol Heart Circ Physiol, 2019. 316(3): p. H435-H445.

2. Pfeffer, M.A. and E. Braunwald, Ventricular remodeling after myocardial infarction. Experimental observations and clinical implications. Circulation, 1990. 81(4): p. 1161-72.

3. Cohn, J.N., R. Ferrari, and N. Sharpe, Cardiac remodeling--concepts and clinical implications: a consensus paper from an international forum on cardiac remodeling. Behalf of an International Forum on Cardiac Remodeling. J Am Coll Cardiol, 2000. 35(3): p. 569-82.

4. Konstam, M.A., et al., Left Ventricular Remodeling in Heart Failure. Current Concepts in Clinical Significance and Assessment, 2011. 4(1): p. 98-108.

5. Barba, I., M. Andres, and D. Garcia-Dorado, Metabolomics and Heart Diseases: From Basic to Clinical Approach. Curr Med Chem, 2019. 26(1): p. 46-59.

6. Cresci, S., et al., Heart Failure in the Era of Precision Medicine: A Scientific Statement From the American Heart Association. Circ Genom Precis Med, 2019: p. HCG0000000000000058.

7. Stenemo, M., et al., The metabolites urobilin and sphingomyelin (30:1) are associated with incident heart failure in the general population. ESC Heart Fail, 2019. 6(4): p. 764-773.

8. Zhu, M.R., et al., The value of serum metabolomics analysis in predicting the response to cardiac resynchronization therapy. J Geriatr Cardiol, 2019. 16(7): p. 529-539.

9. Zhou, J., et al., Comprehensive metabolomic and proteomic analyses reveal candidate biomarkers and related metabolic networks in atrial fibrillation. Metabolomics, 2019. 15(7): p. 96.

10. Zhong, Z., et al., Targeted metabolomic analysis of plasma metabolites in patients with coronary heart disease in southern China. Medicine (Baltimore), 2019. 98(7): p. e14309.

11. Sowton, A.P., J.L. Griffin, and A.J. Murray, Metabolic Profiling of the Diabetic Heart: Toward a Richer Picture. Front Physiol, 2019. 10: p. 639.

12. Pouralijan Amiri, M., et al., Metabolomics in early detection and prognosis of acute coronary syndrome. Clin Chim Acta, 2019. 495: p. 43-53.

13. Muller, O.J., et al., Comprehensive plasma and tissue profiling reveals systemic metabolic alterations in cardiac hypertrophy and failure. Cardiovasc Res, 2019. 115(8): p. 1296-1305.

14. McKirnan, M.D., et al., Metabolomic analysis of serum and myocardium in compensated heart failure after myocardial infarction. Life Sci, 2019. 221: p. 212-223.

15. Goulart, V.A.M., et al., Metabolic Disturbances Identified in Plasma Samples from ST-Segment Elevation Myocardial Infarction Patients. Dis Markers, 2019. 2019: p. 7676189.

16. Kohlhauer, M., et al., Metabolomic Profiling in Acute ST-Segment-Elevation Myocardial Infarction Identifies Succinate as an Early Marker of Human Ischemia-Reperfusion Injury. J Am Heart Assoc, 2018. 7(8).

17. Chen, L., J. Song, and S. Hu, Metabolic remodeling of substrate utilization during heart failure progression. Heart Fail Rev, 2019. 24(1): p. 143-154.